

Department of Companion Animals and Horses

University of Veterinary Medicine Vienna

Institute of Small Animal Surgery

(Head: Ass.-Prof. Dr.med.vet. Britta Vidoni)

**Evaluation of a newly described rostromentorial craniotomy
approach in brachycephalic dogs for consistency in size and shape
in comparison with mesaticephalic breeds**

Diploma thesis

University of Veterinary Medicine Vienna

submitted by

Martin Schlager

Vienna, 16.04.2021

Academic advisor: Dr. med. vet. Gabriele Gradner Dipl. ECVS

Clinical Unit of Small Animal Surgery of Vetmeduni Vienna

Department of Companion Animals and Horses

University of Veterinary Medicine Vienna

Assessor:

Acknowledgement

First and foremost, I want to thank my whole **family**, who always supported me both, mentally as well as financially. Without them, I would not have been able to go through this whole journey from the beginning to the end.

Furthermore, I want to thank all my **friends** at University and elsewhere, for always staying on my side, even during tough times and helping me to stay focused on the important things.

Special thanks go out to my assessor **Dr.med.vet. Gabriele Gradner Dipl.ECVS** for letting me work on such a fascinating project and providing me with advice, guidance and help throughout the thesis.

I particularly thank **Dr.rer.nat. Stephan Handschuh** for instructing me with all the necessary knowledge regarding the visualization and simulation as well as the **VetCORE – Facility for Research** for providing the necessary equipment.

Moreover, I need to thank **Univ.-Prof. Dr.med.vet. Eberhard Ludewig** and the team of the **Clinical Unit of Diagnostic Imaging of Vetmeduni Vienna** for providing me with the required scans for this thesis.

In addition, my thanks also go to **Ao.Univ.-Prof. Dr.med.vet. Sabine Breit** for supplying specimen and help on how to approach these as well as the correct nomenclature of the Gyri and Sulci.

Likewise, many thanks go to **Dr.rer.nat. Alexander Tichy** from the Department of Biomedical Sciences.

Table of content

1	Introduction	1
1.1	The Rostrotentorial Approach in Veterinary Medicine.....	1
1.2	Anatomy.....	3
1.2.1	The Skull	3
1.2.2	Morphometric Analysis of the Canine Skull.....	5
1.2.3	The Encephalon	9
1.2.4	The Cerebral Lobes.....	12
1.2.5	The Meninges.....	13
1.2.6	The Sinus Durae Matris.....	13
2	Material and Methods	16
2.1	Diagnostic Imaging.....	16
2.2	Visualization.....	16
2.3	Morphometric Analysis	18
2.4	The Rostrotentorial Approach.....	21
2.4.1	Drill Holes „Approach Brachycephalic“ (Figure 21)	21
2.4.2	Crista Sagittalis Externa	23
2.4.3	Sinus Frontalis.....	24
2.4.4	Drill Holes “Approach Mesaticephalic”	24
2.4.5	Calculations and Statistics	27
3	Results	29
3.1	Morphometric Analysis	29
3.2	Craniotomy Area on the Skull.....	30

3.3	Accessible Gyri	33
3.4	Craniotomy Area in comparison with Brain Area	40
3.5	Sinus frontalis	44
4	Discussion	45
5	Summary	49
6	Zusammenfassung	51
7	Appendix	53
7.1	Translation-sheet	53
7.2	Measurements from Amira	57
7.3	Statistics.....	63
7.4	Standard Operating Procedure.....	85
7.5	List of Figures	154
7.6	List of Tables.....	162
7.7	References.....	165
	References	165

List of Abbreviations

Abbreviation	
3D	three dimensional
A.	Arteria
Aa.	Arteriae
BC	brachycephalic dogs
CKCS	Cavalier King Charles Spaniel
cm	centimetres
CNS	central nervous system
CT	computed tomography
Fig.	Figure
For.	Foramen
MC	mesaticephalic dogs
MLO	Multilobular osteochondrosarcoma
mm	millimetres
MRI	magnetic resonance imaging
N.	Nervus
NAV	Nomina Anatomica Veterinaria
Nn.	Nervi
OSA	Osteosarcoma
R.	Ramus
Rr.	Rami
SD	Standard deviation
sqcm	Square centimetres
sqmm	Square Millimetres
SRA	surgical resection alone
ST	Survival time
Tab.	Table
V.	Vena
VUW	University of Veterinary Medicine Vienna
Vv.	Venae

1 Introduction

1.1 The Rostrotentorial Approach in Veterinary Medicine

With advanced diagnostic imaging getting more precise and readily available, our possibilities of diagnosing intracranial masses in their early stages rise dramatically. This is especially important as “Intracranial neoplasia is frequently encountered in dogs.” (Song et al. 2013) and “Intracranial neoplasia represent a major cause of morbidity and mortality.” (Dickinson 2014) It is suggested that certain brachycephalic breeds, namely Boxers, Boston Terriers and Bulldogs are especially prone to astrocytomas and oligodendrogliomas. (Dickinson 2014)

In dogs, five standard approaches, namely the lateral rostrtentorial, the bilateral rostrtentorial, the suboccipital caudotentorial, the ventral and the transfrontal approach were developed (Oliver et al. 1987, Oliver JE Jr 1966, 1968). The possibility of combining these approaches is used to expose most areas of the brain. (Pluhar et al. 1996)

The rostrtentorial approach is a surgical opening of the calvarium mainly in the area of the os parietale but also the os frontale and os temporale can be involved. The purpose of this surgery is the exposition and removal of pathologies in this region, originating from the soft tissue, nervous tissue, or bone. It provides ready access for fragment removal, fracture repair, intracranial decompression, intracranial abscessation, or masses. (Kramer et al. 2007) The research and advancement in this area is becoming more important as intracranial surgery in dogs is becoming more commonplace, especially for resection of brain tumours or to obtain biopsies for a definitive histopathologic diagnosis. (Dickinson 2014, Pluhar et al. 1996) A definitive diagnosis of intracranial pathologies is only possible by histopathologic examination oftentimes followed by additional tests of the affected tissue. Acquisition of pathologic tissue requires either specialized biopsy instruments or an already highly invasive surgery. Most neuro-oncological studies in veterinary medicine are limited by a lack of histopathologic evaluation and a small number of cases. (Dickinson 2014) In human medicine molecular genetic analysis of tumors has become commonplace for grading besides histopathologic examinations. (Dickinson 2014, Park et al. 2017) Removal of intracranial masses is very challenging, but should be manageable with a standard operating procedure which also includes a histological diagnosis, staging and 3D imaging prior to surgery. (Boston 2010) Previous studies indicate a comparatively positive outcome after removal surgery of rostrtentorial masses with mean survival times longer than for infratentorial neoplasms. (Dickinson 2014, Suñol et al. 2017) However, it is important to mention that the outcome of surgery is highly dependent on the equipment, the expertise and knowledge of the surgeon. (Dickinson 2014, Steyrer 2018)

For a craniotomy, the osseous part of the calvarium will be preserved and later re-established, contrary to the craniectomy where part of the calvarium is removed and cranioplasty will be performed afterwards. Craniectomy usually is performed for tumors which affect the bones of the calvarium, like primary bone tumors or soft tissue neoplasia that invades the osseous structures. (Boston 2010) Cranioplasty can be performed to recover and replace bones that had to be altered or removed due to any pathologies, but is not thought to be necessary in dogs if the temporalis muscle can be used to cover the defect. (Boston 2010)

Craniotomy approaches in animals are often derived from its human counterparts, albeit with modifications as a result of the anatomic differences such as the larger cranial muscles. (Pluhar et al. 1996)

The rostromentorial approach has been used in dogs as well as in cats, calves and horses. (Braun et al. 1977, Gouille et al. 2011, Janicek et al. 2006, Kramer et al. 2007, Wouters et al. 2011)

Dewey et al. (2007) evaluated cases with a combined rostromentorial and suboccipital craniotomy with the rostral border being 1-2cm caudal of the sutura coronalis. The only intraoperative complication was a haemorrhage from the sinus transversus in one of the dogs. They suggest this was due to them choosing to create a larger window for better decompression. A smaller window would decrease the risk of sinus transversus haemorrhage, but if a haemorrhage occurs, the possibility of intervention might not be sufficient enough.

There is a number of different variations surgeons have used and published. Bilderback and Faissler (2009) performed a modified rostromentorial craniectomy on a defect centred on the os parietale. 32 months after surgery the dog was still doing well with occasional seizure activity which was treated with Levetiracetam.

Suñol et al. (2017) did a retrospective study of 29 cases with intracranial masses in a rostromentorial location. Three different approaches were performed including transfrontal in 20 dogs, frontoparietal in five dogs and parietotemporal in four dogs. The median survival time for dogs with meningiomas was 422 days, for dogs with gliomas 66 days. Although they state that the secondary changes evaluated on MRI like the presence of a midline shift and ventricular compression have a significant impact on the survival time, their study showed a longer survival time than previously reported.

Past studies only vaguely described the surgical part of the craniotomies or craniectomies they performed and did not exactly specify how the procedure took place. Only recently a study on the rostromentorial approach was carried out (Steyrer 2018), which described every step and evaluated its procedure on safety and reproducibility in mesaticephalic dogs. The drill holes for mesaticephalic dogs were determined on a virtual skull for gaining the biggest possible rostromentorial approach without damaging vital structures. The percentage of the exposed brain surface and of the different gyri was calculated. The gyrus ectosylvius medius was the most exposed gyrus in the rostromentorial approach (99.92%). The venous or pneumatized sinus systems were not damaged. (Steyrer 2018)

Aim of this diploma thesis is to create a reproducible rostromentorial approach in brachycephalic dogs. By determining bony landmarks on virtual skulls, the rostromentorial approach will be evaluated for consistency and safety.

The drill points determined for brachycephalic dogs are compared with the drill entry points in mesaticephalic dogs evaluated in a diploma thesis. (Steyrer 2018) The hypothesis is that the specific drill holes for brachycephalic dogs are not applicable for mesaticephalic dogs or vice versa.

1.2 Anatomy

1.2.1 The Skull

The skeleton of the skull is divided into the bones of the cranium, which surrounds the brain, and the bones of the face. In this chapter, we only focus on the anatomy of the cranium because of its relevance for the rostromentorial approach.

The cavum cranii consists of following bones: os frontale, os parietale, os interparietale, os occipitale, os temporale, os praesphenoidale, os ethmoidale, os basisphenoidale. (Figure 1 and Figure 2)

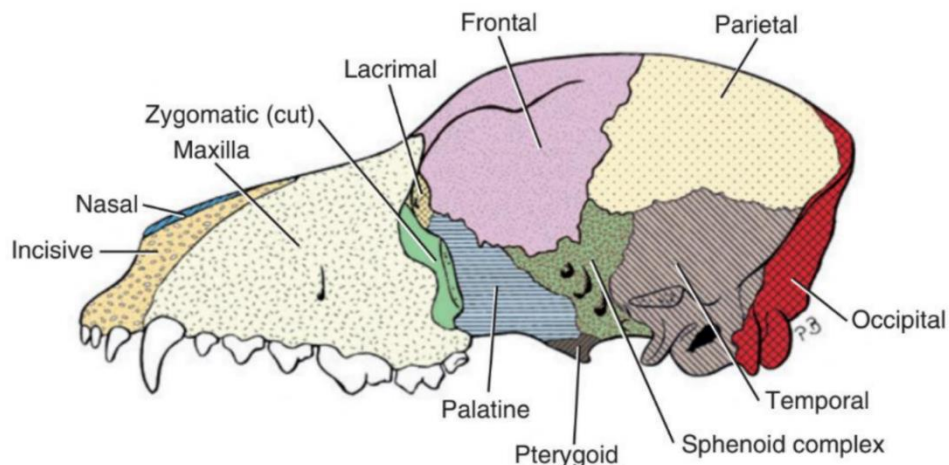


Figure 1: Bones of the skull, lateral aspect. (Hermanson et al.

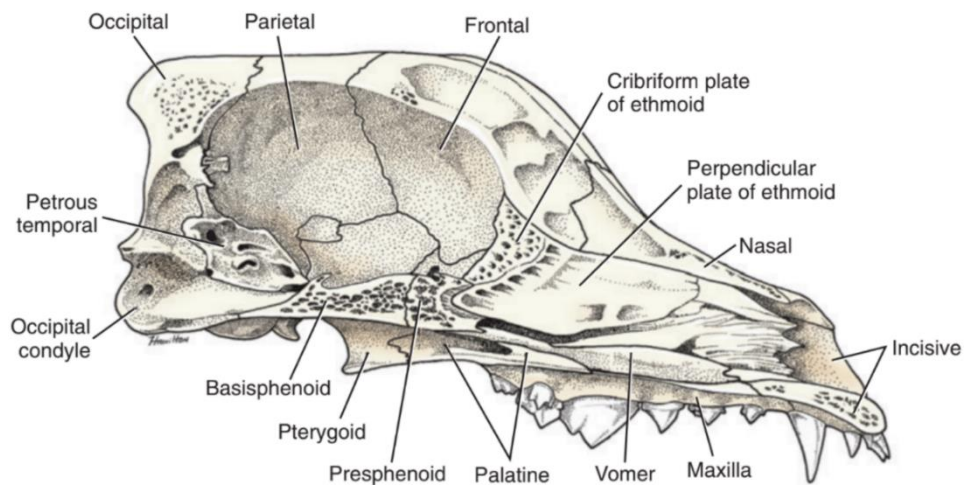


Figure 2: Bones of the skull, medial aspect of sagittal section. (Hermanson et al. 2020)

The cavum cranii has one big opening rostrally which is called the lamina cribrosa and another one caudally, which is called the foramen magnum. The lamina cribrosa connects the cavum cranii with the cavum nasii and contains the fibres of the nervus olfactorius. (Figure 2) The foramen magnum on the other hand is the opening where the systema nervosum centrale leaves the skull as medulla oblongata and then continues as medulla spinalis into the canalis vertebralis.

1.2.1.1 The Sinus Paranasales

The sinus paranasales are air cavities inside the skull bones and are covered in mucosa. These cavities all are connected to the cavum nasi, and therefore connected to the outer environment. In dogs, we differentiate the recessus maxillaris and the sinus frontalis. The most important sinus for this study is the sinus frontalis and it lies within the os frontale. It is separated into three compartments, namely the rostral, medial, and lateral sinus frontalis with the latter being the biggest. It is important to mention that the sinus frontalis is the cavity with the biggest variations in the skull and brachycephalic dogs often are reported to have a small or absent sinus frontalis. (Figure 3) (Evans and Miller 1979, Hermanson et al. 2020)

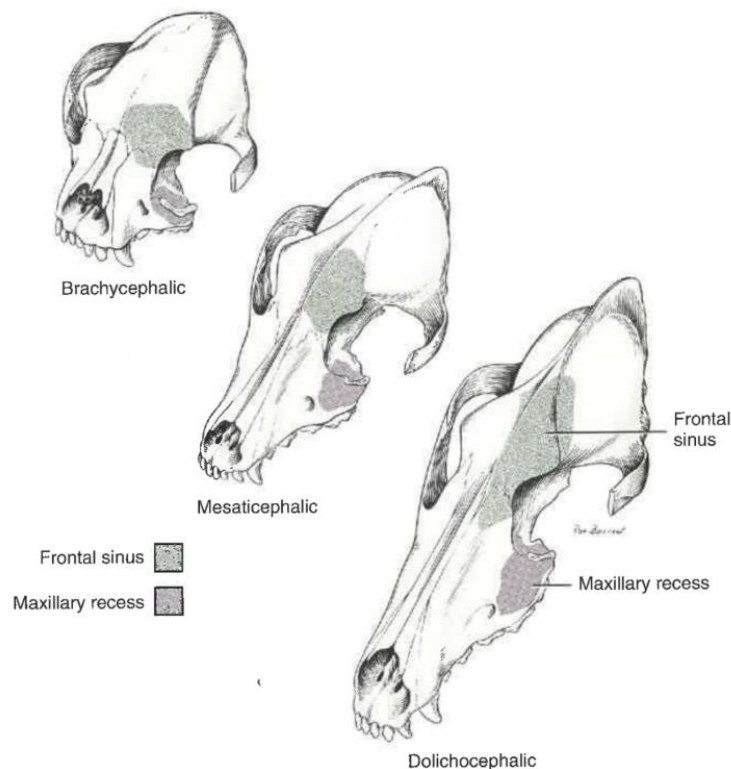


Figure 3: Paranasal sinuses in three types of skulls (Hermanson et al. 2020)

The sinus frontalis is important for the rostromentorial approach, as an unintentional trephination can cause major complications such as pneumocephalus – also known as pneumatocele or intracranial aerocele –, which is caused by air breaking into the cavum epidurale, cavum subdurale or cavum subarachnoidale. (M Das and Bajaj 2020) This condition can develop when the cranium is connected to the external environment and the pressure gradient favours an inflow of air. (Cavanaugh et al. 2008)

1.2.2 Morphometric Analysis of the Canine Skull

“Skulls differ more in size and shape among domestic dogs than in any other mammalian species.” (Hermanson et al. 2020) The different breeds vary so much in size and proportion, for example, toy breeds compared to Great Danes, that it could appear they are different genera, but domesticated dogs clearly are members of the same species. (Wayne 1986)

Bony landmarks to take measurements and to classify different skulls have been described before. (Onar 1999, Stockard et al. 1941) (Figure 4, Figure 5, Figure 6)

Inion: Central surface point on the protuberantia occipitalis externa.

Bregma: Junction on the median plane of the right and left sutura coronalis, or the point of the crossing of the sutura coronalis and sutura sagittalis.

Nasion: Junction on the median plane of the right and left sutura frontonasalis.

Prosthion: Rostral end of the sutura interincisiva, located between the roots of the dorsal central dentes incisivi.

Basion: Middle of the ventral margin of the foramen magnum.

Centre of the meatus acusticus externus: Although unnamed, this spot also serves as a reference point.

These terms (Inion, Bregma, Nasion, Prosthion and Basion) are not referenced in the Nomina Anatomica Veterinaria, but they have obtained popularity among clinicians. (Hermanson et al. 2020)

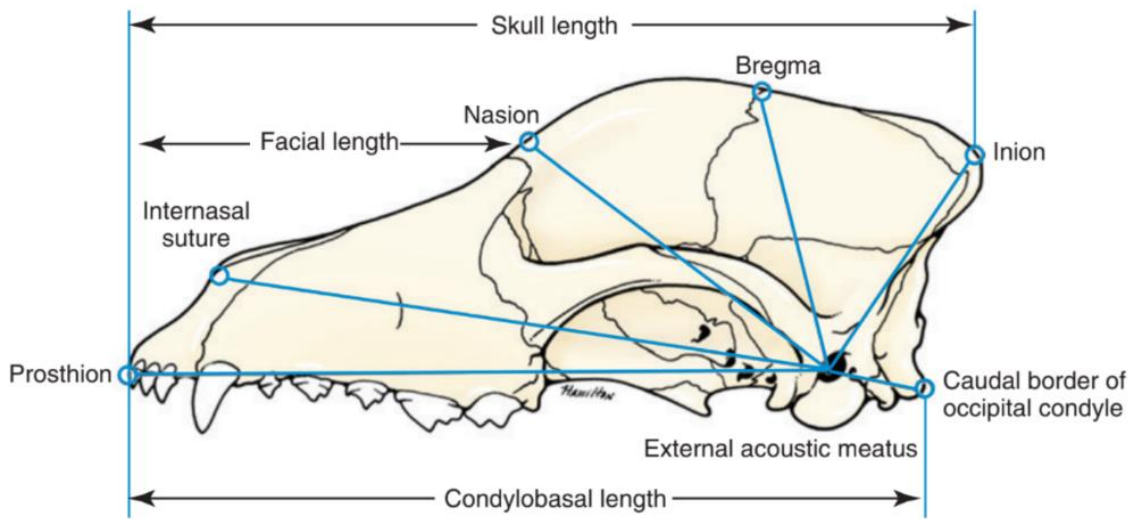


Figure 4: Skull, lateral view showing craniometric points. (Hermanson et al. 2020)

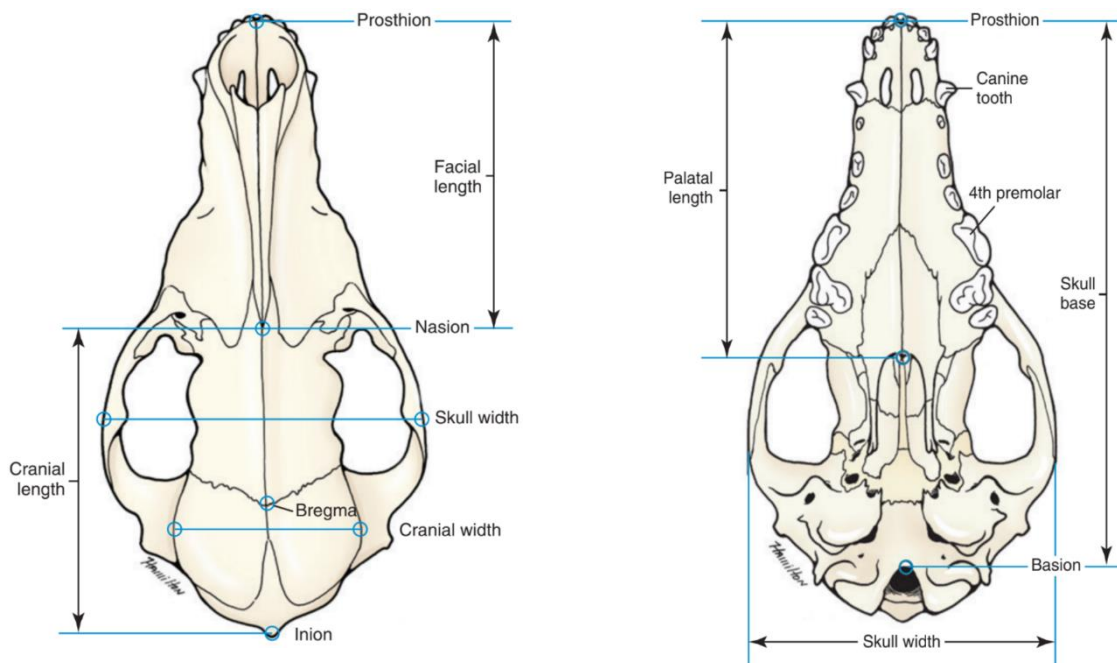


Figure 5: Skull, dorsal view showing craniometric points. (Hermanson et al. 2020)

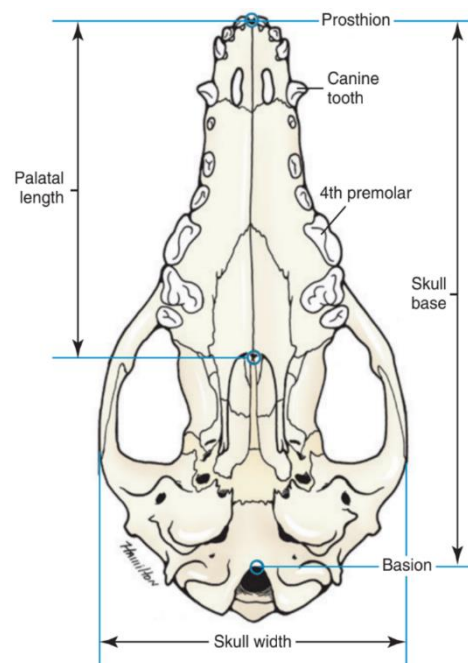


Figure 6: Skull, ventral view showing craniometric points (Hermanson et al. 2020)

Table 1 shows average measurements of the three different skull types, namely brachycephalic, mesaticephalic and dolichocephalic. The measurements were taken from randomly selected dogs. The skull measurements vary vastly between these three types, especially in the facial measures. (Hermanson et al. 2020)

Table 1: Average measurements of three skull types. (Hermanson et al. 2020)

Measurement		Brachycephalic	Mesaticephalic	Dolichocephalic
Facial length	Nasion to prosthion	48 mm	89 mm	114 mm
Facial width	Widest interzygomatic distance	103 mm	99 mm	92 mm
Cranial length	Inion to nasion	99 mm	100 mm	124 mm
Cranial width	Widest interparietal distance	56 mm	56 mm	59 mm
Cranial height	Middle of external acoustic meatus to bregma	54 mm	60 mm	61 mm
Mandibular length	Caudal border of condyle to pogonion	85 mm	134 mm	163 mm
Skull length	Inion to prosthion	127 mm	189 mm	238 mm
Skull width	Widest interzygomatic distance	103 mm	99 mm	92 mm
Indices				
Skull base length	Basion to prosthion	107 mm	170 mm	216 mm
Skull index		81	52	39
Cranial index		57	56	48
Facial index		215	111	81

For differentiation of the skull types, the Cephalic index and Cranial index are used. The Cephalic index puts the facial width and skull length in relation whereas the Cranial index does the same with the cranial width and the cranial length. We distinguish between brachycephalic, mesaticephalic and dolichocephalic skulls.

The bones of the skull which build the facial area is called the viscerocranium and show the greatest variation in between the breeds. Dolichocephalic breeds show a smaller width of the rostrum as well as the arcus zygomaticus, whereas brachycephalic breeds show a greater width than mesaticephalic dogs. Dolichocephalic dogs also have an elongated rostrum and brachycephalics a shorter one. (Schoenebeck and Ostrander 2013)

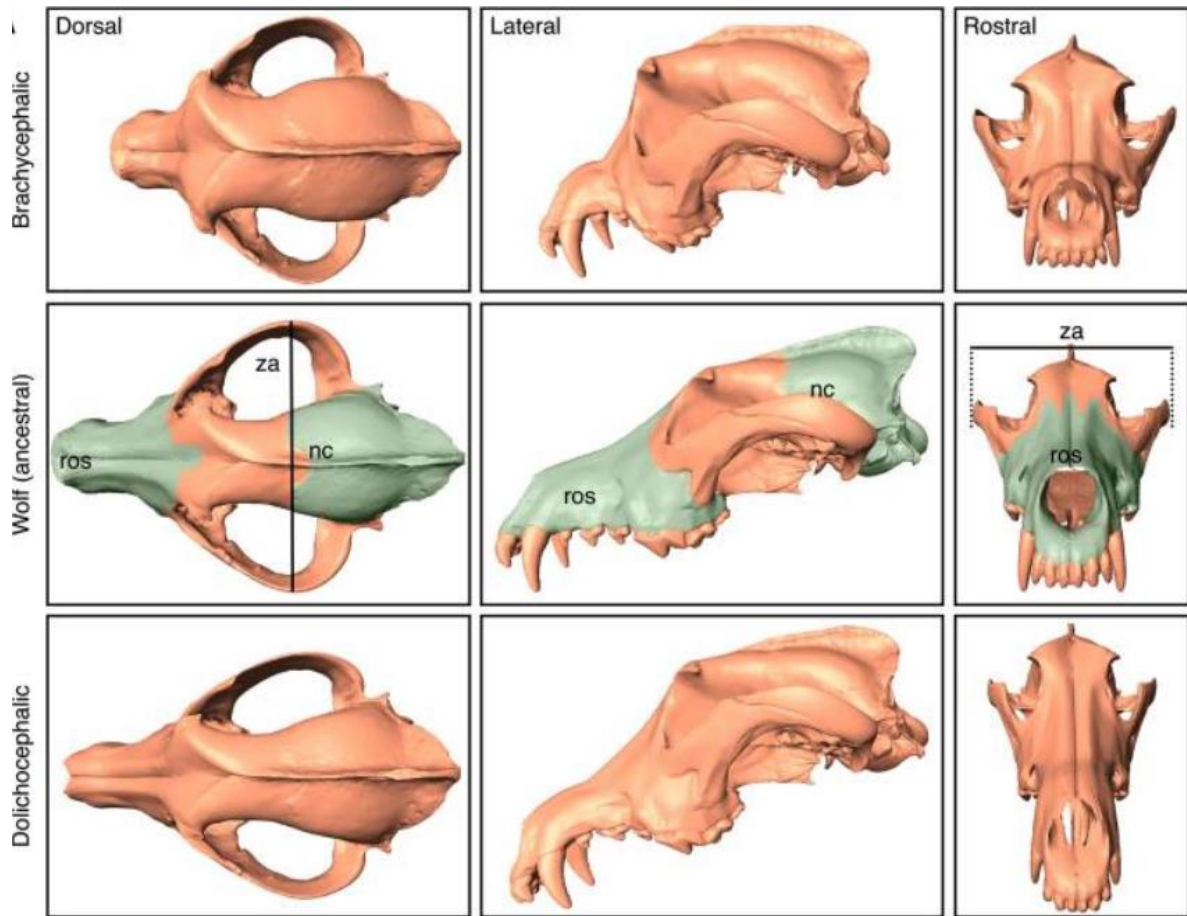


Figure 7: Differences between skull types (modified from Schoenebeck and Ostrander (2013))

ros=rostrum, za=zygomatic arch, nc=neurocranium

A short nose, which may appear as if it were pushed-in, relatively big orbits and brachygnathia inferior are typical for brachycephalic breeds, such as bulldogs and pugs. The term “brachycephalic” originates from human medicine and means “short head”. (Schoenebeck and Ostrander 2013) Cavum cranii of brachycephalic breeds often resembles those of human hydrocephalus. The most extreme resemblance is found in Chihuahuas, whose American Kennel Club breed standard describes the desirable skull as having an “apple dome” and also normalizes open fontanelles which are based on a non-closure of the cranial sutures. (Schoenebeck and Ostrander 2013) Brachycephalia in dogs can be accompanied by a variety of craniofacial anomalies such as a reduction in the length of bones that form the rostrum, chondrodysplasia of the basis cranii interna, and changes in the position of the palatum durum relative to the basis cranii interna. (Schoenebeck and Ostrander 2013) Skeletal growth in brachycephalic dogs is known to be decreased due to hormonal deficits or epiphyseal dysfunction of long bones and the spine, however brain growth does not seem to be affected as much. (Schmidt et al. 2014) A defective growth reaction of the basicranial physal cartilages results in the typical brachycephalic skull shape and is driven by a deficiency in the cartilaginous matrix which grows to become the os basioccipitale and the os basisphenoidale. (Stockard et al. 1941) A disproportion of the basis cranii interna compared to the overall body size (Lüps 1973, Stockard et al. 1941) suggests, that the regulation of growth at the synchondroses plays a role in the origin of brachycephalic and dolichocephalic skull shapes.

(Schoenebeck and Ostrander 2013) Studies suggest a strong correlation between brain and skull volumes and bodyweight as brachycephalic dogs have a significantly larger total brain volume relative to bodyweight compared to mesaticephalic breeds. Factoring in the usually overall smaller body size compared to the other two types, brachycephalic dogs also have less space in their skull that is not occupied by the brain. (Schmidt et al. 2014) The brain growth in brachycephalic breeds follows a lateral expansion which also becomes visible by the relatively large facial width. This is due to the fact that the neurocranial growth in brachycephalic dogs is limited in its anterior-posterior dimension. (Schmidt et al. 2009)

1.2.3 The Encephalon

The *systema nervosum centrale* consists of the encephalon and the *medulla spinalis* and both are made of the *substantia grisea* and the *substantia alba*. The *substantia grisea* mostly includes perikaryons from the neurons and forms the cortex and the nuclei in the encephalon. The *substantia alba* contains mostly myelinated axons and together with the *substantia grisea* forms the *formatio reticularis* and the *truncus encephali*. Furthermore, the encephalon can be divided into three parts: the cerebrum, the cerebellum and the *truncus encephali*. (Hermanson et al. 2020)

1.2.3.1 The Cerebrum

The cerebrum, being the biggest of the three parts, is built by the two *hemispheria cerebri* and the *fissura longitudinalis* which separates these. The two *hemispheria cerebri* are only connected via the *corpus callosum*, the *fornix*, the *hippocampus* and the *commissura rostralis*.

The

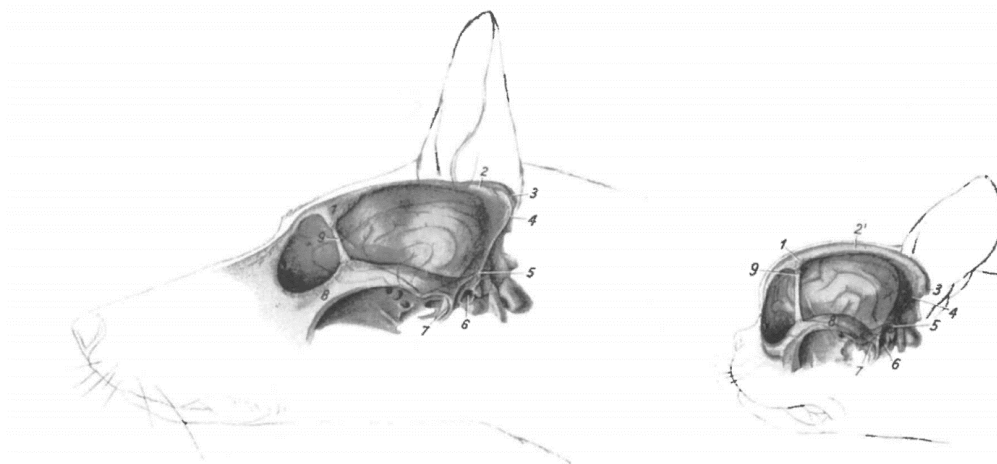
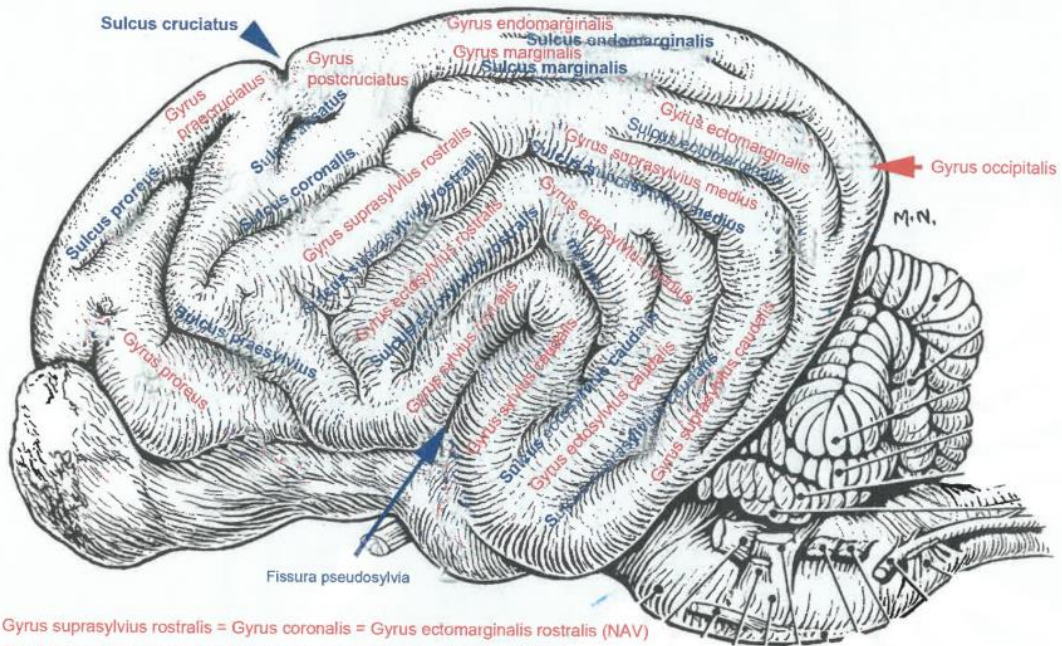


Figure 8: Compared portrayal of the brain location in a German Shepherd (dolichocephalic breed) and a French Bulldog (brachycephalic breed). (Nickel et al. 2004)

1 *processus zygomaticus ossis frontalis*; 2 *crista sagittalis externa*; 2' *planum parietale*; 3 *protuberantia occipitalis externa*; 4 *crista nuchae*; 5 *crista supramastoidea* (6) *meatus acusticus externus*; 7 *fossa mandibularis of the articulatio temporomandibularis*; 8 *arcus zygomaticus*; 9

cortex cerebri is made of three layers, namely the archicortex (means old cortex), paleocortex (means very old cortex) and the biggest of the three, the neocortex (new cortex). (Hermanson et al. 2020) The following Figure 9 and Figure 10 were provided by Ao.Univ.-Prof. Dr.med.vet. Sabine Breit of the VUW and show the correct nomenclature for the gyri and sulci which build the surface of the *hemispheria cerebri*.



Gyrus suprasylvius rostralis = Gyrus coronalis = Gyrus ectomarginalis rostralis (NAV)
 Gyrus suprasylvius medius = Gyrus ectomarginalis, Pars lateralis (NAV)
 Gyrus suprasylvius caudalis = Gyrus ectomarginalis caudalis (NAV)

Sulcus ectosylvius = 1. Bogenfurche
 Sulcus suprasylvius = 2. Bogenfurche
 Sulcus marginalis = 3. Bogenfurche

Figure 9: Nomenclature of the gyri and sulci (lateral view) (Breit Sabine)

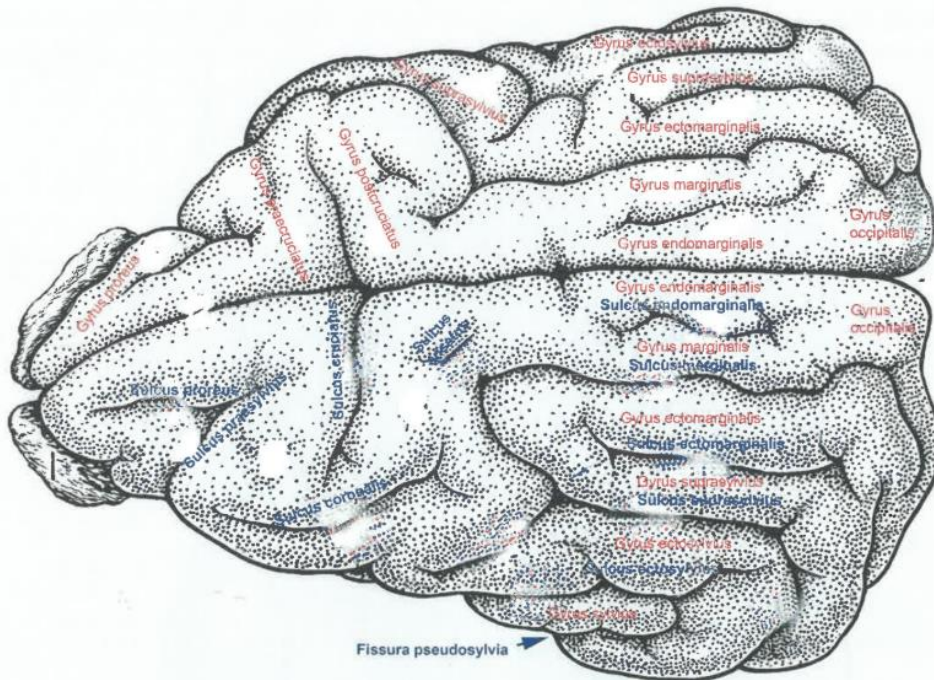


Figure 10: Nomenclature of the gyri and sulci (dorsal view) (Breit Sabine)

The anatomic literature does not completely agree with the exact nomenclature of the gyri and sulci, so the one taught at the VUW is used in this study. In the following Table 2 and Table 3 the different naming schemes of certain structures are represented.

Table 2: Gyri with different naming

Gyri with different naming		
gyrus suprasylvius rostralis	gyrus coronalis	gyrus ectomarginalis rostralis (NAV)
gyrus suprasylvius medius	gyrus ectomarginalis, pars lateralis (NAV)	
gyrus suprasylvius caudalis	gyrus ectomarginalis caudalis (NAV)	

The following Table 3 shows the terms for the gyri and sulci used in this thesis.

Table 3: List of Gyri and Sulci

Gyrus	Sulcus
gyrus sylvius rostralis	fissura pseudosylvia
gyrus sylvius caudalis	sulcus ectosylvius caudalis
gyrus ectosylvius rostralis	sulcus ectosylvius rostralis
gyrus ectosylvius medius	sulcus ectosylvius medius
gyrus ectosylvius caudalis	sulcus suprasylvius caudalis
gyrus suprasylvius rostralis	sulcus suprasylvius medius
gyrus suprasylvius medius	sulcus ectomarginalis
gyrus suprasylvius caudalis	sulcus coronalis
gyrus ectomarginalis	sulcus ansatus
gyrus occipitalis	sulcus praesylvius
gyrus marginalis	sulcus proreus
gyrus endomarginalis	sulcus ansatus
gyrus postcruciatus	sulcus cruciatus
gyrus praecruciatus	sulcus marginalis
gyrus proreus	sulcus endomarginalis

1.2.3.2 The Truncus Encephali

The truncus encephali lies in between the rostral cerebrum and the caudal medulla spinalis. Apart from the nervus olfactorius, all nervi craniales originate from the truncus encephali. The diencephalon builds the rostral segment which links to the cerebrum. The mesencephalon builds the middle section and also contains the aqueductus mesencephali. The caudal part of the truncus encephali is named the medulla oblongata which connects to the medulla spinalis directly. The rostral and ventral part of the medulla oblongata is called the pons. (Hermanson et al. 2020)

1.2.3.2.1 The Mesencephalon

The mesencephalon consists of three segments which are called the tegmentum, substantia nigra and the crus cerebri. The nervus oculomotorius and the nervus trochlearis derive from this part of the encephalon. The aqueductus mesencephali, which lies in the middle of the mesencephalon, forms the connection of the ventriculus quartus and the ventriculus tertius of the diencephalon. (Hermanson et al. 2020)

1.2.3.2.2 The Diencephalon

This rostral section of the truncus encephali is built by the thalamus, metathalamus, hypothalamus, epithalamus and the subthalamus. It holds the ventriculus tertius and has bilateral connections to the hemispheria cerebri. (Hermanson et al. 2020)

1.2.3.3 The Cerebellum

The cerebellum is the major coordinator of the body movements as well as the ability to assess distances which is an important function for precise moves. Just like the cerebrum it has two hemispheria cerebelli and a vermis which lies in the median. The surface has many ridges and grooves, which are not specified any further. The fissura uvulonodularis splits the cerebellum into the corpus cerebelli and the lobus flocculonodularis. (Hermanson et al. 2020)

1.2.4 The Cerebral Lobes

The hemispheria cerebri can be divided into five cerebral lobes each. The most rostral is called the cortex frontalis, caudal and dorsal to that lies the lobus parietalis. The cortex occipitalis is the most caudal part, and the lateral lobe is called the cortex temporalis. (Figure 11) The phylogenetically oldest and most ventral lobe is called the lobus piriformis. (Hermanson et al. 2020) Because of the high anatomic variability, the differentiation of the lobes is rather vague but some structures to separate them are agreed on. (Uemura 2015)

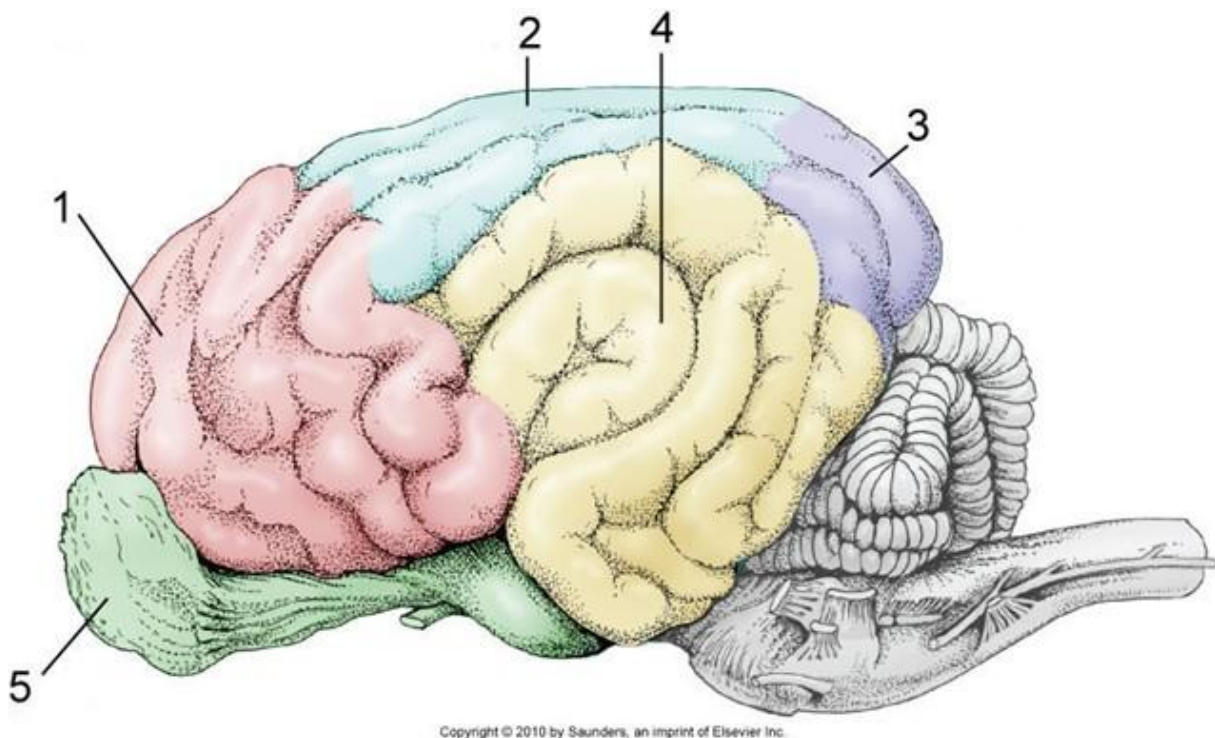


Figure 11: Cerebral lobes (Copyright 2010 by Saunders, an imprint of Elsevier Inc.)
<https://slideplayer.com/slide/8421143/> (accessed May 18, 2020)

(1) cortex frontalis, (2) cortex parietalis, (3) cortex occipitalis, (4) cortex temporalis, (5) lobus piriformis including bulbus olfactorius

1.2.5 The Meninges

The systema nervosum centrale is covered in different layers of meninges with spaces in between. For this study, we only describe the meninges of the brain. The meninges are called the dura mater encephali, the arachnoidea encephali and the pia mater encephali.

1.2.5.1 The Dura mater encephali

The dura mater encephali is composed mainly of collagen bundles, fibroblasts, elastic fibres, vessels, and sensory nerves. "It lines the cranial cavity, simultaneously covering the brain and serving as periosteum for the cranial cavity." (Hermanson et al. 2020) The dura mater originates embryologically as a double layer and where these layers separate, a venous sinus is generally present. The falx cerebri is its biggest partition and separates both cerebral hemispheres from each other. Caudally the dura mater encephali builds the tentorium cerebelli membranaceum which extends over the tentorium cerebelli osseum and separates the cerebral hemispheres from the cerebellum. The third partition is the diaphragma sellae and separates the hypophysis from the truncus encephali.

1.2.5.2 The Arachnoidea Encephali

The arachnoidea encephali is composed by flattened fibroblasts and collagen fibres. It adheres to the inner surface of the dura mater encephali and only separates from it in case of a pathologic condition. Furthermore, it is connected to the pia mater via trabeculae but also separated from it by the cavum subarachnoidale.

1.2.5.3 The Cavum Subarachnoidale

The cavum subarachnoidale is filled with liquor cerebrospinalis and big vessels. It has four bigger enlargements called cisternae subarachnoidales which are called the cisterna cerebellomedullaris, cisterna valliculae lateralis cerebri, cisterna chiasmatis and cisterna interpeduncularis. The cisterna cerebellomedullaris is commonly known for the ability to obtain liquor cerebrospinalis and is located where the caudal surface of the cerebellum meets the dorsal surface of the medulla oblongata.

1.2.5.4 The Pia Mater Encephali

The pia mater follows every irregularity of the brain surface and is very vascular because all vessels entering and leaving the systema nervosum centrale must travel in pia mater.

1.2.6 The Sinus Durae Matris

As mentioned before, the dura mater encephali has two layers in between which the sinus durae matris is found. These sinuses appear in certain large osseous canals. The sinuses differentiate from the regular venous system in its consistent lumen, the lack of valves, the tunica media and tunica adventitia.

We differentiate the dorsal and the ventral sinuses which freely intercommunicate. (Figure 12) The dorsal sinus consists of the unpaired sinus sagittalis dorsalis, sinus rectus and the paired sinus transversus, sinus petrosus dorsalis, sinus temporalis and sinus sigmoideus.

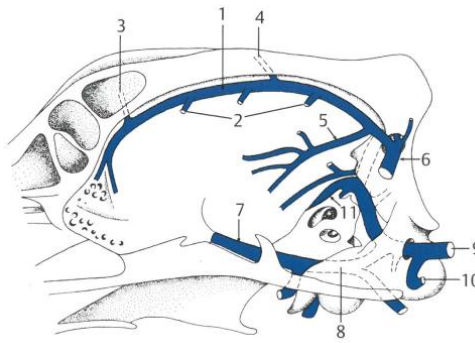


Figure 12: Sinus durae matris, simplified, medial aspect (Salomon et al. 2020)

(1) sinus sagittalis dorsalis, (2) vv. Cerebri dorsales, (3) v. diploica frontalis, (4) v. diploica parietalis, (5) sinus rectus, (6) sinus transversus, (7) sinus cavernosus, (8) sinus petrosus ventralis, (9) sinus basilaris, (10) sinus interbasilaris, (11) sinus temporalis

1.2.6.1 The Dorsal Sinus

The sinus sagittalis dorsalis begins rostrally, takes the right and left veins that come from the nasal cavity and then runs caudally inside a channel of the falx cerebri close to the crista sagittalis interna and the sutura sagittalis. It collects the vv. cerebri dorsales as well as most of the vv. diploicae and joins the sinus rectus at its end. (Hermanson et al. 2020)

The sinus rectus begins at the caudal end of the falx cerebri where the v. cerebri magna and the v. corporis callosi join together and then runs through the caudal part of the falx cerebri. There the right and left parts of the tentorium cerebelli membranaceum join it and the sinus rectus lies rostradorsal to the tentorium cerebelli osseum. (Hermanson et al. 2020)

The part where the sinus sagittalis dorsalis merges with both sinus transversus and usually the sinus rectus, is called confluens sinuum and is located within the dorsal part of the os occipitale.

Starting at the confluens sinuum, the sinus transversus runs laterally in the canalis sinus transversi and then continues in the sulcus sinus transversi for its last third. At the end it divides into the sinus temporalis and the sinus sigmoideus.

The sinus sigmoideus is an S-shaped continuation from the sinus transversus and merges with the sinus petrosus ventralis. It bends ventromedially and caudally before it enters the foramen jugulare, the sinus basilaris divides from it and runs in the canalis condylaris and then continues as plexus venosus vertebralis internus. (Hermanson et al. 2020)

The sinus temporalis is a continuation of the sinus transversus and runs in the rostral direction inside the meatus temporalis. (Hermanson et al. 2020)

The sinus petrosus dorsalis builds a connection between the rostral end of the sinus sagittalis dorsalis and the sinus transversus close to the ventral end of the sulcus sinus transversi. (Hermanson et al. 2020)

1.2.6.2 The Ventral Sinus

The ventral sinus consists of the paired sinus cavernosus, sinus basilaris, sinus condylaris, sinus petrosus ventralis and the unpaired sinus intercavernosus rostralis and caudalis. (Figure 13)

The sinus cavernosus is paired and is the major drainage for the ventral parts of the brain. Each sinus starts rostrally at the fissura orbitalis, where they also intercommunicate through the plexus opthalmicus, then runs on the floor of the fossa cranii media to the canalis petrooccipitalis. There it continues as the sinus petrosus ventralis and is connected to the plexus venosus vertebralis internus. Medially the two sinus cavernosus are connected through the two sinus intercavernosus, one being rostrally and one caudally to the stalk of the dorsum sellae. (Hermanson et al. 2020)

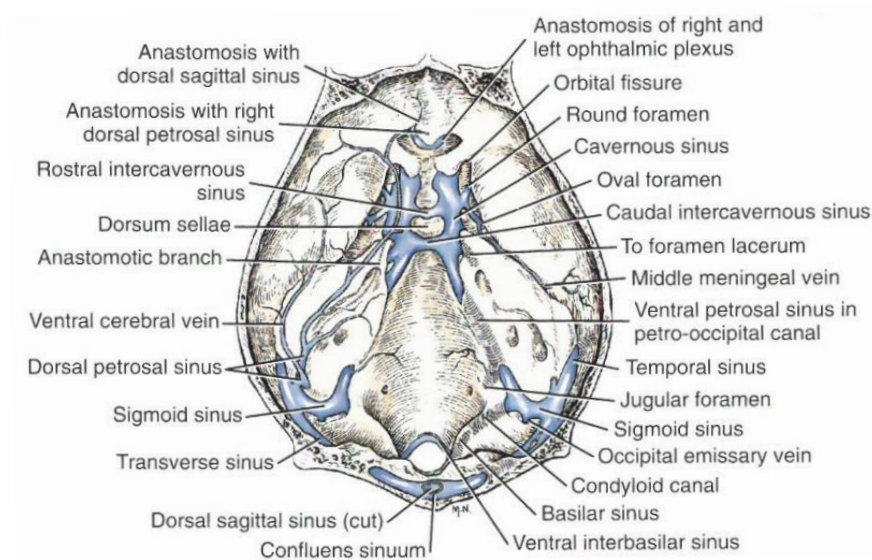


Figure 13: Cranial venous sinuses, dorsal aspect (calvaria removed.) (Reinhard et al. 1962)

The following chapters will guide the reader through the process of visualisation and simulation of the craniotomies as well as the subsequent measurements and calculations which were performed.

2 Material and Methods

2.1 Diagnostic Imaging

The CT and MRI images were provided by the Clinical Unit of Diagnostic Imaging at the VUW and then reviewed for usability in this study. The database search included all brachycephalic dogs which had a CT and an MRI scan of the head in the time between 1.1.2014 and 13.12.2018 as well as every mesaticephalic dog which had a CT and an MRI scan of the head between 1.1.2010 and 11.03.2019.

Inclusion criteria were completeness of the scans and lack of pathologic conditions affecting the systema nervosum centrale as well as the osseous part of the cranium. The remaining scans included four French bulldogs, one Golden Retriever and three mesaticephalic crossbreeds. (Table 4)

Table 4: Information about the dogs

Information about dogs from whom the databases were used				
Dog Number	Breed	Sex	Age	Weight in kg
Dog1	Golden Retriever	female spayed	7a 8m	36
Dog2	Mix	female spayed	14a 6m	23.7
Dog3	Mix	female spayed	6a 6m	n.a
Dog4	Mix	male spayed	16a 2m	5.4
Dog5	French Bulldog	female spayed	13a 7m	9.3
Dog6	French Bulldog	male	7a 1m	11.6
Dog7	French Bulldog	male spayed	11a 9m	17
Dog8	French Bulldog	male	9a 5m	19.6

Dogs 1-4 are in the mesaticephalic group, dog 5-8 in the brachycephalic group. a = years, m= months, n.a. = not available

2.2 Visualization

The chosen scans were loaded onto the University server for further processing of the images. The workstation was situated at the VetCORE facility for Research of VUW and the programme Amira 2019.01 (Thermo Fischer Scientific) was used for the 3D visualization of the provided scans. A standard operating procedure will be attached to this thesis for further traceability and reproducibility. (Appendix pages) Nonetheless, I will explain the basic process here.

First the CT scans, saved as DICOM files, were loaded into Amira, and then saved as Amira files. Each patient had its own project folder to avoid any possibility of confusion. A basic 3D model of the skull was created by using the "Isosurface" tool with a threshold of 350 Hounsfield Units. This 3D model then was aligned on a global axis after setting 34 landmarks in a specific order.

Table 5 contains these points of interest. The points we chose are a modified version of the publication of Drake and Klingenberg, 2010.

Table 5: Landmarks used to align the skulls

Number	Designation
1	Bregma
2	Inion
3	midpoint of Bregma and Inion
4	processus nasalis sinister
5	processus nasalis dexter
6	sutura internasalis, most rostral point
7	Nasion
8	processus frontalis ossis zygomaticus sinister
9	processus zygomaticus ossis frontalis sinister
10	canalis opticus sinister, medioventrally
11	meatus acusticus externus sinister, craniolaterally
12	dens caninus sinister (204), posterior buccal corner
13	dens praemolaris 3 sinister (207), posterior buccal corner
14	dens praemolaris 4 sinister (208), posterior buccal corner
15	processus frontalis ossis zygomaticus dexter
16	processus zygomaticus ossis frontalis dexter
17	canalis opticus dexter, medioventrally
18	meatus acusticus externus dexter, craniolaterally
19	dens caninus dexter (104), posterior buccal corner
20	dens praemolaris 3 dexter (107), posterior buccal corner
21	dens praemolaris 4 sinister (108)
22	processus mastoideus sinister
23	processus mastoideus dexter
24	processus paracondylaris sinister
25	processus paracondylaris dexter
26	tuberculum nuchale sinister
27	tuberculum nuchale dexter
28	condylus occipitalis sinister
29	condylus occipitalis dexter
30	Basion
31	os palatinum, most caudal point
32	hamulus pterigoidei sinister
33	hamulus pterigoidei dexter
34	Prosthion

2.3 Morphometric Analysis

After the alignment of the 3D model on the global axis, the different types of skull shapes are differentiated by using the morphometric analysis including the cranial and cephalic index. Its goal is to quantify the huge variability of the skull in dogs.

The cranial measurements are taken by setting the render mode to “orthographic”, using the “Scalebar” tool and then zooming in and out until the scalebar fits the landmarks. Table 6 contains the cranial measurements which were used in this study and the Figure 14 and Figure 15 show the measurements in the dorsal and the lateral view, illustrated by Onar (1999). The Figure 15 has been been modified to resemble the measurements in dorsal view as they were taken in this study.

Table 6: Measurements for the cranial index

Measurements	Landmarks	Info
Facial length	Nasion to Prosthion	dorsal view
Facial width	widest interzygomatic distance	dorsal view
Cranial length	Inion to Nasion	dorsal view
Cranial width	widest interparietal distance	dorsal view
Cranial height	middle of Meatus acusticus externus to bregma	lateral view
Skull length	Inion to Prosthion	dorsal view
Skull base length	Basion to Prosthion	ventral view

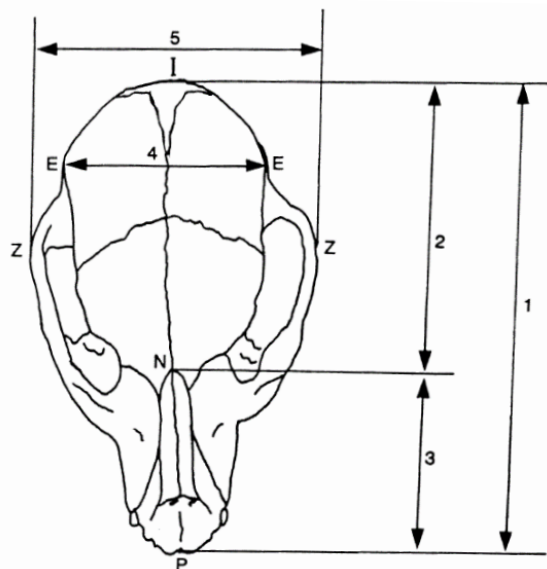


Figure 14: Measurements of the cranium (dorsal view) (Onar 1999)

(I) Inion, (N) Nasion, (P) Prosthion, (E) Euryon, (Z) Zygion, (1) skull length, (2) cranial length, (3) viscerocranial length, (4) maximum width of neurocranium, (5) maximum zygomatic width

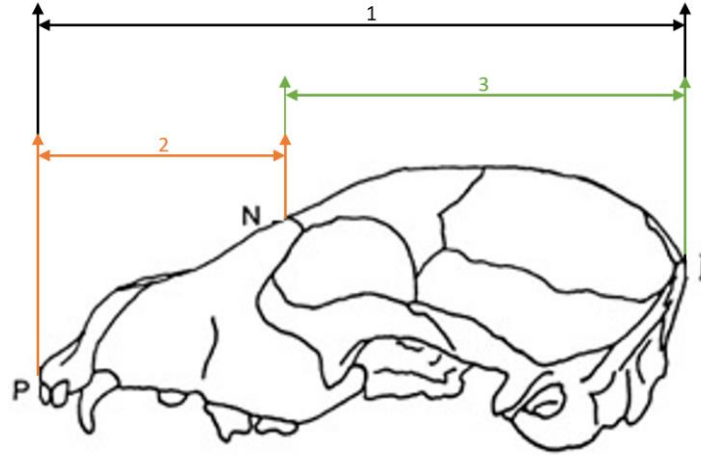


Figure 15: Modified measurements of the cranium (lateral view) (Onar 1999)

(I) Inion, (P) Prosthion, (N) nasion, (1) skull length, (2) viscerocranial length and (3) cranial length

These cranial measurements were then used to calculate the Cranial and the Cephalic index.

$$\text{Cranial index} = \frac{\text{cranial width} * 100}{\text{cranial length}}$$

$$\text{Cephalic index} = \frac{\text{facial width} * 100}{\text{skull length}}$$

To further differentiate between mesaticephalic and brachycephalic, the median of the Cephalic index (CI) of all dogs will be calculated and used as breakpoint. The Dogs were split at the median of the CI and the skulls below the median are classified as “Low CI” representing the mesaticephalic group and dogs with a CI higher than the median are classified as “High CI” and represent the brachycephalic group. (Roberts et al. 2010)

To further evaluate this method, a t-test for sample pairs was performed between both groups to provide information about its significance.

Afterwards the MRI files, saved as DICOM files, are loaded into Amira, roughly aligned to the CT images and then with help of the “Register Images” tool properly aligned. After everything was aligned perfectly, the brain was cropped out of the MRI images and the resolution increased drastically. Then a surface of the resampled brain was created in order to be able to do measurements. This freshly created surface was used to identify the cortex and the gyri.

Table 7 contains every surface which was measured for this thesis and Figure 16 is used to illustrate them.

Table 7: Gyri used in this study

Number	Surface name
1	cortex
2	gyrus sylvius rostralis
3	gyrus sylvius caudalis
4	gyrus ectosylvius rostralis
5	gyrus ectosylvius medius
6	gyrus ectosylvius caudalis
7	gyrus suprasylvius rostralis
8	gyrus suprasylvius medius
9	gyrus ectomarginalis
10	gyrus suprasylvius caudalis
11	gyrus occipitalis
12	gyrus marginalis
13	gyrus endomarginalis
14	gyrus postcruciatu
15	gyrus praecruciatu
16	gyrus proreus

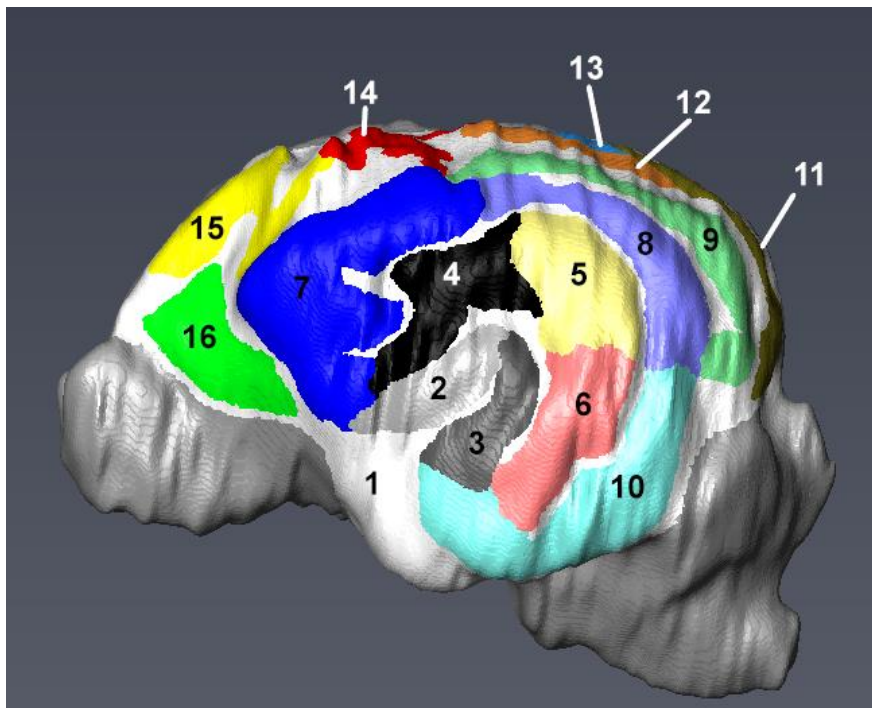


Figure 16: Brain with all Gyri drawn in

(1) cortex (2) gyrus sylvius rostralis (3) gyrus sylvius caudalis (4) gyrus ectosylvius rostralis (5) gyrus ectosylvius medius (6) gyrus ectosylvius caudalis (7) gyrus suprasylvius rostralis (8) gyrus suprasylvius medius (9) gyrus

ectomarginalis (10) gyrus suprasylvius caudalis (11) gyrus occipitalis (12) gyrus marginalis (13) gyrus endomarginalis (14) gyrus postcruciatu (15) gyrus praecruciatu (16) gyrus proreus

2.4 The Rostrotentorial Approach

The rostrtentorial approach in mesaticephalic dogs has been evaluated in a diploma thesis at the VUW. (Steyrer 2018)

For ease of use, the described approach in Steyrer (2018) will be called "Approach Mesaticephalic" and the one developed in this thesis will be called "Approach Brachycephalic". Mesaticephalic dogs will be named Dog 1 to 4 and the brachycephalic dogs will be named Dog 5 to 8 in the following chapters.

First, the approach and landmarks of the „Approach Brachycephalic“ are described. Landmarks for the drilling points were based on palpable osseous structures and imaginary lines between those.

2.4.1 Drill Holes „Approach Brachycephalic“ (Figure 21)

For the first drill hole, draw an imaginary line between the Processus zygomaticus ossis frontalis and the ipsilateral Crista supramastoidea. In order to allow a safety margin to stay clear of the Sinus frontalis, you must measure 10mm in the caudal direction on this line, starting at the Processus zygomaticus ossis frontalis.

For the second drill hole, draw an imaginary line between the Processus zygomaticus ossis frontalis and the caudal end of the Crista supramastoidea. The drill hole will be in the exact middle of this line and is later used as a reference point for drill hole four.

For the third drill hole, start by measuring the length of the Crista supramastoidea. Then, beginning at the base of the Arcus zygomaticus, go straight dorsally for just this length.

Drill hole four lies exactly dorsally of drill hole two. Draw an imaginary line straight up from drill hole two to the midline of the skull. On this line, measure 20mm away from the midline in order to provide a safety margin. The reason why this safety margin is so big, once again is the variable shape of brachycephalic skulls. This drill hole will be used as a reference point for drill hole five.

For the fifth and last drill hole, draw an imaginary line between drill hole four and the most caudal point of the Protuberantia occipitalis. This drill hole will be on the exact middle of this line. Variable skull shapes prohibit the declaration of a simple safety margin from the most caudal point in brachycephalic dogs.

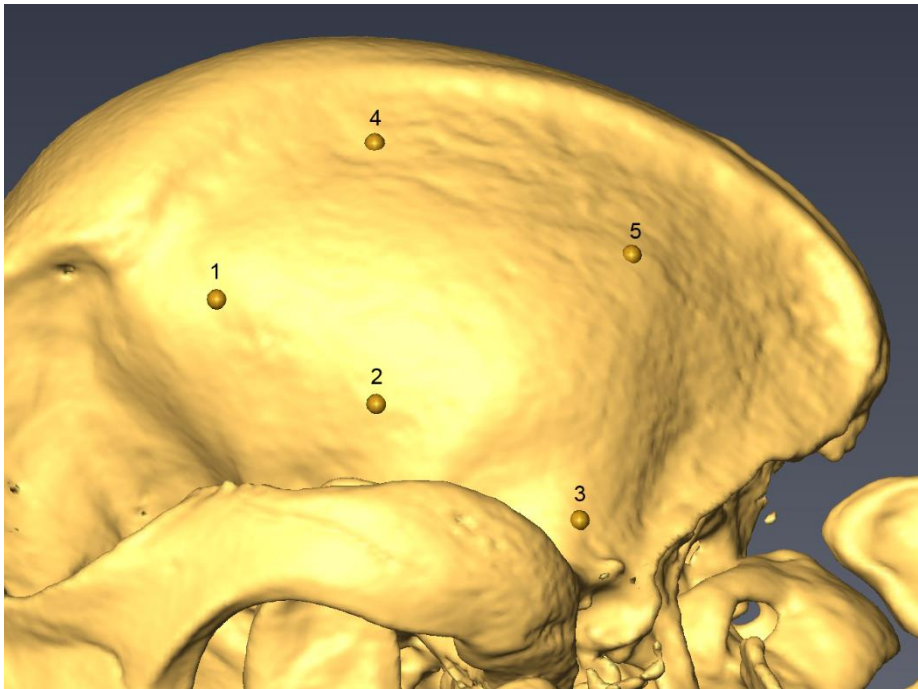


Figure 17: „Approach Brachycephalic“ on a brachycephalic dog – Drill holes 1 to 5
 (1) drill hole 1 (2) drill hole 2 (3) drill hole 3 (4) drill hole 4 (5) drill hole 5

Figure 18 illustrates the guiding lines used for the “Approach Brachycephalic” in mm.

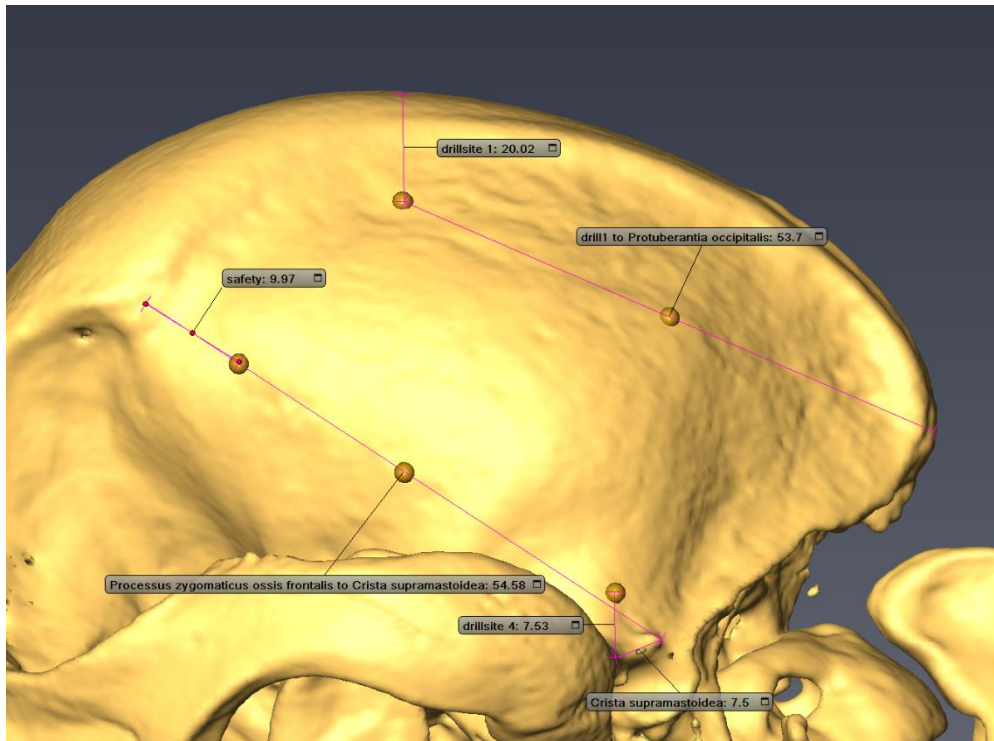


Figure 18: „Approach Brachycephalic“ on a brachycephalic dog – Drill holes 1 to 5 with guiding lines in mm

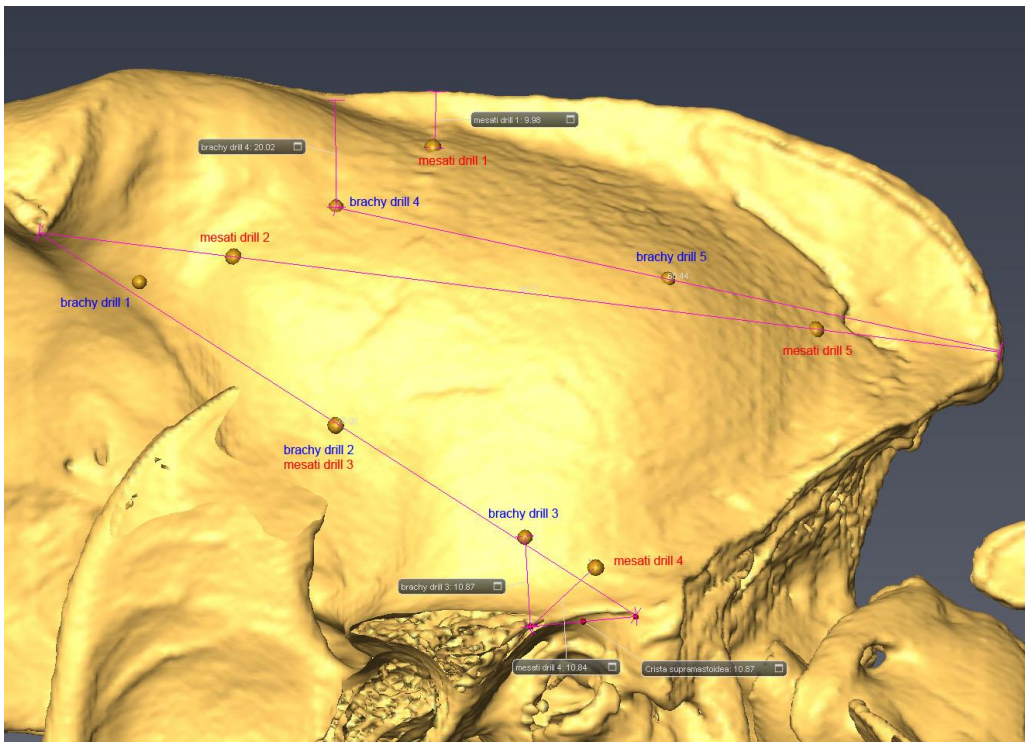


Figure 19: Comparison „Approach Mesaticephalic“ and „Approach Brachycephalic“ on a mesaticephalic dog

Blue: „Approach Brachycephalic“; Red: „Approach Mesaticephalic“ at the end of both approaches

After setting the landmarks for the drill holes, the craniotomy area was drawn onto the skull, measured, and then deleted to show the underlying brain and the accessible gyri. The now accessible area of the brain and its Gyri were measured as well and then used for various calculations.

2.4.2 Crista Sagittalis Externa

To evaluate the safety of the approaches regarding laceration of the dorsal sinus system and the sinus sagittalis dorsalis, measurements from the most dorsal and therefore closest point of the craniotomy to the crista sagittalis externa have been done. These were done in Amira with help of the “measurement” tool. (Figure 20)

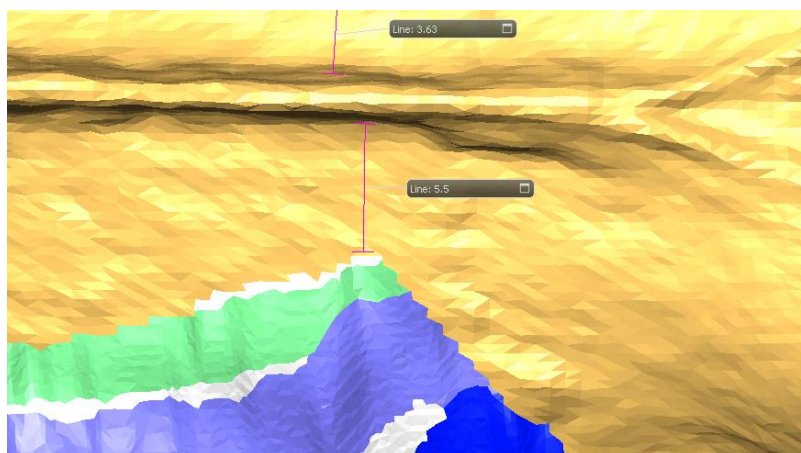


Figure 20: Measuring the distance of the craniotomy area to the crista sagittalis externa (in mm)

2.4.3 Sinus Frontalis

After simulating the craniotomy, the skulls were scanned for the existence of the Sinus frontalis. Furthermore, it was important to find out if the Sinus frontales were opened using the craniotomy approaches. This was done in Amira by creating an Ortho Slice tool of the CT scan and moving it one slice rostral to the craniotomy. (Figure 21)

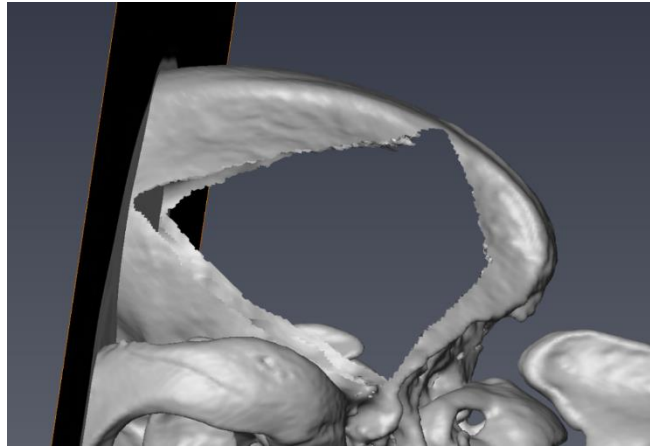


Figure 21: Ortho Slice tool set one slice rostrally to the craniotomy

The frontal sinus was evaluated in the transverse view for any damages caused by the simulated drill holes. (Figure 22) Once the Ortho slice tool was in position, the 3D visualisation was used to check the Sinus frontales for trepanation by the craniotomy.

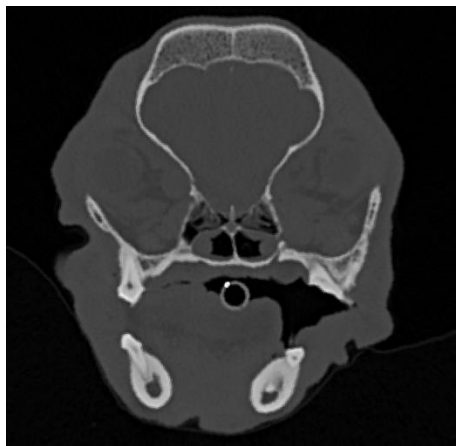


Figure 22: CT scan one slice rostral of the simulated craniotomy – the Sinus frontalis in this dog is cranial to the craniotomy and therefore unopened.

2.4.4 Drill Holes “Approach Mesaticephalic”

“Find the impression, indicated in red, between the sutura parietofrontalis and the temporal line, that indicates the border of the frontal sinuses. One centimetre laterally of the sagittal crest and 0.5 centimetres caudoventrally of this line (toward the centre of the neurocranium) The first hole is drilled as seen in Figure 23.” (Steyrer 2018)

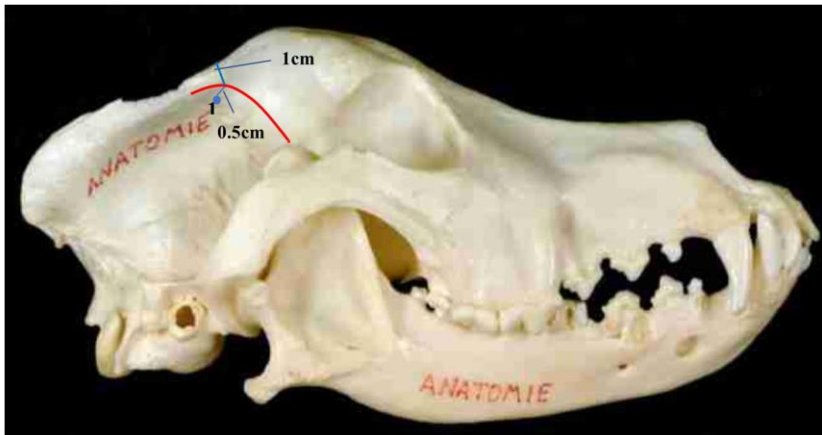


Figure 23: Location of the first hole (Steyrer 2018)

“For the second hole (Figure 24) draw an imaginary line (straight red line) connecting the most lateral aspect of the zygomatic process of the frontal bone to the most caudal point of the occipital protuberance. Drill the second hole directly on this line, 0.5 centimetres caudally to the point where the impression described for hole number one (curved red line) intersects with it.” (Steyrer 2018)

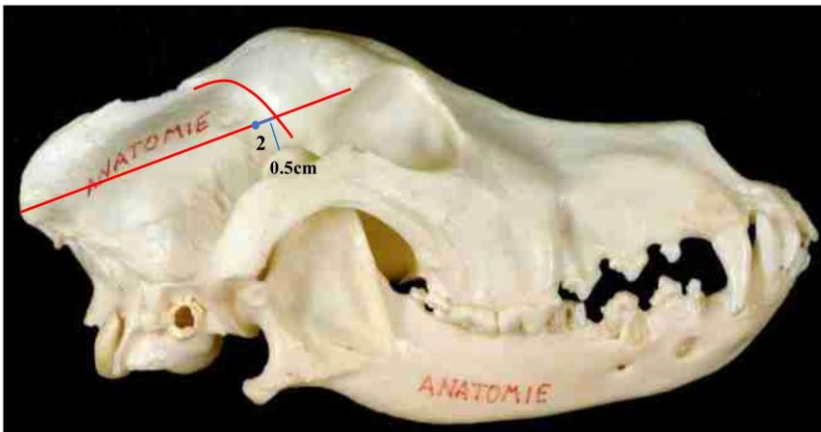


Figure 24: Location of the second hole (Steyrer 2018)

“To locate the drilling site for hole number three (Figure 25) draw an imaginary line (straight red line) connecting the most lateral aspect of the zygomatic process of the frontal bone to the point where the nuchal crest meets the supramastoid crest. Drill the third hole exactly at the midpoint of this line.” (Steyrer 2018)

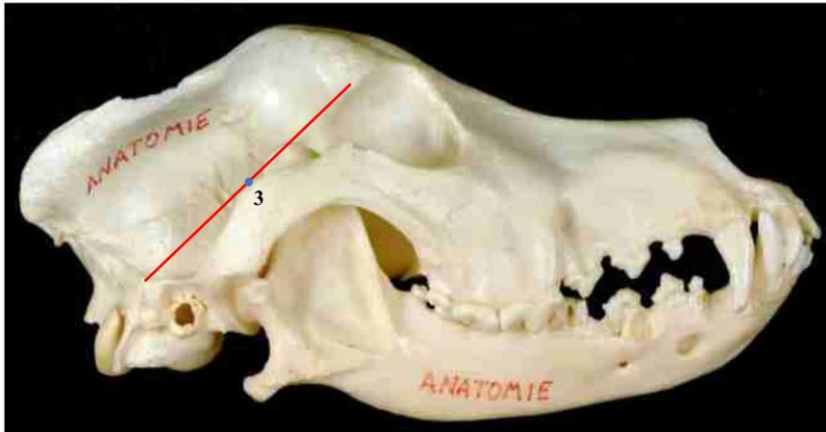


Figure 25: Location of the third hole (Steyrer 2018)

“For hole number four measure the length of the supramastoid crest and project it from the base of the zygomatic process dorsally, parallel to the nuchal crest to locate the fourth drilling site as depicted in Figure 26.” (Steyrer 2018)



Figure 26: Location of the fourth hole (Steyrer 2018)

“For the last hole (Figure 27) draw an imaginary line (straight red line) connecting the most lateral aspect of the zygomatic process of the frontal bone to the most caudal point of the occipital protuberance. Find the impression at the base of the nuchal crest/external sagittal crest (curved red line). Drill the fifth hole directly on the connection line, 0.5 centimetres cranially from where the line intersects with the indentation.” (Steyrer 2018)

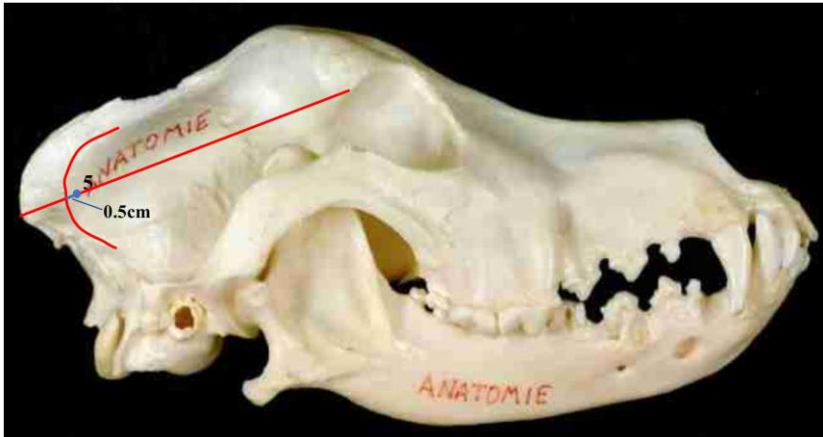


Figure 27: Location of the fifth hole (Steyrer 2018)

2.4.5 Calculations and Statistics

- Morphometric Analysis

The measurements of the different lengths and widths necessary for the morphometric analysis (Table 6) were performed in Amira and then the Cranial and Cephalic index were calculated with the following formulas:

$$\text{Cranial index} = \frac{\text{cranial width} * 100}{\text{cranial length}}$$

$$\text{Cephalic index} = \frac{\text{facial width} * 100}{\text{skull length}}$$

The Median of the Cephalic index then was calculated in Microsoft Excel with the function "MEDIAN()". The results were evaluated by performing a t-test for independent samples with a significance level of 0.95. This means that a $p \leq 0.05$ is a statistically significant result.

- Craniotomy area on the skull in sqmm

The craniotomy area has been extracted from Amira (paragraph 10.15 of the SOP on page 142).

Then the mean value was calculated in Microsoft Excel with the function "MITTELWERT()" and the standard deviation with "STABW.N()". These calculations were performed from the whole population (n=8) and both CI groups, respectively.

$$\text{Mittelwert } \bar{X} = \frac{a_1 + a_2 + \dots + a_n}{n}$$

$$\text{Standardabweichung } s_x = \sqrt{\frac{1}{N-1} * \sum_{i=1}^N (\chi_i - \chi)^2}$$

- Comparison of the craniotomy areas of both approaches
The size comparison for one was portrayed by showing them next to each other for each dog but also by dividing the area of the "Approach Mesaticephalic" through the "Approach Brachycephalic".

$$\text{size comparison} = \frac{\text{craniotomy area "Approach Mesaticephalic"}}{\text{craniotomy area "Approach Brachycephalic"}}$$

To further validate the results, a t-test for independent samples with a significance level of 0.95 has been performed.

- Measurements to the crista sagittalis externa
These measurements were taken in Amira with the "measurement" tool and written down.
- Access to gyri
To calculate in how many % of the dogs each separate gyrus has been accessed, the number of times it was exposed x in each CI group was divided through the number of dogs in each group ($n = 4$) and then multiplied by 100.

$$\text{gyrus accessed in \%} = \frac{x \text{ times exposed gyrus}}{n \text{ dogs in each CI group}} * 100$$

This calculation was performed for the mesaticephalic as well as the brachycephalic group. The significance of the results was validated with a chi-square test based on Pearson and an exact test based on Fisher. The chi-square test requires a minimum sample size of five, which is not provided in these calculations and therefore, another test which does not require a minimum sample size was performed, which in this case was the exact test based on Fisher.

- Accessible gyri area in sqmm
The total and the exposed area of the individual gyri in each approach and dog and also the total area of accessible brain area were extracted from Amira. The mean area of each gyrus was calculated by adding up the area (a_n) in sqmm of all measurements and dividing them by the number n of measured gyri.

$$\text{Mittelwert } \bar{X} = \frac{a_1 + a_2 + \dots + a_n}{n}$$

To calculate the % how much each gyrus has been exposed with each approach, the mean accessible gyrus area for the individual gyrus in each CI group was divided through the mean total gyrus area of each CI group.

$$\text{mean accessible gyrus area in sqmm} = \frac{\text{mean accessible gyrus area in sqmm}}{\text{mean total gyrus area in sqmm}}$$

- Craniotomy area in comparison with the brain area
The craniotomy area was compared to the accessible brain area. A mean value and a standard deviation have been calculated of the whole population ($n = 8$) and both CI groups, respectively. Again, a t-test for independent samples with a significance level of 0.95 was performed.

3 Results

3.1 Morphometric Analysis

The skull measurements taken for this study show proportions as expected with the longer facial lengths in the “Low CI” group (mesaticephalic dogs) and wider facial width in the “High CI” group (brachycephalic). It also becomes apparent that the cranial width in both groups is relatively similar even though the facial measurements vary so widely.

Table 8: Measurements of the skull in mm

Measurements of the skull in mm										
Dog	Facial length	Facial width	Cranial length	Cranial width	Cranial height	Skull length	Skull base length	Cranial Index	Cephalic index	
Dog1	97.10	115.00	112.30	67.74	71.48	208.10	187.30	60.32	55.26	Low CI
Dog2	91.40	102.40	115.00	60.75	59.24	205.60	181.50	52.83	49.81	Low CI
Dog3	84.39	104.00	108.00	62.54	56.77	192.10	174.40	57.91	54.14	Low CI
Dog4	49.36	77.45	73.58	48.91	46.04	123.80	109.70	66.47	62.56	Low CI
Dog5	38.72	125.90	93.64	61.67	55.31	132.70	114.60	65.86	94.88	High CI
Dog6	40.25	127.00	84.18	57.70	54.97	125.50	109.30	68.54	101.20	High CI
Dog7	24.29	95.43	84.43	60.26	53.93	108.60	89.51	71.37	87.87	High CI
Dog8	31.61	112.80	89.47	63.09	51.99	121.10	97.38	70.52	93.15	High CI

The median CI for this thesis was 75.22 with a standard deviation in the whole population of 21.35, in the “Low CI” group of 5.30 and in the “High CI” group of 5.49. The t-test for independent samples between low and high CI shows $p = 0.006$ for the facial length, $p = 0.026$ for the skull length, $p = 0.019$ for the skull base length, $p = 0.02$ for the cranial index and $p < 0.001$ for the CI itself. (Figure 28)

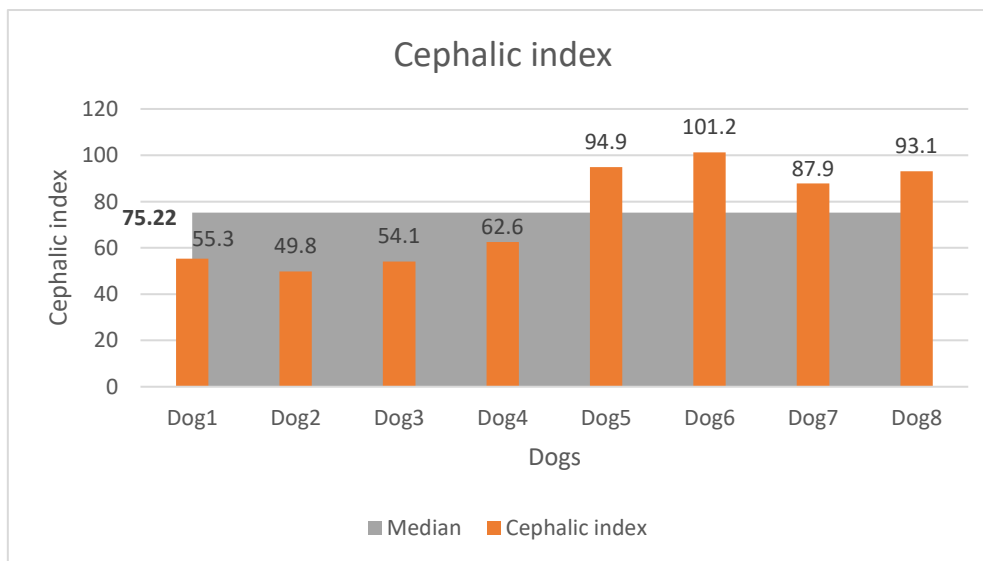


Figure 28: Cephalic index for each dog and median

These results show that the separation between mesaticephalic and brachycephalic was performed correctly and the dogs represent each group appropriately.

3.2 Craniotomy Area on the Skull

The area listed is in square millimetres (sqmm) with a mean value of the craniotomy area for the „Approach Brachycephalic“ of all dogs of 1276.22 sqmm (SD +/- 394.95 sqmm). For mesaticephalic dogs the mean value was 1286.39 sqmm (SD +/- 519.65 sqmm) and for brachycephalic dogs 1266.06 sqmm (SD +/- 204.29 sqmm). (Figure 29)

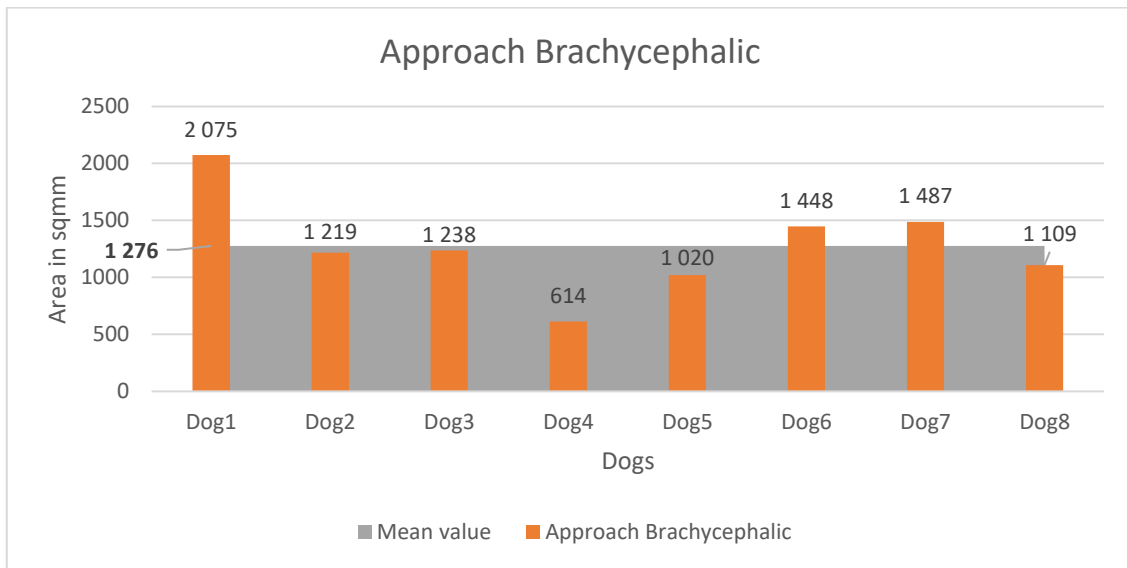


Figure 29: Craniotomy areas of „Approach Brachycephalic“

The mean value of all dogs for the „Approach Mesaticephalic“ of 1694.65 sqmm (SD +/- 370.38 sqmm), the mean value of mesaticephalic dogs 1738.60 sqmm (SD +/- 485.79 sqmm) and of brachycephalic dogs 1650.71 sqmm (SD +/- 185.76 sqmm). The greatest but also the smallest area was present in mesaticephalic dogs. (Figure 30)

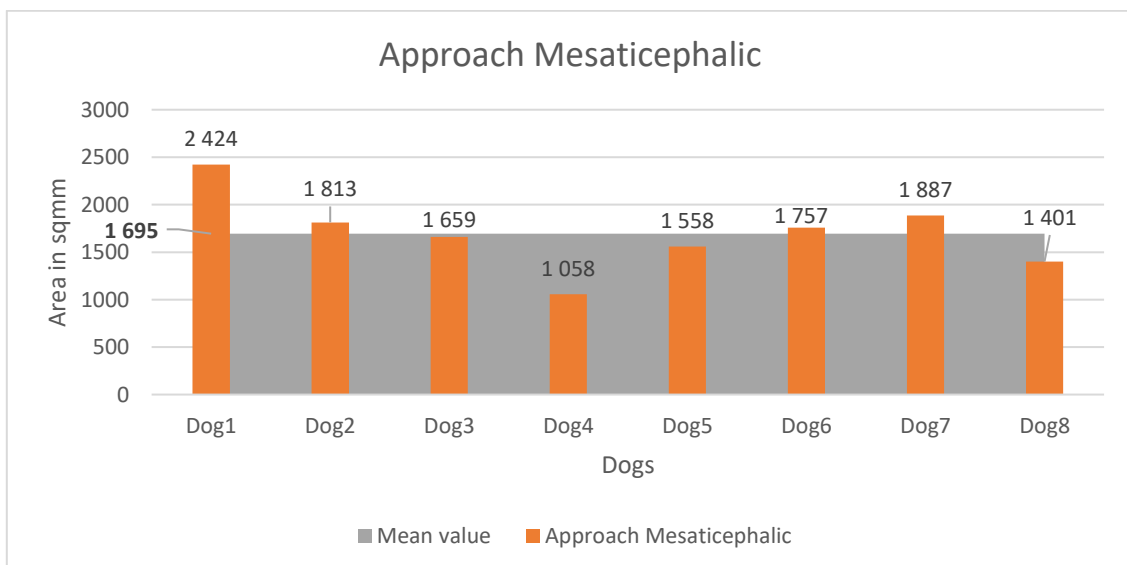


Figure 30: Craniotomy areas of „Approach Mesaticephalic“

As suggested by the previous diagrams, the craniotomy area of the „Approach Mesaticephalic“ throughout both CI groups is approximately 1.33 times bigger than in the „Approach Brachycephalic“. In the „Approach Brachycephalic“ the measured area is 1.30 times bigger in mesaticephalic dogs compared to brachycephalic dogs. (Figure 31)

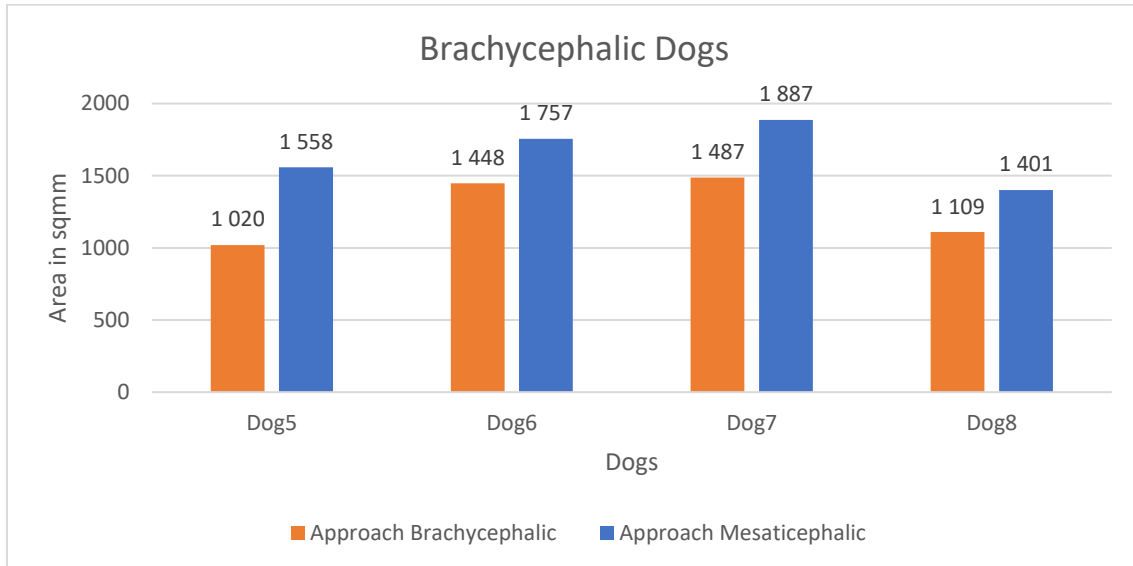


Figure 31: Comparison of craniotomy areas for brachycephalic dogs

The craniotomy area of the „Approach Mesaticephalic“ is 1.35 times bigger in mesaticephalic dogs than in brachycephalic dogs. (Figure 32)

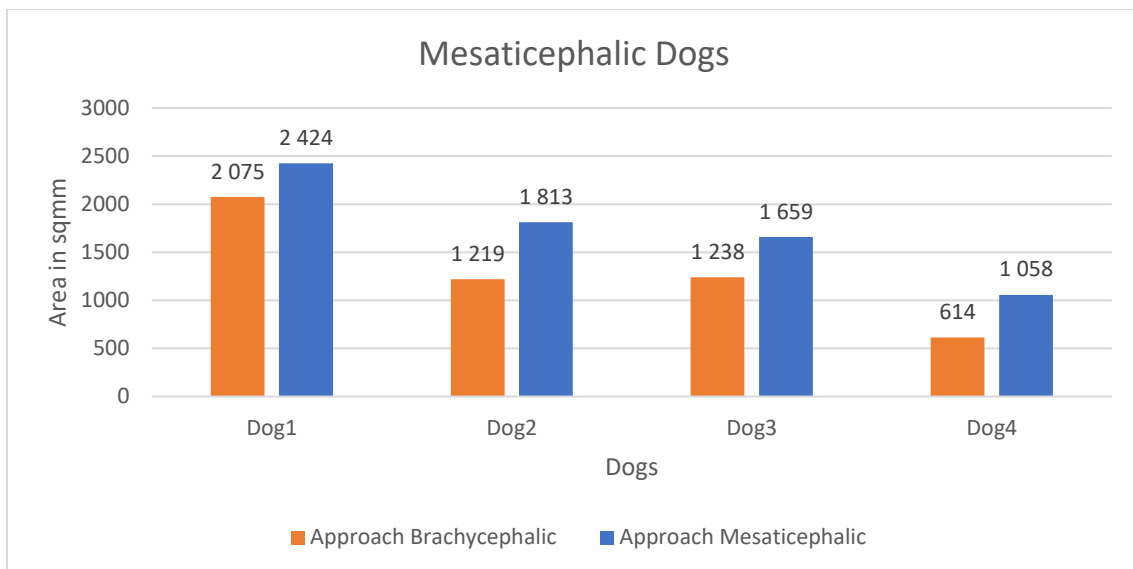


Figure 32: Comparison of craniotomy areas for mesaticephalic dogs

The biggest difference between both approaches was in Dog 4 where the „Approach Mesaticephalic“ showed a 1.72 times bigger area than the „Approach Brachycephalic“. Dog 1 showed the smallest difference with 1.17 times.

When comparing the craniotomy area of the two approaches, the t-test for sample pairs has a $p < 0.001$ for the craniotomy area on both sides. This means that the “Approach Mesaticephalic” is providing a significantly bigger craniotomy area than the “Approach Brachycephalic”.

The Figure 34 and Figure 33 provide an overview of the location and size of both craniotomy approaches in one of the mesaticephalic dogs. It is clearly visible that the craniotomy area in the “Approach Mesaticephalic” is bigger.

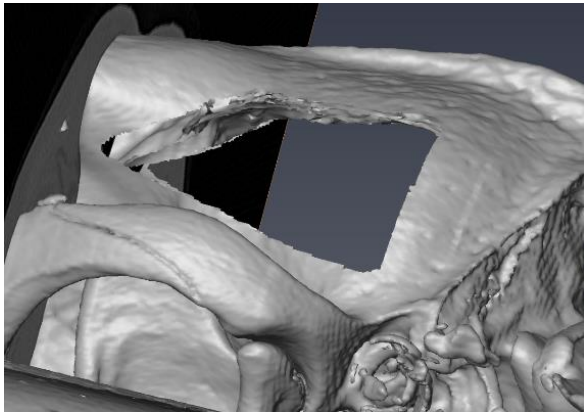


Figure 34: "Approach Brachycephalic" in Dog 3 (mesaticephalic dog)

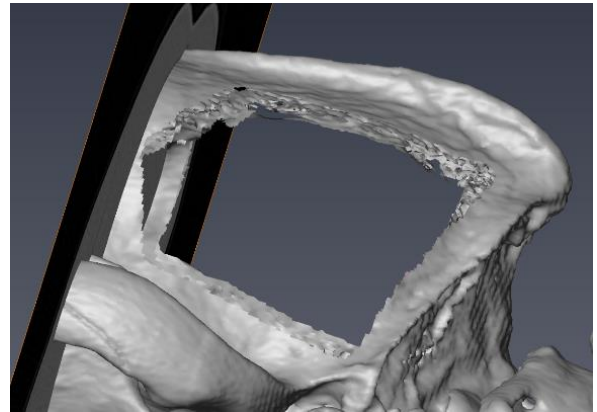


Figure 33: "Approach Mesaticephalic" in Dog 3 (mesaticephalic dog)

Figure 35 and Figure 36 compare both approaches in one of the brachycephalic dogs. Again the “Approach Mesaticephalic” shows a bigger craniotomy area. But also, its borders are coming dangerously close to the crista sagittalis externa which also poses some risks.

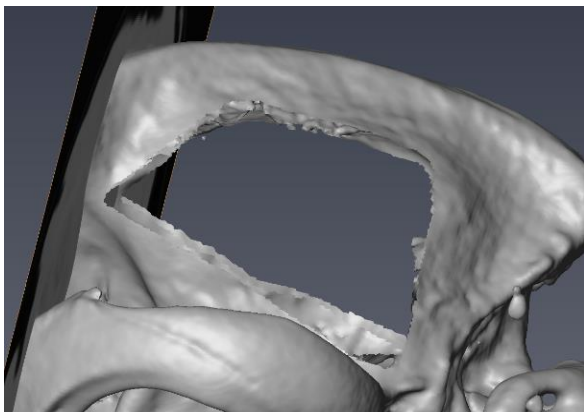


Figure 35: "Approach Brachycephalic" in Dog 7 (brachycephalic dog)

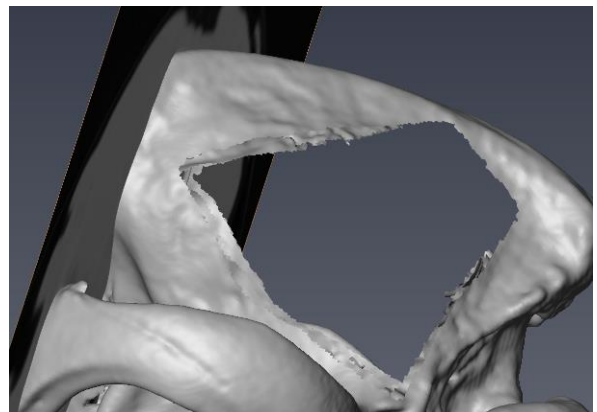


Figure 36: "Approach Mesaticephalic" in Dog 7 (brachycephalic dog)

The measurements to assess how close the craniotomy is to the crista sagittalis externa showed that the “Approach Brachycephalic” consistently provides a more reasonable safety margin so that the dorsal sinus system is not damaged. Although it is worth to mention that the planned safety margin from the drill hole 4 should be 20 mm but has been slightly less in all participants. The “Approach Mesaticephalic” is very close (< 1 cm) to the median of the skull and therefore very close to the dorsal sinus system in every single dog with the smallest margin being 3.63 mm and the biggest 9.63 mm. (Table 9)

Table 9: Measurements from the craniotomy to the crista sagittalis externa

Measurements from the craniotomy to the crista sagittalis externa				
Dog	Approach Brachycephalic		Approach Mesaticephalic	
	left	right	left	right
Dog 1	16.09	18.49	9.28	9.54
Dog 2	16.87	16.99	3.63	5.50
Dog 3	18.97	18.30	6.66	6.82
Dog 4	19.47	19.32	9.63	9.07
Dog 5	18.56	19.08	5.85	7.18
Dog 6	18.48	18.85	8.77	9.04
Dog 7	19.26	18.50	7.43	5.12
Dog 8	19.42	18.66	8.03	9.12

3.3 Accessible Gyri

The following two tables show in how many dogs each specific gyrus could be accessed. It does not give any information of how much of the individual gyrus is visible.

In brachycephalic dogs, the gyrus sylvius rostralis, gyrus ectosylvius rostralis, gyrus ectosylvius medius, gyrus ectosylvius caudalis, gyrus ectosylvius caudalis, gyrus suprasylvius medius, gyrus ectomarginalis and gyrus suprasylvius caudalis were exposed in all dogs and both approaches. Furthermore, the „Approach Mesaticephalic“ exposed the gyrus sylvius caudalis and the gyrus occipitalis in all brachycephalic dogs and the “Approach Brachycephalic” the gyrus suprasylvius rostralis. (Table 10)

Table 10: Access to gyri in brachycephalic dogs

Access to gyri in brachycephalic dogs						
gyrus	Approach Brachycephalic			Approach Mesaticephalic		
	left	right	mean	left	right	mean
gyrus sylvius rostralis	100%	100%	100%	100%	100%	100%
gyrus sylvius caudalis	100%	75%	88%	100%	100%	100%
gyrus ectosylvius rostralis	100%	100%	100%	100%	100%	100%
gyrus ectosylvius medius	100%	100%	100%	100%	100%	100%
gyrus ectosylvius caudalis	100%	100%	100%	100%	100%	100%
gyrus suprasylvius rostralis	100%	100%	100%	75%	75%	75%
gyrus suprasylvius medius	100%	100%	100%	100%	100%	100%
gyrus ectomarginalis	100%	100%	100%	100%	100%	100%
gyrus suprasylvius caudalis	100%	100%	100%	100%	100%	100%
gyrus occipitalis	50%	50%	50%	100%	100%	100%
gyrus marginalis	0%	75%	38%	50%	50%	50%
gyrus endomarginalis	0%	25%	13%	25%	75%	50%
gyrus postcruciatatus	75%	75%	75%	50%	50%	50%
gyrus praecruciatatus	25%	25%	25%	0%	0%	0%
gyrus proreus	0%	0%	0%	0%	0%	0%

The “Approach Brachycephalic” failed to expose the left gyrus marginalis, left gyrus endomarginalis and both sides of the gyrus proreus altogether in brachycephalic dogs. The “Approach Mesaticephalic” did not expose the gyrus praecruciatu and the gyrus proreus at all. (Table 10) This shows that the “Approach Brachycephalic” is superior in exposing the rostral gyri, whereas the “Approach Mesaticephalic” is more likely to expose the caudal gyri.

In mesaticephalic dogs, the gyrus sylvius rostralis, gyrus sylvius caudalis, gyrus ectosylvius rostralis, gyrus ectosylvius medius, gyrus ectosylvius caudalis, gyrus suprasylvius rostralis and Gyrus suprasylvius medius can be accessed in all dogs and with both approaches. Furthermore, the „Approach Mesaticephalic“ exposed the gyrus ectomarginalis, gyrus suprasylvius caudalis, gyrus marginalis and the gyrus postcruciatu in all mesaticephalic dogs. The gyrus marginalis can be visualized more often in the “Approach Mesaticephalic” than in the “Approach Brachycephalic” on the left side ($p = 0.028$; chi-square test). The Gyrus proreus is significantly better accessible in the “Approach Brachycephalic” on both sides ($p = 0.028$; chi-square test). Both Gyri do not show a significance in the exact test according to Fisher ($p = 0.143$ respectively). (Table 11)

Table 11: Access to gyri in mesaticephalic dogs

Access to gyri in mesaticephalic dogs						
gyrus	Approach Brachycephalic			Approach Mesaticephalic		
	left	right	mean	left	right	mean
gyrus sylvius rostralis	100%	100%	100%	100%	100%	100%
gyrus sylvius caudalis	100%	100%	100%	100%	100%	100%
gyrus ectosylvius rostralis	100%	100%	100%	100%	100%	100%
gyrus ectosylvius medius	100%	100%	100%	100%	100%	100%
gyrus ectosylvius caudalis	100%	100%	100%	100%	100%	100%
gyrus suprasylvius rostralis	100%	100%	100%	100%	100%	100%
gyrus suprasylvius medius	100%	100%	100%	100%	100%	100%
gyrus ectomarginalis	75%	75%	75%	100%	100%	100%
gyrus suprasylvius caudalis	75%	100%	88%	100%	100%	100%
gyrus occipitalis	0%	0%	0%	75%	75%	75%
gyrus marginalis	25%	50%	38%	100%	100%	100%
gyrus endomarginalis	25%	0%	13%	75%	100%	88%
gyrus postcruciatu	75%	75%	75%	100%	100%	100%
gyrus praecruciatu	75%	75%	75%	25%	25%	25%
gyrus proreus	75%	75%	75%	0%	25%	13%

The „Approach Brachycephalic“ failed to access the gyrus occipitalis in mesaticephalic dogs completely. Again the “Approach Brachycephalic” is better used for the rostral gyri and the “Approach Mesaticephalic” for the caudal and dorsal gyri.

The Figure 39 provides an approximate overview of the accessible gyri in brachycephalic dogs if the “Approach Brachycephalic” is performed. The craniotomy lies centrally on the lateral part of the cranium and exposes a big variety of gyri.

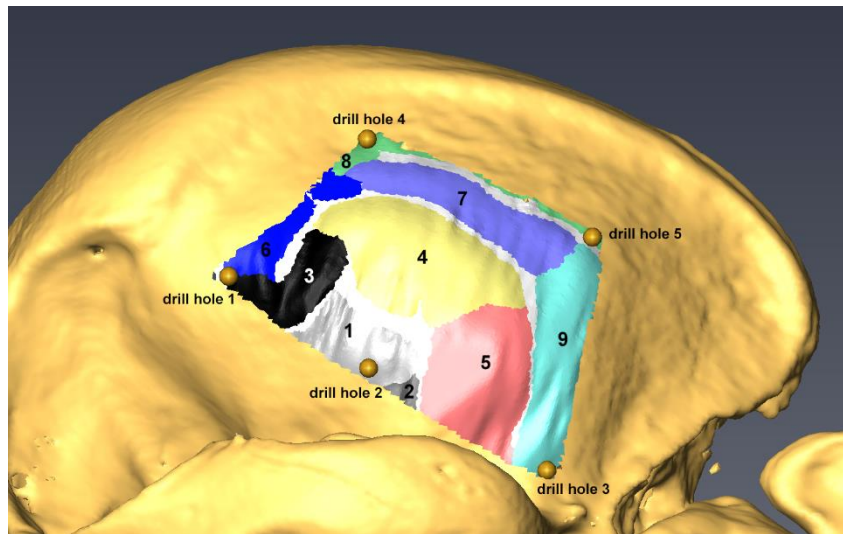


Figure 37: „Approach Brachycephalic“ on a brachycephalic skull (Dog 5)

(1) gyrus sylvius rostralis (2) gyrus sylvius caudalis (3) gyrus ectosylvius rostralis (4) gyurs ectosylvius medius (5) gyrus ectosylvius caudalis (6) gyrus suprasylvius rostralis (7) gyrus suprasylvius medius (8) gyrus ectomarginalis (9) gyrus suprasylvius caudalis

The “Approach Mesaticephalic” in brachycephalic dogs is portrayed in the Figure 40 to provide an overview. In this dog the gyrus occipitalis was exposed additionally to the ones from the “Approach Brachycephalic”. But with a bigger craniotomy comes the potential risk of exposing irrelevant or hazardous tissue like seen in Figure 40 where caudally to the brain only bony tissue is removed and structures like the dorsal sinus system are at risk.

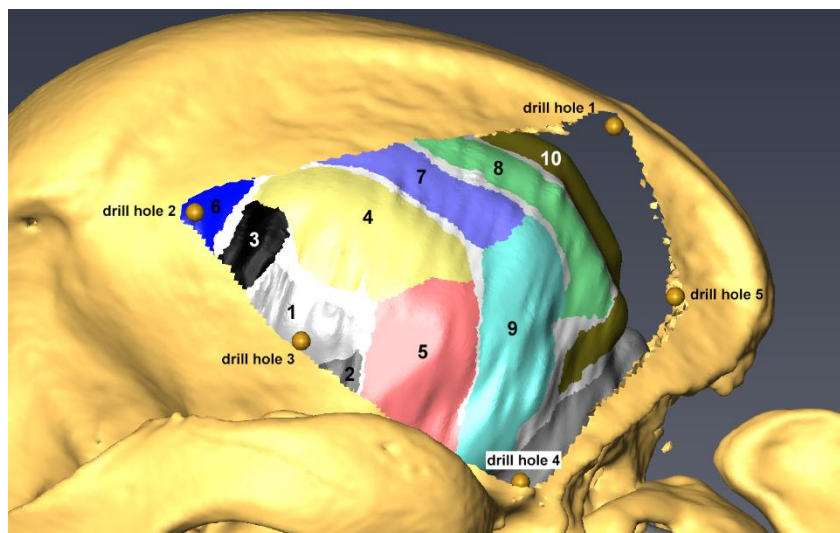


Figure 38: „Approach Mesaticephalic“ on a brachycephalic dog (Dog 5)

(1) gyrus sylvius rostralis (2) gyrus sylvius caudalis (3) gyrus ectosylvius rostralis (4) gyurs ectosylvius medius (5) gyrus ectosylvius caudalis (6) gyrus suprasylvius rostralis (7) gyrus suprasylvius medius (8) gyrus ectomarginalis (9) gyrus suprasylvius caudalis (10) gyrus occipitalis

The „Approach Brachycephalic“ managed to expose 100% of the gyrus ectosylvius medius in all brachycephalic dogs and failed to access the gyrus proreus altogether. The „Approach Mesaticephalic“ did not expose the gyrus praecruciatum and gyrus proreus. (Table 12) In the „Approach Mesaticephalic“ 100% of the gyrus ectosylvius medius and the gyrus suprasylvius medius were accessible in all mesaticephalic dogs, but the „Approach Brachycephalic“ missed the gyrus occipitalis completely. (Table 13)

The exposed area of the gyrus suprasylvius caudalis and the gyrus endomarginalis show a big difference in the „Approach Brachycephalic“ in between sides. The biggest differences (> 20%) between the left and right side are showing up in the gyrus ectosylvius caudalis, gyrus suprasylvius caudalis, gyrus marginalis and the gyrus endomarginalis. The gyrus occipitalis was not exposed in the „Approach Brachycephalic“ at all. (Table 12) The „Approach Mesaticephalic“ does not show differences as big as the other approach. (Table 13)

The 111.43% access of the gyrus endomarginalis in the „Approach Brachycephalic“ in mesaticephalic dogs is due to a mathematical calculation. The unfortunately only accessed area of the gyrus endomarginalis in the „Approach Brachycephalic“ on the left side of mesaticephalic dogs (59.72 sqmm) is divided through the mean area of the left gyrus endomarginalis in mesaticephalic dogs (53.59 sqmm) and then multiplied by 100 to get the result in percent. ($59.72/53.59*100 = 1.1143*100=111.43\%$). (Table 13)

Table 13: Mean accessible gyri area in mesaticephalic dogs in sqmm and %

Mean accessible gyri area in mesaticephalic dogs in sqmm and %												
gyrus	Approach Brachycephalic						Approach Mesaticephalic					
	left		right		mean		left		right		mean	
	sqmm	%	sqmm	%	sqmm	%	sqmm	%	sqmm	%	sqmm	%
gyrus sylvius rostralis	113.02	77.73	94.01	69.34	103.51	73.54	109.73	75.47	86.41	63.73	98.07	69.60
gyrus sylvius caudalis	58.14	46.35	64.30	42.12	61.22	44.24	53.28	42.48	73.08	47.86	63.18	45.17
gyrus ectosylvius rostralis	127.55	98.34	151.49	98.18	139.52	98.26	125.40	96.68	141.95	92.00	133.68	94.34
gyrus ectosylvius medius	120.48	95.50	121.97	99.66	121.22	97.58	126.15	100.00	122.39	100.00	124.27	100.00
gyrus ectosylvius caudalis	99.53	66.78	52.49	43.24	76.01	55.01	109.03	73.16	69.98	57.64	89.51	65.40
gyrus suprasylvius rostralis	221.86	91.38	176.28	85.98	199.07	88.68	182.34	75.10	166.24	81.08	174.29	78.09
gyrus suprasylvius medius	80.77	52.08	100.17	57.72	90.47	54.90	155.08	100.00	173.55	100.00	164.32	100.00
gyrus ectomarginalis	37.83	17.39	51.44	22.02	44.64	19.71	185.03	85.06	211.26	90.41	198.14	87.74
gyrus suprasylvius caudalis	3.95	1.63	78.62	36.37	41.28	19.00	128.18	53.04	133.03	61.54	130.60	57.29
gyrus occipitalis	0.00	0.00	0.00	0.00	0.00	0.00	64.76	43.17	68.17	45.01	66.47	44.09
gyrus marginalis	25.49	50.59	13.08	27.88	19.29	39.24	37.00	73.42	41.46	88.42	39.23	80.92
gyrus endomarginalis	59.72	111.43	0.00	0.00	29.86	55.72	46.89	87.49	34.33	71.24	40.61	79.37
gyrus postcruciatius	152.93	71.59	152.77	74.02	152.85	72.81	124.39	58.23	129.18	62.59	126.78	60.41
gyrus praecruciatius	110.68	64.23	83.85	62.56	97.26	63.40	1.78	1.03	23.21	17.32	12.50	9.18
gyrus proreus	43.71	23.38	36.89	18.57	40.30	20.98	0.00	0.00	33.77	16.99	16.88	8.50

In brachycephalic dogs, both approaches provide comparatively similar access to the gyrus sylvius rostralis, gyrus sylvius caudalis, gyrus ectosylvius medius and the gyrus ectosylvius caudalis. The „Approach Brachycephalic“ exposes a greater area for the gyrus ectosylvius rostralis, gyrus suprasylvius rostralis, gyrus suprasylvius medius and the gyrus postcruciatus. The „Approach Mesaticephalic“ provides better access to the gyrus ectomarginalis, gyrus suprasylvius caudalis, gyrus occipitalis, gyrus marginalis and gyrus endomarginalis. (Figure 39)

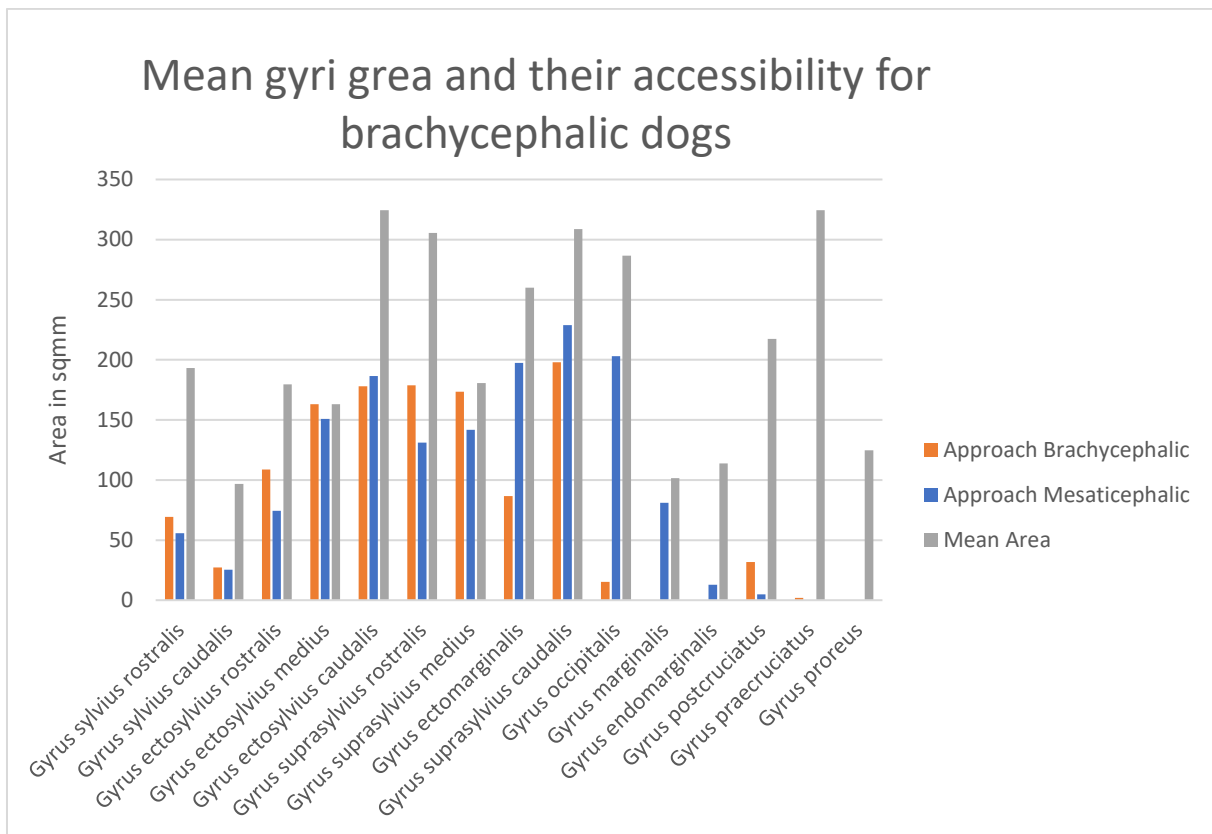


Figure 39: Mean gyri area and their accessibility in brachycephalic dogs

For brachycephalic dogs, the “Approach Brachycephalic” should be preferred for the gyrus ectosylvius rostralis, gyrus suprasylvius rostralis, gyrus suprasylvius medius and the gyrus postcruciatus whereas the „Approach Mesaticephalic“ is preferred for the gyrus ectomarginalis, gyrus suprasylvius caudalis, gyrus occipitalis, gyrus marginalis and gyrus endomarginalis. However, the pros and cons of a very dorsal approach need to be balanced as there is the pro of a bigger exposed area of certain gyri, but also the con of the risk of lacerating the dorsal sinus system.

In mesaticephalic dogs, the accessibility of the gyrus sylvius rostralis, gyrus sylvius caudalis, gyrus ectosylvius rostralis and the gyrus ectosylvius medius are similar in both approaches. The „Approach Mesaticephalic“ exposes more of the gyrus suprasylvius medius, gyrus ectomarginalis, gyrus suprasylvius caudalis, gyrus occipitalis, gyrus marginalis and the gyrus endomarginalis. The „Approach Brachycephalic“ outweighs for access to the gyrus suprasylvius rostralis, gyrus postcruciatus, gyrus praecruciatatus and the gyrus proreus. (Figure 40)

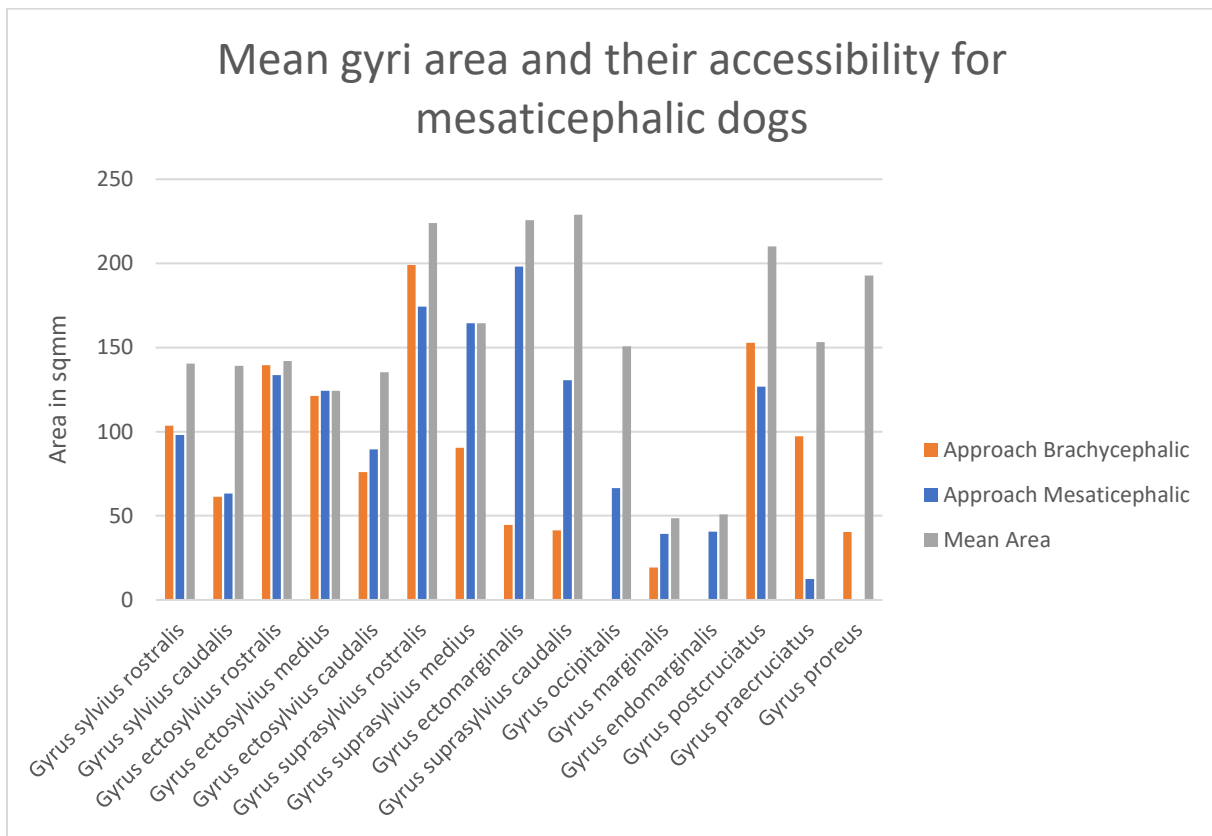


Figure 40: Mean Gyri Area and their accessibility in mesaticephalic dogs

This shows that the “Approach Mesaticephalic” should be preferred to expose the gyrus suprasylvius medius, gyrus ectomarginalis, gyrus suprasylvius caudalis, gyrus occipitalis, gyrus marginalis and the gyrus endomarginalis and the „Approach Brachycephalic“ preferred for access to the gyrus suprasylvius rostralis, gyrus postcruciatius, gyrus praecruciatius and the gyrus proreus in mesaticephalic dogs.

3.4 Craniotomy Area in comparison with Brain Area

The area of the bone removed, and the underlying brain were compared.

In the „Approach Brachycephalic“, seven of eight dogs showed a greater brain area than craniotomy area. Same as in the „Approach Mesaticephalic“, Dog 1 showed a greater craniotomy area than brain area. The mean brain area was 1372.99 sqmm (SD +/- 339.84 sqmm) and the mean craniotomy area 1276.22 sqmm (SD +/- 394.95 sqmm). (Figure 41)

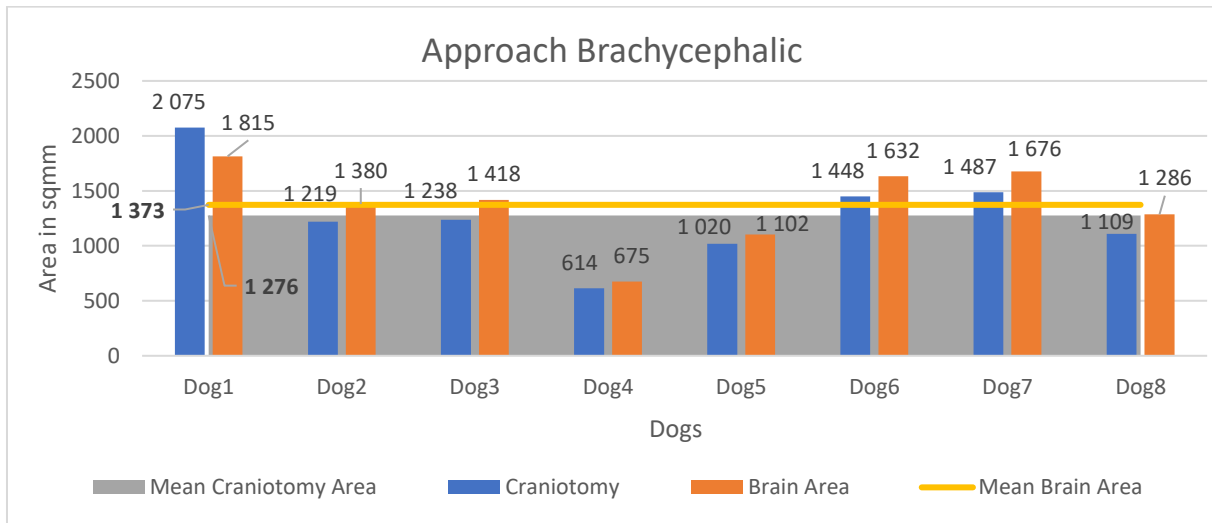


Figure 41: Craniotomy area compared to the accessible brain area in the „Approach Brachycephalic“

In seven of eight dogs, the brain area was bigger than the craniotomy area in the „Approach Mesaticephalic“. The mean brain area was 1749.71 sqmm (SD +/- 306.70 sqmm) and the mean craniotomy area 1694.65 sqmm (SD +/- 370.38 sqmm). (Figure 42)

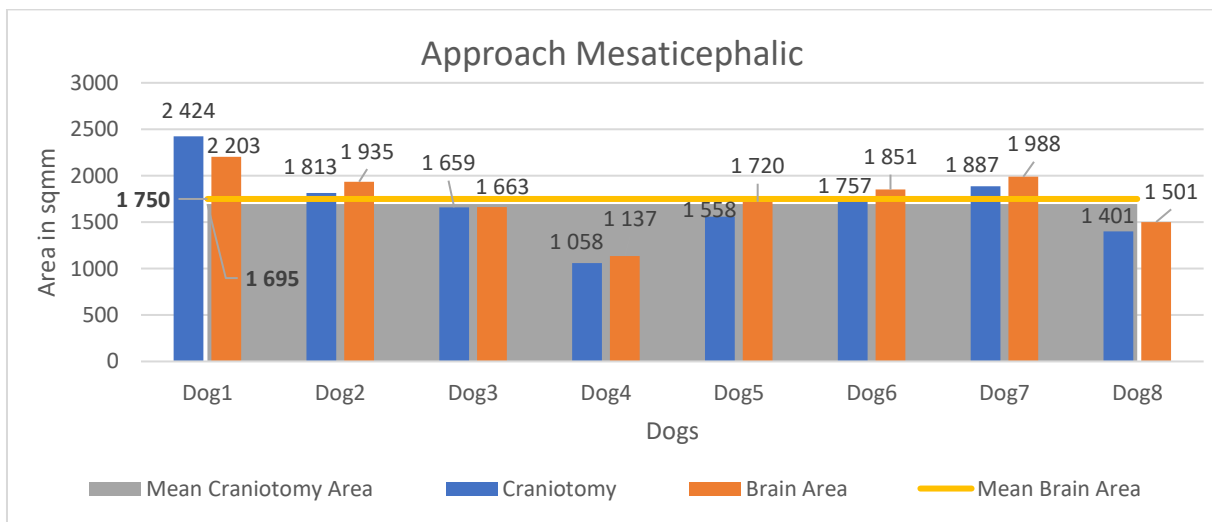


Figure 42: Craniotomy area compared to accessible brain area in the „Approach Mesaticephalic“

When the exposed brain area of the two approaches in all participants is compared, the t-test for sample pairs has a $p < 0.001$ for on the left side. The exposed brain area on the right side has a $p = 0.003$. This means that the „Approach Mesaticephalic“ is providing a significantly bigger exposed brain area than the „Approach Brachycephalic“ in all participants.

In the „Approach Brachycephalic“ in mesaticephalic dogs, the mean brain area with 1321.87 sqmm (SD +/- 410.39 sqmm) was greater than the mean craniotomy area with 1286.39 sqmm (SD +/- 519.65 sqmm). Again, only Dog 1 had a greater craniotomy area than brain area. (Figure 43)

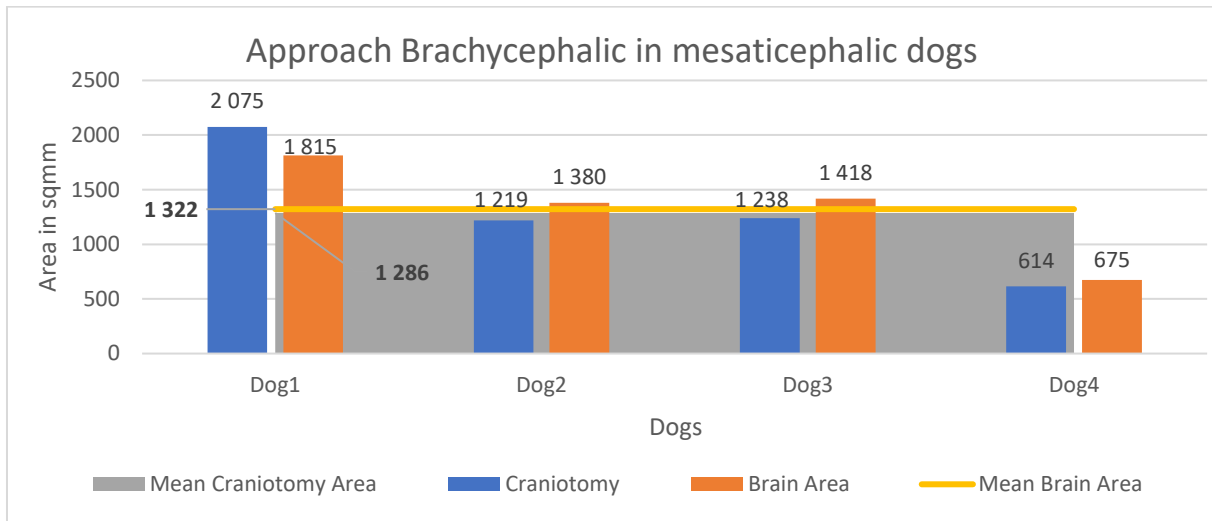


Figure 43: Craniotomy Area compared to the accessible brain area in the „Approach Brachycephalic“ in mesaticephalic dogs

For the „Approach Mesaticephalic“ in mesaticephalic dogs, the mean craniotomy area with a value of 1738.60 sqmm (SD +/- 465.79 sqmm) was greater than the mean brain area with a value of 1734.47 sqmm (SD +/- 394.34 sqmm), although only one of four dogs had a greater craniotomy area than brain area. (Figure 44)

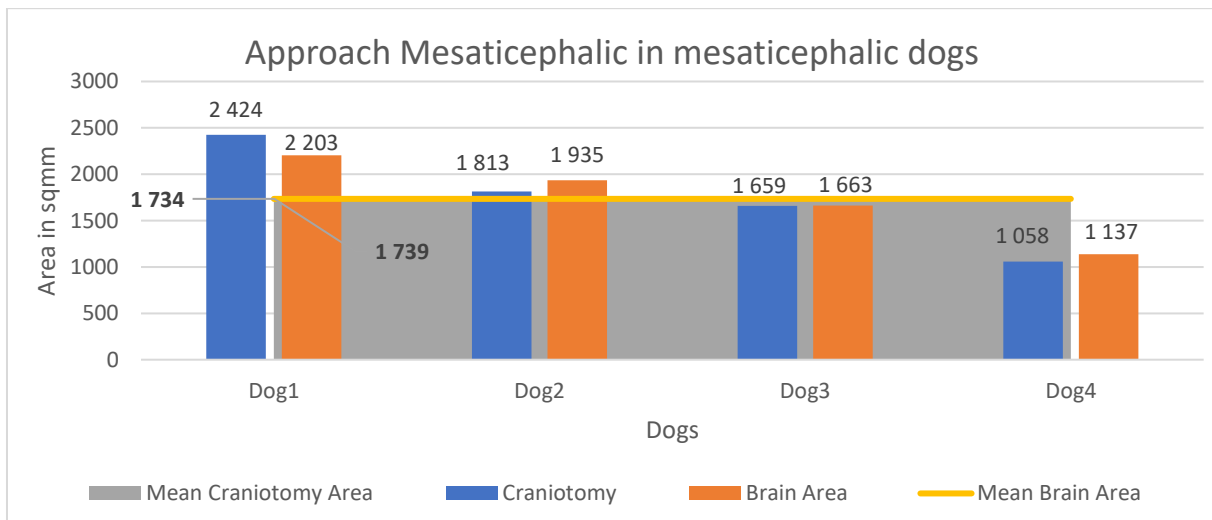


Figure 44: Craniotomy Area compared to the accessible brain area in the „Approach Mesaticephalic“ in mesaticephalic dogs

The „Approach Brachycephalic“ in brachycephalic dogs exposed a greater brain area than craniotomy area in all four dogs as well. The mean brain area was 1424.10 sqmm (SD +/- 239.45 sqmm) and the mean craniotomy area was 1266.06 sqmm (SD +/- 204.29 sqmm). This difference of almost 2 sqcm could result in a better practicability due to smaller approaches necessary for extracranial masses. (Figure 45)

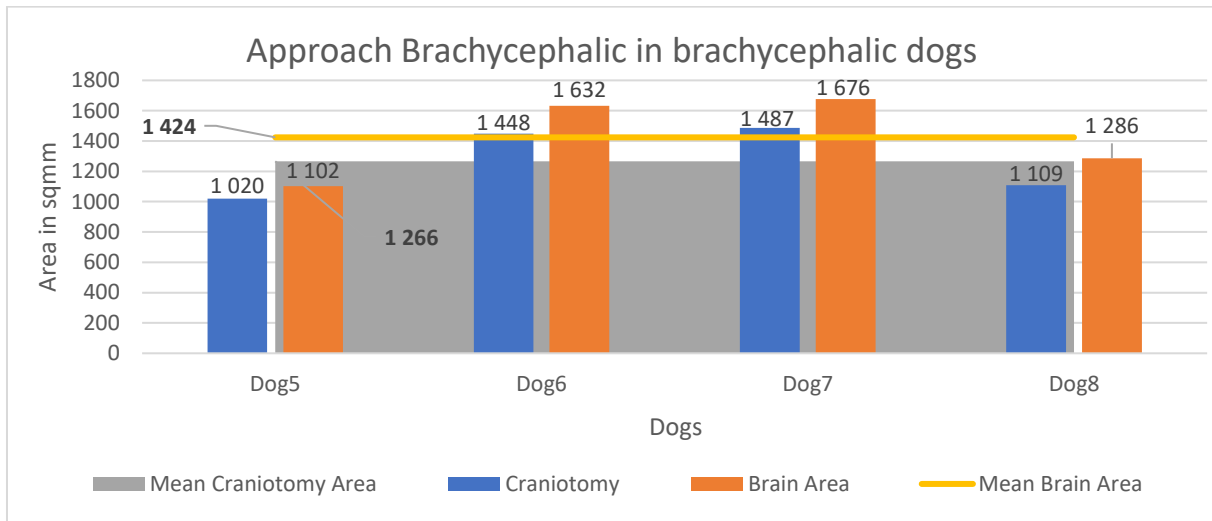


Figure 45: Craniotomy area compared to the accessible brain area in the „Approach Brachycephalic“ on brachycephalic dogs

In the „Approach Mesaticephalic“ in brachycephalic dogs, all four dogs showed a greater brain area than craniotomy area which also shows in the mean brain area of 1764.95 sqmm (SD +/- 179.33 sqmm) being greater than the mean craniotomy area of 1650.71 sqmm (SD +/- 185.76 sqmm). (Figure 46)

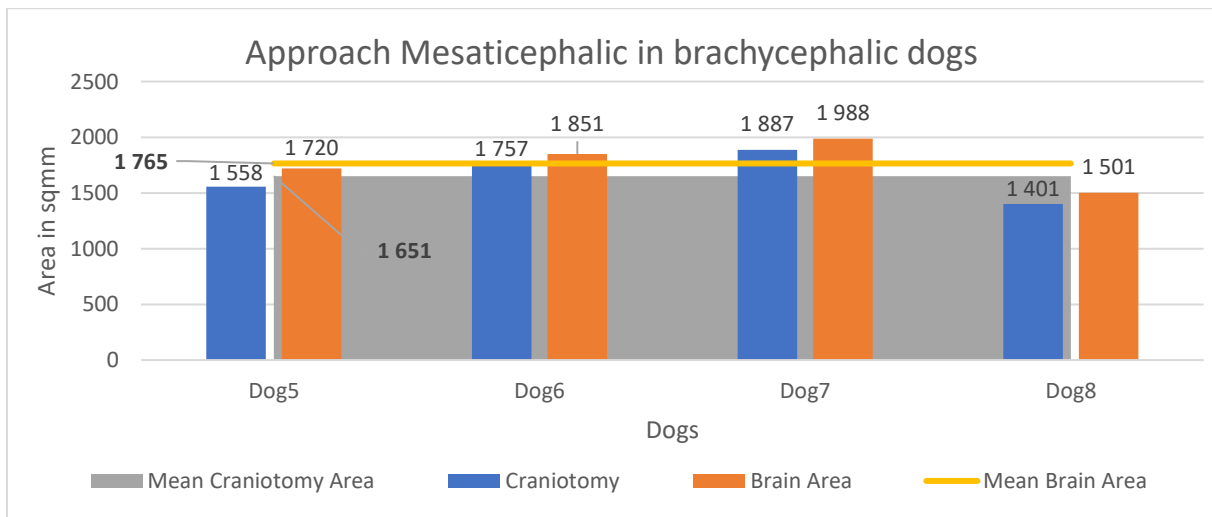


Figure 46: Craniotomy area compared to the accessible brain area in the „Approach Mesaticephalic“ on brachycephalic dogs

In mesaticephalic dogs, the „Approach Mesaticephalic“ exposed only 99.76% brain area of the craniotomy area and the „Approach Brachycephalic“ 102.76%. In brachycephalic dogs, both approaches granted access to more brain area than the craniotomy area with the „Approach Mesaticephalic“ exposing 106.92% and the „Approach Brachycephalic“ 112.48%. There is no statistical significance in the craniotomy area nor in the exposed brain area in a t-test for independent samples.

3.5 Sinus frontalis

All four mesaticephalic dogs and Dog 7 and Dog 8 from the brachycephalic dogs have got a sinus frontalis on both sides. The brachycephalic Dog 5 only has got a sinus frontalis on its right side. This agrees with the previous findings that the sinus frontalis is inconsistent in brachycephalic dogs.

In none of the brachycephalic dogs sinus frontales were opened by the “Approach Brachycephalic”, but three out of four left sinus frontales and three out of four right sinus frontales of the mesaticephalic dogs.

In this study the “Approach Mesaticephalic” opened two out of four left sinus frontales of mesaticephalic dogs, no right sinus frontales of mesaticephalic dogs and none of the brachycephalic dogs.

This result suggests that both approaches are safe regarding trepanation of the sinus frontales for brachycephalic dogs and the “Approach Mesaticephalic” is safer in mesaticephalic dogs.

4 Discussion

Craniotomies in veterinary medicine have become more important and more advanced over time. The fact that diagnostic imaging today is more precise and used more often for neurologic cases, leads to more pathologies being diagnosed and consequently also being treated. Craniotomies are not used only for removal of tissue, but also for intracranial decompression or to take samples for biopsies. (Dickinson 2014, Kramer et al. 2007, Marquez-Grados et al. 2020, Pluhar et al. 1996, Sharkey et al. 2004) The goal of this diploma thesis is to ensure a safe and reproducible access to the lateral regions of the brain in brachycephalic dogs. To achieve this, the database of the VUW was searched for dogs which had CT and MRI scans of the skull done (n = 8) which then were merged for a simulation and visualisation of the newly amended rostral approach as well as the approach evaluated by Steyrer (2018). This was done in four brachycephalic and four mesaticephalic dogs to then compare both approaches in the different skull types. The results of this study show that the "Approach Brachycephalic" is a safe way to access a number of gyri in brachycephalic dogs without damaging the sinus frontales or the dorsal sinus system. The "Approach Mesaticephalic" on the other hand results in an unfeasible and hazardous craniotomy because of its very dorsal location and the thereby arising complications.

When loading the MRI scans into Amira, it is important to decide which sequence shows the best quality. (Steyrer 2018) used the T2-weighted sequence in his study but I considered the T1 to be the better option for my study. Moreover, the quality of MRI scans seemed to differ greatly between the dogs which resulted in variable outcome of generated brain surfaces as well as in the possibility to differentiate the gyri. This problem appeared especially in brachycephalic dogs as their brain is smaller in absolute numbers than the brain of mesaticephalic dogs. The varying quality of the scans may have a negative effect on how accurate each gyrus is definable and could therefore lead to an inaccurately measured area of the gyri.

There is a big variety and inconsistency regarding Cranial and Cephalic Index in the different studies. The approach of Roberts et al. (2010) represents the differentiation between mesaticephalic and brachycephalic in this thesis best, because the standard deviation of the CI within each group is low, but higher throughout the whole population and the $p < 0.001$. Nevertheless, it must be pointed out that their approach depends on each individual study as the breakpoint is calculated from its own population and does not provide an absolute number to separate mesaticephalic from brachycephalic dogs. This means that this approach can theoretically calculate a "High CI" group, which indicates brachycephalic, in a homogenous mesaticephalic group.

The craniotomy area on the skull in sqmm throughout both CI groups was 1.33 times bigger in the „Approach Mesaticephalic“ compared to the „Approach Brachycephalic“ and also is significant with a $p < 0.001$. Mesaticephalic dogs showed the biggest difference within the group and included the smallest and biggest overall area in the whole population of both approaches. This is represented by the relatively high standard deviation in the mesaticephalic group compared to the group of brachycephalic dogs.

There seems to be an inconsistency regarding accessibility of the gyri on the left and right side of the brain in both approaches and both groups. This is especially prominent in brachycephalic dogs where for example the gyrus marginalis in the „Approach Brachycephalic“ was not exposed on the left side, but in three out of four dogs exposed on the right side. This also

shows in Table 13 where the gyrus endomarginalis in the „Approach Brachycephalic“ is exposed 111.43% on the left and 0.00% on the right side for mesaticephalic dogs. Another cause for this high variance is the fact that this gyrus was only accessed in one dog with a rather big, exposed gyrus area (compared to the mean gyrus endomarginalis area in mesaticephalic dogs) on the left and not at all on the right side. The 111.43% therefore are a mathematical problem. A possible explanation for the inconsistency in accessibility could be the lack of quality and resolution in some of the scans and as a consequence of this, an inaccuracy in the drawing of the gyri, or the positioning of the affected gyri close to the edge of the craniotomy area. Another cause could be a certain degree of biological variance and asymmetry in the hemispheres (Toga and Thompson 2003). Furthermore, it is necessary to mention that the gyrus marginalis and gyrus endomarginalis could not be separated visually in Dog 7 (brachycephalic) and therefore it statistically only shows up as gyrus endomarginalis.

The variability in the exposition of the different gyri in each approach might be due to the „Approach Mesaticephalic“ lying more caudally and dorsally and therefore not exposing the area just caudal to the sinus frontales, but also being bigger in general compared to the „Approach Brachycephalic“. However, it is important to mention that because of the high variety of skull shapes in brachycephalic dogs even throughout the same breeds and similar sizes. The location of the drill holes in the „Approach Brachycephalic“ was more directed towards safety and reproducibility throughout these dogs and as a consequence led to a smaller craniotomy area than anticipated. Drill hole 1 of the „Approach Mesaticephalic“ appears to be appropriate for mesaticephalic dogs, but because of the different skull shapes of brachycephalics, and the drill holes' reliance on the sutura parietofrontalis, its location varied highly. It led to a borderline impossible craniotomy in this area because of its extremely dorsal location (< 1 cm to the crista sagittalis externa) and the risk to lacerate the sinus sagittalis dorsalis. Therefore, the sutura parietofrontalis is not a recommended reference point in brachycephalic dogs but appears to be appropriate for mesaticephalic dogs, although the craniotomy comes close to the crista sagittalis externa as well. This very dorsal drill hole also affected the craniotomy area and the accessibility of gyri. As a result of these points, the comparison of both approaches in brachycephalic dogs must be treated with caution.

To further improve accessibility of the brain in a craniotomy, it may be necessary to occlude parts of the sinus durae matris. Previous studies indicate no risk of an elevation of the intracranial pressure and no or transient neurologic deficits after unilateral acute or permanent occlusion of a sinus transversus. (Bagley et al. 1997, Boston 2010, Pluhar et al. 1996) Although a moderate increase of the intracranial pressure can be compensated, these mechanisms cannot cope with a persistent increase in intracranial pressure which can lead to life threatening conditions like cerebral ischemia and brain herniation. Therefore, an increased intracranial pressure influences the postoperative mortality rate. (Seki et al. 2019) Laceration or incision of the sinus durae matris leads to heavy bleeding, followed by cerebral hypotension as well as increased intracranial pressure due to haematoma. (Steyrer 2018)

The accessible brain area was bigger than the craniotomy area in seven of eight dogs in the „Approach Mesaticephalic“, with the Dog 1 being the outlier. In general, it must be considered that however big the craniotomy area is, the exposed area underneath it should be at least the same. However, in Dog 1 the difference in these two areas is due to the generally dorsal and caudal positioning of this particular approach („Approach Mesaticephalic“) and the subsequently „misaligned“ craniotomy which exposes tissue that isn't counted towards brain tissue. This leads to a bigger craniotomy area, but the exposed brain area beneath it is smaller. Figure 48 and Figure 47 portray the difference of both approaches in Dog 1.

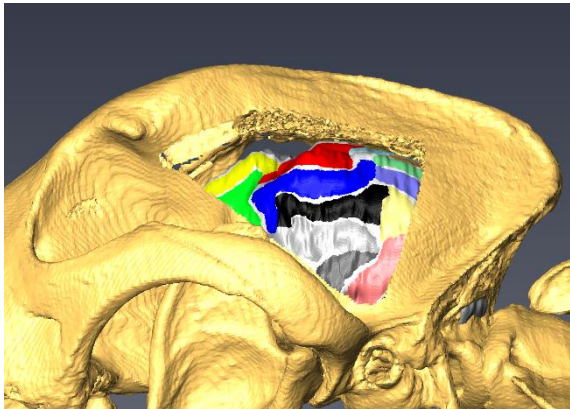


Figure 48: „Approach Brachycephalic“ in Dog 1

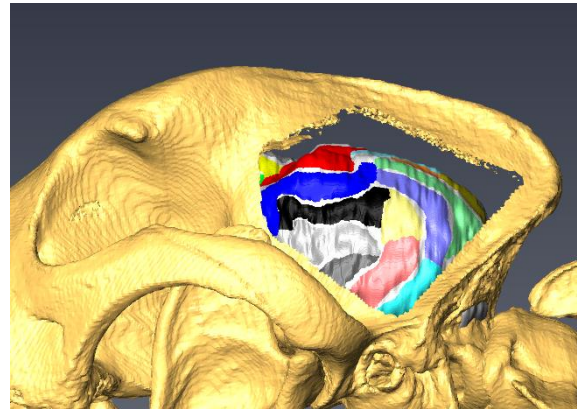


Figure 47: „Approach Mesaticephalic“ in Dog 1

A sinus frontalis is present in 7 out of 8 dogs, albeit one of these dogs has the sinus frontalis only on one side. This inconsistency regarding the presence of a sinus frontalis is only apparent in the brachycephalic group which corresponds with previous studies in this field. (Hermanson et al. 2020) Although there was an effort in the „Approach Brachycephalic“ not to damage the sinus frontalis, because there is a risk of bleeding, infection, and a possible occurrence of a pneumocephalus, both sides of the sinus frontalis in three out of four mesaticephalic dogs were opened.

The „Approach Mesaticephalic“ only opened the left sinus frontalis of two dogs from the mesaticephalic group and none of the brachycephalics, which could be due to the more caudal craniotomy position of his approach. To cope with this result in the „Approach Brachycephalic“ either a bigger safety margin for the drill hole 1 should be considered, or the pre-operative use of diagnostic imaging, namely CT, to determine how much safety margin is necessary to avoid any trepanation of the sinus frontalis. On one hand trepanation of the sinus frontalis bears a short term risk like bleeding of the mucosa - on the other hand postoperative complications like seizures, surgical site infection, intracranial haemorrhage, pneumocephalus, increasing intracranial pressure, CSF leakage and pneumonia are possible complications after a craniotomy. (Cavanaugh et al. 2008, M Das and Bajaj 2020, Marras et al. 1998, Seki et al. 2019, Wohlgemuth 1985)

One drawback of this study is the low number of cases. I was only able to obtain both, CT and MRI scans of the head, of four brachycephalic and four mesaticephalic dogs which is not an appropriate sample size to be diagnostically conclusive. For definitive conclusions regarding reproducibility and significance, further studies and greater case numbers are needed. Moreover, the brachycephalic group consisted only of French Bulldogs whereas the mesaticephalic group was more heterogeneous with one Golden Retriever and three mixed breeds who also were quite different in size and weight. Furthermore, a certain degree of inaccuracy is expected due to the visualization of a 3D object on a 2D screen. Moving and

rotating the visualization on the screen often leads to a small variation of areas and therefore should be seen as source of error, albeit negligible.

When both approaches are compared it is important to not only look at the sizes of the craniotomies or the accessible gyri, but also to look at the practicability and safety. In brachycephalic dogs the "Approach Mesaticephalic" provides a larger craniotomy area and a bigger access to some gyri, but safety must be considered when strictly following the guide. The craniotomy lies very dorsal which can provoke laceration of the sinus sagittalis dorsalis and then cause major complications. It needs to be considered, that such a big craniotomy might be viable when simulated on a computer and only bony structures are taken into account, but then in real life could interfere with the anatomy of the soft tissue and therefore decrease its practicability. In conclusion the newly designed "Approach Brachycephalic" is more feasible in brachycephalic dogs due to its safety and reproducibility and the "Approach Mesaticephalic" is best reserved for mesaticephalic dogs.

5 Summary

A rostromental craniotomy approach in brachycephalic dog breeds is described with its anatomical features and circumstances of brachycephalia and then compared to an already described approach in mesaticephalic dogs (Steyrer 2018) regarding its safety and consistency.

For this, the Institute of Topographic Anatomy of the VUW provided specimen of brachycephalic dog breeds prior to the study which were examined for possible anatomical differences.

Afterwards the Clinical Unit of Diagnostic Imaging of the VUW made the database available for the study. All mesati- and brachycephalic dogs with available CT and MRI scans of the skull since the year 2010 without pathologies of the brain were included in this study. The processing of these scans was done in Amira (Thermo Fischer Scientific) in the version 2019.01.

The skulls were measured in Amira and based on follow-up calculations split into two groups (mesati- and brachycephalic). Additionally, they were scanned for anatomical variations inside the skull. A substantial difference in these two skull shapes is the presence and extent of the bilateral sinus frontalis as well as the median crista sagittalis externa and the protuberantia occipitalis.

To ensure a safe surgical approach, the maximal expansion of the sinus frontales, the protuberantia occipitalis and the crista sagittalis externa were measured and the approach from Steyrer (2018) under consideration of appropriate safety margins was amended.

Subsequently the already described as well as the newly designed craniotomy approaches were simulated virtually on all skulls. The craniotomy area together with the according gyri area was measured and furthermore both approaches were compared and statistically analysed.

The results show that the newly adapted craniotomy approach in brachycephalic dogs exposes a variety of gyri. The majority of the gyrus ectosylvius rostralis, gyrus ectosylvius caudalis, gyrus suprasylvius rostralis, gyrus suprasylvius medius, gyrus suprasylvius caudalis and entire gyrus ectosylvius media are exposed.

The following Table 14 compares the mean accessible area of each gyrus in percent of both approaches and both skull shapes.

Table 14: Comparison of the mean access to the area of each individual gyrus in %

Comparison of the mean access to the gyri area in %				
gyrus	brachycephalic dogs		mesaticephalic dogs	
	Approach brachycephalic	Approach mesaticephalic	Approach brachycephalic	Approach mesaticephalic
gyrus sylvius rostralis	35.53	28.79	73.54	69.60
gyrus sylvius caudalis	28.15	26.31	44.24	45.17
gyrus ectosylvius rostralis	62.47	43.23	98.26	94.34
gyrus ectosylvius medius	100.00	92.48	97.58	100.00
gyrus ectosylvius caudalis	54.92	57.51	55.01	65.40
gyrus suprasylvius rostralis	58.74	43.00	88.68	78.09
gyrus suprasylvius medius	96.74	80.17	54.90	100.00
gyrus ectomarginalis	33.37	76.00	19.71	87.74
gyrus suprasylvius caudalis	64.15	74.05	19.00	57.29
gyrus occipitalis	5.34	70.77	0.00	44.09
gyrus marginalis	6.84	80.23	39.24	80.92
gyrus endomarginalis	4.22	10.59	55.72	79.37
gyrus postcruciatus	15.13	2.37	72.81	60.41
gyrus praecruciatus	0.65	0.00	63.40	9.18
gyrus proreus	0.00	0.00	20.98	8.50

The comparability to the approach from Steyrer (2018) is to be taken cautiously, because strictly following the guide leads to an impossible craniotomy in brachycephalic dogs which would risk a laceration of the sinus sagittalis dorsalis.

Furthermore, this study agrees with previous findings, that the sinus frontalis is inconsistent in brachycephalic dogs. The "Approach Mesaticephalic" opened at least one sinus frontalis in two out of eight dogs, both mesaticephalic. The "Approach Brachycephalic" lead to trepanation of no brachycephalic, but three mesaticephalic dogs. This means that in this study both approaches were safe regarding opening of the sinus frontales in brachycephalic, but not for mesaticephalic dogs.

In conclusion the newly designed "Approach Brachycephalic" is more feasible in brachycephalic dogs due to its safety and reproducibility and the "Approach Mesaticephalic" is best for mesaticephalic dogs.

6 Zusammenfassung

Ein bereits beschriebener rostrotentorialer Kraniotomiezugang bei mesaticephalen Hunderassen (Steyrer 2018) wird auf die anatomischen Gegebenheiten und Besonderheiten von brachycephalen Hunden angepasst um auch bei diesen einen möglichst sicheren und dennoch zweckdienlichen chirurgischen Zugang zu erhalten.

Dazu wurden im Vorfeld Schädelknochenpräparate von brachycephalen Hunderassen des Instituts für Topographische Anatomie der VUW auf allfällige Besonderheiten in deren Anatomie untersucht und größere Auffälligkeiten festgehalten.

In der Folge stellte die klinische Abteilung für Bildgebende Diagnostik der VUW Ihre Datenbank für den eigentlichen Versuch zur Verfügung. Alle seit 2010 verfügbaren CT und MRI Scans physiologischer Schädel von mesati- und brachycephalen Hunden wurden in die Studie inkludiert. Die Verarbeitung dieser Scans erfolgte mithilfe des Programms Amira (Thermo Fischer Scientific) in der Version 2019.01.

Die Schädelknochen wurden in Amira vermessen und auf Basis der anschließenden Berechnungen in zwei Gruppen (mesati- und brachycephal) eingeteilt. Zusätzlich wurden sie auf anatomische Variationen innerhalb des Schädelknochens untersucht. Ein wesentlicher Unterschied der beiden Schädelformen ist das Vorhandensein und die Ausprägung des beidseitigen Sinus frontalis sowie der medianen Crista sagittalis externa und der Protuberantia occipitalis.

Um einen sicheren Zugang zu gewährleisten wurde die Maximalausdehnung der Sinus frontales, der Protuberantia occipitalis und der Crista sagittalis externa in Amira ausgemessen und der von Steyrer (2018) beschriebene Zugang unter Bedachtnahme auf entsprechende Sicherheitsabstände abgeändert.

Danach wurden sowohl der bereits beschriebene als auch der neu konzipierte Kraniotomiezugang virtuell an allen Schädeln simuliert und die Kraniotomieflächen sowie die freigelegte Fläche des Gehirns und der Gyri ausgemessen. Weiterführend wurden die beiden Zugänge miteinander verglichen und statistisch ausgewertet.

Die Ergebnisse zeigen, dass der neu angepasste Kraniotomiezugang bei brachycephalen Hunderassen eine Vielzahl an Gyri freilegt. Der Großteil des Gyrus ectosylvius rostralis, Gyrus ectosylvius caudalis, Gyrus suprasylvius rostralis, Gyrus suprasylvius medius, Gyrus suprasylvius caudalis und der gesamte Gyrus ectosylvius medius werden dargestellt.

Die folgende Table 15 vergleicht die durchschnittlich zugängliche Fläche jedes einzelnen Gyri in Prozent von beiden Zugängen und Schädelformen.

Table 15: Vergleich der durchschnittlich zugänglichen Fläche der einzelnen Gyri in %

Vergleich der durchschnittlich zugänglichen Gyri Fläche in %				
Gyrus	Brachycephale Hunde		Mesaticephale Hunde	
	Zugang brachycephal	Zugang mesaticephal	Zugang brachycephal	Zugang mesaticephal
Gyrus sylvius rostralis	35.53	28.79	73.54	69.60
Gyrus sylvius caudalis	28.15	26.31	44.24	45.17
Gyrus ectosylvius rostralis	62.47	43.23	98.26	94.34
Gyrus ectosylvius medius	100.00	92.48	97.58	100.00
Gyrus ectosylvius caudalis	54.92	57.51	55.01	65.40
Gyrus suprasylvius rostralis	58.74	43.00	88.68	78.09
Gyrus suprasylvius medius	96.74	80.17	54.90	100.00
Gyrus ectomarginalis	33.37	76.00	19.71	87.74
Gyrus suprasylvius caudalis	64.15	74.05	19.00	57.29
Gyrus occipitalis	5.34	70.77	0.00	44.09
Gyrus marginalis	6.84	80.23	39.24	80.92
Gyrus endomarginalis	4.22	10.59	55.72	79.37
Gyrus postcruciatius	15.13	2.37	72.81	60.41
Gyrus praecruciatius	0.65	0.00	63.40	9.18
Gyrus proreus	0.00	0.00	20.98	8.50

Die Vergleichbarkeit mit dem Zugang von Steyrer (2018) ist vorsichtig zu beurteilen, da dieser bei strikter Ausführung bei brachycephalen Hunden zu nicht geeigneten Kraniotomien führt welche ein Risiko der Verletzung des Sinus sagittalis dorsalis bergen.

Weiters stimmt diese Diplomarbeit mit vorherigen Berichten einer Inkonsistenz der Sinus frontales bei brachycephalen Hunden überein. Der „Approach Mesaticephalic“ öffnete mindestens einen Sinus frontalis bei zwei von acht Hunden, beide mesaticephal. Der „Approach Brachycephalic“ führte zu keiner Öffnung bei brachycephalen, aber zur Öffnung des Sinus frontalis von drei mesaticephalen Hunden. Daher kann man sagen, dass beide Zugänge sicher für brachycephale, aber nicht für mesaticephale Hunde sind.

Zusammenfassend kann man sagen, dass der neu beschriebene „Approach Brachycephalic“ aufgrund der höheren Gefahrlosigkeit und Reproduzierbarkeit bei brachycephalen Hunden besser geeignet ist und daher bei diesen bevorzugt werden sollte. Der „Approach Mesaticephalic“ erzielt bei mesaticephalen Hunden gute Ergebnisse und sollte deswegen auch bei diesen angewandt werden.

7 Appendix

7.1 Translation-sheet

By virtue of the nomenclatures used in this thesis being Latin, but many other publications using English as their terminology, I have added a Translation-sheet.

Nomina Anatomica Veterinaria	English
A. basilaris	basilar artery
A. carotis communis	common carotid artery
A. carotis interna	internal carotid artery
A. cerebri caudalis	caudal cerebral artery
A. cerebri media	middle cerebral artery
A. cerebri rostralis	rostral cerebral artery
A. choroidea rostralis	rostral choroidal artery
A. communicans caudalis	Caudal communicating artery
A. ethmoidalis interna	internal ethmoidal artery
A. hypophysialis caudalis	caudal hypophyseal artery
A. intercarotica caudalis	caudal intercarotid artery
A. intercarotica rostralis	rostral intercarotid artery
A. ophthalmica interna	internal ophthalmic artery
A. vertebralis	vertebral artery
Aa. cerebelli caudales	caudal cerebellar arteries
Aa. labyrinthi	labyrinth arteries
Aqueductus mesencephali	Mesencephalic aqueduct
Arachnoidea encephali	Arachnoid mater
Basis cranii interna	Cranial base
Bulbus olfactorius	Olfactory bulb
C. magna cerebri	great cerebral vein
Canalis carotideus	carotid canal
Canalis opticus	Optic canal
Canalis petrooccipitalis	Petrooccipital canals
Canalis sinus transversi	Transverse canal
Canalis vertebralis	Vertebral canal
Cavum cranii	Cranial cavity
Cavum nasii	Nasal cavity
Cavum subarachnoidale	Subarachnoid space
Cavum subarachnoidale	Subarachnoid space
Chiasma opticum	Optic chiasm
Chiasma opticum	optic chiasm
Cisterna cerebellomedullaris	Cisterna magna
Cisterna chiasmatis	Chiasmatic cistern
Cisterna interpeduncularis	Interpeduncular cistern
Cisterna valleculae lateralis cerebri	Cistern of lateral cerebral fossa
Commissura rostralis	Rostral commissure
Condylus occipitalis	Occipital condyle
Confluens sinuum	Confluence of the sinuses
Cortex auditivus (human med)	Auditory cortex
Cortex cerebri	Cerebral cortex
Cortex frontalis	Frontal lobe

Cortex occipitalis	Occipital lobe
Cortex parietalis	Parietal lobe
Cortex temporalis	Temporal lobe
Crus cerebri	Crus cerebri
Dentes canini	Canine
Dentes praemolares	Premolar
Dentes incisivi	Incisor
Diaphragma sellae	Sellar diaphragm
Encephalon	Brain
Epithalamus	Epithalamus
Fissura longitudinalis cerebri	Median longitudinal fissure
Fissura longitudinalis cerebri	longitudinal fissure
Fissura orbitalis	Orbital fissure
Fissura pseudosylvia	pseudosylvian fissure
Fissura tympanooccipitalis	tympanooccipital fissure
Fissura uvulonodularis	Uvulonodular fissure
Foramen jugulare	Jugular foramen
Foramen vertebrale	Vertebral foramen
Formatio reticularis	Reticular formation
Fossa cranii media	Middle cranial fossa
Gyrus proreus	prorean gyrus
Hamulus pterigoidei	Pterygoid hamulus
Hemisphaeria cerebri	Cerebral hemispheres
Lamina cribrosa	Cribriform plate
Lamina cribrosa	cribriform plate
Liquor cerebrospinalis	Cerebrospinal fluid
Ln. retropharyngeus medialis	medial retropharyngeal lymph node
Lobus flocculonodularis	Flocculonodular lobe
Lobus piriformis	Piriform lobe
Lobus piriformis	Piriform lobe
Meatus acusticus externus	External acoustic meatus
Meatus acusticus externus	External acoustic meatus
Meatus temporalis	Temporal meatus
Medulla spinalis	Spinal cord
Mesencephalon	Midbrain
Nervi craniales	Cranial nerves
Nervus olfactorius	Olfactory nerve
Nervus trochlearis	Fourth cranial nerve
Nuclei basales	basal nuclei
Nuclei geniculi	geniculate nucleus
Nuclei olivares	olives
Nucleus accumbens	Accumbens
Nucleus caudatus	caudate nucleus
Nucleus endopeduncularis	endopeduncular nucleus
Nucleus ruber	red nucleus
Nucleus subthalamicus	subthalamic nucleus
Os basisphenoidale	Basisphenoid bone
Os ethmoidale	Ethmoid bone
Os frontale	Frontal bone
Os interparietale	Interparietal bone
Os occipitale	Occipital bone
Os parietale	Parietal bone

Os praesphenoidale	Presphenoid bone
Os temporale	Temporal bone
Pedunculus cerebri	Cerebral peduncles
Plexus choroideus	choroid plexus
Plexus choroideus	choroid plexus
Plexus ophtalmicus	Ophtalmic plexus of veins
Plexus venosus vertebralis internus	Ventral internal vertebral venous plexus
Polus caudalis	Occipital pole
Polus rostralis	Frontal pole
Processus frontalis ossis zygomaticus	Frontal process of zygomatic bone
Processus interparietalis ossis occipitalis	Interparietal process of the occipital bone
Processus mastoideus	Mastoid process
Processus nasalis	Nasal process
Processus zygomaticus ossis frontalis	Zygomatic process of frontal bone
Protuberantia occipitalis externa	Occipital protuberance
Rr. Ad pontem	Pontine branches
Rr. centrales	Central branches
Rr. corticales	Cortical branches
Rr. striati	Striatic branches
Septum nasi osseum	Osseous nasal septum
Sinus basilaris	Basilar sinus
Sinus caroticus	carotid sinus
Sinus durae matris	Sinus of the dura mater
Sinus frontalis	Frontal sinus
Sinus intercavernosi	Intercavernous sinus
Sinus petrosus dorsalis	Dorsal petrosal sinus
Sinus petrosus ventralis	Ventral petrosal sinus
Sinus petrosus ventralis	Ventral petrosal sinus
Sinus rectus	Straight sinus
Sinus sagittalis dorsalis	Dorsal sagittal sinus
Sinus sagittalis dorsalis	Dorsal sagittal venous sinus
Sinus sigmoideus	Sigmoid sinus
Sinus sigmoideus	Sigmoid sinus
Sinus temporalis	Temporal sinus
Sinus transversus	Transverse sinus
Substantia alba	White matter
Substantia grisea	Grey matter
Subthalamus	Subthalamus
Sulcus ansatus	ansate sulcus
Sulcus coronalis	coronal sulcus
Sulcus cruciatus	cruciate sulcus
Sulcus hippocampi	hippocampal sulcus
Sulcus sinus transversi	Transverse groove
Sutura coronalis	Frontoparietal suture
Sutura frontonasalis	Frontonasal suture
Sutura interincisiva	Inter incisive suture
Sutura internasalis	Internasal suture
Sutura sagittalis	Sagittal suture
Systema nervosum centrale	Central nervous system
Tentorium cerebelli membranaceum	Membranous cerebellar tentorium
Tentorium cerebelli osseum	Osseous cerebellar tentorium
Tractus olfactorius	Olfactory tract

Truncus encephali	Brainstem
Tuberculum nuchale	Nuchal tubercle
Tunica adventitia	Adventitia
Tunica media	Middle coat
V. angularis oculi	angular vein of the eye
V. cerebri magna	Great cerebral vein
V. corporis callosi	Vein of the corpus callosum
V. diploica	Diploic vein
V. diploica frontalis	frontal diploic vein
V. diploica occipitalis	occipital diploic vein
V. diploica parietalis	parietal diploic vein
V. diploica parietalis	parietal diploic vein
V. emissaria foraminis ovalis	emissary vein of the oval foramen
V. thalamostriata	thalamostriate vein
Ventriculus lateralis	Lateral ventricle
Ventriculus quartus	Fourth ventricle
Ventriculus tertius	Third ventricle
Ventriculus tertius	third ventricle
Vermis	Median vermis
Viscerocranium (human med)	viscerocranium
Vv. Cerebelli dorsales	dorsal cerebellar veins
Vv. cerebri dorsales	Dorsal cerebral veins
Vv. Cerebri dorsales	dorsal cerebral veins
Vv. Cerebri interna	Internal cerebral veins
Vv. choroidea	Choroidal veins
Vv. diploicae	Diploic veins
Vv. medullares	Medullary veins
Vv. meningeae	meningeal veins
Vv. pontis	pontine veins

7.2 Measurements from Amira

Table 16: Morphometric measurements in mm

Morphometric measurements in mm							
	Facial length	Facial width	Cranial length	Cranial width	Cranial height	Skull length	Skull base length
Dog 1	97.10	115.00	112.30	67.74	71.48	208.10	187.30
Dog 2	91.40	102.40	115.00	60.75	59.24	205.60	181.50
Dog 3	84.39	104.00	108.00	62.54	56.77	192.10	174.40
Dog 4	49.36	77.45	73.58	48.91	46.04	123.80	109.70
Dog 5	24.29	95.43	84.43	60.26	53.93	108.60	89.51
Dog 6	31.61	112.80	89.47	63.09	51.99	121.10	97.38
Dog 7	38.72	125.90	93.64	61.67	55.31	132.70	114.60
Dog 8	40.25	127.00	84.18	57.70	54.97	125.50	109.30

Table 17: Craniotomy area Approach Schlager in mm

Craniotomy area in mm		
	Approach Schlager left	Approach Schlager right
Dog 1	2101.95	2047.12
Dog 2	1211.06	1226.38
Dog 3	1175.94	1300.62
Dog 4	594.91	633.16
Dog 5	953.43	1086.99
Dog 6	1395.03	1501.44
Dog 7	1448.56	1524.79
Dog 8	1053.52	1164.69

Table 18: Craniotomy area Approach Steyrer in mm

Craniotomy area in mm		
	Approach Steyrer left	Approach Steyrer right
Dog 1	2349.87	2497.22
Dog 2	1927.74	1698.74
Dog 3	1718.64	1600.20
Dog 4	1017.29	1099.07
Dog 5	1511.92	1603.53
Dog 6	1867.89	1645.71
Dog 7	1808.47	1965.71
Dog 8	1413.71	1388.72

Table 19: Gyri area in mm Dog 1

Gyri area in mm						
Dog 1	brain		Approach Schlager		Approach Steyrer	
	left	right	left	right	left	right
total area	6959.53	6767.55	1955.82	1673.26	2160.55	2244.88
undefined	2782.24	2516.44				
Cortex	4177.29	4251.11				
Gyrus sylvius rostralis	195.75	107.30	185.79	78.05	174.09	87.43
Gyrus sylvius caudalis	112.94	127.10	78.40	82.15	63.39	97.11
Gyrus ectosylvius rostralis	166.35	128.74	166.78	128.74	166.35	128.74
Gyrus ectosylvius medius	100.78	111.53	87.53	111.53	100.78	111.53
Gyrus ectosylvius caudalis	189.89	115.50	134.45	44.17	155.61	68.26
Gyrus suprasylvius rostralis	251.65	293.08	251.65	275.42	239.26	278.45
Gyrus suprasylvius medius	203.95	172.73	77.45	133.68	203.95	172.73
Gyrus ectomarginalis	243.10	291.45	57.30	55.52	217.44	288.80
Gyrus suprasylvius caudalis	247.35	287.50	0.12	60.46	103.61	134.59
Gyrus occipitalis	222.44	210.70			90.57	72.78
Gyrus marginalis	36.65	51.80	25.49	23.32	36.65	51.80
Gyrus endomarginalis	74.43	74.29	59.72		45.77	61.04
Gyrus postcruciatius	330.01	352.53	330.01	292.57	219.31	300.00
Gyrus praecruciatius	137.06	95.31	98.66	51.75		
Gyrus proreus	230.84	259.82	97.87	76.31		33.77

Table 20: Gyri area in mm Dog 2

Gyri area in mm						
Dog 2	brain		Approach Schlager		Approach Steyrer	
	left	right	left	right	left	right
total area	6247.73	6579.66	1355.92	1404.23	1921.84	1948.63
undefined	2298.55	2690.78				4.48
Cortex	3949.18	3888.87				
Gyrus sylvius rostralis	126.61	172.43	120.46	121.00	117.58	90.39
Gyrus sylvius caudalis	186.44	219.62	77.12	79.60	66.98	86.56
Gyrus ectosylvius rostralis	146.40	221.53	137.34	220.38	132.12	194.92
Gyrus ectosylvius medius	128.95	148.56	128.95	148.56	128.95	148.56
Gyrus ectosylvius caudalis	174.82	153.92	136.90	60.62	125.16	77.62
Gyrus suprasylvius rostralis	242.24	149.45	217.22	142.92	189.05	140.98
Gyrus suprasylvius medius	156.06	258.15	106.61	108.62	156.06	258.15
Gyrus ectomarginalis	243.11	220.89	20.90	6.78	208.92	172.62
Gyrus suprasylvius caudalis	198.57	165.08	9.65	90.20	132.29	127.45
Gyrus occipitalis	145.14	137.21			40.40	58.23
Gyrus marginalis	62.47	43.34			62.47	43.34
Gyrus endomarginalis	67.65	56.07			48.93	53.56
Gyrus postcruciatius	237.47	170.75	36.77	53.13	146.69	139.79

Gyrus praecruciatius	236.17	227.42	89.24	100.74	1.78	23.21
Gyrus proreus	255.04	216.20	10.68	18.47		

Table 21: Gyri area in mm Dog 3

Gyri area in mm						
Dog 3	brain		Approach Schlager		Approach Steyrer	
	left	right	left	right	left	right
total area	6852.56	6765.42	1319.51	1516.13	1723.80	1602.78
undefined	3167.88	3111.68				
Cortex	3684.68	3653.74				
Gyrus sylvius rostralis	195.85	142.34	90.34	91.48	92.04	92.41
Gyrus sylvius caudalis	141.30	164.39	32.50	34.98	32.94	50.44
Gyrus ectosylvius rostralis	110.16	179.82	110.16	174.18	107.16	157.06
Gyrus ectosylvius medius	166.31	120.61	159.19	120.61	166.31	120.61
Gyrus ectosylvius caudalis	129.65	109.67	59.46	34.75	65.53	60.22
Gyrus suprasylvius rostralis	220.10	149.67	216.58	136.29	165.15	76.76
Gyrus suprasylvius medius	128.23	146.66	114.73	144.10	128.23	146.66
Gyrus ectomarginalis	222.33	255.31	35.30	92.03	190.70	224.02
Gyrus suprasylvius caudalis	326.25	252.46	2.07	115.65	187.35	181.76
Gyrus occipitalis	114.10	157.44			63.31	73.50
Gyrus marginalis	42.12	49.23		2.83	42.12	49.23
Gyrus endomarginalis	50.44	27.93			45.96	20.94
Gyrus postcruciatius	180.05	174.91	92.01	112.63	124.22	53.80
Gyrus praecruciatius	194.12	148.53	144.15	99.05		
Gyrus proreus	164.08	173.98	22.58	15.89		

Table 22: Gyri area in mm Dog 4

Gyri area in mm						
Dog 4	brain		Approach Schlager		Approach Steyrer	
	left	right	left	right	left	right
total area	4602.65	4613.87	659.83	690.27	1081.66	1191.63
undefined	1992.39	2167.81			0.49	1.09
Cortex	2610.25	2446.06				
Gyrus sylvius rostralis	63.40	120.23	55.49	85.51	55.20	75.39
Gyrus sylvius caudalis	61.03	99.61	44.53	60.49	49.83	58.20
Gyrus ectosylvius rostralis	95.94	87.08	95.94	82.66	95.98	87.08
Gyrus ectosylvius medius	108.55	108.86	106.22	107.19	108.55	108.86
Gyrus ectosylvius caudalis	101.81	106.56	67.33	70.43	89.84	73.82
Gyrus suprasylvius rostralis	257.19	227.93	201.98	150.48	135.90	168.77
Gyrus suprasylvius medius	132.08	116.68	24.28	14.28	132.08	116.68
Gyrus ectomarginalis	161.53	166.97			123.07	159.59
Gyrus suprasylvius caudalis	194.54	159.61		48.16	89.49	88.31
Gyrus occipitalis	118.38	100.45				

Gyrus marginalis	60.32	43.20			6.76	21.48
Gyrus endomarginalis	21.85	34.49				1.79
Gyrus postcruciatu	106.89	127.38			7.32	23.11
Gyrus praecruciatu	122.01	64.84				
Gyrus proreus	97.85	144.84				

Table 23: Gyri area in mm Dog 5

Gyri area in mm						
Dog 5	brain		Approach Schlager		Approach Steyrer	
	left	right	left	right	left	right
total area	6371.50	6601.42	1058.23	1146.10	1714.42	1724.93
undefined	2060.18	2308.48			152.37	89.88
Cortex	4311.32	4292.94				
Gyrus sylvius rostralis	255.82	222.70	70.39	51.94	63.61	45.00
Gyrus sylvius caudalis	119.52	202.17	7.81	17.17	10.89	23.27
Gyrus ectosylvius rostralis	122.75	304.11	67.59	142.46	42.07	111.08
Gyrus ectosylvius medius	216.80	147.79	216.80	147.79	216.80	147.79
Gyrus ectosylvius caudalis	196.86	242.60	155.17	157.94	166.72	173.04
Gyrus suprasylvius rostralis	207.46	158.42	52.34	114.58	31.65	29.88
Gyrus suprasylvius medius	148.58	277.38	148.58	232.04	112.92	181.61
Gyrus ectomarginalis	262.21	367.66	54.00	1.07	161.14	306.37
Gyrus suprasylvius caudalis	375.41	235.84	149.82	114.70	240.44	160.61
Gyrus occipitalis	286.58	233.17			238.48	196.83
Gyrus marginalis	53.87	58.36				
Gyrus endomarginalis	59.74	36.47				
Gyrus postcruciatu	294.26	252.57				
Gyrus praecruciatu	258.12	323.68				
Gyrus proreus	168.12	151.12				

Table 24: Gyri area in mm Dog 6

Gyri area in mm						
Dog 6	brain		Approach Schlager		Approach Steyrer	
	left	right	left	right	left	right
total area	8087.50	7821.14	1591.06	1673.27	1925.33	1776.03
undefined	3268.54	3280.30	16.52	30.40	198.93	188.07
Cortex	4818.96	4540.84				
Gyrus sylvius rostralis	196.09	211.77	101.90	85.48	71.21	52.93
Gyrus sylvius caudalis	146.32	118.92	43.76	62.22	42.24	63.43
Gyrus ectosylvius rostralis	189.56	287.56	131.96	132.14	65.94	26.01
Gyrus ectosylvius medius	175.22	153.76	175.22	153.76	137.22	95.30
Gyrus ectosylvius caudalis	391.13	370.13	276.96	231.27	269.66	252.38
Gyrus suprasylvius rostralis	356.84	142.60	132.89	84.87		
Gyrus suprasylvius medius	115.01	210.53	115.01	210.53	79.20	84.77

Gyrus ectomarginalis	287.13	290.91	78.55	179.78	180.05	155.15
Gyrus suprasylvius caudalis	208.06	302.56	203.20	237.35	207.91	260.07
Gyrus occipitalis	343.58	337.58	25.11	20.97	343.07	325.56
Gyrus marginalis	80.62	94.25		5.23		
Gyrus endomarginalis	153.81	207.64			4.07	22.93
Gyrus postcruciatius	278.86	166.46	1.91	0.46		
Gyrus praecruciatius	271.85	302.99				
Gyrus proreus	151.61	90.56				

Table 25: Gyri area in mm Dog 7

Gyri area in mm						
Dog 7	brain		Approach Schlager		Approach Steyrer	
	left	right	left	right	left	right
total area	6765.00	6564.62	1599.57	1752.20	1977.30	1998.80
undefined	2514.78	2120.78		9.02	60.67	23.66
Cortex	4250.22	4443.84				
Gyrus sylvius rostralis	187.53	78.19	111.82	40.06	74.59	45.40
Gyrus sylvius caudalis	61.39	32.58	53.35	3.67	48.28	11.89
Gyrus ectosylvius rostralis	95.90	108.44	95.90	74.26	89.91	68.81
Gyrus ectosylvius medius	135.33	191.06	135.33	191.06	135.33	191.06
Gyrus ectosylvius caudalis	290.38	442.32	176.53	183.07	163.11	202.57
Gyrus suprasylvius rostralis	408.06	532.85	286.14	308.87	169.24	181.90
Gyrus suprasylvius medius	126.17	221.22	125.85	215.85	126.17	205.90
Gyrus ectomarginalis	214.21	147.11	56.54	84.48	214.21	147.11
Gyrus suprasylvius caudalis	435.61	461.71	292.65	308.86	269.51	374.61
Gyrus occipitalis	306.63	305.12	4.19	10.89	273.24	191.16
Gyrus marginalis	238.95	84.39		29.39	95.68	69.37
Gyrus endomarginalis		166.58		10.62		35.32
Gyrus postcruciatius	170.03	216.12	61.24	68.98	5.72	2.21
Gyrus praecruciatius	269.56	396.79	2.52			
Gyrus proreus	136.37	102.28				

Table 26: Gyri area in mm Dog 8

Gyri area in mm						
Dog 8	brain		Approach Schlager		Approach Steyrer	
	left	right	left	right	left	right
total area	6329.12	6666.73	1259.77	1312.62	1536.54	1466.23
undefined	2187.77	2870.10		12.73	18.31	9.76
Cortex	4141.36	3796.62				
Gyrus sylvius rostralis	239.65	154.07	47.16	44.99	48.10	45.26
Gyrus sylvius caudalis	71.73	20.96	1.71		1.86	1.52
Gyrus ectosylvius rostralis	150.02	178.01	102.78	121.76	89.28	101.41
Gyrus ectosylvius medius	163.61	120.22	163.61	120.22	163.61	120.22

Gyrus ectosylvius caudalis	383.04	278.70	124.37	117.57	124.68	140.34
Gyrus suprasylvius rostralis	323.25	313.95	237.90	211.80	205.49	168.46
Gyrus suprasylvius medius	162.55	183.28	160.37	179.82	162.55	181.70
Gyrus ectomarginalis	281.02	229.08	121.30	117.76	239.84	176.39
Gyrus suprasylvius caudalis	170.30	279.98	126.86	149.88	145.56	171.31
Gyrus occipitalis	226.47	253.66			18.11	37.55
Gyrus marginalis	101.44	101.02		0.06	87.68	71.32
Gyrus endomarginalis	91.37	93.42				6.64
Gyrus postcruciatu	229.74	130.38	12.76	44.58	2.97	9.03
Gyrus praecruciatu	351.06	421.36		1.47		
Gyrus proreus	115.10	83.07				

Table 27: Sinus frontalis

Sinus frontalis						
	existence		Approach Schlager		Approach Steyrer	
	left	right	left	right	left	right
Dog 1	Yes	Yes	Yes	Yes	No	No
Dog 2	Yes	Yes	Yes	Yes	Yes	No
Dog 3	Yes	Yes	Yes	Yes	Yes	No
Dog 4	Yes	Yes	No	No	No	No
Dog 5	No	Yes	No	No	No	No
Dog 6	No	No	No	No	No	No
Dog 7	Yes	Yes	No	No	No	No
Dog 8	Yes	Yes	No	No	No	No

7.3 Statistics

Table 28: Statistics Gyrus sylvius rostralis

Kreuztabelle

Anzahl

Methode Name			Gyrus sylvius rostralis	
			1	Gesamt
Approach Schlager left	Gruppe	1	4	4
		2	4	4
		Gesamt	8	8
Approach Schlager right	Gruppe	1	4	4
		2	4	4
		Gesamt	8	8
Approach Steyrer left	Gruppe	1	4	4
		2	4	4
		Gesamt	8	8
Approach Steyrer right	Gruppe	1	4	4
		2	4	4
		Gesamt	8	8

Chi-Quadrat-Tests

Methode Name		Wert
Approach Schlager left	Chi-Quadrat nach Pearson	a
	Anzahl der gültigen Fälle	8
Approach Schlager right	Chi-Quadrat nach Pearson	a
	Anzahl der gültigen Fälle	8
Approach Steyrer left	Chi-Quadrat nach Pearson	a
	Anzahl der gültigen Fälle	8
Approach Steyrer right	Chi-Quadrat nach Pearson	a
	Anzahl der gültigen Fälle	8

a. Es werden keine Statistiken berechnet, da Gyrus sylvius rostralis eine Konstante ist

Table 29: Statistics *Gyrus sylvius caudalis*

Kreuztabelle

Anzahl

Methode Name			Gyrus sylvius caudalis		Gesamt
			0	1	
Approach Schlager left	Gruppe	1		4	4
		2		4	4
		Gesamt		8	8
Approach Schlager right	Gruppe	1	0	4	4
		2	1	3	4
		Gesamt	1	7	8
Approach Steyrer left	Gruppe	1		4	4
		2		4	4
		Gesamt		8	8
Approach Steyrer right	Gruppe	1		4	4
		2		4	4
		Gesamt		8	8

Chi-Quadrat-Tests

Methode Name		Wert	df	Asymptotische Signifikanz (2-seitig)
Approach Schlager left	Chi-Quadrat nach Pearson	^a .		
	Anzahl der gültigen Fälle	8		
Approach Schlager right	Chi-Quadrat nach Pearson	1,143 ^b	1	,285
	Kontinuitätskorrektur ^c	,000	1	1,000
	Likelihood-Quotient	1,530	1	,216
	Zusammenhang linear-mit-linear	1,000	1	,317
	Anzahl der gültigen Fälle	8		
Approach Steyrer left	Chi-Quadrat nach Pearson	^a .		
	Anzahl der gültigen Fälle	8		
Approach Steyrer right	Chi-Quadrat nach Pearson	^a .		
	Anzahl der gültigen Fälle	8		

a. Es werden keine Statistiken berechnet, da *Gyrus sylvius caudalis* eine Konstante ist

b. 4 Zellen (100,0%) haben eine erwartete Häufigkeit kleiner 5. Die minimale erwartete Häufigkeit ist ,50.

c. Wird nur für eine 2x2-Tabelle berechnet

Chi-Quadrat-Tests

Methode Name		Exakte Signifikanz (2-seitig)	Exakte Signifikanz (1-seitig)
Approach Schlager right	Exakter Test nach Fisher	1,000	,500

Table 30: Statistics *Gyrus ectosylvius rostralis***Kreuztabelle**

Anzahl			Gyrus ectosylvius rostralis	
Methode Name			1	Gesamt
Approach Schlager left	Gruppe	1	4	4
		2	4	4
		Gesamt	8	8
Approach Schlager right	Gruppe	1	4	4
		2	4	4
		Gesamt	8	8
Approach Steyrer left	Gruppe	1	4	4
		2	4	4
		Gesamt	8	8
Approach Steyrer right	Gruppe	1	4	4
		2	4	4
		Gesamt	8	8

Chi-Quadrat-Tests

Methode Name		Wert
Approach Schlager left	Chi-Quadrat nach Pearson	a
	Anzahl der gültigen Fälle	8
Approach Schlager right	Chi-Quadrat nach Pearson	a
	Anzahl der gültigen Fälle	8
Approach Steyrer left	Chi-Quadrat nach Pearson	a
	Anzahl der gültigen Fälle	8
Approach Steyrer right	Chi-Quadrat nach Pearson	a
	Anzahl der gültigen Fälle	8

a. Es werden keine Statistiken berechnet, da *Gyrus ectosylvius rostralis* eine Konstante ist

Table 31: Statistics *Gyrus ectosylvius medius***Kreuztabelle**

Anzahl			Gyrus ectosylvius medius	
Methode Name			1	Gesamt
Approach Schlager left	Gruppe	1	4	4
		2	4	4
		Gesamt	8	8
Approach Schlager right	Gruppe	1	4	4
		2	4	4
		Gesamt	8	8
Approach Steyrer left	Gruppe	1	4	4
		2	4	4
		Gesamt	8	8
Approach Steyrer right	Gruppe	1	4	4
		2	4	4
		Gesamt	8	8

Chi-Quadrat-Tests

Methode Name		Wert
Approach Schlager left	Chi-Quadrat nach Pearson	a
	Anzahl der gültigen Fälle	8
Approach Schlager right	Chi-Quadrat nach Pearson	a
	Anzahl der gültigen Fälle	8
Approach Steyrer left	Chi-Quadrat nach Pearson	a
	Anzahl der gültigen Fälle	8
Approach Steyrer right	Chi-Quadrat nach Pearson	a
	Anzahl der gültigen Fälle	8

a. Es werden keine Statistiken berechnet, da *Gyrus ectosylvius medius* eine Konstante ist

Table 32: Statistics *Gyrus ectosylvius caudalis*

Kreuztabelle

Anzahl

Methode Name			Gyrus ectosylvius caudalis	
			1	Gesamt
Approach Schlager left	Gruppe	1	4	4
		2	4	4
		Gesamt	8	8
Approach Schlager right	Gruppe	1	4	4
		2	4	4
		Gesamt	8	8
Approach Steyrer left	Gruppe	1	4	4
		2	4	4
		Gesamt	8	8
Approach Steyrer right	Gruppe	1	4	4
		2	4	4
		Gesamt	8	8

Chi-Quadrat-Tests

Methode Name		Wert
Approach Schlager left	Chi-Quadrat nach Pearson	a
	Anzahl der gültigen Fälle	8
Approach Schlager right	Chi-Quadrat nach Pearson	a
	Anzahl der gültigen Fälle	8
Approach Steyrer left	Chi-Quadrat nach Pearson	a
	Anzahl der gültigen Fälle	8
Approach Steyrer right	Chi-Quadrat nach Pearson	a
	Anzahl der gültigen Fälle	8

a. Es werden keine Statistiken berechnet, da *Gyrus ectosylvius caudalis* eine Konstante ist

Table 33: Statistics *Gyrus suprasylvius rostralis*

Anzahl

Methode Name			Gyrus suprasylvius rostralis		Gesamt
			0	1	
Approach Schlager left	Gruppe	1		4	4
		2		4	4
		Gesamt		8	8
Approach Schlager right	Gruppe	1		4	4
		2		4	4
		Gesamt		8	8
Approach Steyrer left	Gruppe	1	0	4	4
		2	1	3	4
		Gesamt	1	7	8
Approach Steyrer right	Gruppe	1	0	4	4
		2	1	3	4
		Gesamt	1	7	8

Chi-Quadrat-Tests

Methode Name		Wert	df	Asymptotische Signifikanz (2-seitig)
Approach Schlager left	Chi-Quadrat nach Pearson	^a		
	Anzahl der gültigen Fälle	8		
Approach Schlager right	Chi-Quadrat nach Pearson	^a		
	Anzahl der gültigen Fälle	8		
Approach Steyrer left	Chi-Quadrat nach Pearson	1,143 ^b	1	,285
	Kontinuitätskorrektur ^c	,000	1	1,000
	Likelihood-Quotient	1,530	1	,216
	Zusammenhang linear-mit-linear	1,000	1	,317
	Anzahl der gültigen Fälle	8		
Approach Steyrer right	Chi-Quadrat nach Pearson	1,143 ^b	1	,285
	Kontinuitätskorrektur ^c	,000	1	1,000
	Likelihood-Quotient	1,530	1	,216
	Zusammenhang linear-mit-linear	1,000	1	,317
	Anzahl der gültigen Fälle	8		

a. Es werden keine Statistiken berechnet, da *Gyrus suprasylvius rostralis* eine Konstante ist

b. 4 Zellen (100,0%) haben eine erwartete Häufigkeit kleiner 5. Die minimale erwartete Häufigkeit ist ,50.

c. Wird nur für eine 2x2-Tabelle berechnet

Chi-Quadrat-Tests

Methode Name		Exakte Signifikanz (2-seitig)	Exakte Signifikanz (1-seitig)
Approach Steyrer left	Exakter Test nach Fisher	1,000	,500
Approach Steyrer right	Exakter Test nach Fisher	1,000	,500

Table 34: Statistics Gyrus suprasylvius medius

Anzahl			Gyrus suprasylvius medius	
Methode Name			1	Gesamt
Approach Schlager left	Gruppe	1	4	4
		2	4	4
		Gesamt	8	8
Approach Schlager right	Gruppe	1	4	4
		2	4	4
		Gesamt	8	8
Approach Steyrer left	Gruppe	1	4	4
		2	4	4
		Gesamt	8	8
Approach Steyrer right	Gruppe	1	4	4
		2	4	4
		Gesamt	8	8

Chi-Quadrat-Tests

Methode Name		Wert
Approach Schlager left	Chi-Quadrat nach Pearson	^a .
	Anzahl der gültigen Fälle	8
Approach Schlager right	Chi-Quadrat nach Pearson	^a .
	Anzahl der gültigen Fälle	8
Approach Steyrer left	Chi-Quadrat nach Pearson	^a .
	Anzahl der gültigen Fälle	8
Approach Steyrer right	Chi-Quadrat nach Pearson	^a .
	Anzahl der gültigen Fälle	8

a. Es werden keine Statistiken berechnet, da Gyrus suprasylvius medius eine Konstante ist

Table 35: Statistics *Gyrus ectomarginalis*

Kreuztabelle

Anzahl			Gyrus ectomarginalis		Gesamt
			0	1	
Methode Name					
Approach Schlager left	Gruppe	1	1	3	4
		2	0	4	4
		Gesamt	1	7	8
Approach Schlager right	Gruppe	1	1	3	4
		2	0	4	4
		Gesamt	1	7	8
Approach Steyrer left	Gruppe	1		4	4
		2		4	4
		Gesamt		8	8
Approach Steyrer right	Gruppe	1		4	4
		2		4	4
		Gesamt		8	8

Chi-Quadrat-Tests

Methode Name		Wert	df	Asymptotische Signifikanz (2-seitig)
Approach Schlager left	Chi-Quadrat nach Pearson	1,143 ^a	1	,285
	Kontinuitätskorrektur ^b	,000	1	1,000
	Likelihood-Quotient	1,530	1	,216
	Zusammenhang linear-mit-linear	1,000	1	,317
	Anzahl der gültigen Fälle	8		
Approach Schlager right	Chi-Quadrat nach Pearson	1,143 ^a	1	,285
	Kontinuitätskorrektur ^b	,000	1	1,000
	Likelihood-Quotient	1,530	1	,216
	Zusammenhang linear-mit-linear	1,000	1	,317
	Anzahl der gültigen Fälle	8		
Approach Steyrer left	Chi-Quadrat nach Pearson	. ^c		
	Anzahl der gültigen Fälle	8		
Approach Steyrer right	Chi-Quadrat nach Pearson	. ^c		
	Anzahl der gültigen Fälle	8		

a. 4 Zellen (100,0%) haben eine erwartete Häufigkeit kleiner 5. Die minimale erwartete Häufigkeit ist ,50.

b. Wird nur für eine 2x2-Tabelle berechnet

c. Es werden keine Statistiken berechnet, da *Gyrus ectomarginalis* eine Konstante ist

Chi-Quadrat-Tests

Methode Name		Exakte Signifikanz (2-seitig)	Exakte Signifikanz (1-seitig)
Approach Schlager left	Exakter Test nach Fisher	1,000	,500
Approach Schlager right	Exakter Test nach Fisher	1,000	,500

Table 36: Statistics Gyrus suprasylvius caudalis

Kreuztabelle

Anzahl			Gyrus suprasylvius caudalis		
Methode Name			0	1	Gesamt
Approach Schlager left	Gruppe	1	1	3	4
		2	0	4	4
		Gesamt	1	7	8
Approach Schlager right	Gruppe	1		4	4
		2		4	4
		Gesamt		8	8
Approach Steyrer left	Gruppe	1		4	4
		2		4	4
		Gesamt		8	8
Approach Steyrer right	Gruppe	1		4	4
		2		4	4
		Gesamt		8	8

Chi-Quadrat-Tests

Methode Name		Wert	df	Asymptotische Signifikanz (2-seitig)
Approach Schlager left	Chi-Quadrat nach Pearson	1,143 ^a	1	,285
	Kontinuitätskorrektur ^b	,000	1	1,000
	Likelihood-Quotient	1,530	1	,216
	Zusammenhang linear-mit-linear	1,000	1	,317
	Anzahl der gültigen Fälle	8		
Approach Schlager right	Chi-Quadrat nach Pearson	.c		
	Anzahl der gültigen Fälle	8		
Approach Steyrer left	Chi-Quadrat nach Pearson	.c		
	Anzahl der gültigen Fälle	8		
Approach Steyrer right	Chi-Quadrat nach Pearson	.c		
	Anzahl der gültigen Fälle	8		

a. 4 Zellen (100,0%) haben eine erwartete Häufigkeit kleiner 5. Die minimale erwartete Häufigkeit ist ,50.

b. Wird nur für eine 2x2-Tabelle berechnet

c. Es werden keine Statistiken berechnet, da Gyrus suprasylvius caudalis eine Konstante ist

Chi-Quadrat-Tests

Methode Name		Exakte Signifikanz (2-seitig)	Exakte Signifikanz (1-seitig)
Approach Schlager left	Exakter Test nach Fisher	1,000	,500

Table 37: Statistics Gyrus occipitalis

Anzahl			Gyrus occipitalis		
Methode Name			0	1	Gesamt
Approach Schlager left	Gruppe	1	4	0	4
		2	2	2	4
		Gesamt	6	2	8
Approach Schlager right	Gruppe	1	4	0	4
		2	2	2	4
		Gesamt	6	2	8
Approach Steyrer left	Gruppe	1	1	3	4
		2	0	4	4
		Gesamt	1	7	8
Approach Steyrer right	Gruppe	1	1	3	4
		2	0	4	4
		Gesamt	1	7	8

Chi-Quadrat-Tests

Methode Name		Wert	df	Asymptotische Signifikanz (2-seitig)
Approach Schlager left	Chi-Quadrat nach Pearson	2,667 ^a	1	,102
	Kontinuitätskorrektur ^b	,667	1	,414
	Likelihood-Quotient	3,452	1	,063
	Zusammenhang linear-mit-linear	2,333	1	,127
	Anzahl der gültigen Fälle	8		
Approach Schlager right	Chi-Quadrat nach Pearson	2,667 ^a	1	,102
	Kontinuitätskorrektur ^b	,667	1	,414
	Likelihood-Quotient	3,452	1	,063
	Zusammenhang linear-mit-linear	2,333	1	,127
	Anzahl der gültigen Fälle	8		
Approach Steyrer left	Chi-Quadrat nach Pearson	1,143 ^c	1	,285
	Kontinuitätskorrektur ^b	,000	1	1,000
	Likelihood-Quotient	1,530	1	,216
	Zusammenhang linear-mit-linear	1,000	1	,317
	Anzahl der gültigen Fälle	8		
Approach Steyrer right	Chi-Quadrat nach Pearson	1,143 ^c	1	,285
	Kontinuitätskorrektur ^b	,000	1	1,000
	Likelihood-Quotient	1,530	1	,216
	Zusammenhang linear-mit-linear	1,000	1	,317
	Anzahl der gültigen Fälle	8		

a. 4 Zellen (100,0%) haben eine erwartete Häufigkeit kleiner 5. Die minimale erwartete Häufigkeit ist 1,00.

b. Wird nur für eine 2x2-Tabelle berechnet

c. 4 Zellen (100,0%) haben eine erwartete Häufigkeit kleiner 5. Die minimale erwartete Häufigkeit ist ,50.

Table 38: Fisher test Gyrus occipitalis

Chi-Quadrat-Tests

Methode Name		Exakte Signifikanz (2-seitig)	Exakte Signifikanz (1-seitig)
Approach Schlager left	Exakter Test nach Fisher	,429	,214
Approach Schlager right	Exakter Test nach Fisher	,429	,214
Approach Steyrer left	Exakter Test nach Fisher	1,000	,500
Approach Steyrer right	Exakter Test nach Fisher	1,000	,500

Table 39: Statistics Gyrus marginalis

Kreuztabelle

Anzahl

Methode Name			Gyrus marginalis		Gesamt
			0	1	
Approach Schlager left	Gruppe	1	3	1	4
		2	4	0	4
		Gesamt	7	1	8
Approach Schlager right	Gruppe	1	2	2	4
		2	1	3	4
		Gesamt	3	5	8
Approach Steyrer left	Gruppe	1	0	4	4
		2	3	1	4
		Gesamt	3	5	8
Approach Steyrer right	Gruppe	1	0	4	4
		2	2	2	4
		Gesamt	2	6	8

Table 40: Statistic tests Gyrus marginalis

Chi-Quadrat-Tests				
Methode Name		Wert	df	Asymptotische Signifikanz (2-seitig)
Approach Schlager left	Chi-Quadrat nach Pearson	1,143 ^a	1	,285
	Kontinuitätskorrektur ^b	,000	1	1,000
	Likelihood-Quotient	1,530	1	,216
	Zusammenhang linear-mit-linear	1,000	1	,317
	Anzahl der gültigen Fälle	8		
Approach Schlager right	Chi-Quadrat nach Pearson	,533 ^c	1	,465
	Kontinuitätskorrektur ^b	,000	1	1,000
	Likelihood-Quotient	,541	1	,462
	Zusammenhang linear-mit-linear	,467	1	,495
	Anzahl der gültigen Fälle	8		
Approach Steyrer left	Chi-Quadrat nach Pearson	4,800 ^c	1	,028
	Kontinuitätskorrektur ^b	2,133	1	,144
	Likelihood-Quotient	6,086	1	,014
	Zusammenhang linear-mit-linear	4,200	1	,040
	Anzahl der gültigen Fälle	8		
Approach Steyrer right	Chi-Quadrat nach Pearson	2,667 ^d	1	,102
	Kontinuitätskorrektur ^b	,667	1	,414
	Likelihood-Quotient	3,452	1	,063
	Zusammenhang linear-mit-linear	2,333	1	,127
	Anzahl der gültigen Fälle	8		

b. Wird nur für eine 2x2-Tabelle berechnet

c. 4 Zellen (100,0%) haben eine erwartete Häufigkeit kleiner 5. Die minimale erwartete Häufigkeit ist 1,50.

d. 4 Zellen (100,0%) haben eine erwartete Häufigkeit kleiner 5. Die minimale erwartete Häufigkeit ist 1,00.

Chi-Quadrat-Tests			
Methode Name		Exakte Signifikanz (2-seitig)	Exakte Signifikanz (1-seitig)
Approach Schlager left	Exakter Test nach Fisher	1,000	,500
Approach Schlager right	Exakter Test nach Fisher	1,000	,500
Approach Steyrer left	Exakter Test nach Fisher	,143	,071
Approach Steyrer right	Exakter Test nach Fisher	,429	,214

Table 41: Statistics Gyrus endomarginalis

Kreuztabelle

Anzahl			Gyrus endomarginalis		Gesamt
Methode Name			0	1	
Approach Schlager left	Gruppe	1	3	1	4
		2	4	0	4
		Gesamt	7	1	8
Approach Schlager right	Gruppe	1	4	0	4
		2	3	1	4
		Gesamt	7	1	8
Approach Steyrer left	Gruppe	1	1	3	4
		2	2	2	4
		Gesamt	3	5	8
Approach Steyrer right	Gruppe	1	0	4	4
		2	1	3	4
		Gesamt	1	7	8

Chi-Quadrat-Tests

Methode Name		Wert	df	Asymptotische Signifikanz (2-seitig)
Approach Schlager left	Chi-Quadrat nach Pearson	1,143 ^a	1	,285
	Kontinuitätskorrektur ^b	,000	1	1,000
	Likelihood-Quotient	1,530	1	,216
	Zusammenhang linear-mit-linear	1,000	1	,317
	Anzahl der gültigen Fälle	8		
Approach Schlager right	Chi-Quadrat nach Pearson	1,143 ^a	1	,285
	Kontinuitätskorrektur ^b	,000	1	1,000
	Likelihood-Quotient	1,530	1	,216
	Zusammenhang linear-mit-linear	1,000	1	,317
	Anzahl der gültigen Fälle	8		
Approach Steyrer left	Chi-Quadrat nach Pearson	,533 ^c	1	,465
	Kontinuitätskorrektur ^b	,000	1	1,000
	Likelihood-Quotient	,541	1	,462
	Zusammenhang linear-mit-linear	,467	1	,495
	Anzahl der gültigen Fälle	8		
Approach Steyrer right	Chi-Quadrat nach Pearson	1,143 ^a	1	,285
	Kontinuitätskorrektur ^b	,000	1	1,000
	Likelihood-Quotient	1,530	1	,216
	Zusammenhang linear-mit-linear	1,000	1	,317
	Anzahl der gültigen Fälle	8		

a. 4 Zellen (100,0%) haben eine erwartete Häufigkeit kleiner 5. Die minimale erwartete Häufigkeit ist ,50.

b. Wird nur für eine 2x2-Tabelle berechnet

c. 4 Zellen (100,0%) haben eine erwartete Häufigkeit kleiner 5. Die minimale erwartete Häufigkeit ist 1,50.

Table 42: chi-square test Gyrus endomarginalis

Chi-Quadrat-Tests

Methode	Name	Exakte Signifikanz (2- seitig)	Exakte Signifikanz (1- seitig)
Approach Schlager left	Exakter Test nach Fisher	1,000	,500
Approach Schlager right	Exakter Test nach Fisher	1,000	,500
Approach Steyrer left	Exakter Test nach Fisher	1,000	,500
Approach Steyrer right	Exakter Test nach Fisher	1,000	,500

Table 43: Statistics *Gyrus postcruciatu*s

Kreuztabelle

Anzahl			Gyrus postcruciatu		
			0	1	Gesamt
Approach Schlager left	Gruppe	1	1	3	4
		2	1	3	4
		Gesamt	2	6	8
Approach Schlager right	Gruppe	1	1	3	4
		2	1	3	4
		Gesamt	2	6	8
Approach Steyrer left	Gruppe	1	0	4	4
		2	2	2	4
		Gesamt	2	6	8
Approach Steyrer right	Gruppe	1	0	4	4
		2	2	2	4
		Gesamt	2	6	8

Chi-Quadrat-Tests

Methode Name		Wert	df	Asymptotische Signifikanz (2-seitig)
Approach Schlager left	Chi-Quadrat nach Pearson	,000 ^a	1	1,000
	Kontinuitätskorrektur ^b	,000	1	1,000
	Likelihood-Quotient	,000	1	1,000
	Zusammenhang linear-mit-linear	,000	1	1,000
	Anzahl der gültigen Fälle	8		
Approach Schlager right	Chi-Quadrat nach Pearson	,000 ^a	1	1,000
	Kontinuitätskorrektur ^b	,000	1	1,000
	Likelihood-Quotient	,000	1	1,000
Approach Schlager right	Zusammenhang linear-mit-linear	,000	1	1,000
	Anzahl der gültigen Fälle	8		
Approach Steyrer left	Chi-Quadrat nach Pearson	2,667 ^a	1	,102
	Kontinuitätskorrektur ^b	,667	1	,414
	Likelihood-Quotient	3,452	1	,063
	Zusammenhang linear-mit-linear	2,333	1	,127
	Anzahl der gültigen Fälle	8		
Approach Steyrer right	Chi-Quadrat nach Pearson	2,667 ^a	1	,102
	Kontinuitätskorrektur ^b	,667	1	,414
	Likelihood-Quotient	3,452	1	,063
	Zusammenhang linear-mit-linear	2,333	1	,127
	Anzahl der gültigen Fälle	8		

a. 4 Zellen (100,0%) haben eine erwartete Häufigkeit kleiner 5. Die minimale erwartete Häufigkeit ist 1,00.

b. Wird nur für eine 2x2-Tabelle berechnet

Table 44: Fisher test *Gyrus postcruciatus*

Chi-Quadrat-Tests

Methode Name		Exakte Signifikanz (2-seitig)	Exakte Signifikanz (1-seitig)
Approach Schlager left	Exakter Test nach Fisher	1,000	,786
Approach Schlager right	Exakter Test nach Fisher	1,000	,786
Approach Steyrer left	Exakter Test nach Fisher	,429	,214
Approach Steyrer right	Exakter Test nach Fisher	,429	,214

Table 45: Statistics *Gyrus praecruciatius*

Kreuztabelle

Anzahl

Methode Name			Gyrus praecruciatius		Gesamt
			0	1	
Approach Schlager left	Gruppe	1	1	3	4
Approach Schlager left	Gruppe	2	3	1	4
		Gesamt	4	4	8
Approach Schlager right	Gruppe	1	1	3	4
		2	3	1	4
		Gesamt	4	4	8
Approach Steyrer left	Gruppe	1	3	1	4
		2	4	0	4
		Gesamt	7	1	8
Approach Steyrer right	Gruppe	1	3	1	4
		2	4	0	4
		Gesamt	7	1	8

Table 46: Statistic tests *Gyrus praecruciatu*s

Chi-Quadrat-Tests

Methode Name		Wert	df	Asymptotische Signifikanz (2-seitig)
Approach Schlager left	Chi-Quadrat nach Pearson	2,000 ^a	1	,157
	Kontinuitätskorrektur ^b	,500	1	,480
	Likelihood-Quotient	2,093	1	,148
	Zusammenhang linear-mit-linear	1,750	1	,186
	Anzahl der gültigen Fälle	8		
Approach Schlager right	Chi-Quadrat nach Pearson	2,000 ^a	1	,157
	Kontinuitätskorrektur ^b	,500	1	,480
	Likelihood-Quotient	2,093	1	,148
	Zusammenhang linear-mit-linear	1,750	1	,186
	Anzahl der gültigen Fälle	8		
Approach Steyrer left	Chi-Quadrat nach Pearson	1,143 ^c	1	,285
	Kontinuitätskorrektur ^b	,000	1	1,000
	Likelihood-Quotient	1,530	1	,216
	Zusammenhang linear-mit-linear	1,000	1	,317
Approach Steyrer left	Anzahl der gültigen Fälle	8		
Approach Steyrer right	Chi-Quadrat nach Pearson	1,143 ^c	1	,285
	Kontinuitätskorrektur ^b	,000	1	1,000
	Likelihood-Quotient	1,530	1	,216
	Zusammenhang linear-mit-linear	1,000	1	,317
	Anzahl der gültigen Fälle	8		

Chi-Quadrat-Tests

Methode Name		Exakte Signifikanz (2-seitig)	Exakte Signifikanz (1-seitig)
Approach Schlager left	Exakter Test nach Fisher	,486	,243
Approach Schlager right	Exakter Test nach Fisher	,486	,243
Approach Steyrer left	Exakter Test nach Fisher	1,000	,500
Approach Steyrer right	Exakter Test nach Fisher	1,000	,500

Table 47: Statistics *Gyrus proreus*

Kreuztabelle

Anzahl			Gyrus proreus		
Methode Name			0	1	Gesamt
Approach Schlager left	Gruppe	1	1	3	4
		2	4	0	4
		Gesamt	5	3	8
Approach Schlager right	Gruppe	1	1	3	4
		2	4	0	4
		Gesamt	5	3	8
Approach Steyrer left	Gruppe	1	4		4
		2	4		4
		Gesamt	8		8
Approach Steyrer right	Gruppe	1	3	1	4
		2	4	0	4
		Gesamt	7	1	8

Chi-Quadrat-Tests

Methode Name		Wert	df	Asymptotische Signifikanz (2-seitig)
Approach Schlager left	Chi-Quadrat nach Pearson	4,800 ^a	1	,028
	Kontinuitätskorrektur ^b	2,133	1	,144
	Likelihood-Quotient	6,086	1	,014
	Zusammenhang linear-mit-linear	4,200	1	,040
	Anzahl der gültigen Fälle	8		
Approach Schlager right	Chi-Quadrat nach Pearson	4,800 ^a	1	,028
	Kontinuitätskorrektur ^b	2,133	1	,144
	Likelihood-Quotient	6,086	1	,014
	Zusammenhang linear-mit-linear	4,200	1	,040
	Anzahl der gültigen Fälle	8		
Approach Steyrer left	Chi-Quadrat nach Pearson	. ^c		
	Anzahl der gültigen Fälle	8		
Approach Steyrer right	Chi-Quadrat nach Pearson	1,143 ^d	1	,285
	Kontinuitätskorrektur ^b	,000	1	1,000
	Likelihood-Quotient	1,530	1	,216
	Zusammenhang linear-mit-linear	1,000	1	,317
	Anzahl der gültigen Fälle	8		

a. 4 Zellen (100,0%) haben eine erwartete Häufigkeit kleiner 5. Die minimale erwartete Häufigkeit ist 1,50.

b. Wird nur für eine 2x2-Tabelle berechnet

c. Es werden keine Statistiken berechnet, da Gyrus proreus eine Konstante ist

d. 4 Zellen (100,0%) haben eine erwartete Häufigkeit kleiner 5. Die minimale erwartete Häufigkeit ist ,50.

Table 48: Fisher test Gyrus proreus

Chi-Quadrat-Tests

Methode Name		Exakte Signifikanz (2-seitig)	Exakte Signifikanz (1-seitig)
Approach Schlager left	Exakter Test nach Fisher	,143	,071
Approach Schlager right	Exakter Test nach Fisher	,143	,071
Approach Steyrer right	Exakter Test nach Fisher	1,000	,500

Table 49: Statistics craniotomy and gyri area

Gruppenstatistiken

	group	N	Mittelwert	Standardabweichung	Standardfehler des Mittelwertes
Craniotomy_Site_Schlager_left	1	4	1270,9665	621,88202	310,94101
	2	4	1212,6335	245,91894	122,95947
Craniotomy_Site_Schlager_right	1	4	1301,8176	579,73434	289,86717
	2	4	1319,4805	226,03344	113,01672
Craniotomy_Site_Steyrer_left	1	4	1753,3850	556,54953	278,27477
	2	4	1650,4940	221,72501	110,86251
Craniotomy_Site_Steyrer_right	1	4	1723,8064	578,60798	289,30399
	2	4	1650,9187	238,12893	119,06446
Brain_Area_Schlager_left	1	4	1322,7681	529,57577	264,78788
	2	4	1377,1552	265,02442	132,51221
Brain_Area_Schlager_right	1	4	1320,9728	434,70530	217,35265
	2	4	1471,0462	289,04088	144,52044
Brain_Area_Steyrer_left	1	4	1721,9615	462,71207	231,35604
	2	4	1788,3991	202,76063	101,38031
Brain_Area_Steyrer_right	1	4	1746,9809	453,78909	226,89455
	2	4	1741,4953	218,66516	109,33258

Test bei unabhängigen Stichproben

Annahmen=Varianzen sind gleich,
Statistik=T-Test für die Mittelwertgleichheit
Sig. (2-seitig)

Craniotomy_Site_Schlager_left	,867
Craniotomy_Site_Schlager_right	,957
Craniotomy_Site_Steyrer_left	,743
Craniotomy_Site_Steyrer_right	,824
Brain_Area_Schlager_left	,860
Brain_Area_Schlager_right	,586
Brain_Area_Steyrer_left	,801
Brain_Area_Steyrer_right	,983

Table 50: Statistics craniotomy sides compared

Statistik bei gepaarten Stichproben

		Mittelwert	N	Standardabweichung	Standardfehler des Mittelwertes
Paaren 1	Craniotomy_Site_Schlager_left	1241,8000	8	438,90214	155,17534
	Craniotomy_Site_Schlager_right	1310,6490	8	407,46131	144,05933
Paaren 2	Craniotomy_Site_Steyrer_left	1701,9395	8	396,03412	140,01921
	Craniotomy_Site_Steyrer_right	1687,3626	8	411,46133	145,47355
Paaren 3	Brain_Area_Schlager_left	1349,9617	8	388,76751	137,45007
	Brain_Area_Schlager_right	1396,0095	8	351,03603	124,10998
Paaren 4	Brain_Area_Steyrer_left	1755,1803	8	332,62397	117,60033
	Brain_Area_Steyrer_right	1744,2381	8	329,77853	116,59432

Test bei gepaarten Stichproben

Statistik= Sig. (2-seitig)

Paaren 1	Craniotomy_Site_Schlager_left - Craniotomy_Site_Schlager_right	,020
Paaren 2	Craniotomy_Site_Steyrer_left - Craniotomy_Site_Steyrer_right	,802
Paaren 3	Brain_Area_Schlager_left - Brain_Area_Schlager_right	,396
Paaren 4	Brain_Area_Steyrer_left - Brain_Area_Steyrer_right	,751

Table 51: Statistics approaches compared

Statistik bei gepaarten Stichproben

		Mittelwert	N	Standardabweichung	Standardfehler des Mittelwertes
Paaren 1	Craniotomy_Site_Schlager_left	1241,8000	8	438,90214	155,17534
	Craniotomy_Site_Steyrer_left	1701,9395	8	396,03412	140,01921
Paaren 2	Craniotomy_Site_Schlager_right	1310,6490	8	407,46131	144,05933
	Craniotomy_Site_Steyrer_right	1687,3626	8	411,46133	145,47355
Paaren 3	Brain_Area_Schlager_left	1349,9617	8	388,76751	137,45007
	Brain_Area_Steyrer_left	1755,1803	8	332,62397	117,60033
Paaren 4	Brain_Area_Schlager_right	1396,0095	8	351,03603	124,10998
	Brain_Area_Steyrer_right	1744,2381	8	329,77853	116,59432

Test bei gepaarten Stichproben

Statistik= Sig. (2-seitig)

Paaren 1	Craniotomy_Site_Schlager_left - Craniotomy_Site_Steyrer_left	,000
Paaren 2	Craniotomy_Site_Schlager_right - Craniotomy_Site_Steyrer_right	,000
Paaren 3	Brain_Area_Schlager_left - Brain_Area_Steyrer_left	,000
Paaren 4	Brain_Area_Schlager_right - Brain_Area_Steyrer_right	,003

Table 52: Statistics morphometric analysis

Gruppenstatistiken

group		N	Mittelwert	Standardabweichung	Standardfehler des Mittelwertes
Facial length	Low CI	4	80,5625	21,44128	10,72064
	High CI	4	33,7175	7,32616	3,66308
Facial width	Low CI	4	99,7125	15,86329	7,93164
	High CI	4	115,2825	14,72318	7,36159
Cranial length	Low CI	4	102,2200	19,30969	9,65485
	High CI	4	87,9300	4,51989	2,25994
Cranial width	Low CI	4	59,9850	7,95632	3,97816
Cranial width	High CI	4	60,6800	2,29819	1,14909
Cranial height	Low CI	4	58,3825	10,44377	5,22189
	High CI	4	54,0500	1,49354	,74677
Skull length	Low CI	4	182,4000	39,69374	19,84687
	High CI	4	121,9750	10,11776	5,05888
Skull base length	Low CI	4	163,2250	36,07117	18,03558
	High CI	4	102,6975	11,36440	5,68220
Cranial Index	Low CI	4	59,3815	5,66573	2,83287
	High CI	4	69,0725	2,44823	1,22411
Cephalic index	Low CI	4	55,4416	5,29706	2,64853
	High CI	4	94,2725	5,49275	2,74638
Median	Low CI	4	84,8405	13,30328	6,65164
	High CI	4	87,9300	4,51989	2,25994

Test bei unabhängigen Stichproben

Statistik=T-Test für die Mittelwertgleichheit Sig. (2-seitig), Annahmen=Varianzen sind gleich

Facial length	,006
Facial width	,200
Cranial length	,200
Cranial width	,872
Cranial height	,443
Skull length	,026
Skull base length	,019
Cranial Index	,020
Cephalic index	,000
Median	,675

7.4 Standard Operating Procedure

The Standard Operating Procedure was written in collaboration with Dr.rer.nat. Stephan Handschuh.

1 Load and save images:

1.1. Open a new project in Amira.

1.2. "Open Data..." and select all files in the folder "CT", then click "OK"

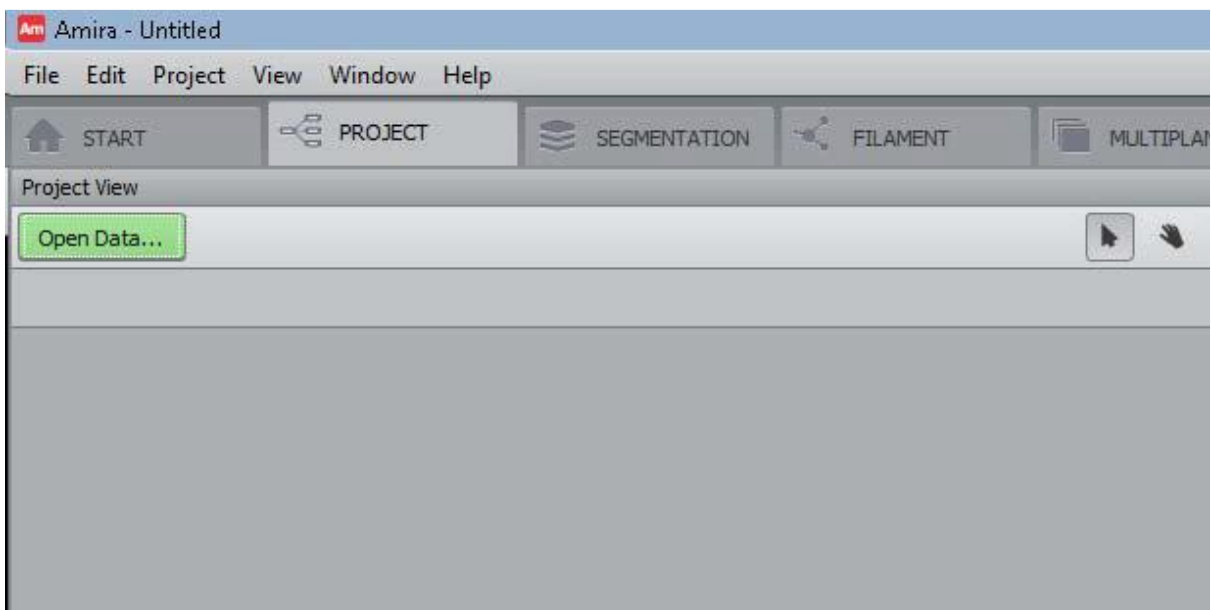


Figure 49: Amira home

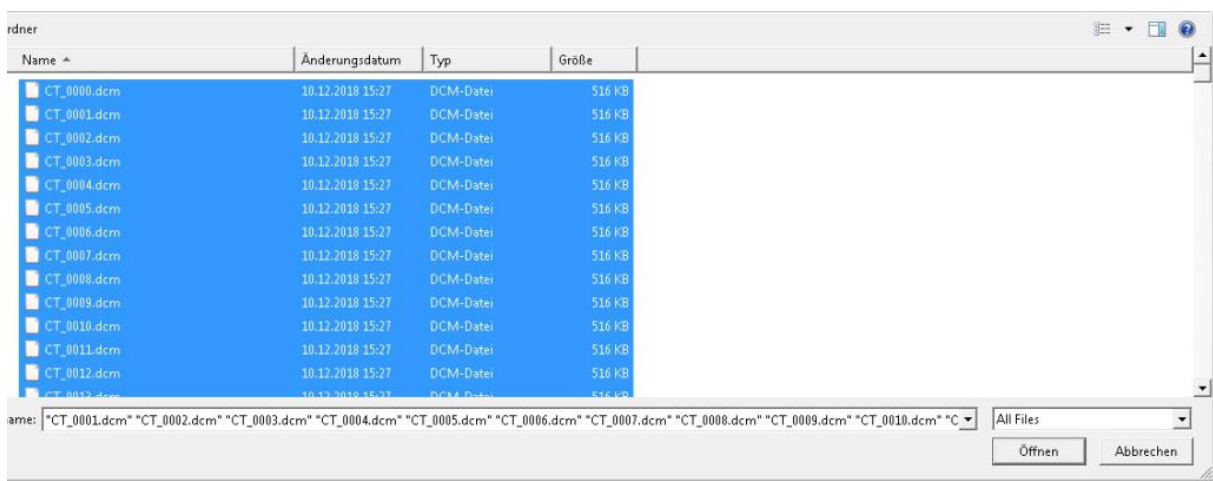


Figure 50: Amira import

1.3. The stack of images is now loaded and can be visualised with “Volren”

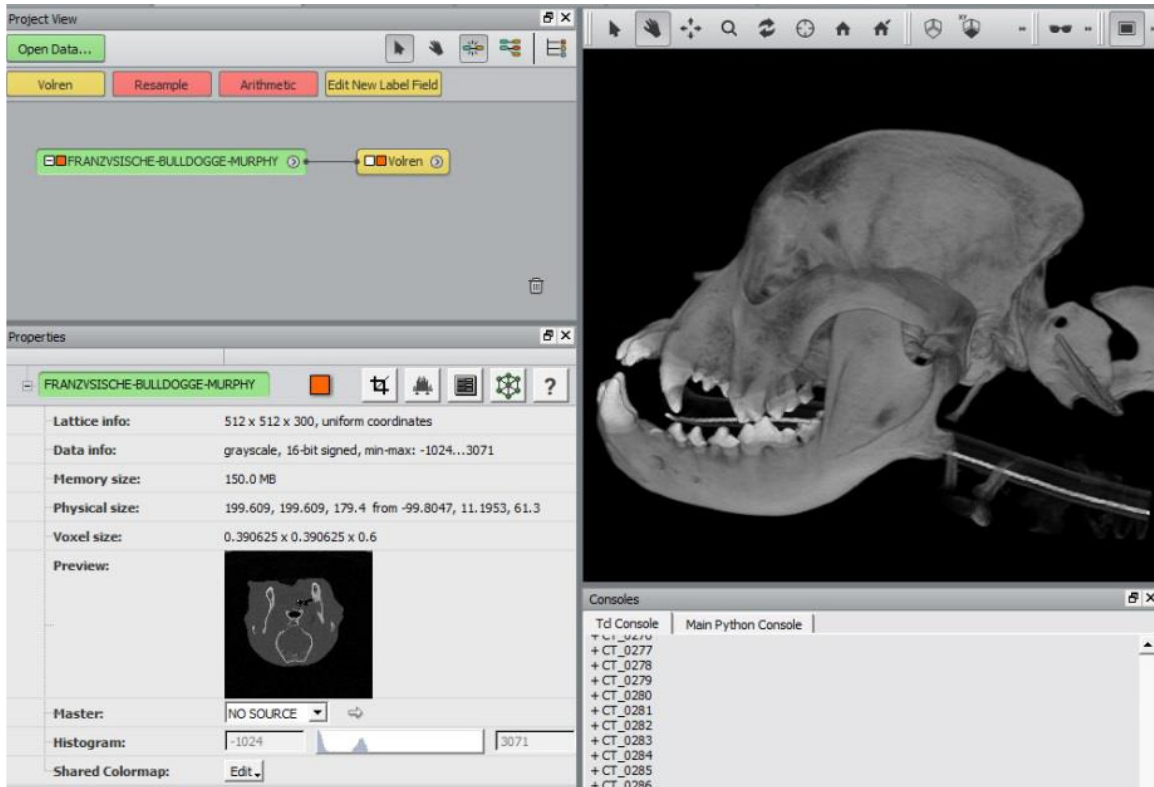
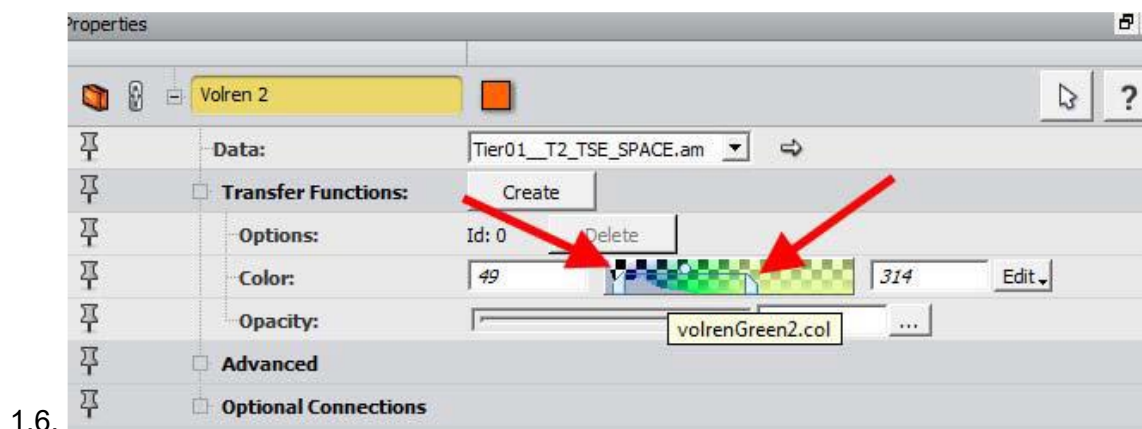


Figure 51: Amira Volren

1.4.

1.5. Load the stack of MRI images. If there are several sequences/weightings available, it is important to check which have the best quality. This is done by loading the stack, visualising it with “Volren” (see 1.3) and then changing the transparency/colour by sliding the brackets. Look for how good the Gyri are definable and how well they are visible.



1.6.

Figure 52: Amira Volren2

1.7. Both stacks are saved as “petname_CT.am” or “petname_Info.am” (example: “name_T2_TSE_SPACE.am”)

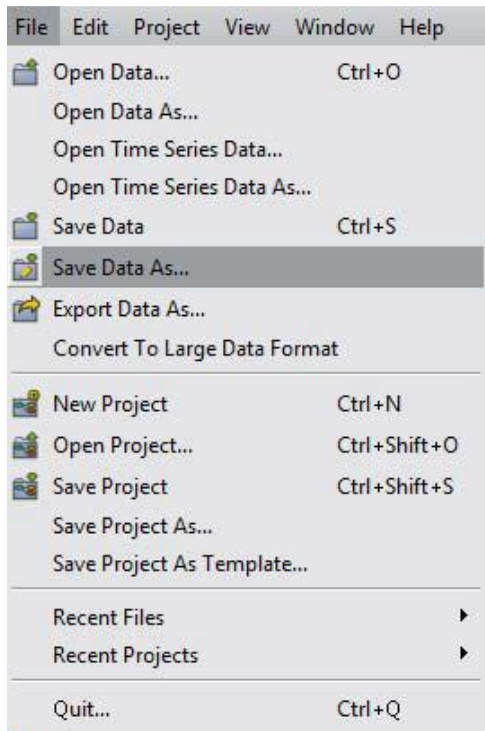


Figure 53: Amira saving

2 Orientation:

2.1. Enable the “Global Axes” in the menu “View” and set the 3D Viewer to “Orthographic” in order to get rid of the otherwise occurring distortion.

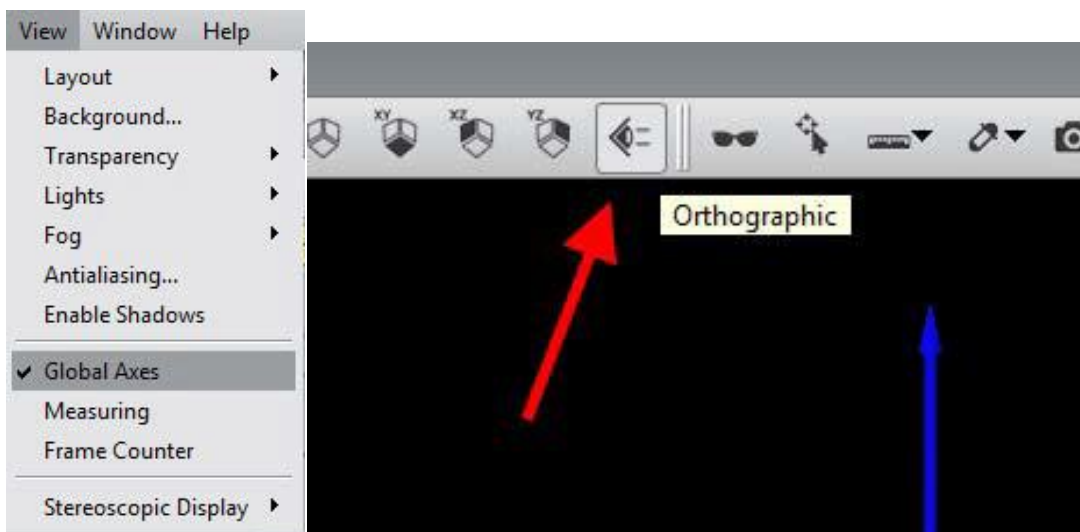


Figure 54: Amira view

Figure 55: Amira axes

2.2. Visualize the CT stack by right clicking it → “Isosurface”

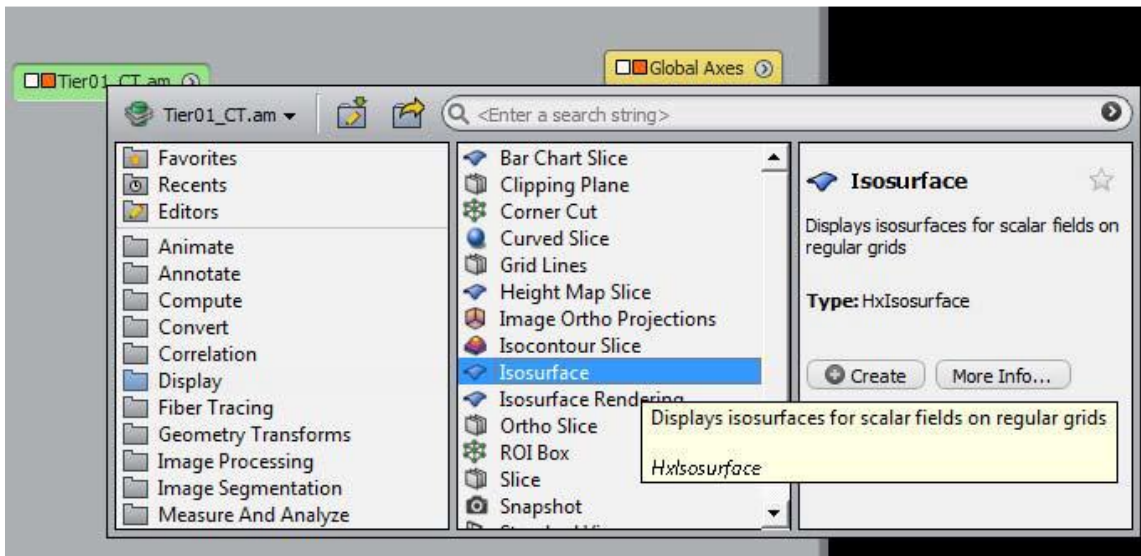


Figure 56: Amira tools

2.3. In the properties, choose a threshold of 350

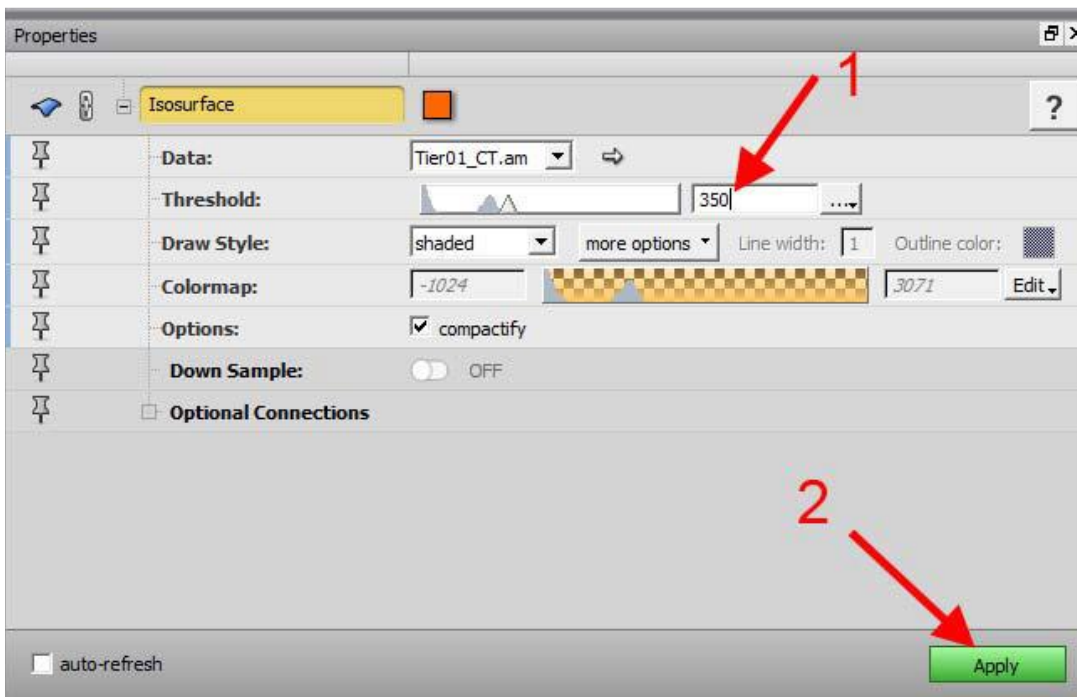


Figure 57: Amira Isosurface

2.4. Turn on the “Transform Editor” and align the skull according to the following images.

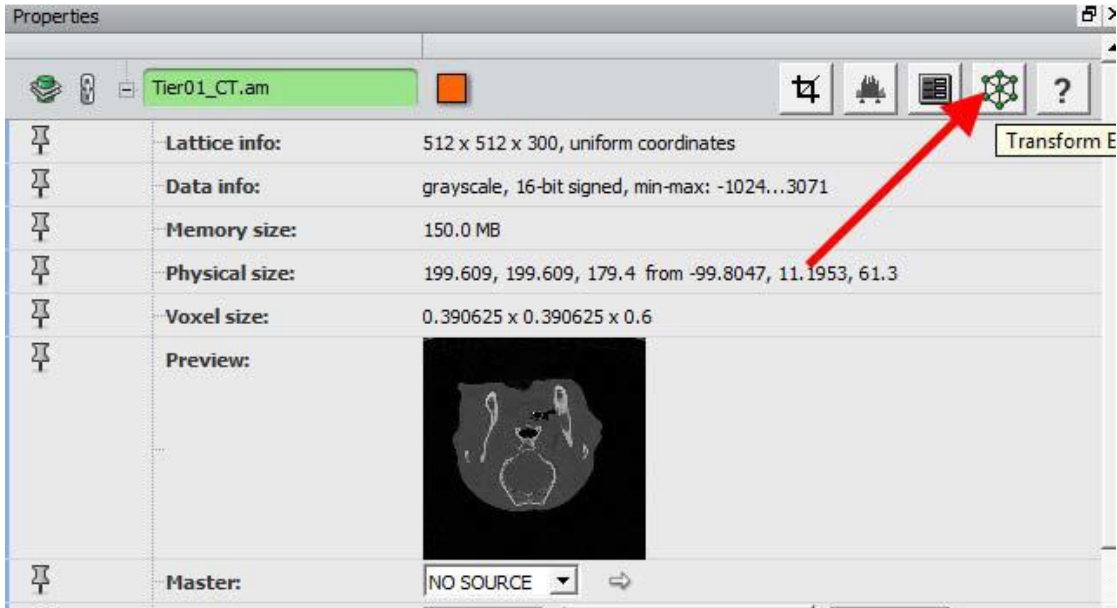
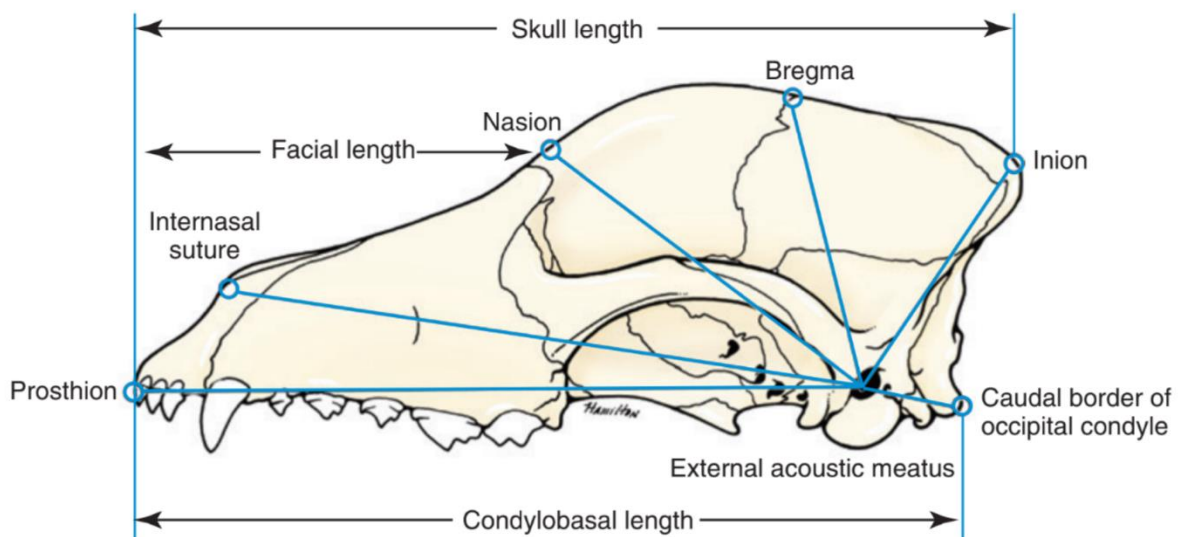


Figure 58: Amira transform

Figure 59: landmarks (Hermanson et al. 2020)



• Fig. 4.6 Skull, lateral view showing craniometric points.

- 2.5. The Prosthion and the Meatus acusticus externus should lie horizontally in one line with the Prosthion on the left side. Use the Global Axes as guidance.

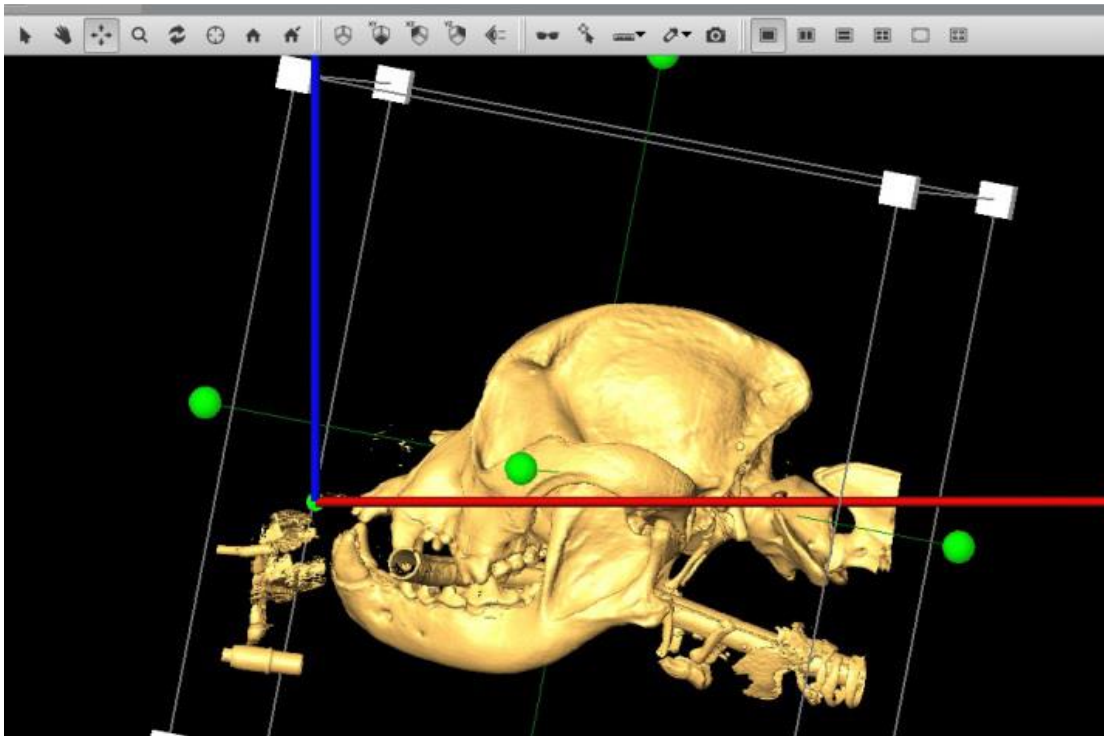


Figure 60: Amira aligning

- 2.6. Switch between "XZ", "XY" and "YZ" view to further align the skull on all axes.

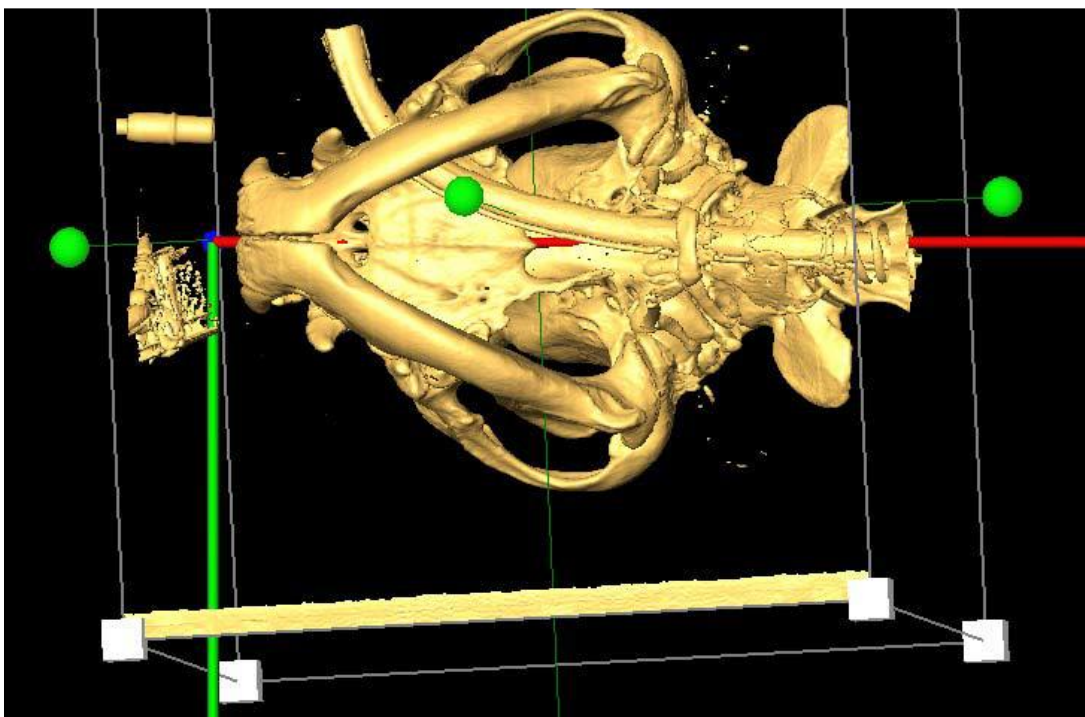


Figure 61: Amira aligning 2

2.7. Now enable the Scalebars by Right Click into the Project View → Create Object → Scalebars and under Properties tick the “Grid” to enable it and precisely align the skull.

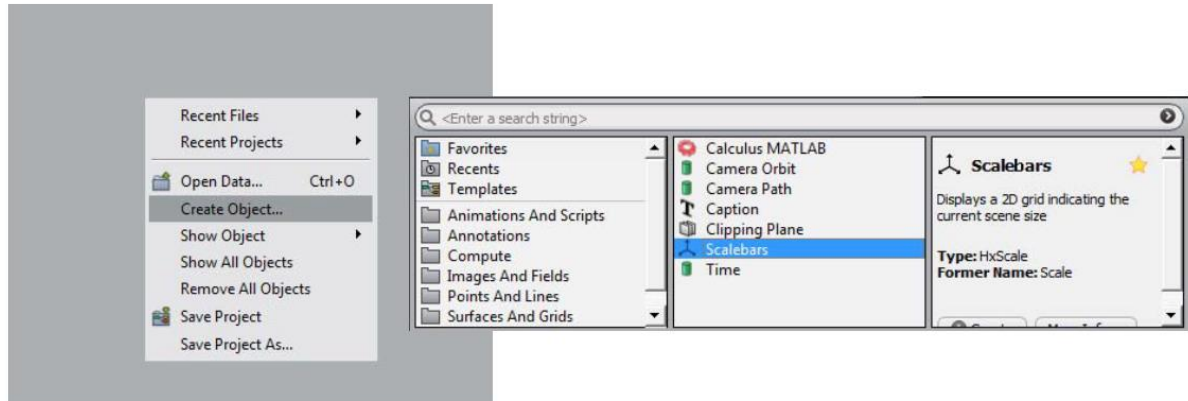


Figure 62: Amira scalebars

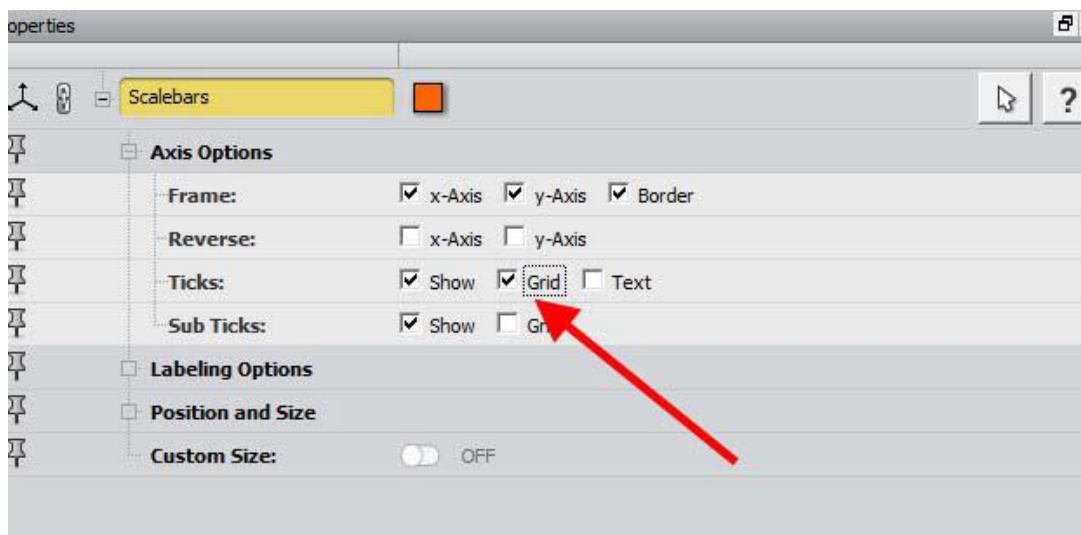


Figure 63: Amira scalebars settings

2.8. Make sure to check the “Transform Editor” if the “Scale factor” is 1 in all three boxes and then save the stack.

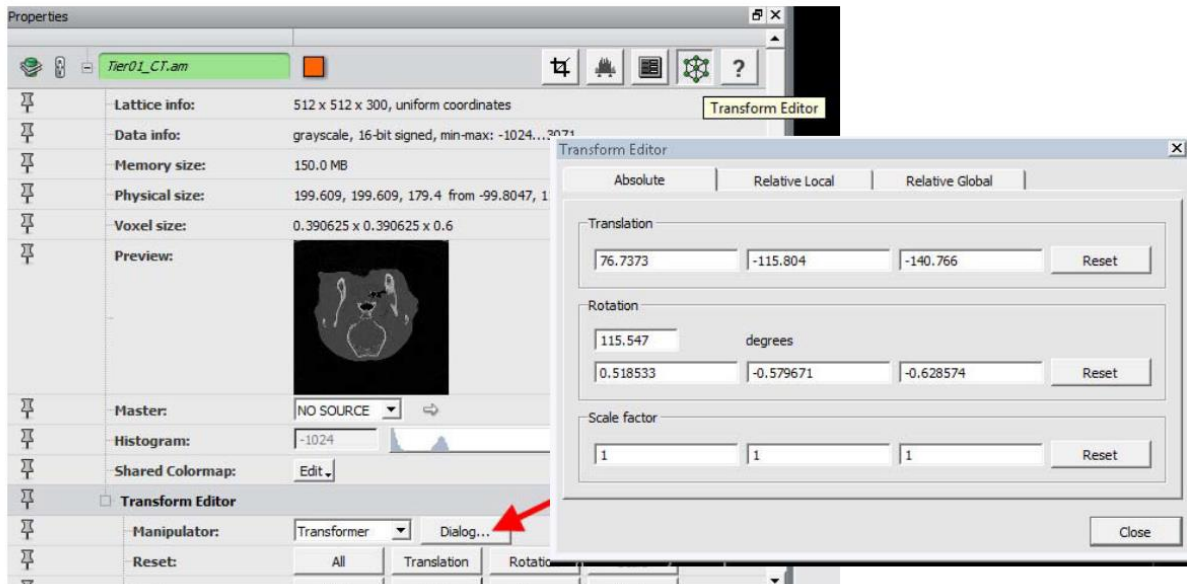


Figure 64: Amira transform editor settings

3 Landmarks:

3.1. Right Click into the Project View → Create Object → Point and Lines → Landmarks

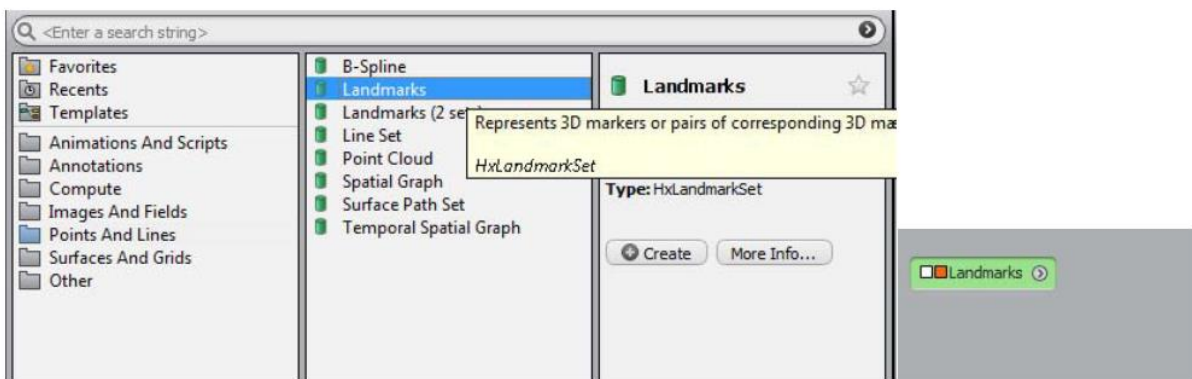


Figure 65: Amira landmarks

3.2. Open the Isosurface tool (Threshold 350, see 2.3), then use the “Landmark Editor” to add and edit landmarks with the “Interact” tool.

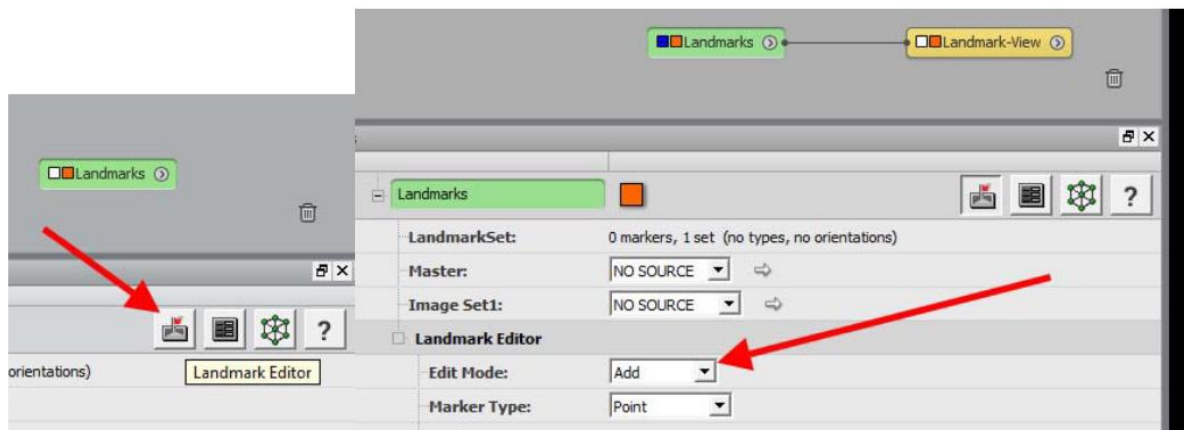


Figure 66: Amira landmark editor

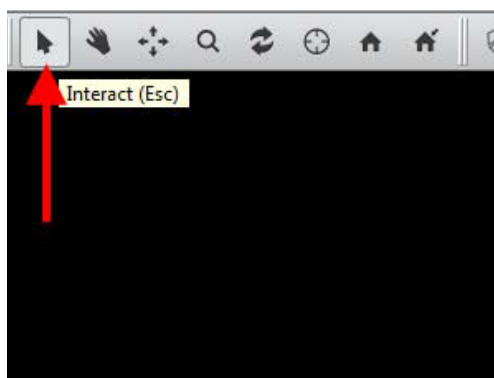


Figure 67: Amira Interact

3.3. Set the following landmarks in the correct order:

Table 53: Amira landmarks

Number	Designation	Info
1	Bregma	Difficult, look for an indentation
2	Inion	Most caudal point of Protuberantia occipitalis
3	Midpoint of Bregma and Inion	“Measurement tool”
4	Processus nasalis sinister	Rostral view
5	Processus nasalis dexter	Rostral view
6	Sutura internasalis, most rostral point	Rostral view
7	Nasion	Indentation
8	Processus frontalis ossis zygomaticus sinister	Dorsal view

9	Processus zygomaticus ossis frontalis sinister	Lateral view
10	Canalis opticus sinister, medioventrally	In Fossa oculi; use "Ortho Slice" and "Clip" for better visibility
11	Meatus acusticus externus sinister, craniolaterally	Ortho Slice and Clip
12	Dens caninus sinister (204), posterior buccal corner	Junction from alveole to tooth
13	Dens praemolaris 3 sinister (207), posterior buccal corner	Junction from alveole to tooth
14	Dens praemolaris 4 sinister (208)	Junction from alveole to tooth
15	Processus frontalis ossis zygomaticus dexter	See left side
16	Processus zygomaticus ossis frontalis dexter	See left side
17	Canalis opticus dexter, medioventrally	See left side
18	Meatus acusticus externus dexter, craniolaterally	See left side
19	Dens caninus dexter (104), posterior buccal corner	See left side
20	Dens praemolaris 3 dexter (107), posterior buccal corner	See left side
21	Dens praemolaris 4 sinister (108)	See left side
22	Processus mastoideus sinister	Caudolateral view
23	Processus mastoideus dexter	Caudolateral view
24	Processus paracondylaris sinister	Ventral view
25	Processus paracondylaris dexter	Ventral view
26	Tuberculum nuchale sinister	Landmark set on the CT image; caudal view
27	Tuberculum nuchale dexter	Landmark set on the CT image; caudal view
28	Condylus occipitalis sinister	Landmark set on the CT image; caudal view
29	Condylus occipitalis dexter	Landmark set on the CT image; caudal view
30	Basion	Ortho Slice and Clip
31	Os palatinum, most caudal point	Caudoventral view
32	Hamulus pterigoidei sinister	Caudoventral view
33	Hamulus pterigoidei dexter	Caudoventral view
34	Prosthion	Rostral view



Figure 68: Amira set landmarks

3.4. Save the landmark file as "petname_morphometric_landmarks_landmarkAscii"

4 Cranial index:

- 4.1. Create a Scalebar with a Grid. Make sure the 3D view is set to orthographic and view an Isosurface of the CT scan. Then align the landmarks you want to measure with the grid by zooming in and out, read the units showed on the axes of the grid (1 unit = 1mm) and write them down in a Microsoft Excel file.

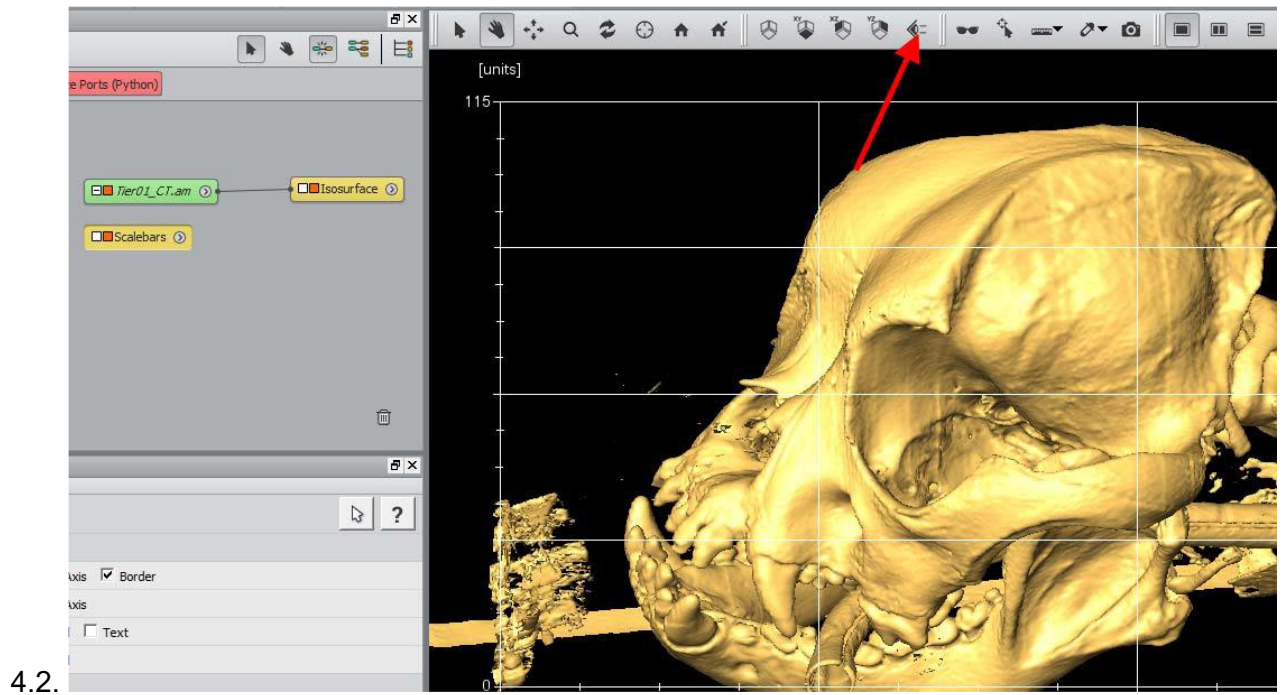


Figure 69: Amira cranial index



Figure 70: Amira Arcus width

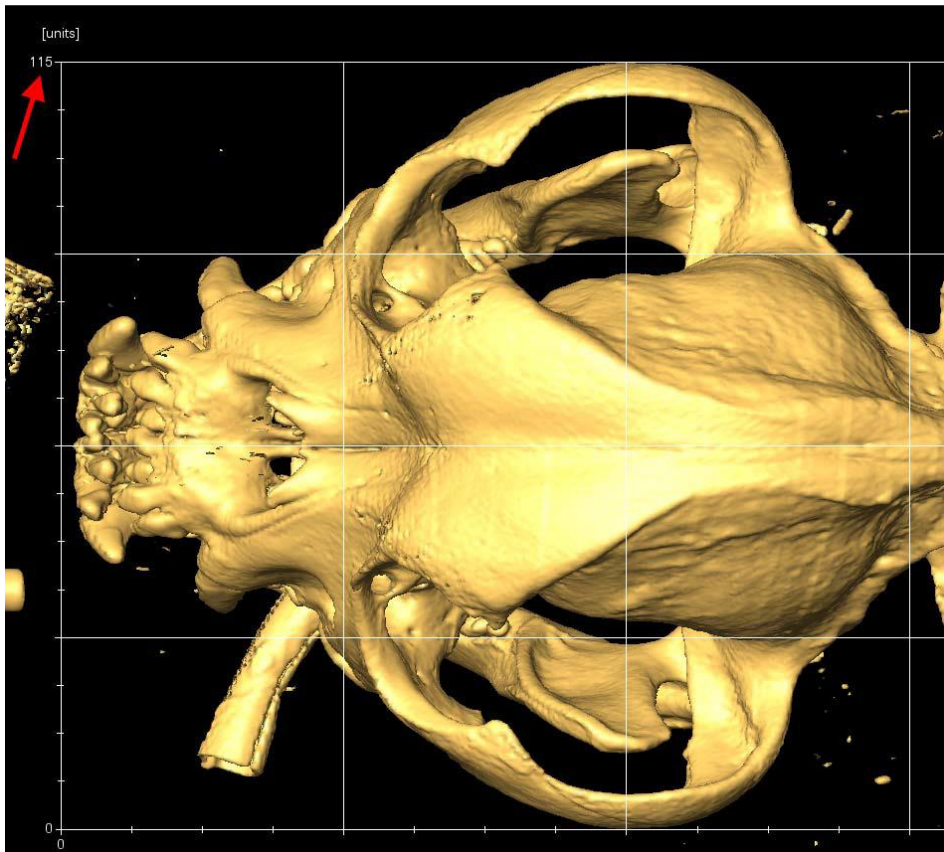


Figure 71: Amira units

4.3. These are the measurements:

Table 54: Amira measurements

Cranial index	Landmarks	Info
Facial length	Nasion to Prosthion	dorsal view
Facial width	Widest interzygomatic distance	dorsal view
Cranial length	Inion to Nasion	dorsal view
Cranial width	Widest interparietal distance	dorsal view
Cranial height	Middle of Meatus acusticus externus to bregma	lateral view
Skull length	Inion to Prosthion	dorsal view
Skull base length	Basion to Prosthion	ventral view

5 Registering CT and MRI files:

- 5.1. Open the already aligned CT file and the MRI file and visualize both with a Volren. For the CT Volren, let the “Transfer function” set to “VolrenRed” and set the MRI Volren to “VolrenGreen”. You can change the transparency for both with the brackets.

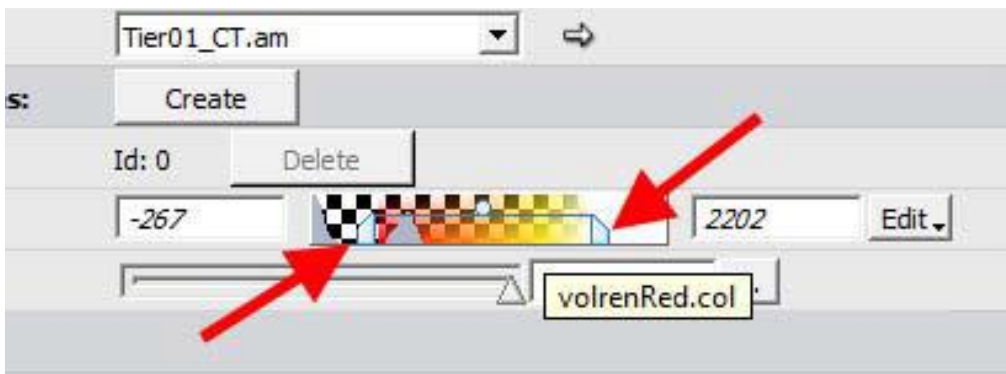


Figure 72: Amira Volren colour

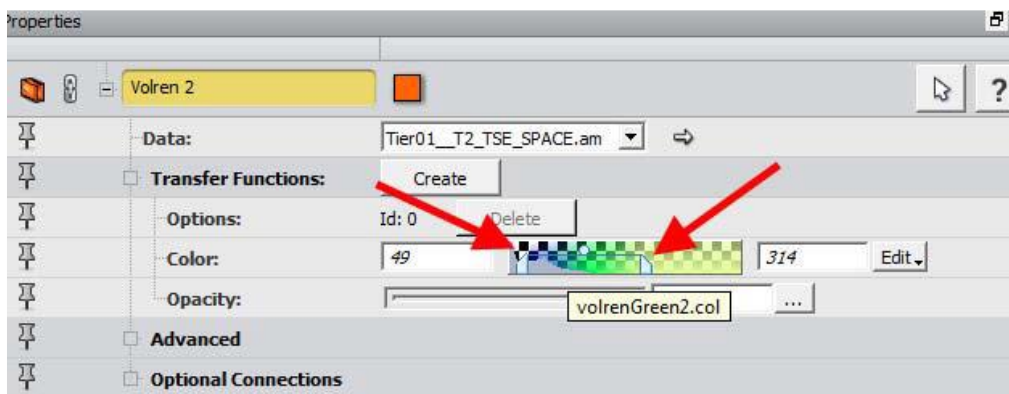


Figure 73: Amira Volren colour green

5.2. Enable the Transform Editor of the MRI file and roughly align it to the already orientated CT file.

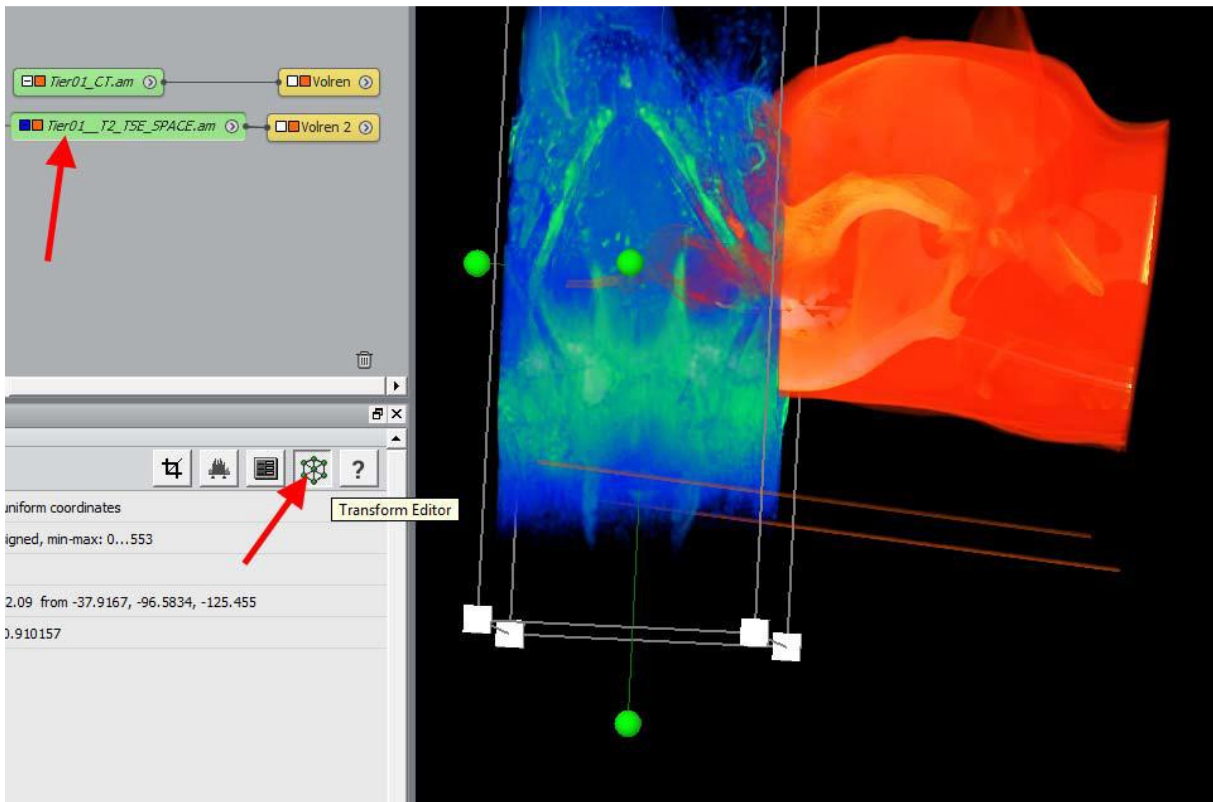


Figure 74: Amira scan alignment

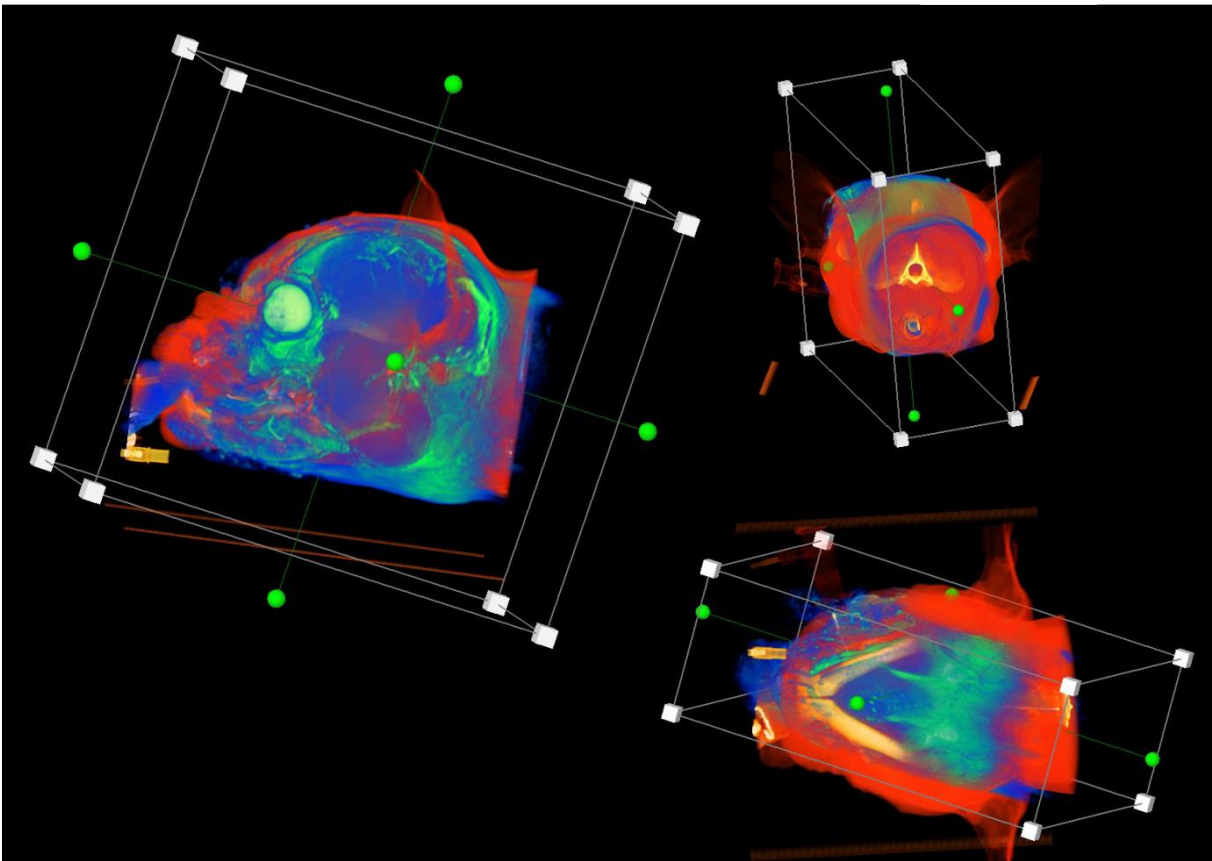


Figure 75: Amira scans aligned

5.3. Right click onto the MRI file → Geometry Transforms → Register Images

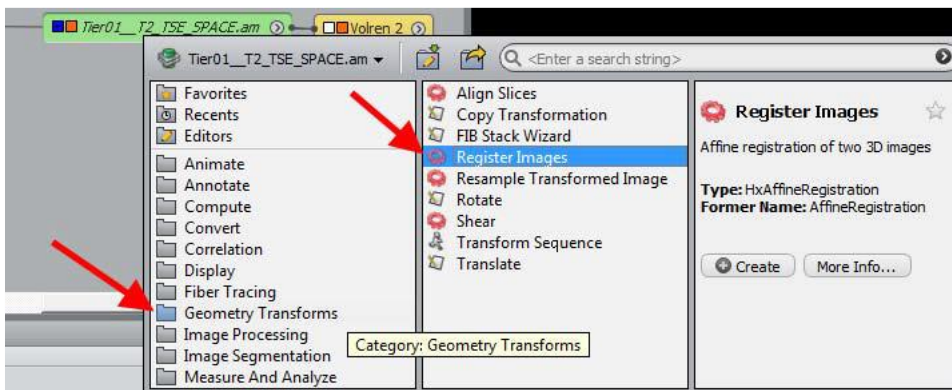


Figure 76: Amira register images

5.4. Select the “Register Images” tool and link the “Reference” to the CT file.

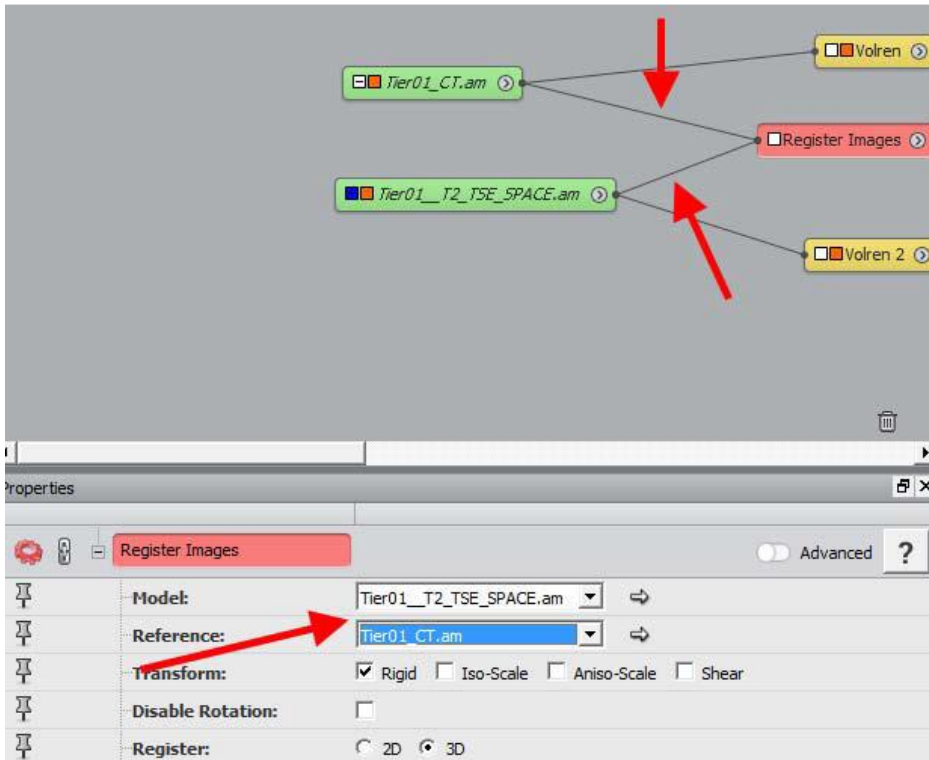


Figure 77: Amira references link

5.5. Now click “Apply” and wait until the rendering is finished.

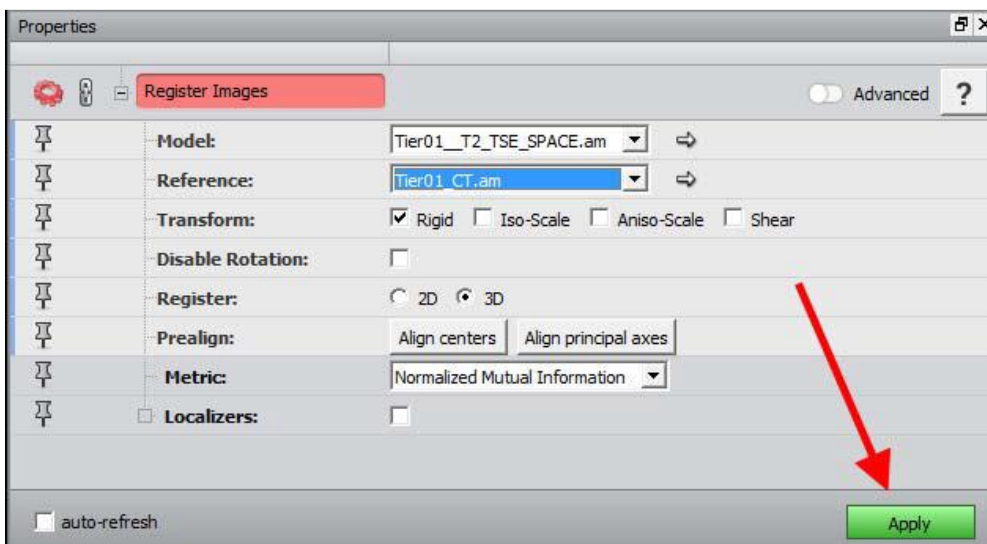


Figure 78: Amira references linked

- 5.6. To inspect the alignment, disable the Volumes of the CT and the MRI file, create an “Orthoslice” for the MRI file and then right click the Ortho Slice → Display → Colour Wash

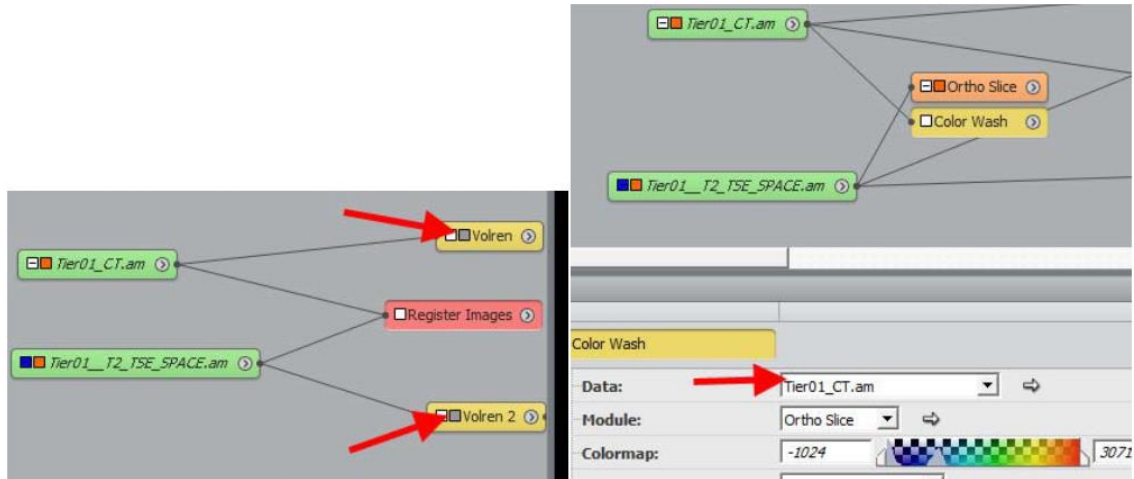


Figure 79: Amira colour wash

- 5.7. Set the Data of the “Colour Wash” as the CT file.
- 5.8. Disable the Transform Editor on the MRI file and with help of the Ortho Slice, check whether the Orientation of both files is appropriate based on the match of the skull and brain contour.

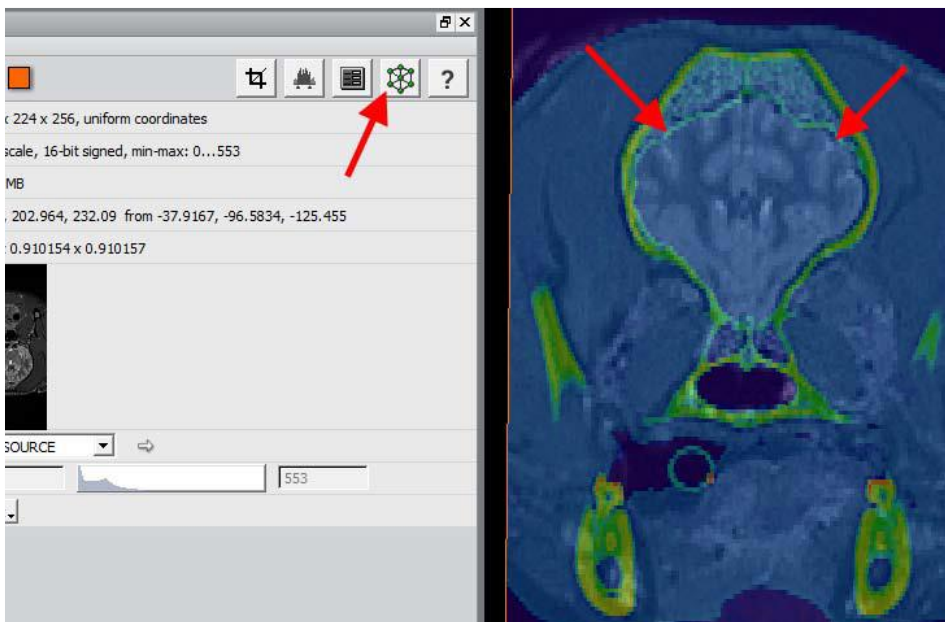


Figure 80: Amira colour wash check

- 5.9. Save the MRI file.

6 Segmentation of the brain:

6.1. The now orientated MRI file is opened.

6.2. Then right click on it → Image Segmentation → Edit New Label Field

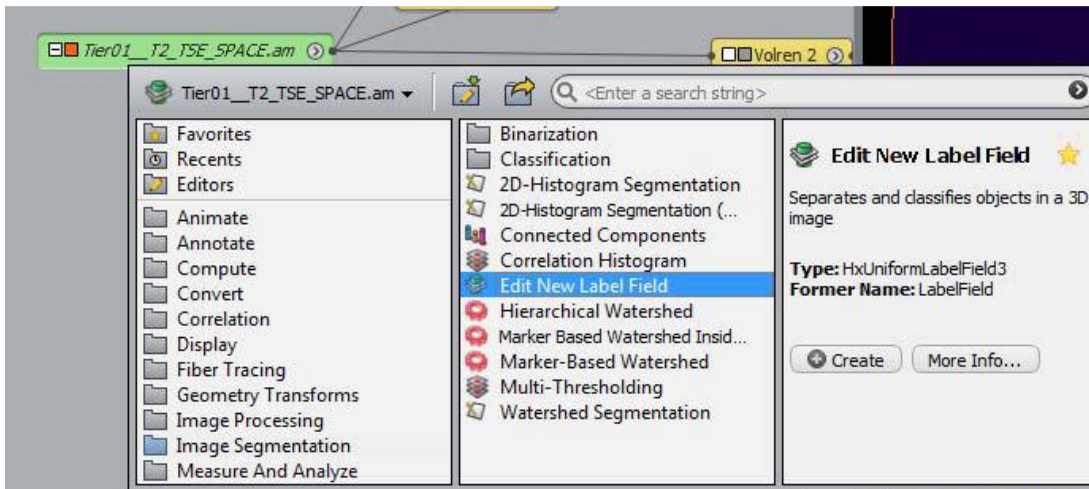


Figure 81: Amira new label field

6.3. The program then switches automatically to the “Segmentation” Tab.



Figure 82: Amira segmentation

6.4. Change the view to “XY” and select the material “Inside”.

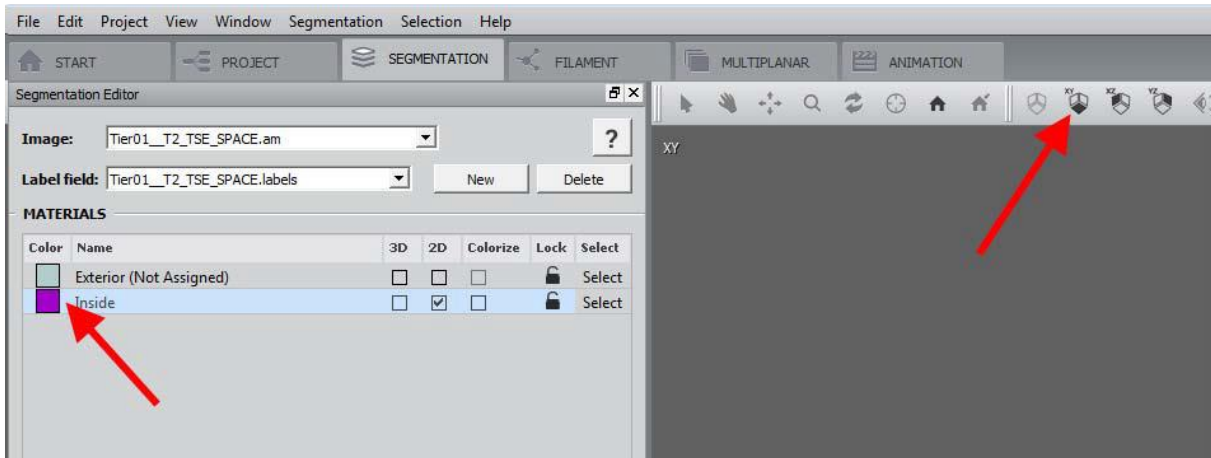


Figure 83: Amira inside material

6.5. Use the “Threshold” tool and set the lower threshold to 150.

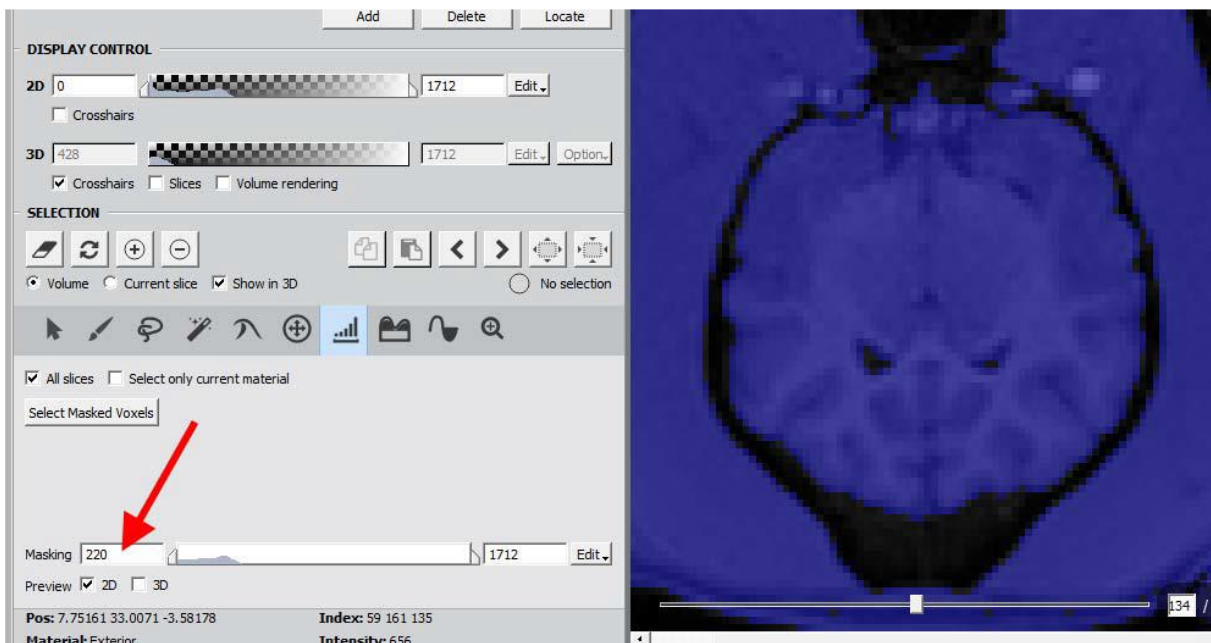


Figure 84: Amira material threshold

6.6. “Select Masked Voxels” → “+” to add the selection to the material “Inside”

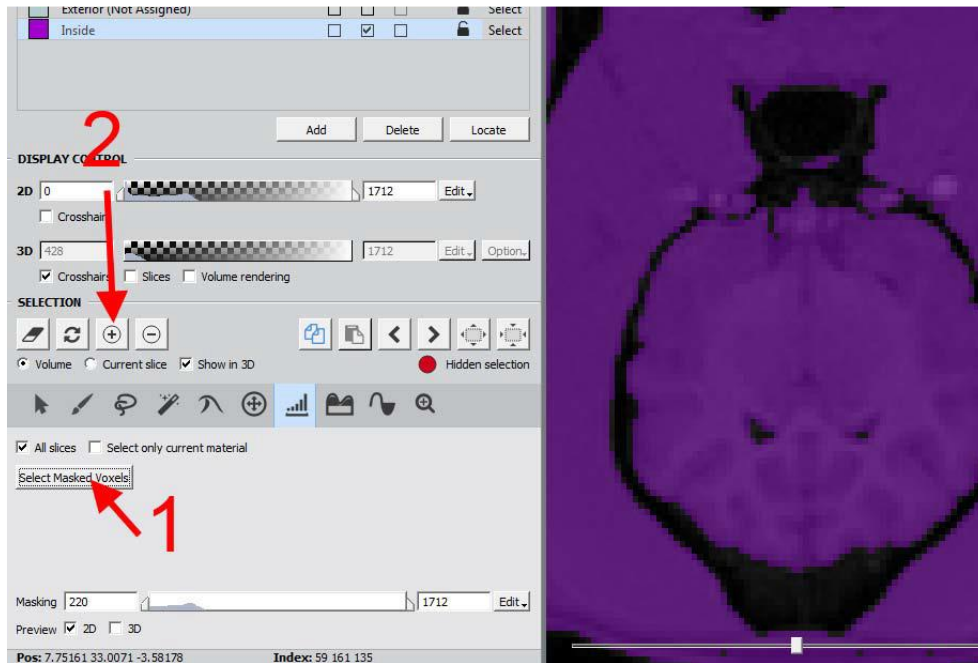


Figure 85: Amira masked voxels

6.7. Set a lower threshold of -114 and an upper threshold of 175 to select the “background”

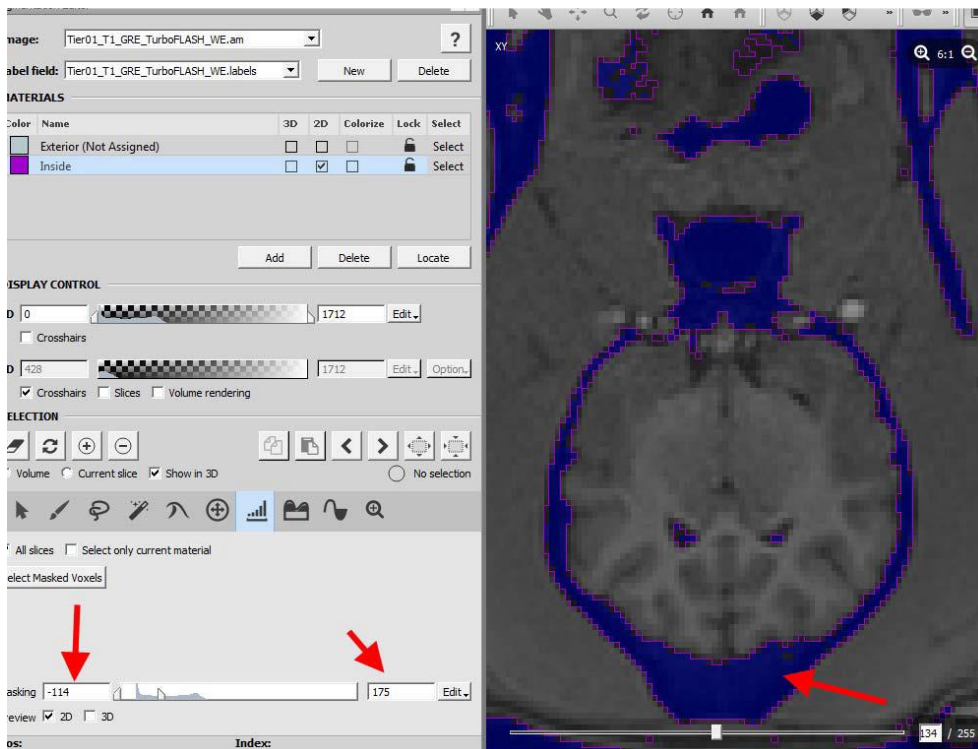


Figure 86: Amira threshold background

6.8. Now “Select Masked Voxels”, then “Grow Selection” three times and then “Shrink Selection” three times again to refine the borders. Remove this selection from the Inside Material by clicking the “-“

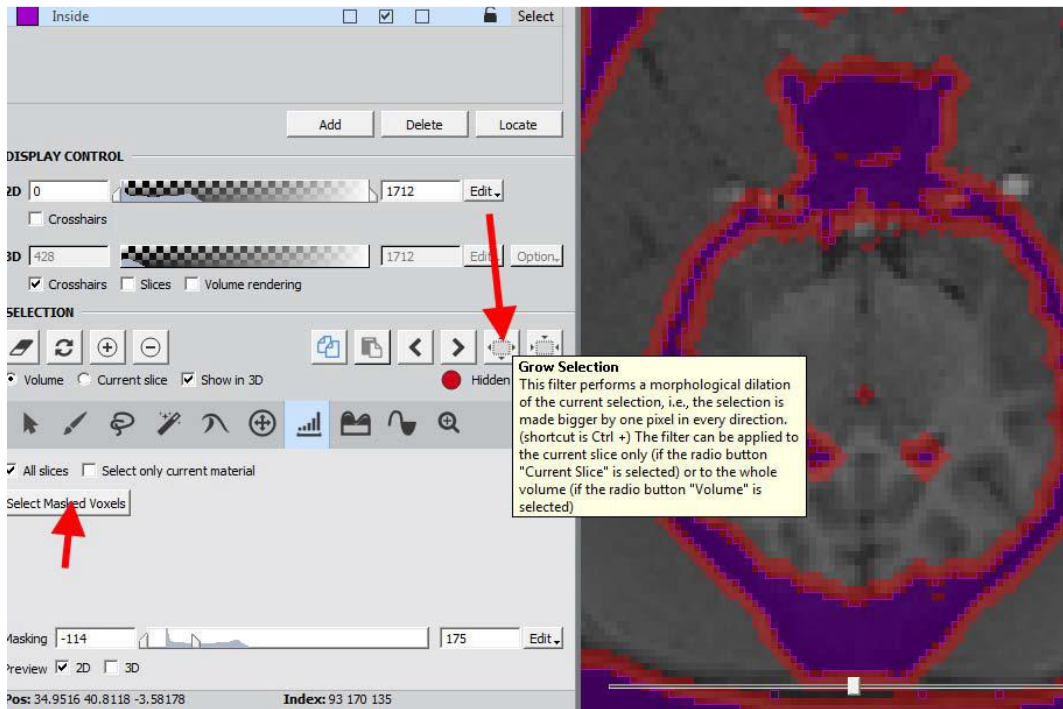


Figure 87: Amira grow selection

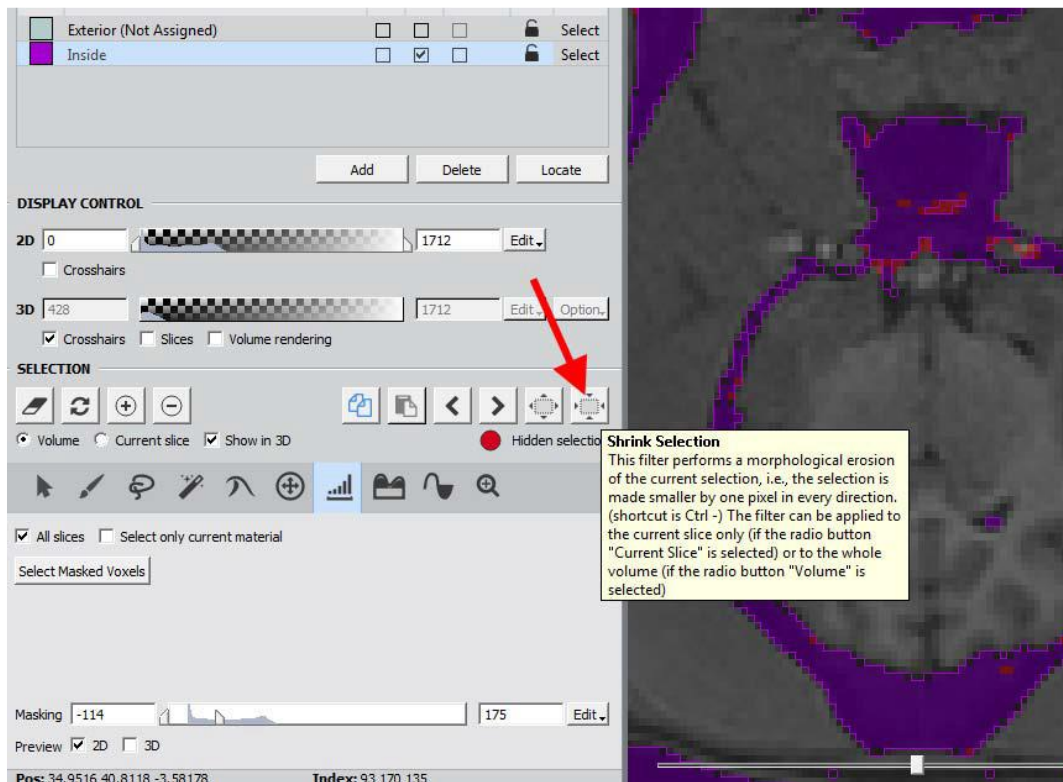


Figure 88: Amira shrink selection

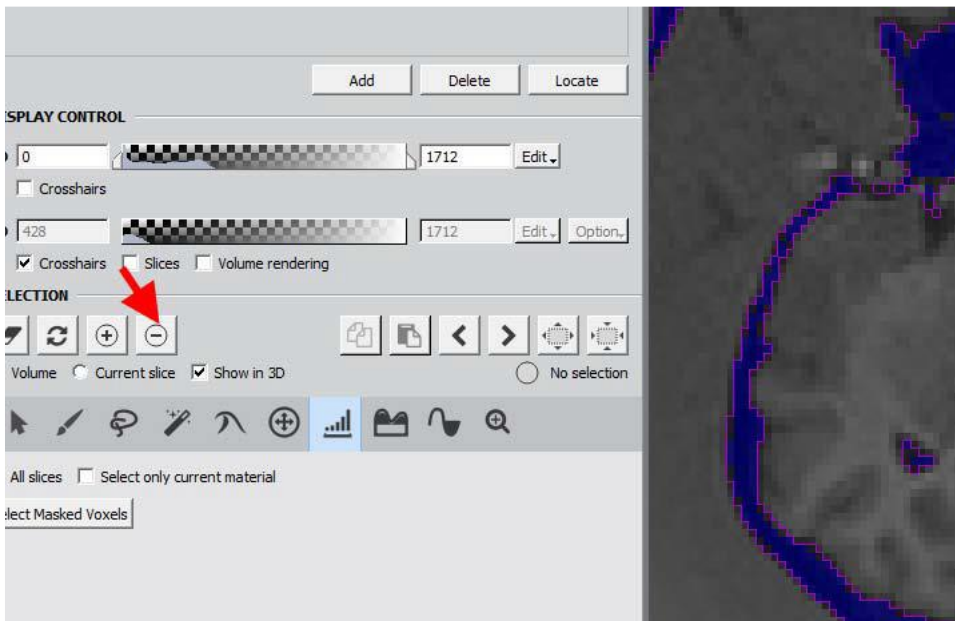


Figure 89: Amira remove selected

6.9. To check the selection, use the “Pick and Move” tool and click into the brain. If only the brain turns red, the brain is extracted. If any surrounding tissue turns red too, there still are connections between the brain and the tissue.

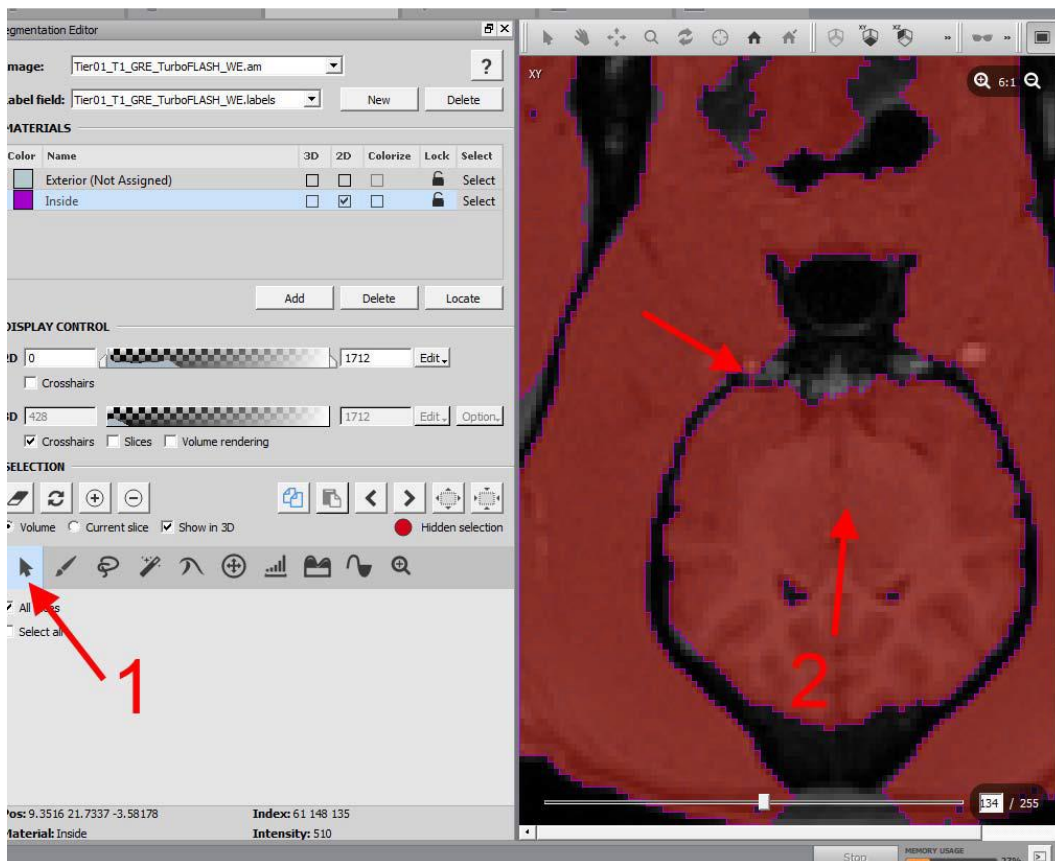


Figure 90: Amira segmentation pick

- 6.10. To remove these connections, “clear” the current selection and then use the “Brush” tool to select and then “-“ to remove them from the Inside material. Make sure all connections are removed by switching between the different views (XZ, XY, YZ) and scrolling through them.

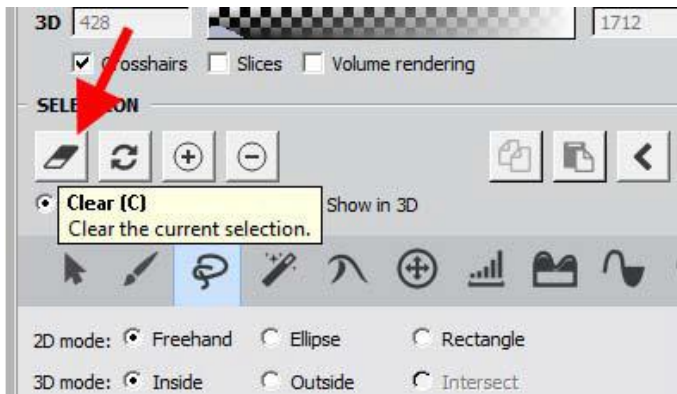


Figure 91: Amira clear selection

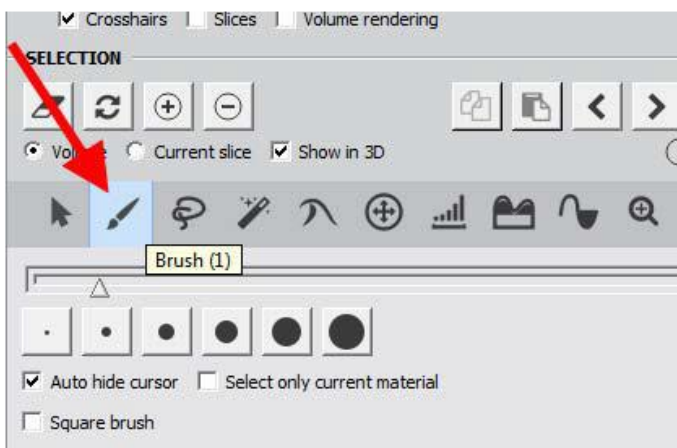


Figure 92: Amira selection brush

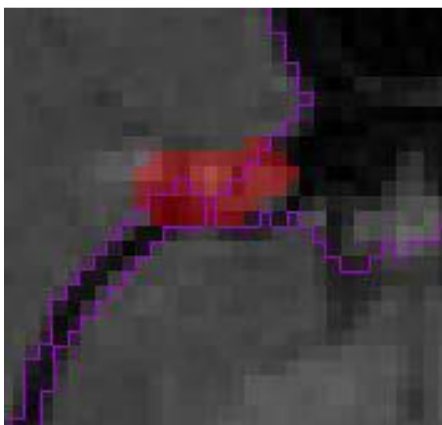


Figure 93: Amira "bridges"

6.11. If only the brain turns red when you click on it, all connections are removed.

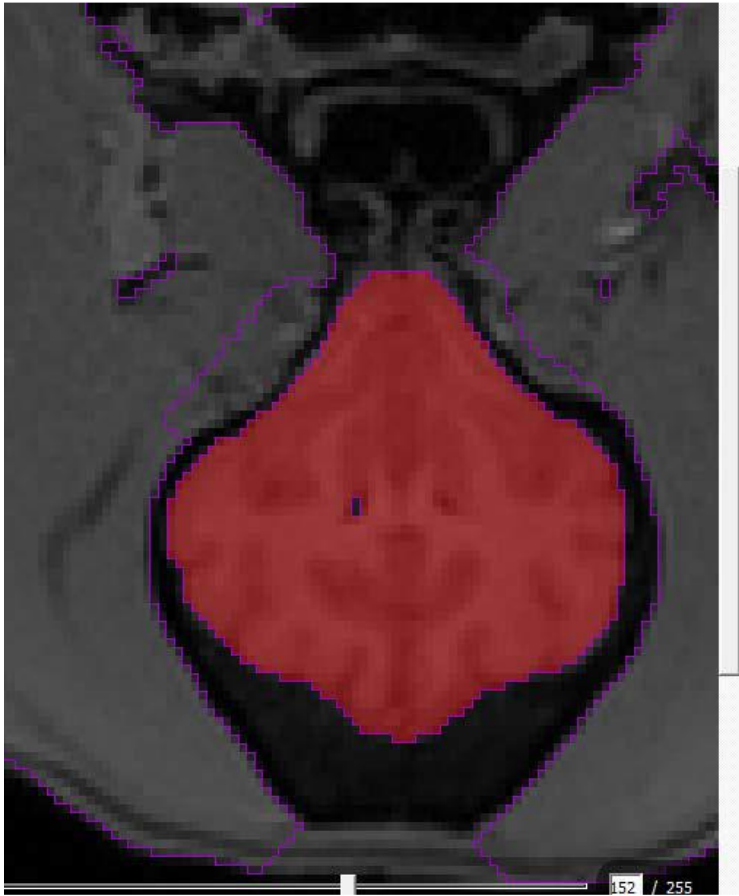


Figure 94: Amira correct selection

6.12. Now invert the selection and remove the background by “Menu Selection” → Invert → All Slices

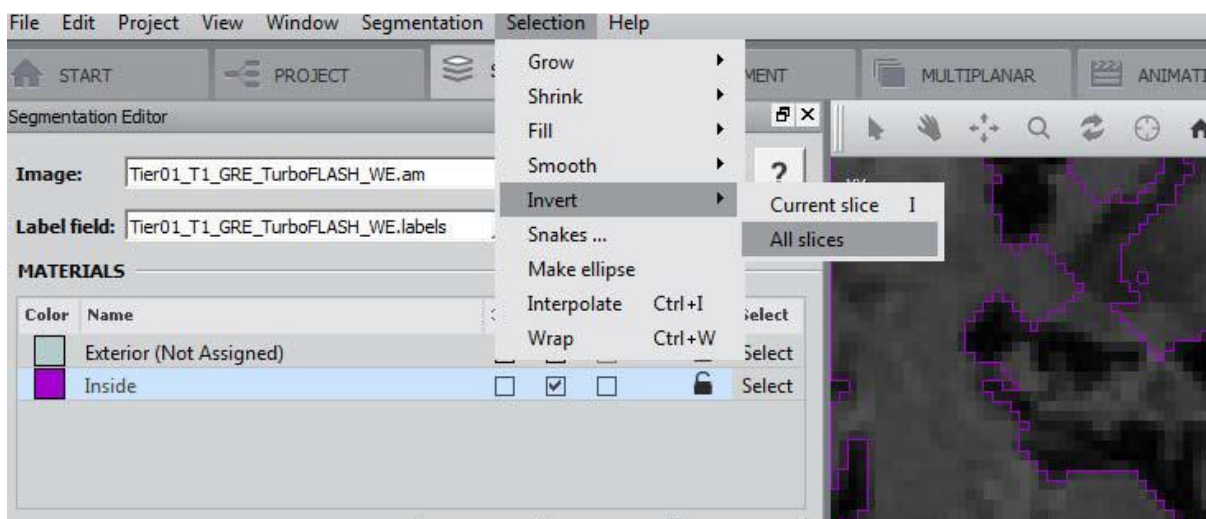


Figure 95: Amira Invert selection

6.13. Now everything except the brain should turn red. Remove (“-“) the background.

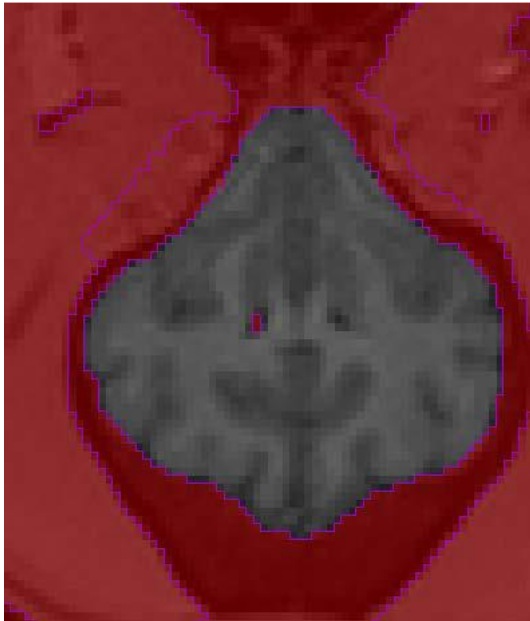


Figure 96: Amira inverted selection

6.14. The violet border should now surround only the brain tissue.

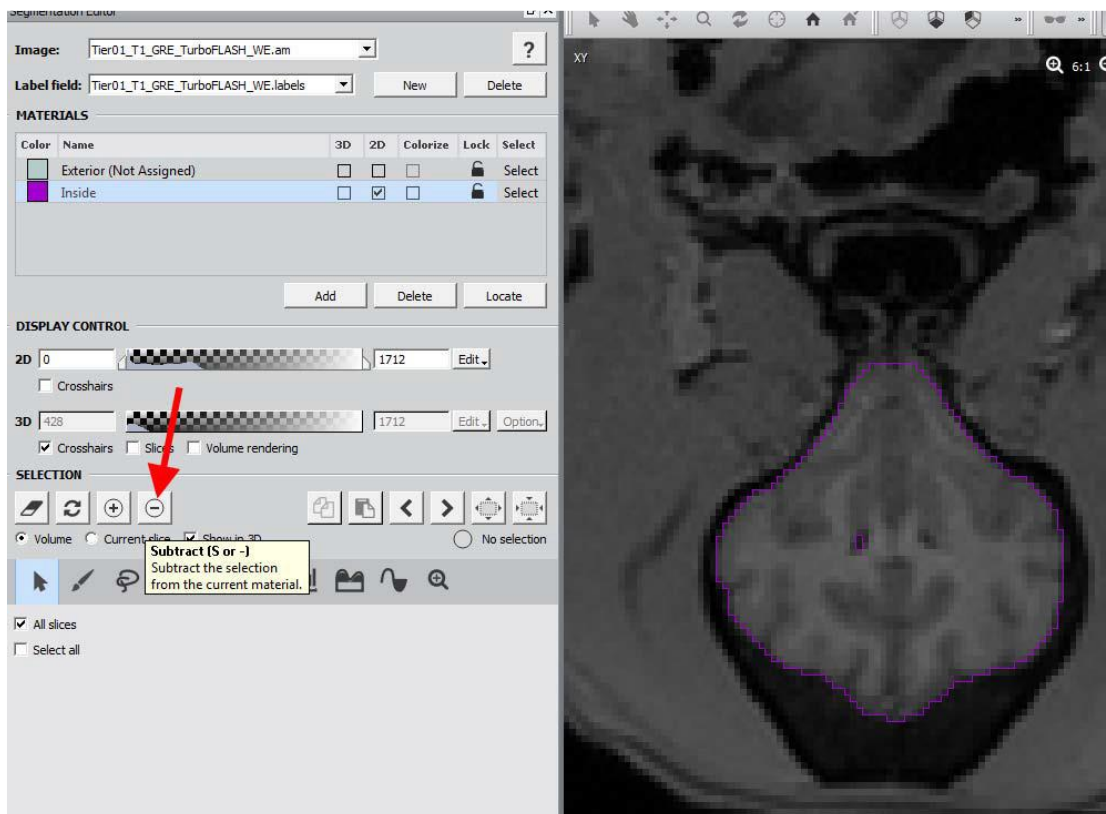


Figure 97: Amira selection border

- 6.15. To remove any holes, select the brain → Grow Selection four times → Shrink Selection four times and then add (“+”)

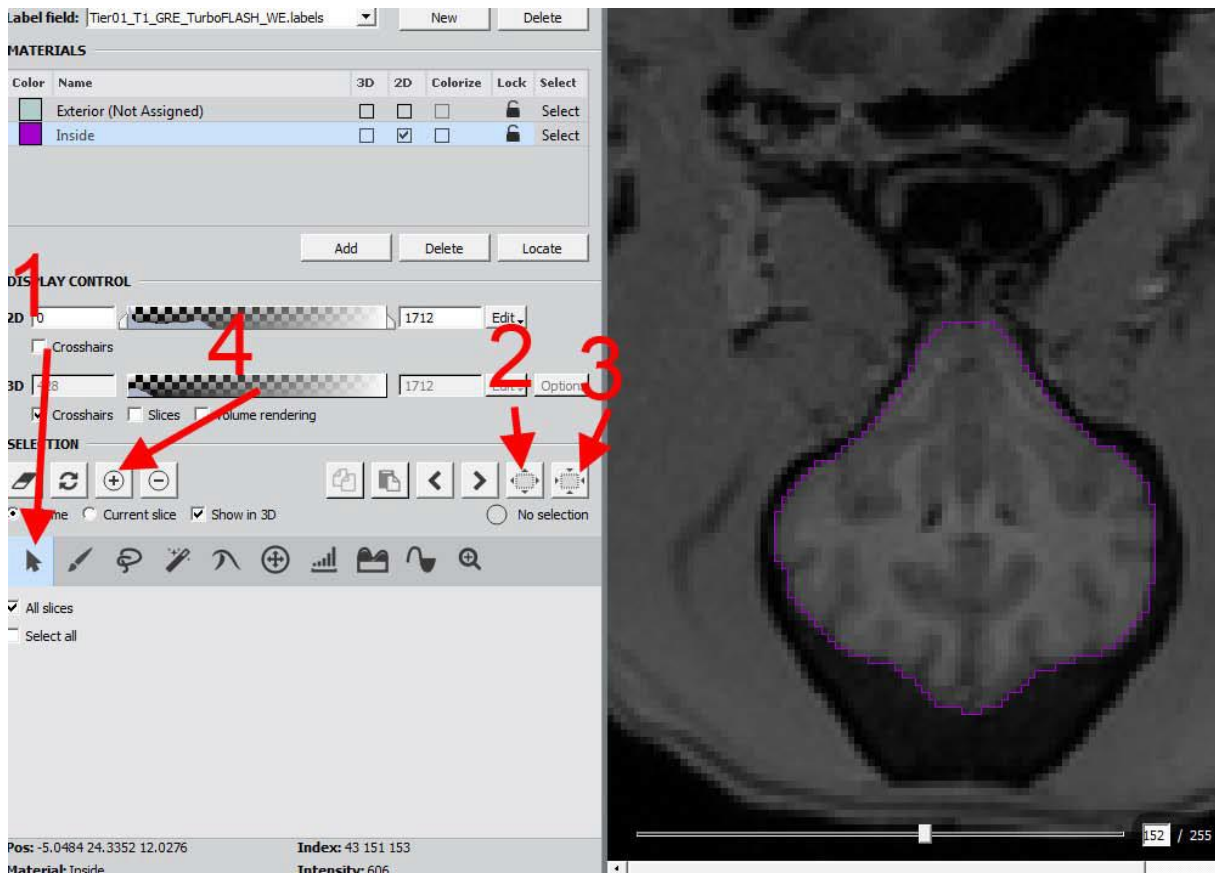


Figure 98: Amira grow and shrink

- 6.16. Additionally, go into the menu “Segmentation” → Fill holes → All Slices and afterwards check the brain in all axes if there still are any holes.

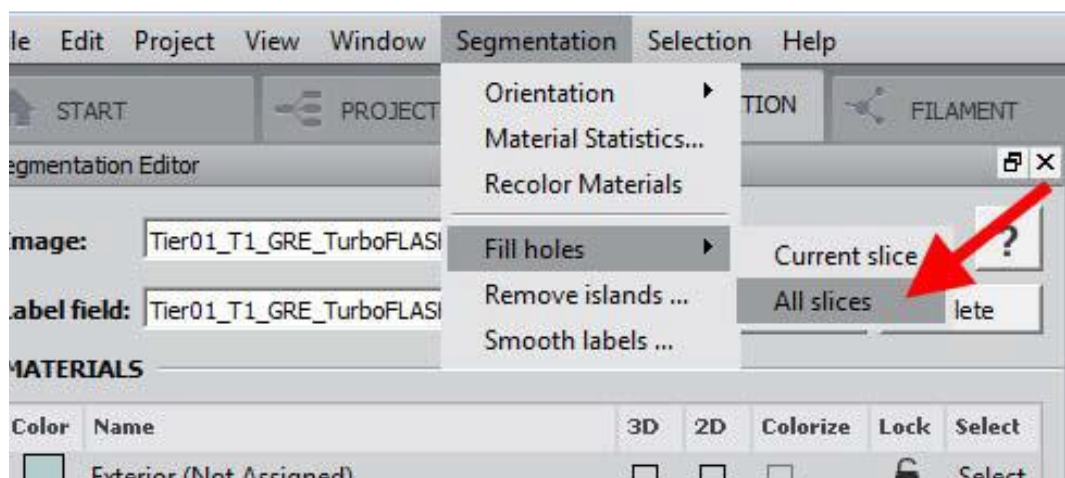


Figure 99: Amira fill holes

- 6.17. The brain will be extended by one Voxel (Grow Selection) and then added (“+”) to the Inside Material

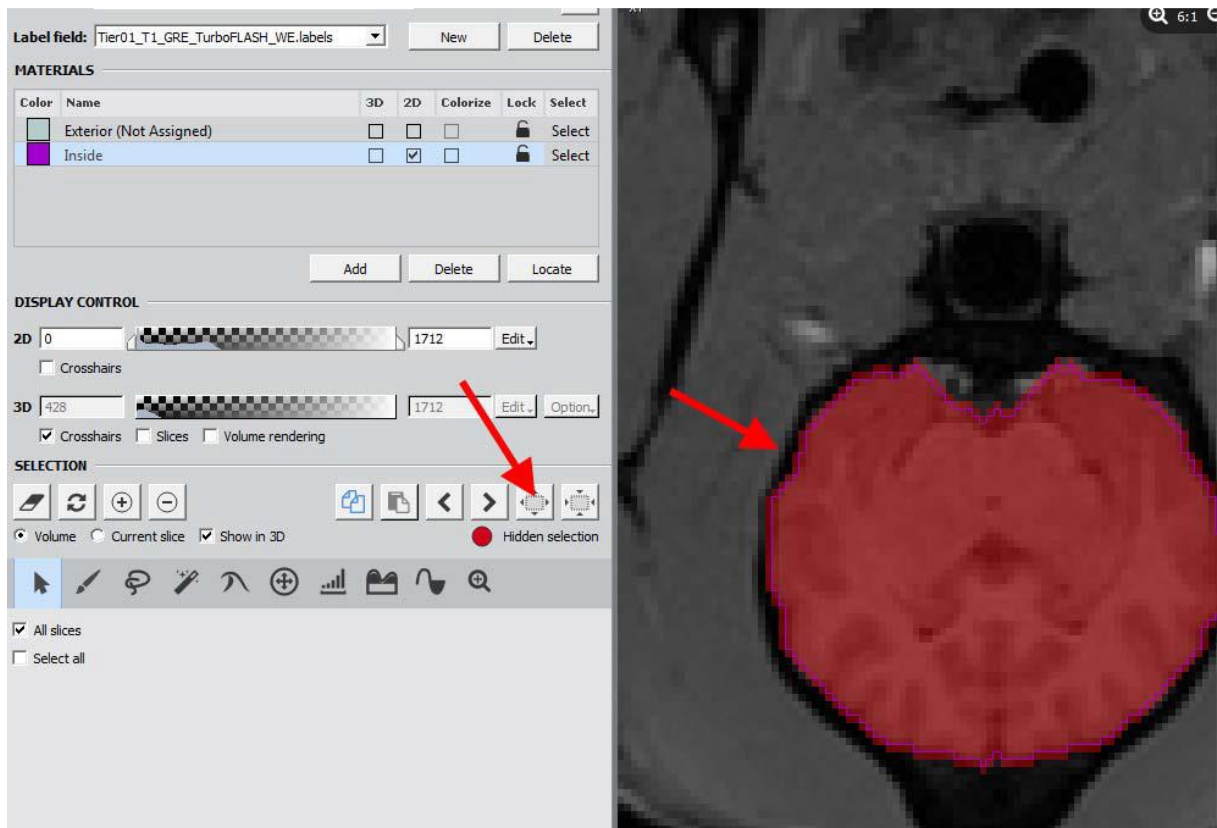


Figure 100: Amira grow selection

- 6.18. Switch into the “Project” tab and save the labels as “petname_MRI_Info_labels.am”

7 Extraction of the brain and improving the resolution:

- 7.1. Right click the MRI file → Compute → Arithmetic



Figure 101: Amira arithmetic

7.2. Right click the white box next to “Arithmetic” and set the “Input B” as the new label file (“petname_MRI_Info_labels.am”)

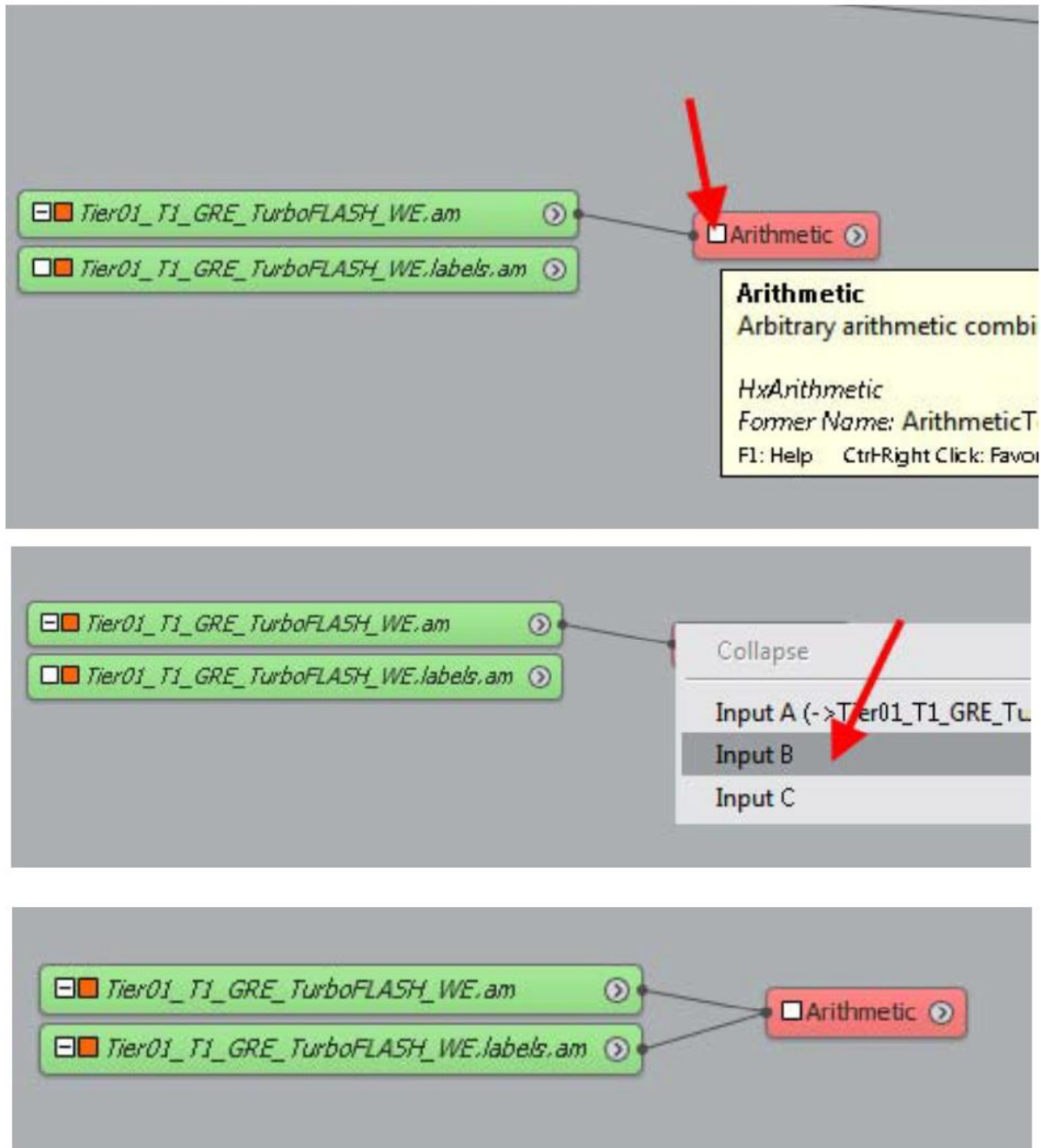


Figure 102: Amira arithmetic input

7.3. Left click on the Arithmetic tool and in its properties, set the “Expression” to “(b==1)*a” (without the quotation marks) and hit “Apply”

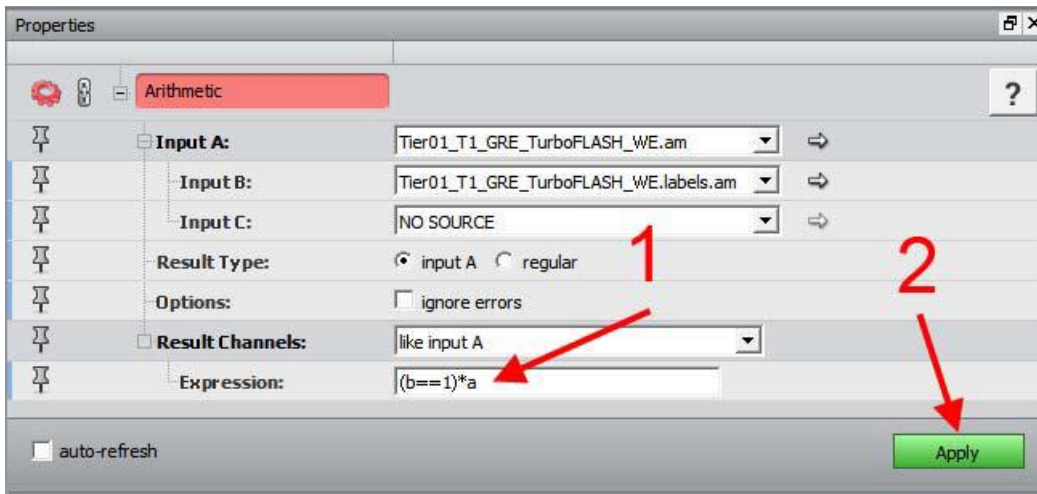


Figure 103: Amira arithmetic expression

7.4. The newly generated “Result” contains only the brain and can be visualized by a Volren tool

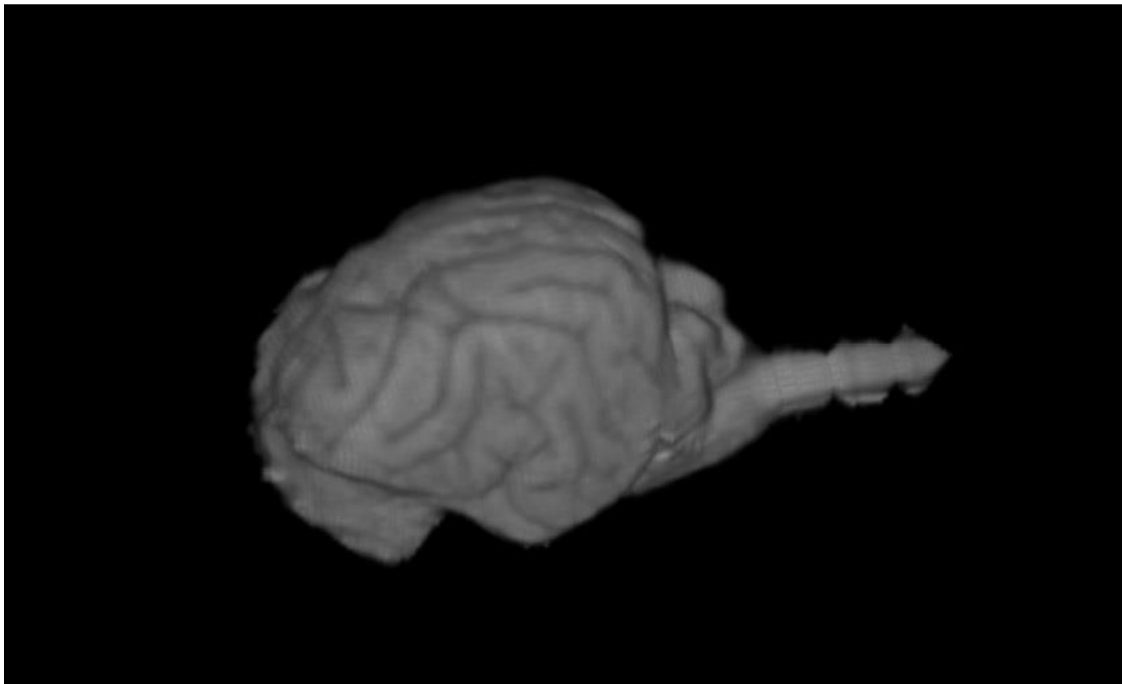


Figure 104: Amira result

- 7.5. Select the “Result” and enable the “Crop Editor” to then crop the box as close as possible to the brain without touching it by moving the green boxes → click OK when finished

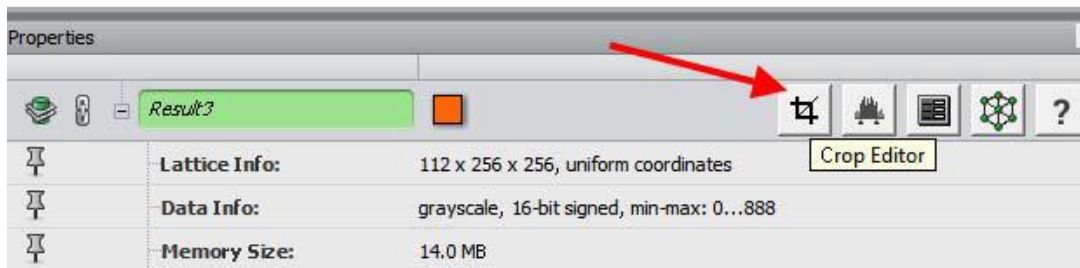


Figure 105: Amira crop editor

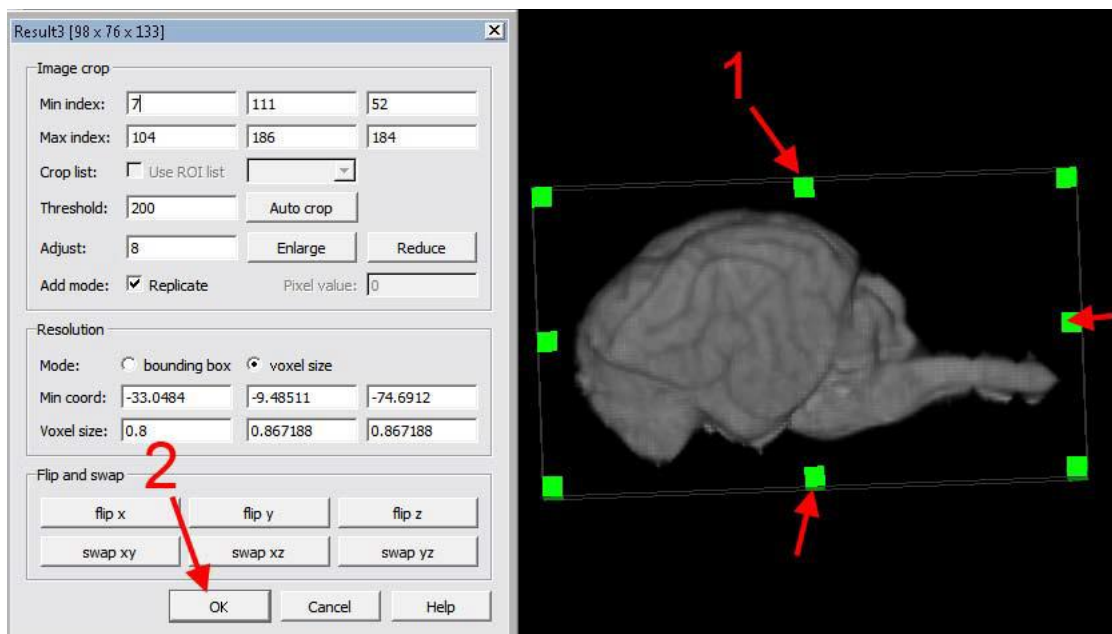


Figure 106: Amira brain crop

- 7.6. Right click the Result → Compute → Volume Operations → Resample

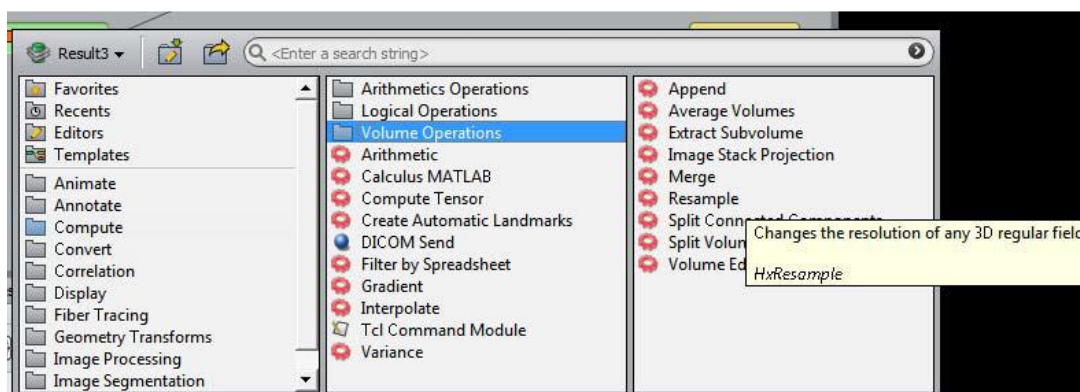


Figure 107: Amira resample

7.7. In the properties of this “Resample” tool, check the “voxel size” box and set all three Voxel Sizes (x, y, and z) to “0.2” → Apply

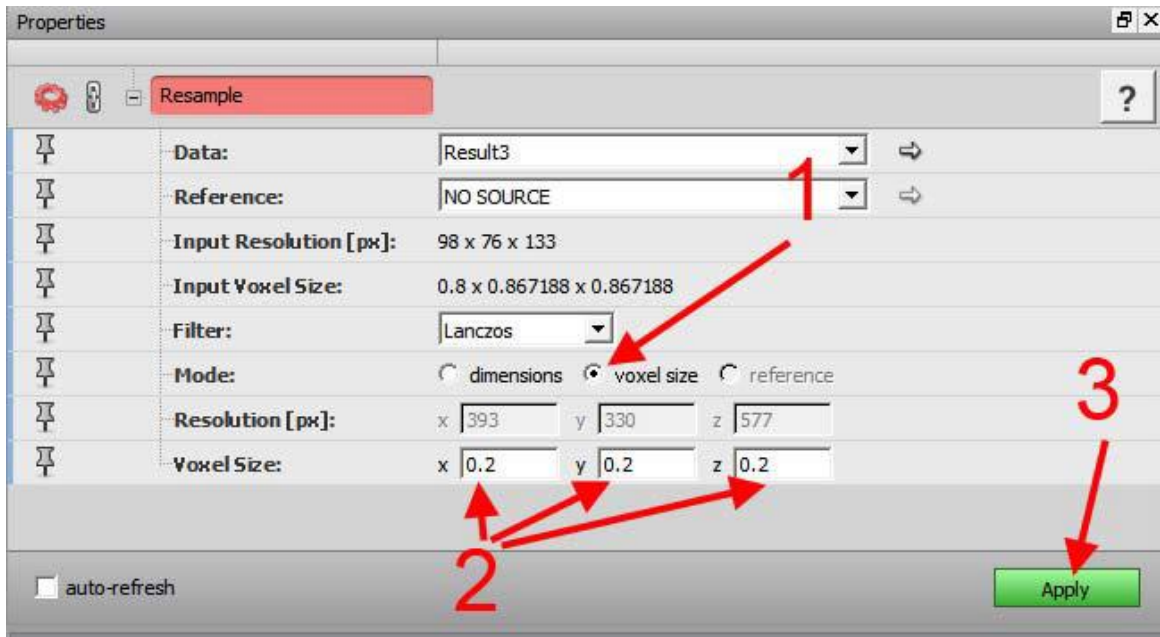


Figure 108: Amira resample settings

7.8. The newly generated “Result.resampled” will be saved as “petname_MRI_Info_brain_resampled.am”

7.9. The “Result” will be saved as “petname_MRI_Info_brain.am”

8 Generating the brain surface:

8.1. Add a new Labelfield (see 6.2) to the “petname_MRI_Info_brain_resampled.am”

8.2. Use the Threshold tool and set the lower value to resemble the edges of the brain →
Select Masked Voxels → “+”

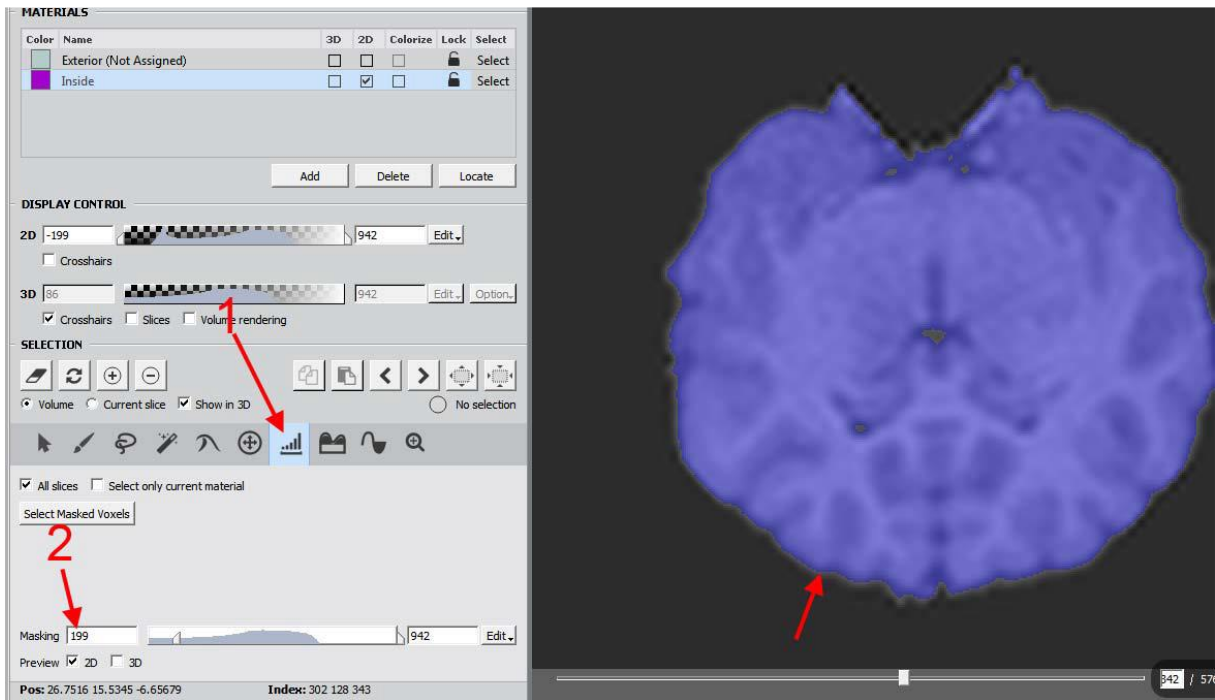


Figure 109: Amira low brain threshold

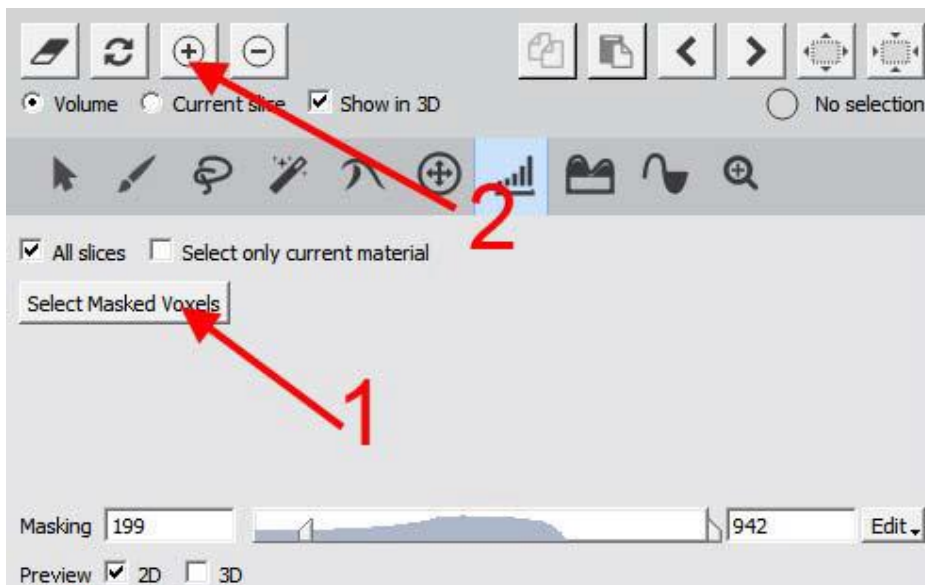


Figure 110: Amira add masked voxels

8.3. Fill the Holes in the menu Segmentation → Fill holes → All slices

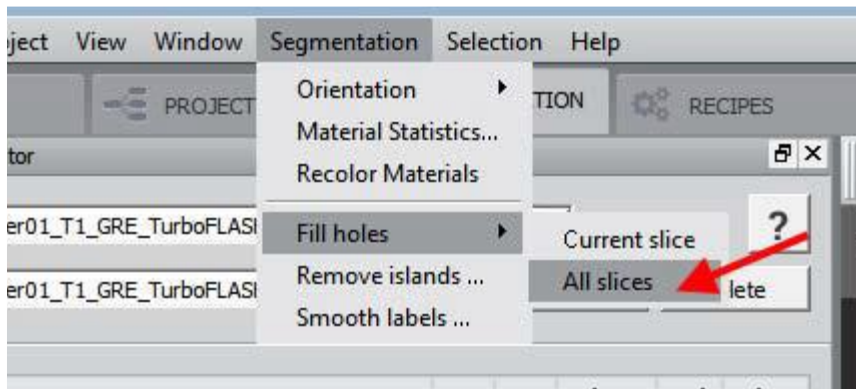


Figure 111: Amira fill holes

8.4. Now soften the brain contour by clicking the menu Segmentation → Smooth labels → Size = 9, Mode = 3D Volume → Apply three times

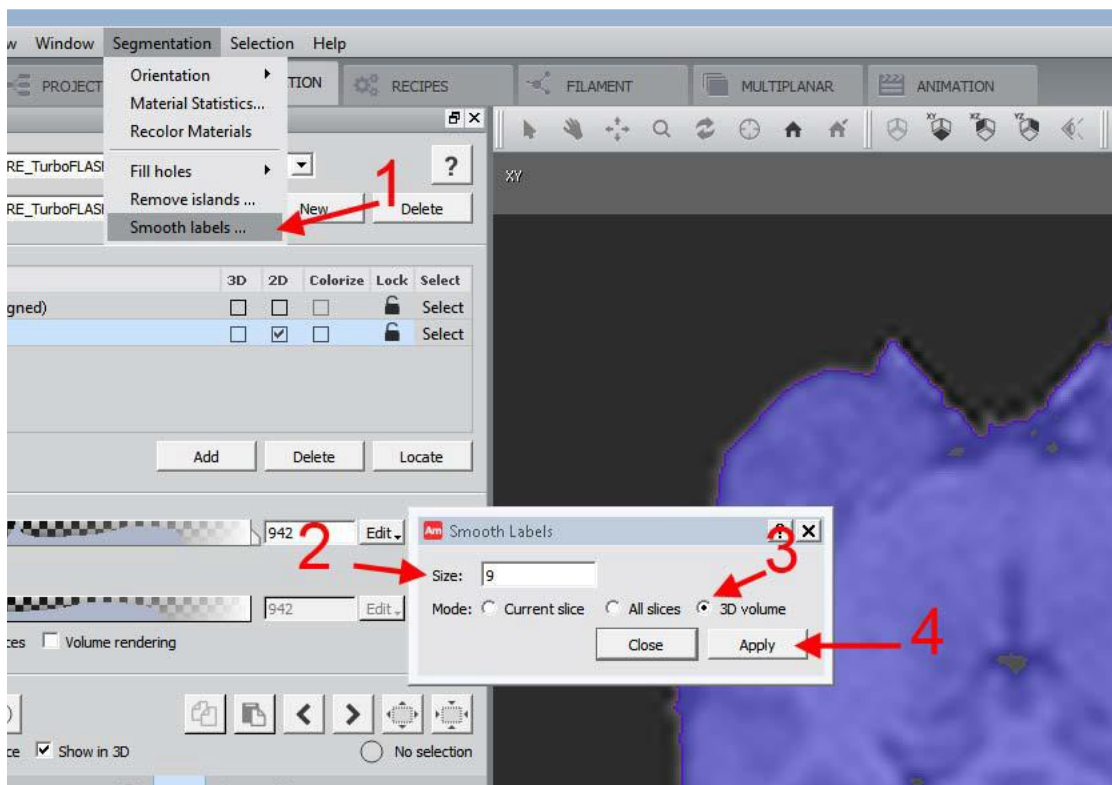


Figure 112: Amira smooth labels

8.5. Switch back to the Project tab and save the labelfile as
 “petname_MRI_Info_brain_resampled.label_brain-contour.am”

8.6. Generate the brain surface by right clicking the new Labelfield → Generate Surface → Apply

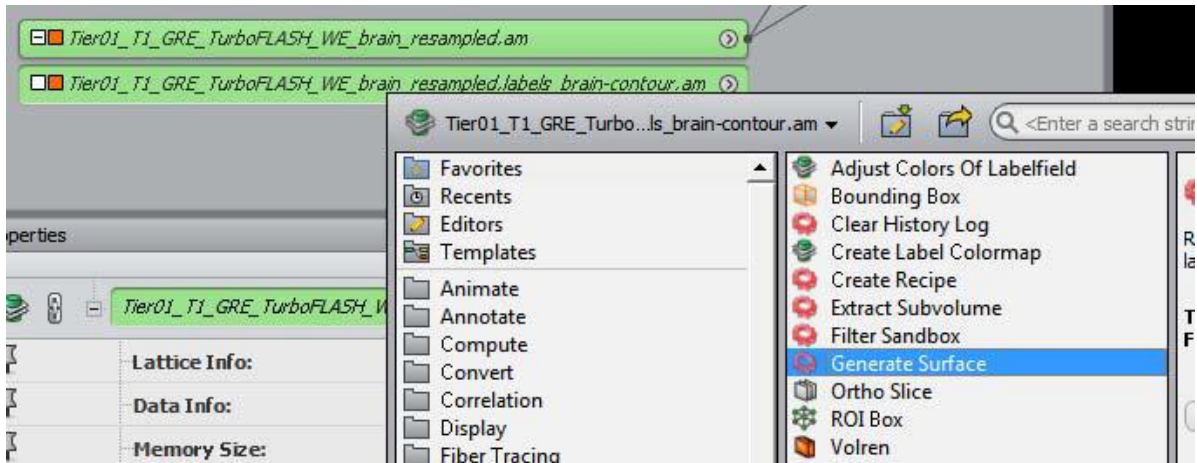


Figure 113: Amira generate surface

8.7. Select the newly generated surface file and reduce the number of triangles by using
 the “Simplification Editor” → Faces = 300 000 → Simplify Now

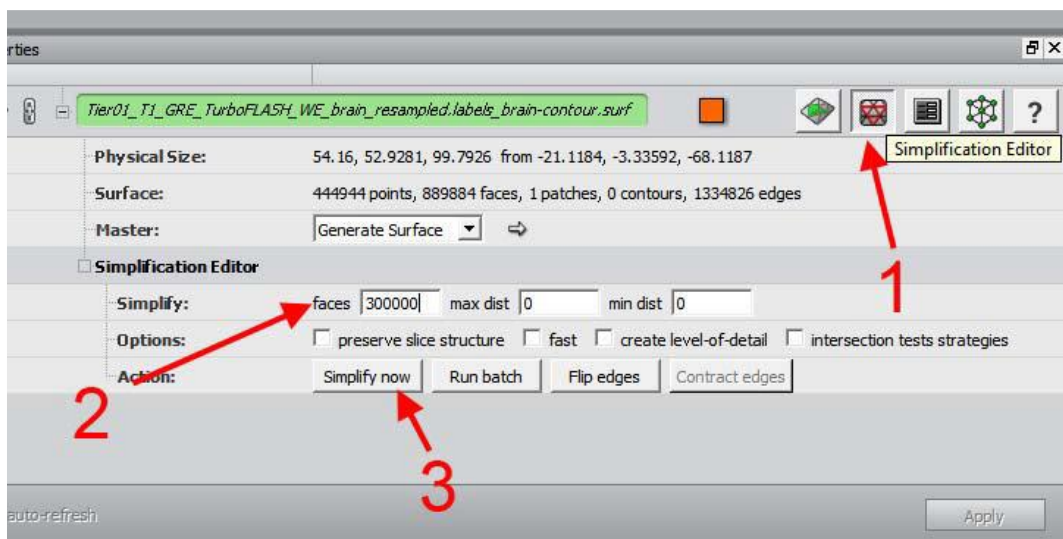


Figure 114: Amira simplification editor

8.8. To check the surface, right click it and choose “Surface View”

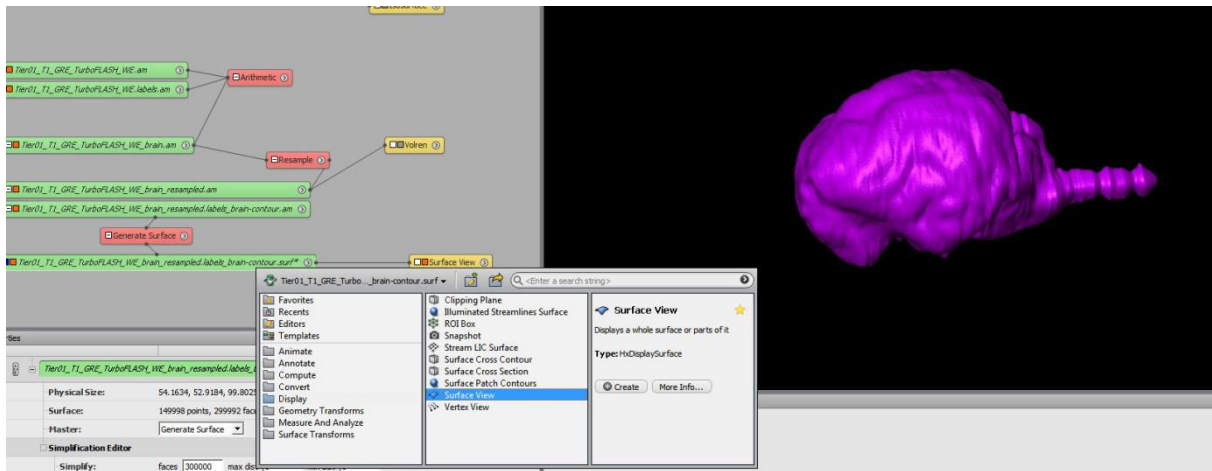


Figure 115: Amira surface view

8.9. This surface will be saved as “petname_brain.surf”. It is important to use the file format “HxSurface binary” (*.surf)!

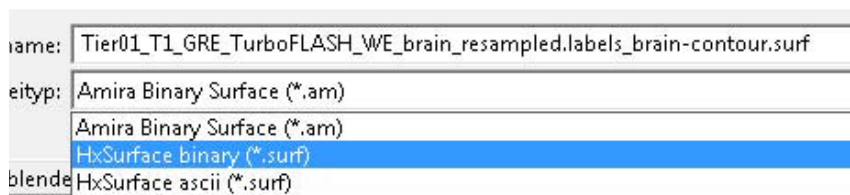


Figure 116: Amira binary

9 Measuring the surface and gyri:

9.1. Open the surface file “petname_brain.surf” and “petname_MRI_Info_brain_resampled.am” and visualize the surface with a Surface View (see 8.8) and the resampled file with a Volren. Hide the Volren by unchecking the orange box next to it and then select the surface to enable the “Surface Editor”.

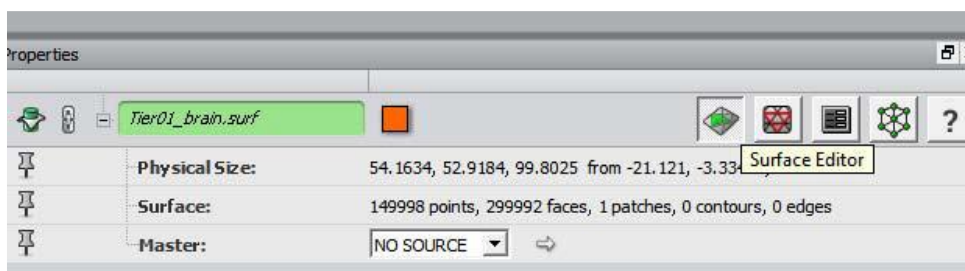


Figure 117: Amira surface editor

9.2. The view automatically switches to “outlined” and the triangles are visible. Use the “Draw contour to highlight faces” tool and uncheck the “Visible triangles only” function.

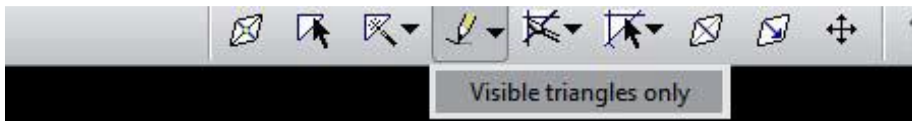


Figure 118: Amira visible triangles

9.3. Set the Surface Draw Style in the properties to “shaded” and then set the view so you see the brain from dorsally.

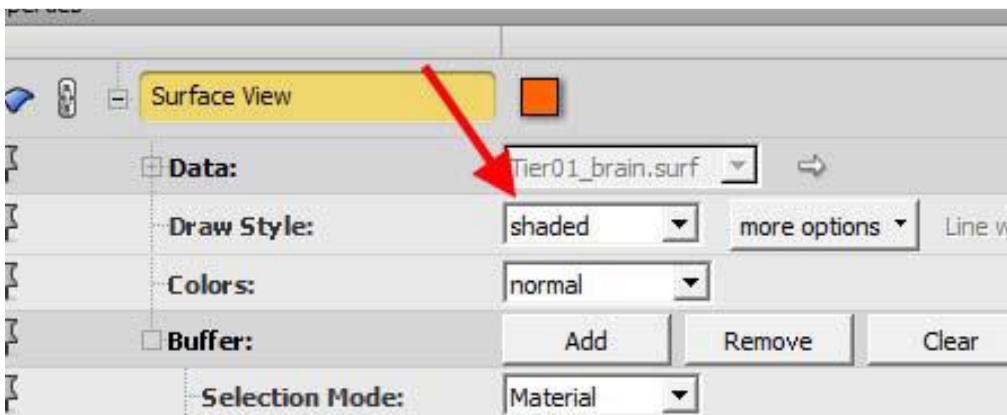


Figure 119: Amira draw style

9.4. Now choose the “Interact” tool and by left clicking and drawing the cursor, you can make a selection on the surface. The first selection should be the right half of the brain, but the selection should be slightly paramedian to the right. Check the selection by viewing the brain from every side and once it is okay, click the menu “Surface” → Edit → Delete Highlighted Faces to delete the red triangles from the surface file.

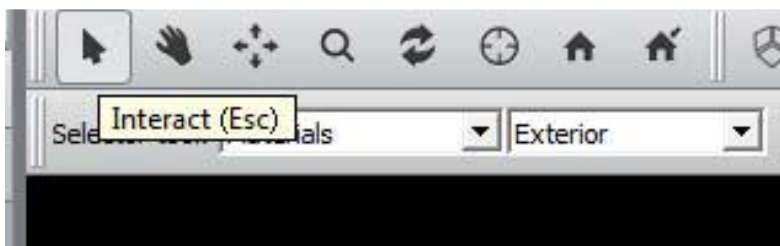


Figure 120: Amira interact tool

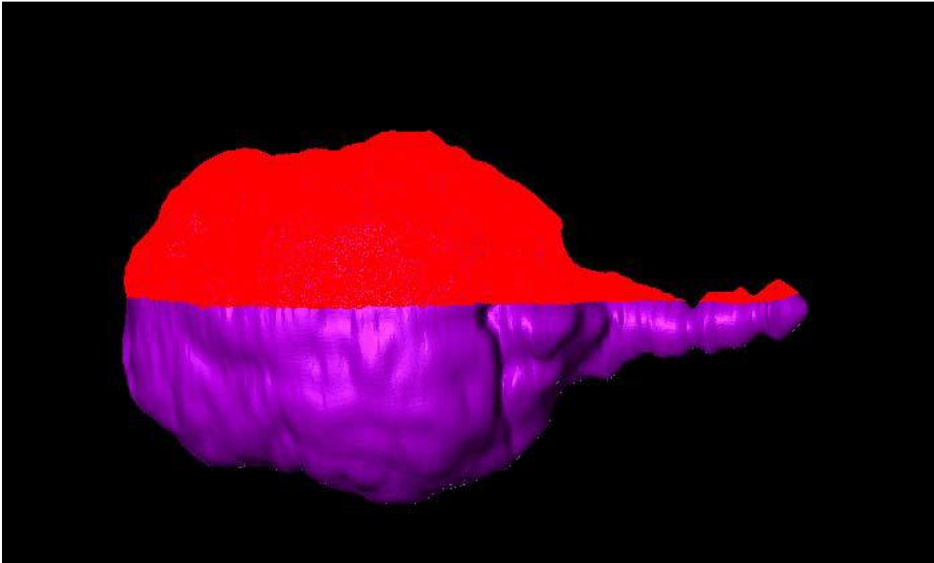


Figure 121: Amira paramedian brain

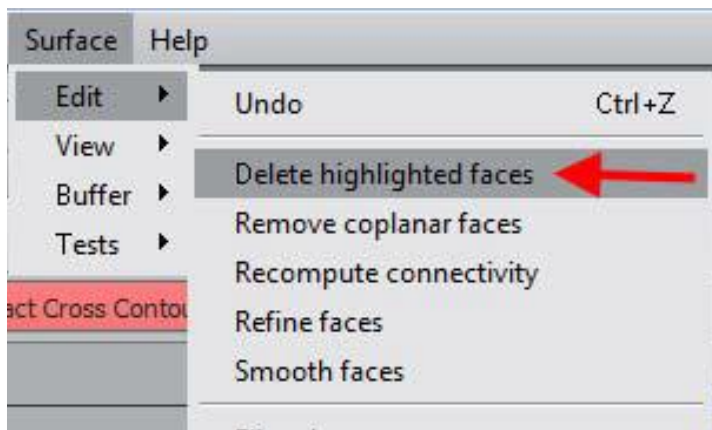


Figure 122: Amira delete highlighted faces

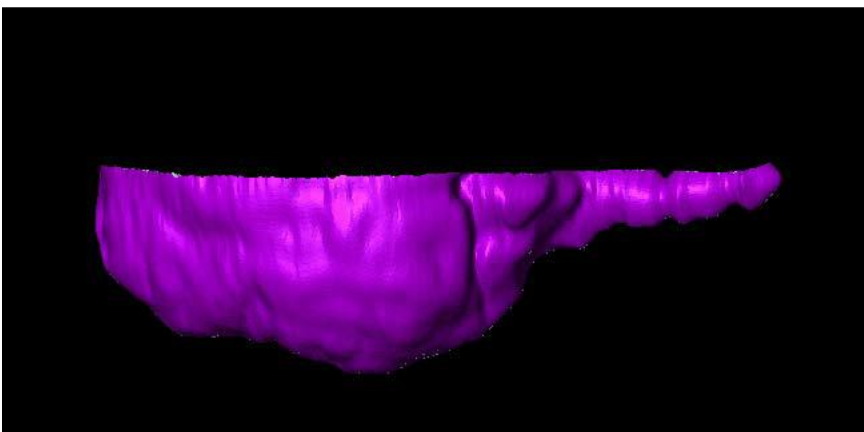


Figure 123: Amira brain half

- 9.5. Close the Surface Editor and save the file as “petname_brain_left.surf” (file format = “HxSurface binary” (*.surf))
- 9.6. Open the original “petname_brain.surf” again and repeat these steps but now with the left side to then save the file as “petname_brain_right.surf”
- 9.7. Open “petname_brain.surf” again, enable the Surface Editor → Draw contour to highlight faces” but leave the “visible triangles only” checked.

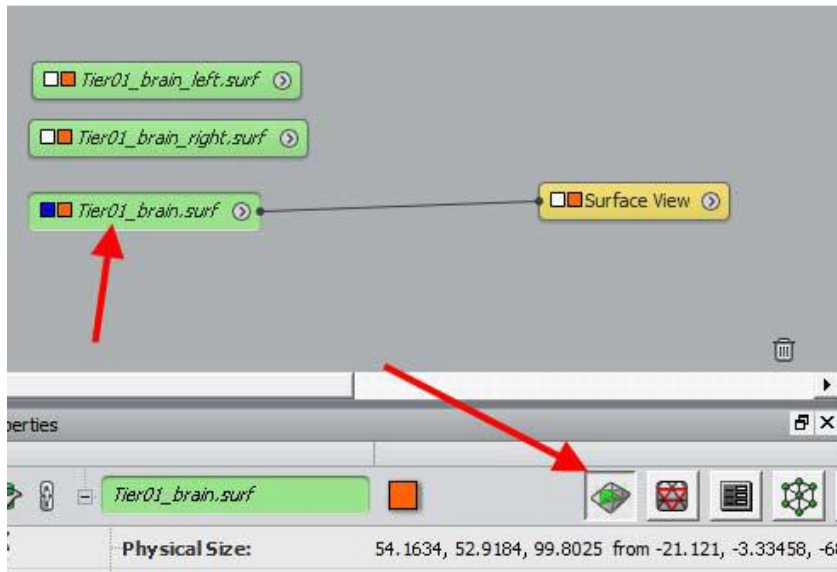


Figure 124: Amira surface editor

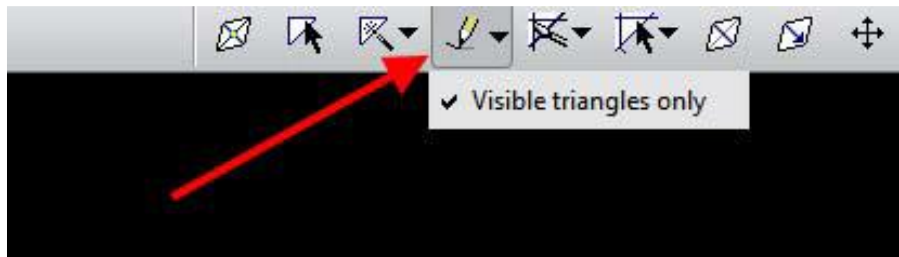


Figure 125: Amira visible triangles

9.8. Set the Surface Draw Style to “shaded” → Interact tool → select the Cortex by turning the brain. It is recommended to now show the Volren file for better visibility of the borders of the Cortex.

9.9. Once the Cortex of one brain half is selected, use the menu Surface → Edit → Set Boundary IDs

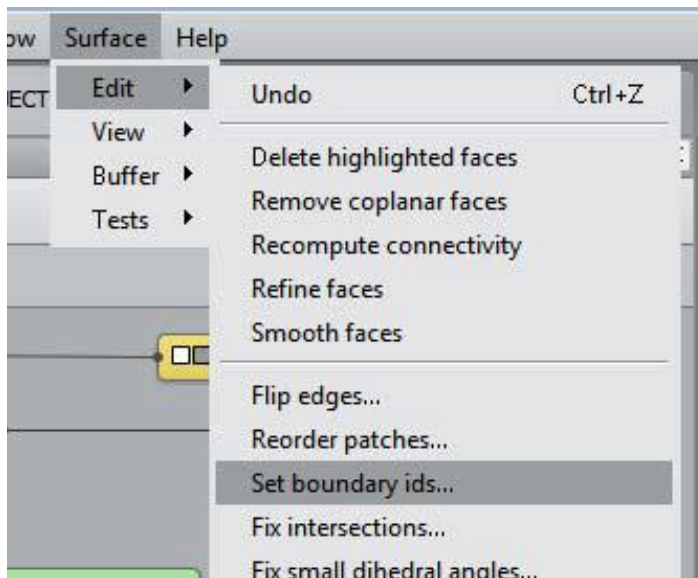


Figure 126: Amira boundary ids

9.10. Then click New → set the Material name in Info and a colour → OK → select new Boundary ID in the list → Set

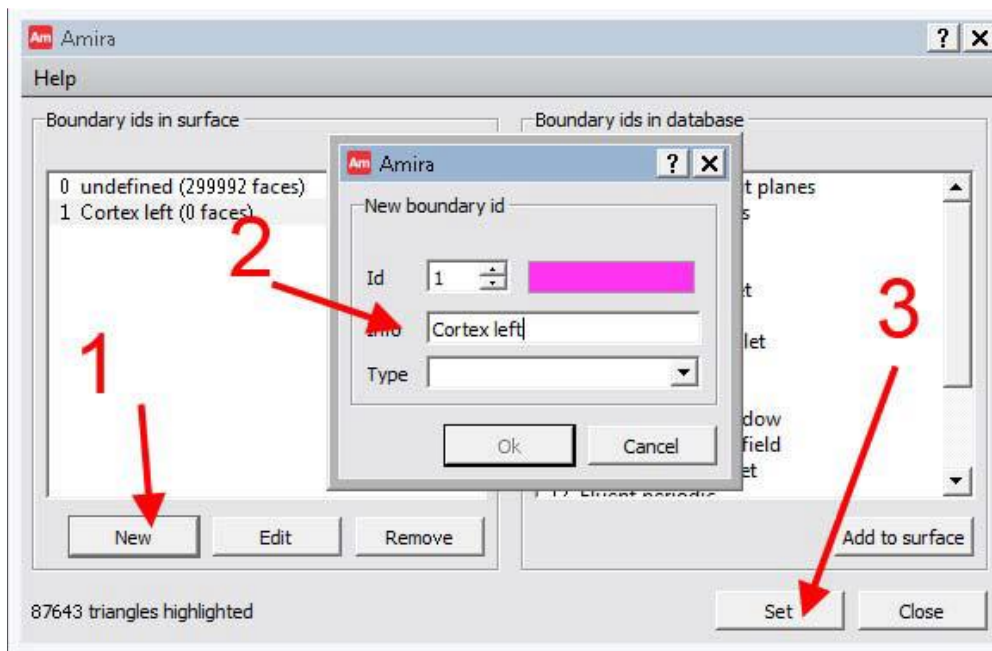


Figure 127: Amira boundary id settings

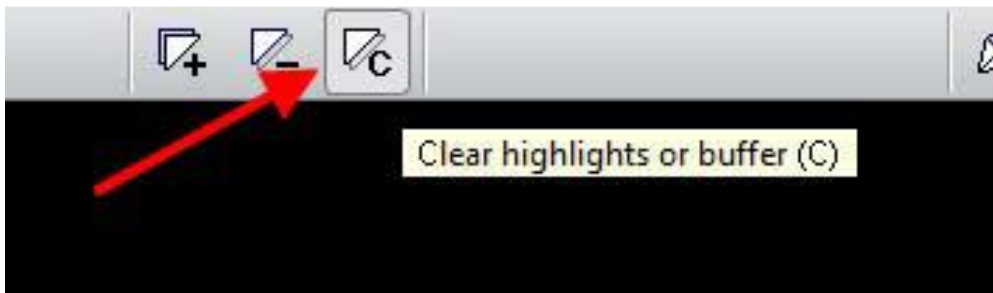


Figure 128: Amira clear buffer

9.11. In the “Surface View”, change the “Colours” to “boundary ids”.

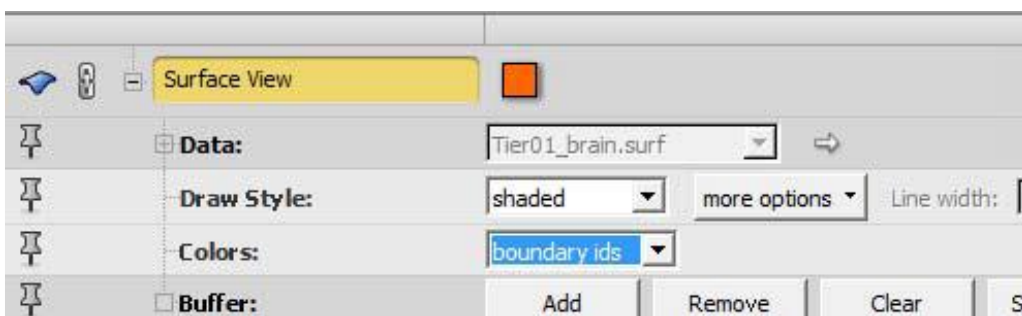


Figure 129: Amira draw style boundary

9.12. Now repeat the same steps to select the right Cortex and set its boundary id.

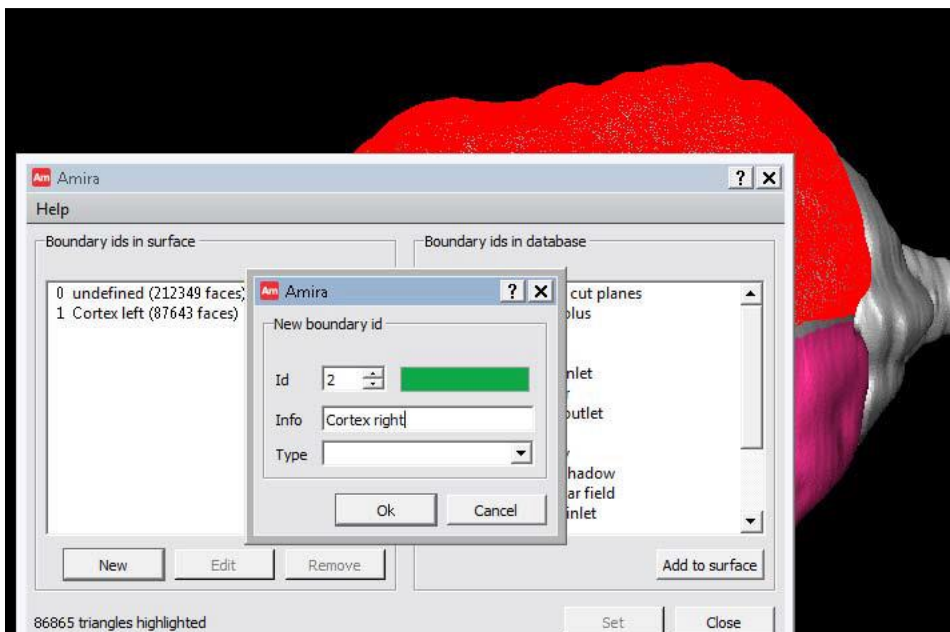


Figure 130: Amira boundary id 2

9.13. Close the Surface Editor and save the file as “petname_brain_cortex-measurements.surf”

9.14. Right Click the surface → Measure and Analyze → Surface Area Volume

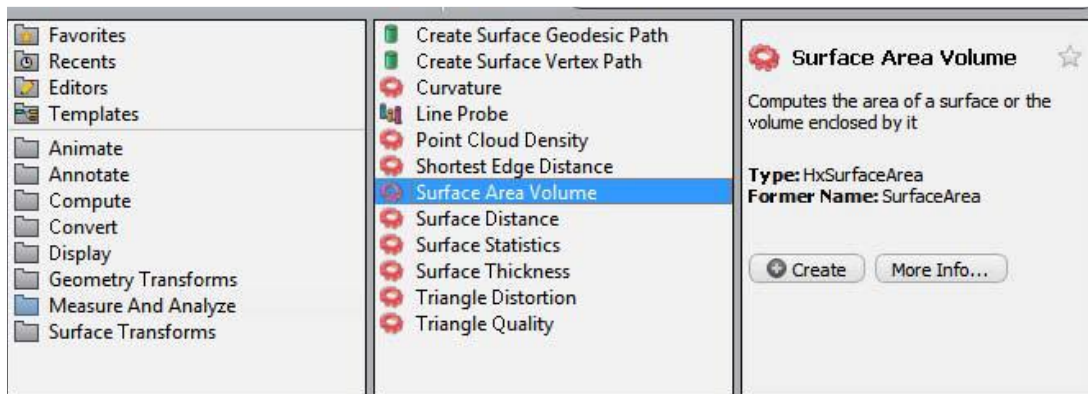


Figure 131: Amira surface area volume

9.15. In properties, set the mode to “patches” and click Apply

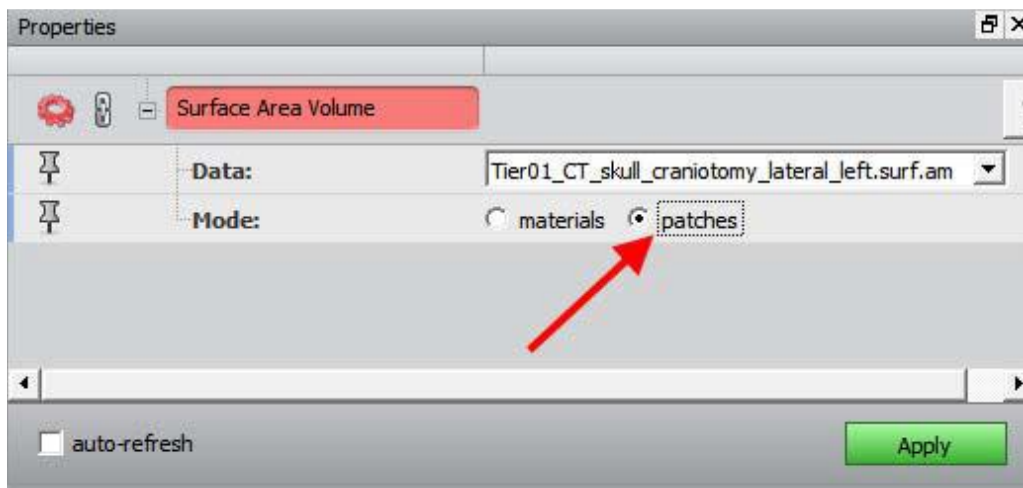
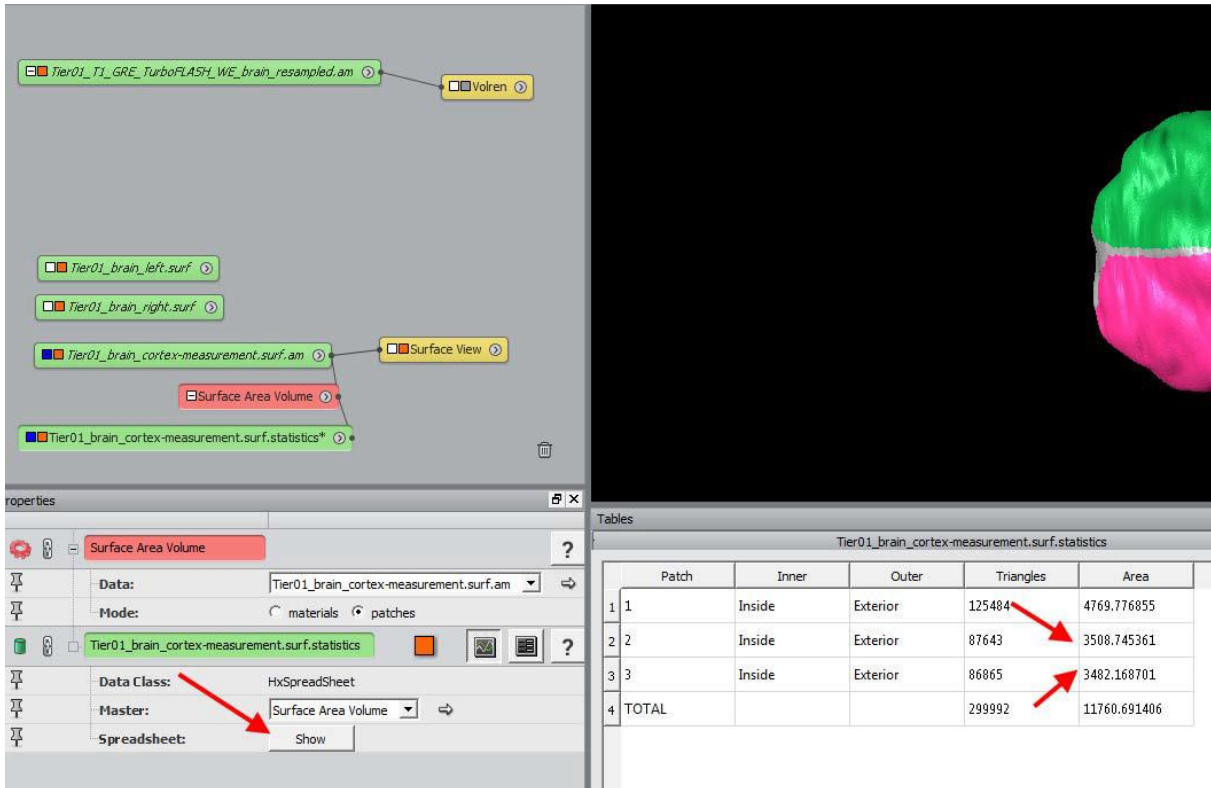


Figure 132: Amira patches

- 9.16. A new table will be generated → Click “show” and now read the table. Patch 1 is the area that was not selected, Patch 2 the left Cortex and Patch 3 the right Cortex



The screenshot shows the Amira software interface. On the left, the Hierarchy panel displays several objects: Tier01_T1_GRE_TurboFLASH_WE_brain_resampled.am (Volren), Tier01_brain_left.surf, Tier01_brain_right.surf, Tier01_brain_cortex-measurement.surf.am (Surface View), Surface Area Volume, and Tier01_brain_cortex-measurement.surf.statistics*. The Properties panel for 'Surface Area Volume' shows 'Data: Tier01_brain_cortex-measurement.surf.am', 'Mode: materials', 'Data Class: HxSpreadSheet', 'Master: Surface Area Volume', and 'Spreadsheet: Show'. The Tables panel displays a table with the following data:

Tier01_brain_cortex-measurement.surf.statistics					
	Patch	Inner	Outer	Triangles	Area
1	1	Inside	Exterior	125484	4769.776855
2	2	Inside	Exterior	87643	3508.745361
3	3	Inside	Exterior	86865	3482.168701
4	TOTAL			299992	11760.691406

Figure 133: Amira show surface area

- 9.17. To draw the Gyri, open “petname_brain_left.surf” and “petname_MRI_Info_brain_resampled.am”. Generate a Volren for the latter.

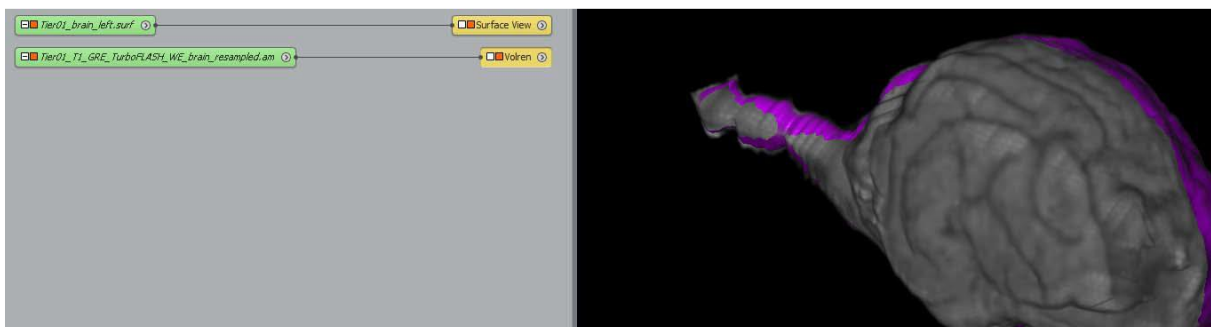


Figure 134: Amira resampled Volren

- 9.18. For the file “petname_brain_left.surf”, the Surface Editor will be opened.
- 9.19. Set the Draw Style in the Surface View to “shaded” and in “more options” the function “Back Face” needs to be selected. The Surface disappears behind the Volren.

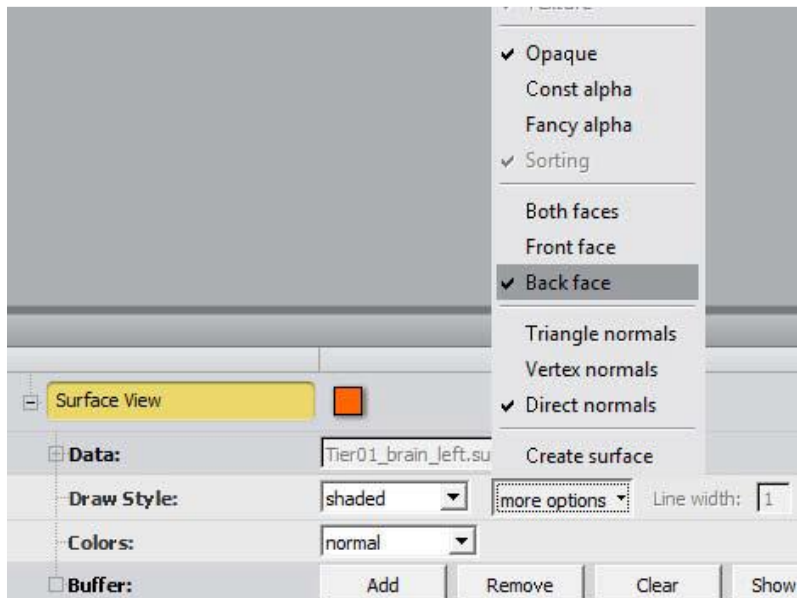


Figure 135: Amira back faces

- 9.20. Now the Gyri need to be drawn in a specific order using the “Draw contour to highlight faces” tool and enable “visible triangles only”.

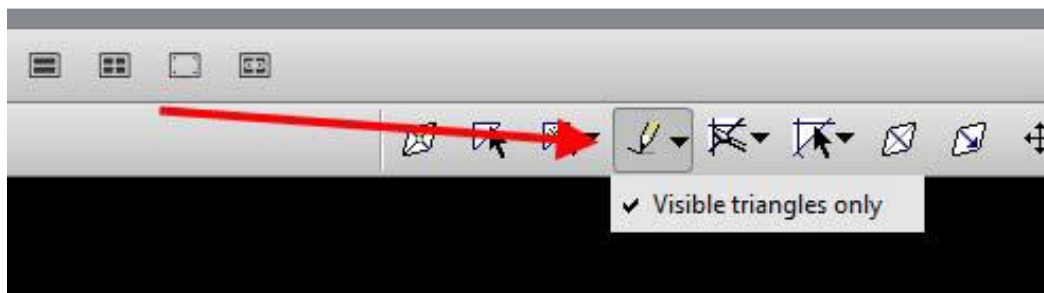


Figure 136: Amira visible triangles

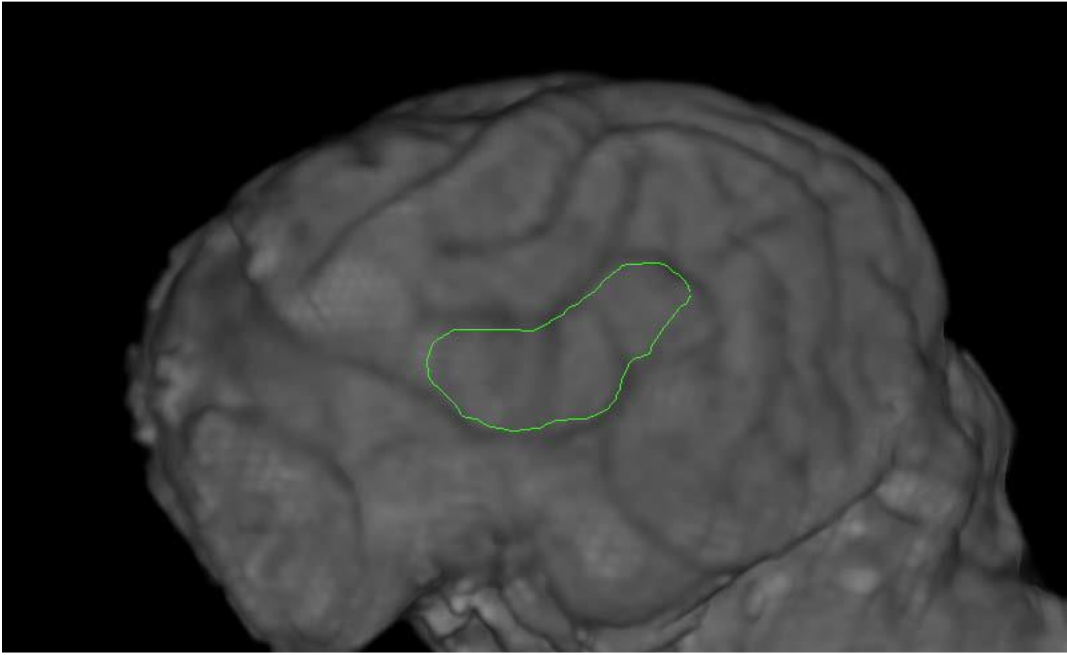


Figure 137: Amira draw Gyrus

- 9.21. To check the selection on the Surface, change the “Draw Style” to “Both faces” again. Always check if other areas of the surface are selected as well (turn the brain around)

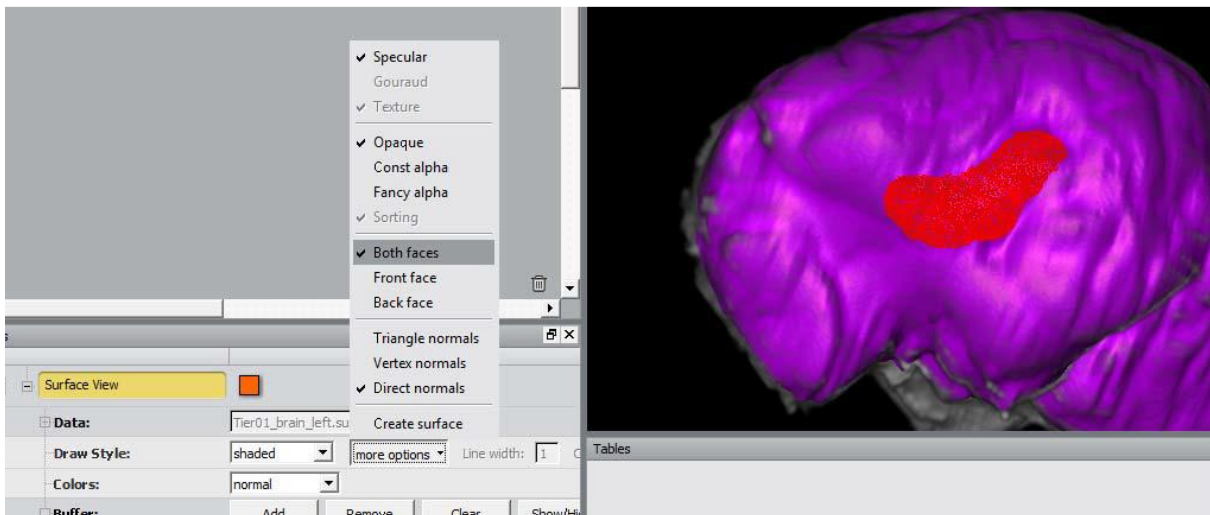


Figure 138: Amira both faces

9.22. If the selection is correct, set the boundary ID, its colour and name.

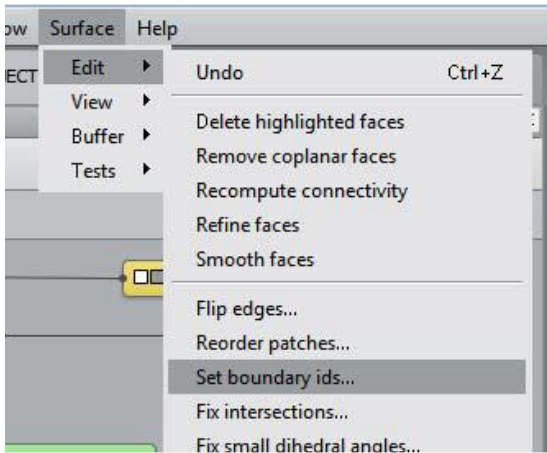


Figure 139: Amira set boundary id

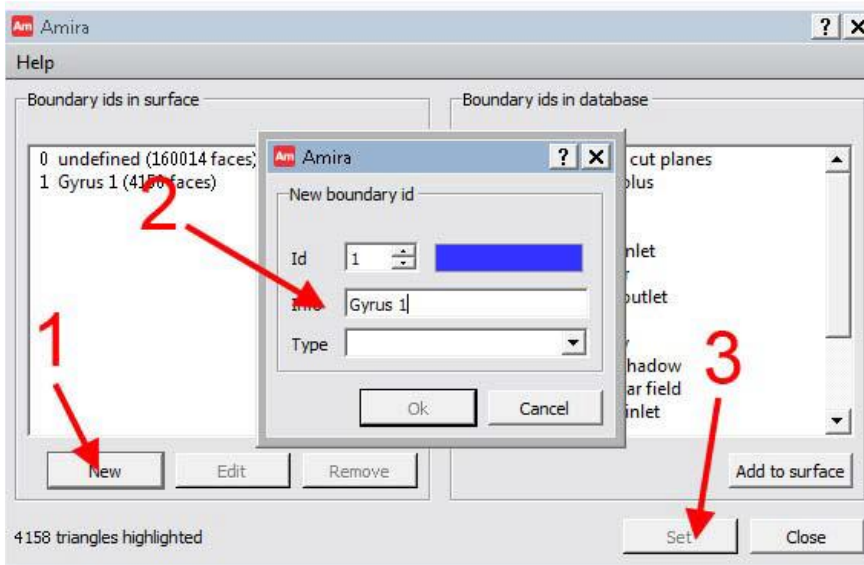


Figure 140: Amira boundary id settings

9.23. "Clear highlights or buffer"

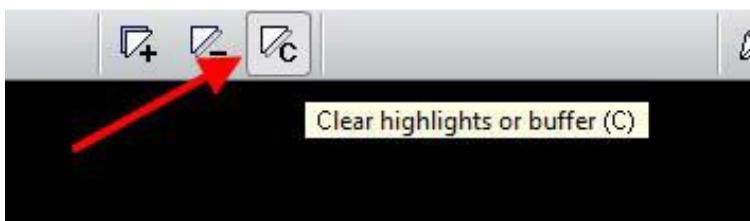


Figure 141: Amira clear highlights

9.24. Change the “Colours” of the surface view to “boundary ids”

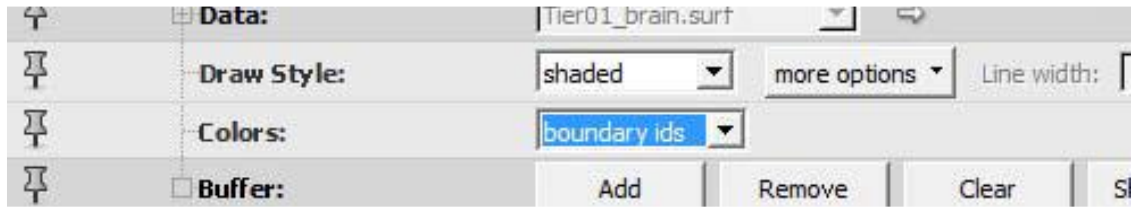


Figure 142: Amira surface view colour

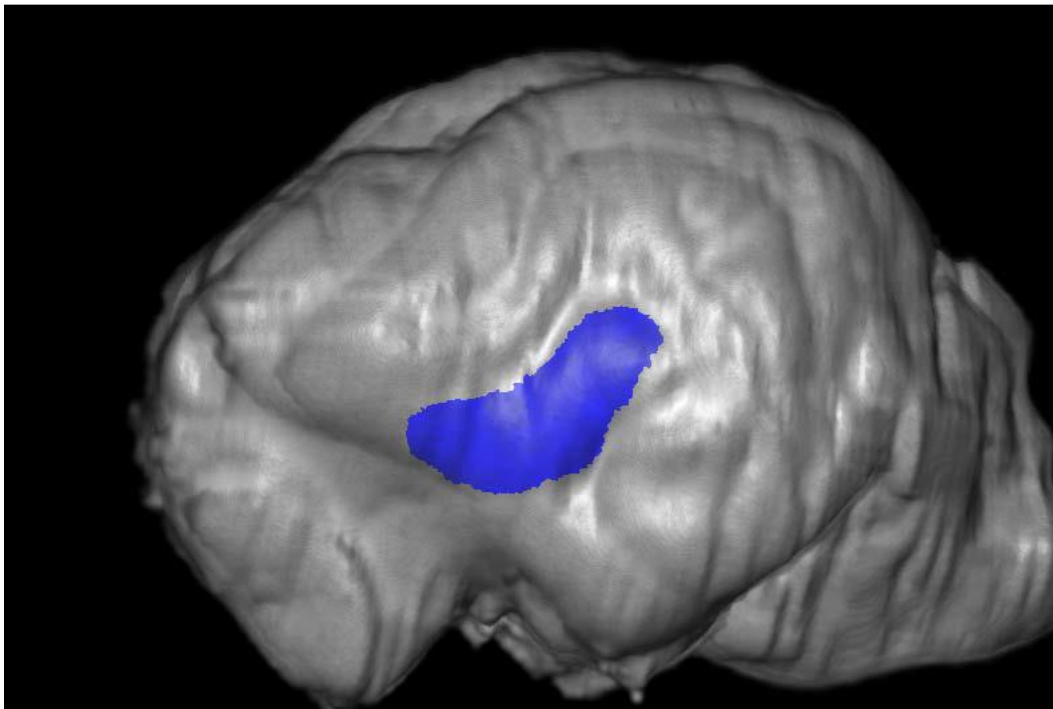


Figure 143: Amira coloured Gyrus

- 9.25. Draw the next Gyrus (repeat steps 9.20 to 9.23) and after setting the view to “both faces” always make sure there is no overlap between these Gyri (delete them with ctrl + left mouse button)

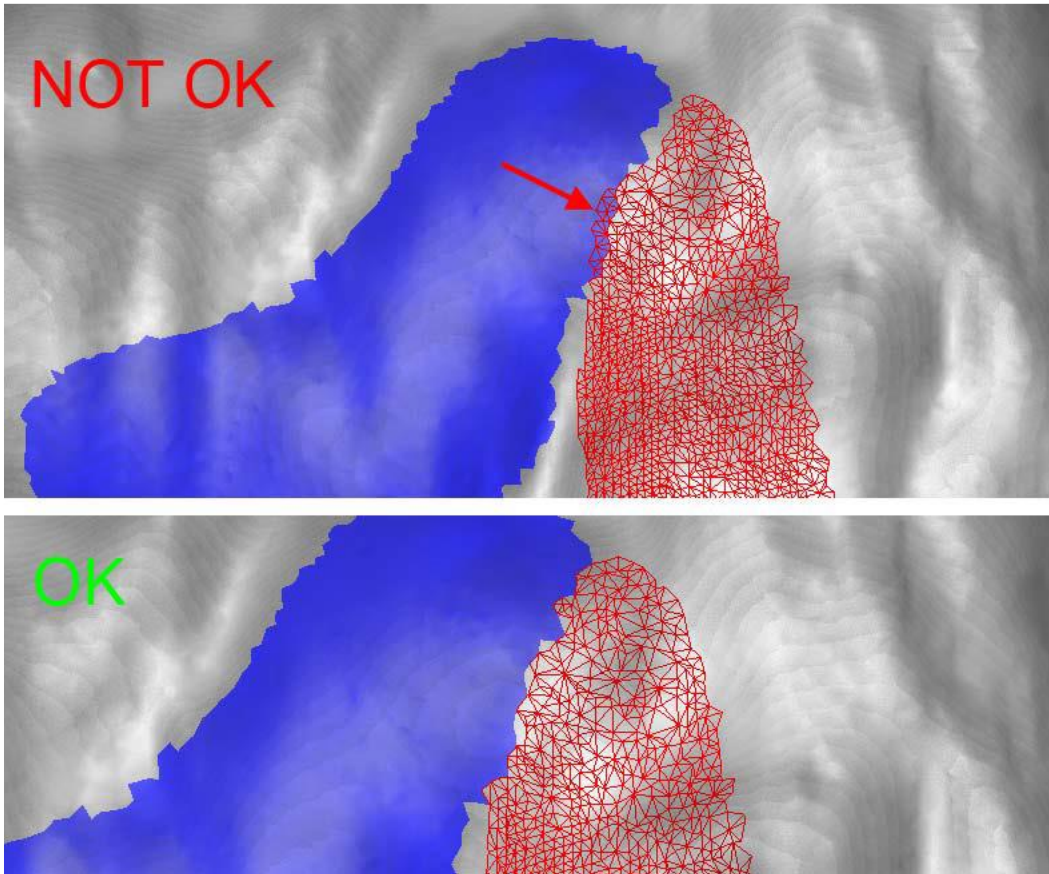


Figure 144: Amira Gyri overlap

- 9.26. The surface should look like this after setting the second boundary id/Gyrus

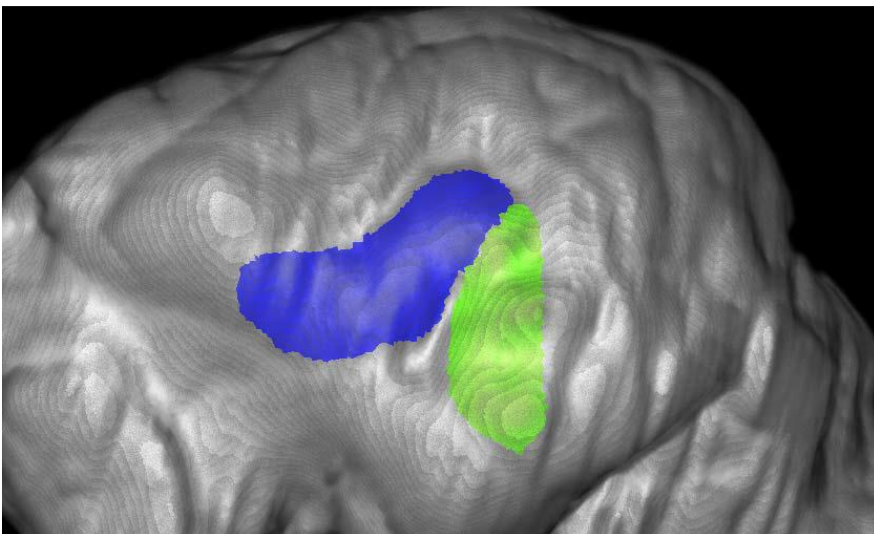


Figure 145: Amira Gyri drawn

9.27. Once all Gyri are added to the surface, save the surface as “petname_brain_left_gyri.surf” (“HxSurface binary”)

9.28. The Gyri can be checked in the Surface Editor by using the “Selector tool” and setting it to “boundary ids”

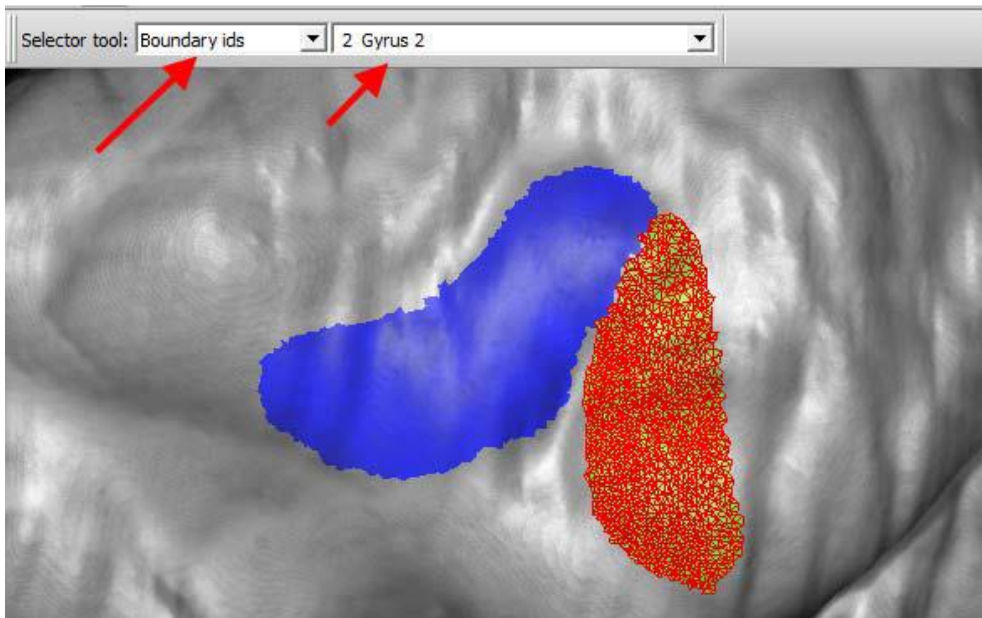


Figure 146: Amira selector tool

9.29. Also set the selector tool to “patches” and make sure the number of patches is the same as the number of boundary ids

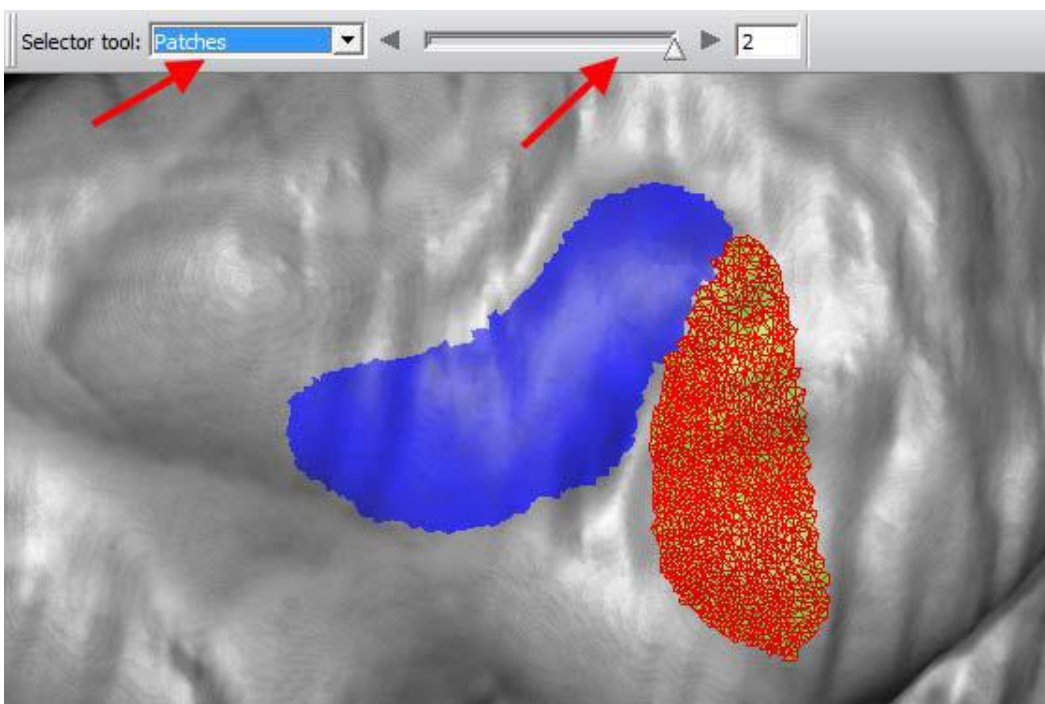


Figure 147: Amira patch selector

- 9.30. Measure the Gyri Area by right clicking the surface file → Measure and Analyze
→ Surface Area Volume

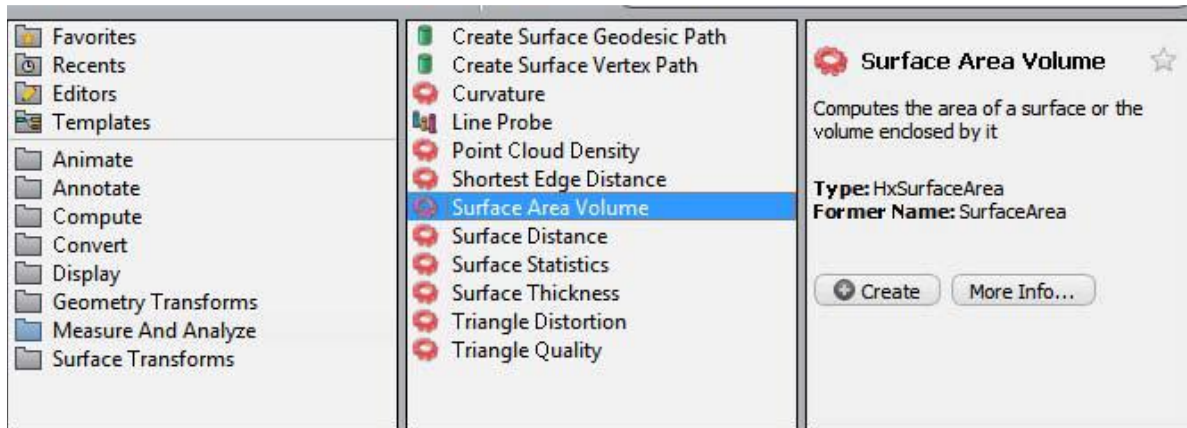


Figure 148: Amira surface area volume

- 9.31. Set the properties to “patches” and hit Apply

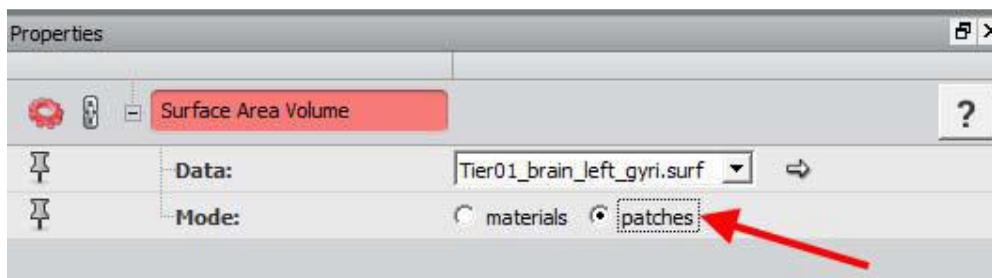


Figure 149: Amira patches apply

- 9.32. A new table will be generated and saved under the suggested name (petname_brain_left_gyri.statistics.am). Then “show” the table and read the values of each patch in mm². The number of the patch resembles the number of the boundary id + 1. So, boundary ID 0 should be Patch 1 in the table.

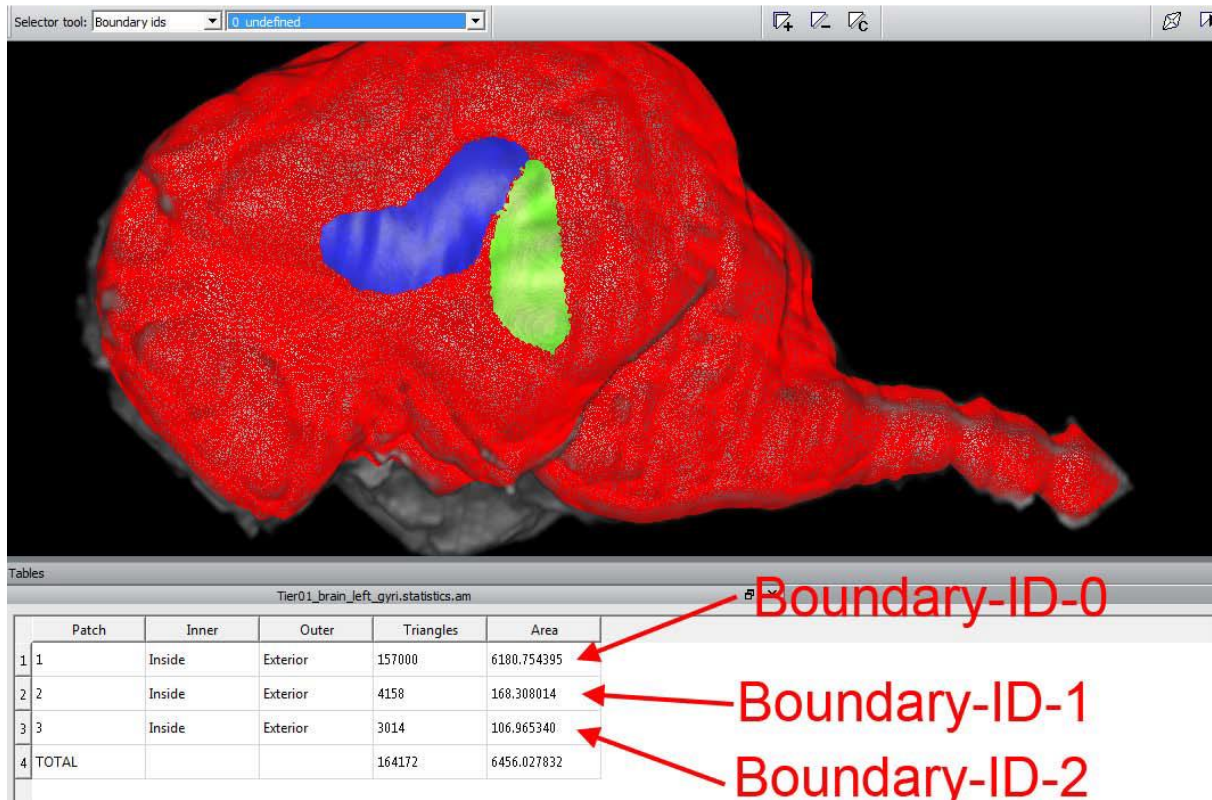


Figure 150: Amira show surface area

- 9.33. Always use the Selector tool (set to patches) to check if the patch and boundary id match.

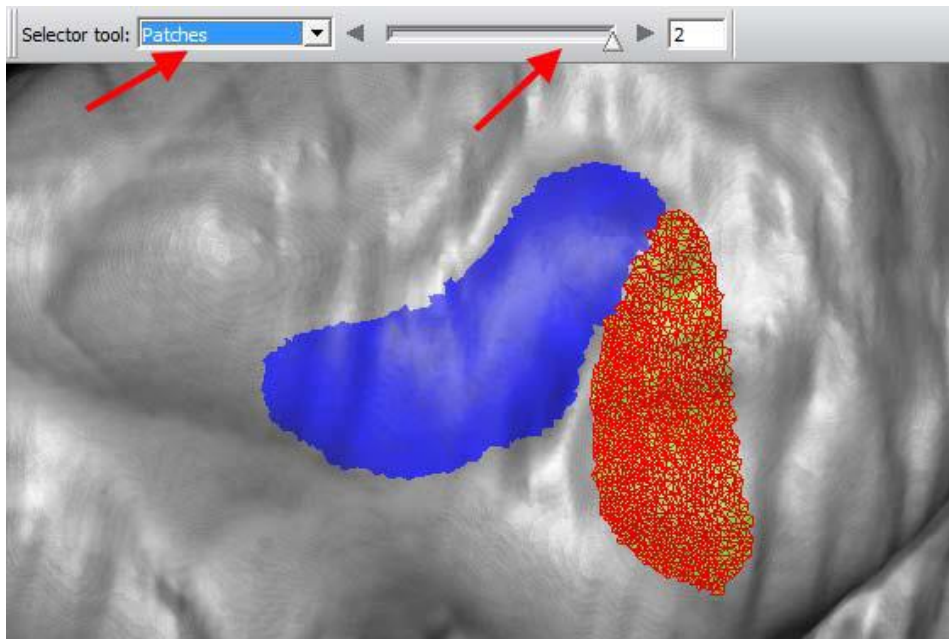


Figure 151: Amira patch selector

- 9.34. Repeat steps 9.17 to 9.33 for the right half of the brain

10 Generating the skull model and measuring the craniotomy area

- 10.1. Generate an Isosurface of the CT scans (see 2.2) with a Threshold of 350
- 10.2. In its properties → more options → Create Surface

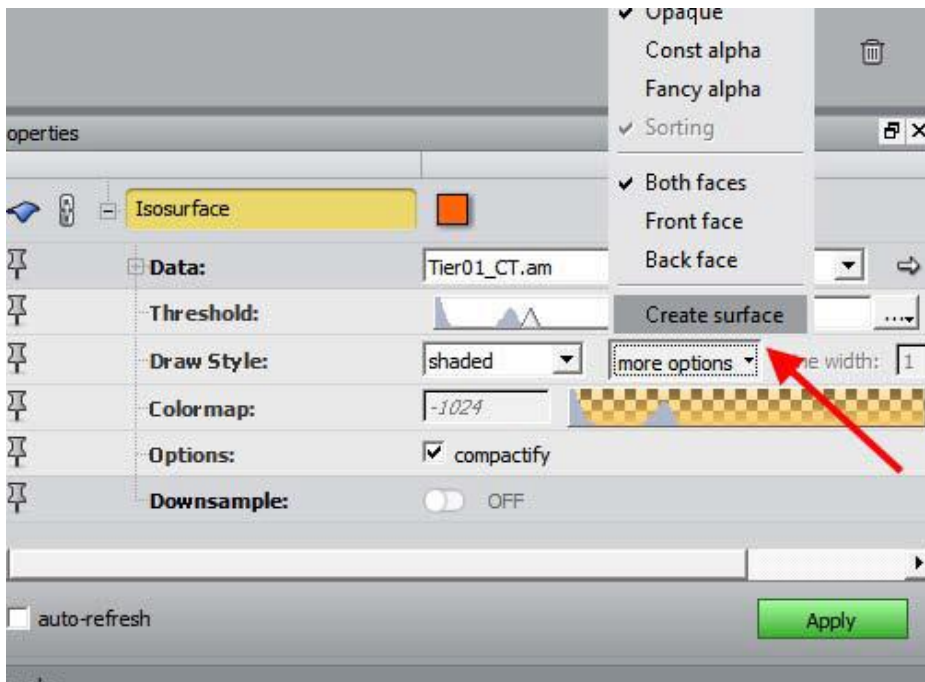


Figure 152: Amira create surface

- 10.3. The newly generated Surface is saved as “petname_CT_skull.surf”
- 10.4. Delete the Isosurface and generate a Surface View (see 2.2) and change the Draw Style → more options → Direct normals

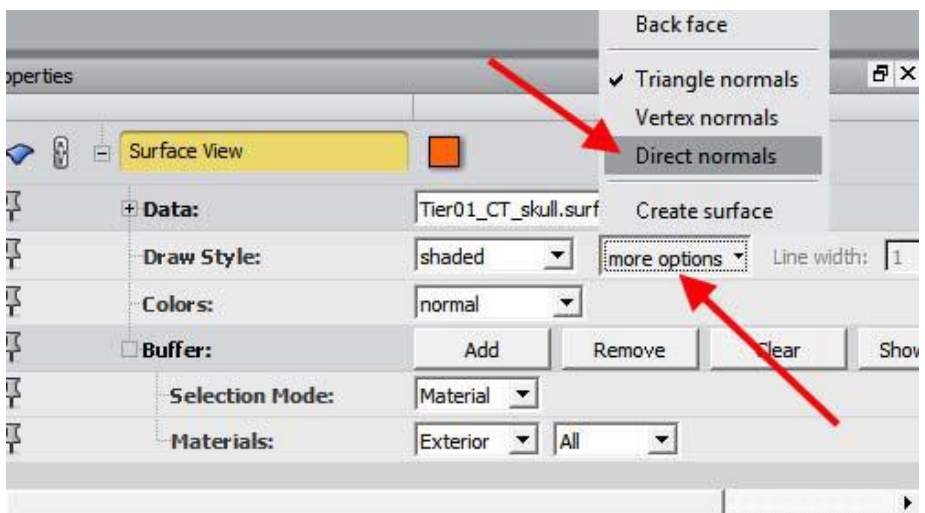


Figure 153: Amira direct normals

- 10.5. Right click into the Project space and create a new object → Points and Lines
→ Landmarks

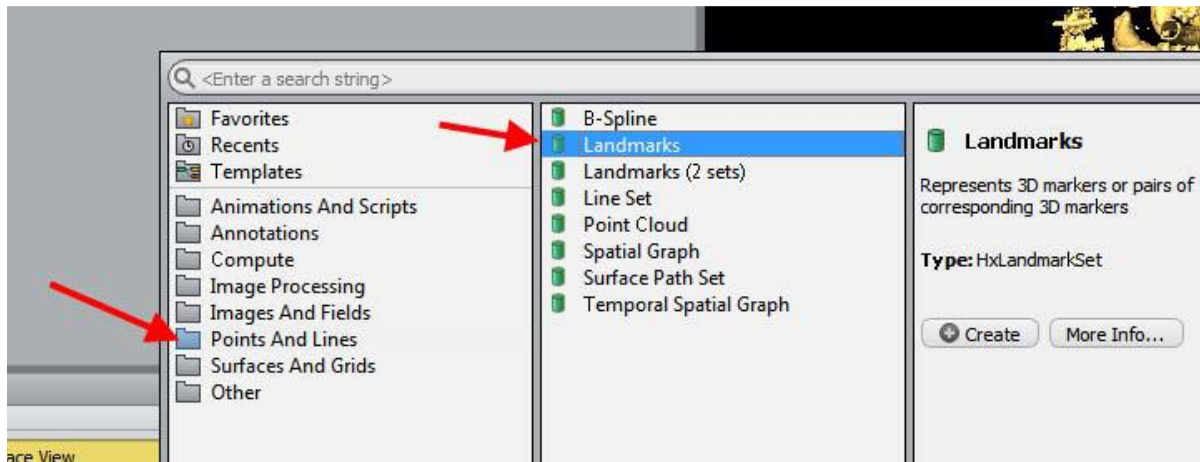


Figure 154: Amira landmarks

- 10.6. Now set the landmarks (see 3) for the drill-holes/burr-holes). You can use the “Measure” tool to measure distances (unit is mm)

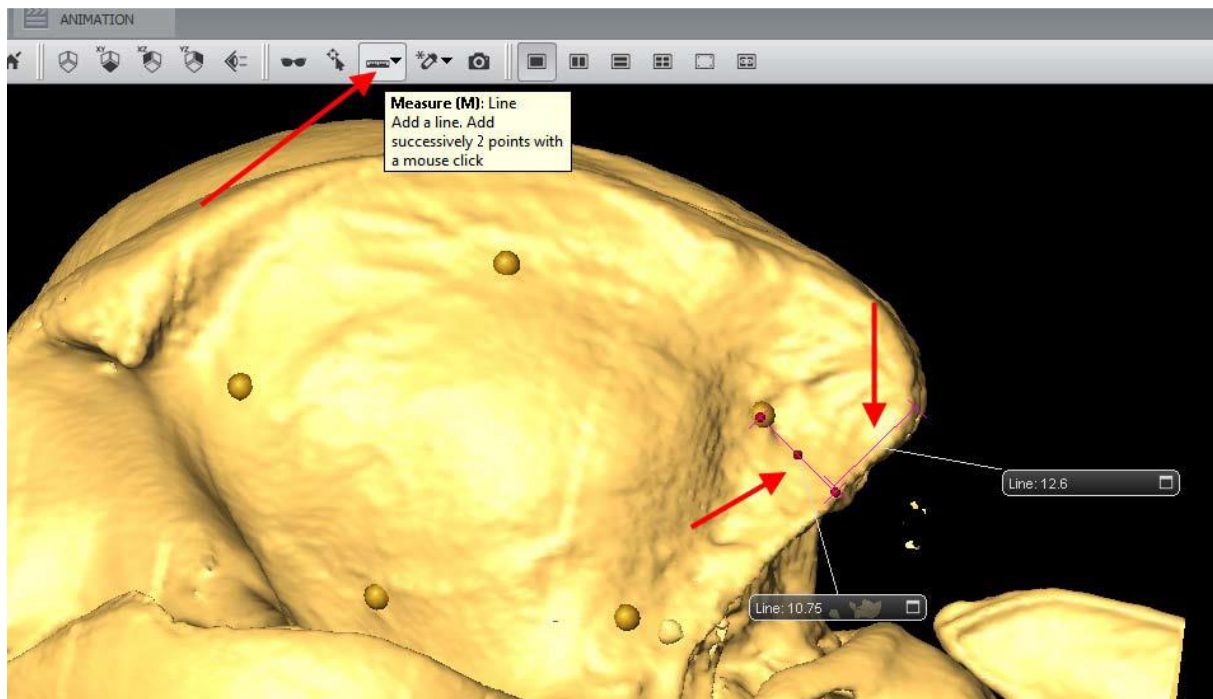


Figure 155: Amira measure tool

- 10.7. Save the landmarks as “petname_CT_drillholes_approach.landmark.Ascii”
- 10.8. Change the landmark size in the properties of the Landmark view to 0.5

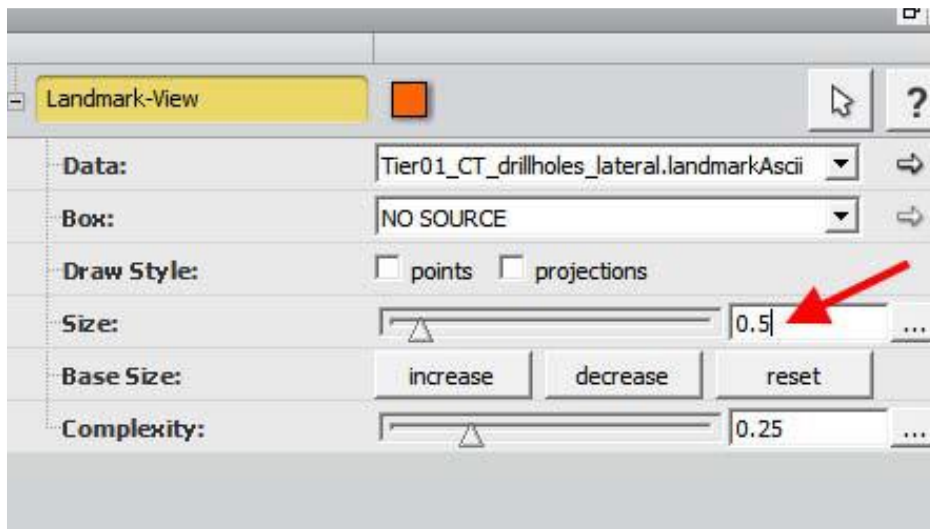


Figure 156: Amira landmark size

- 10.9. Enter the Surface Editor of the “petname_CT_skull.surf”

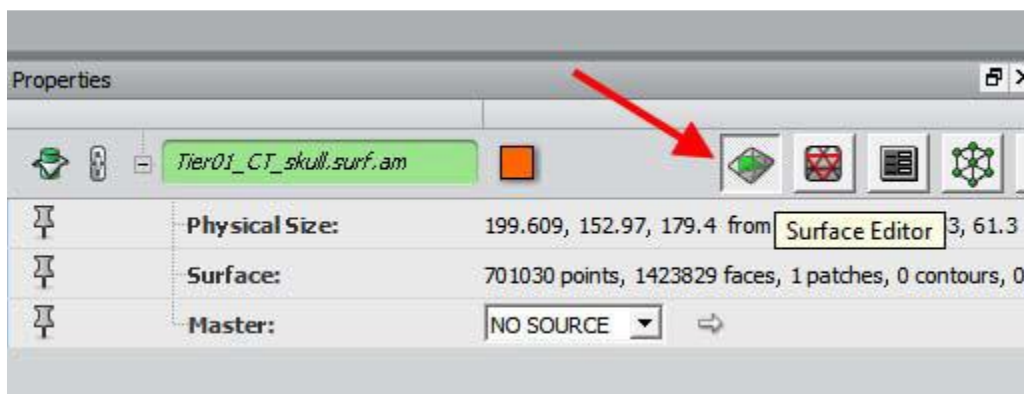


Figure 157: Amira surface editor

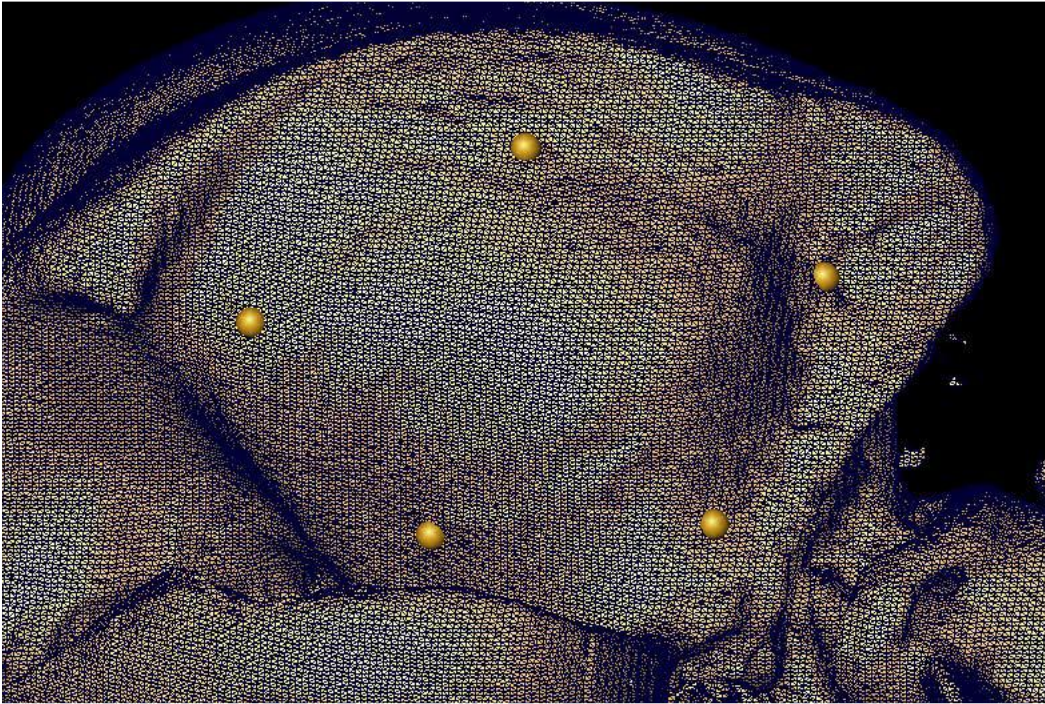


Figure 158: Amira draw contour

10.10. Use the “Draw contour to highlight faces” tool and enable “visible triangles only”



Figure 159: Amira visible triangles

- 10.11. Use the “Interact” tool to draw the selection whilst holding down the left mouse button. (delete with ctrl + left mouse button)

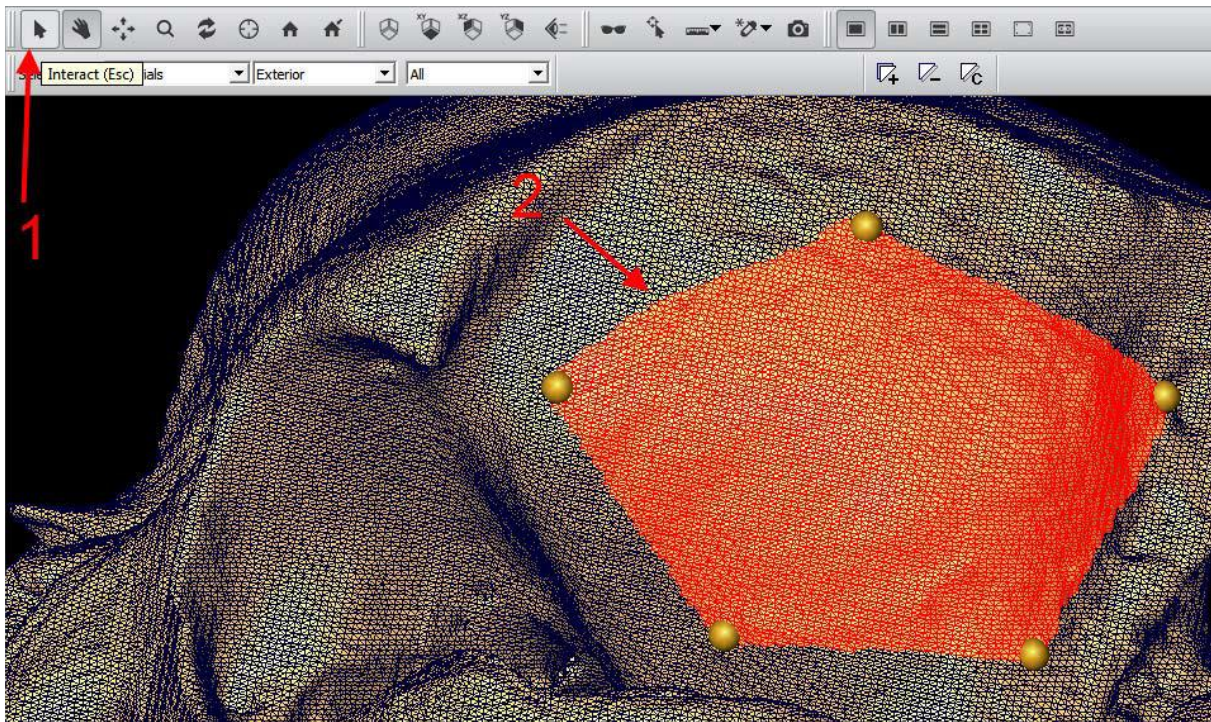


Figure 160: Amira draw craniotomy

- 10.12. Check the selection by rotating the whole skull
 10.13. When the selection is complete, set a new boundary id

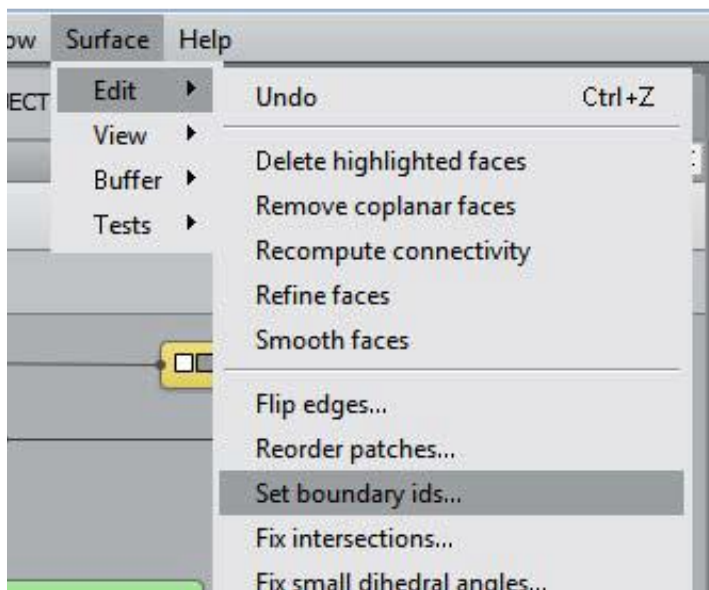


Figure 161: Amira set boundary ids

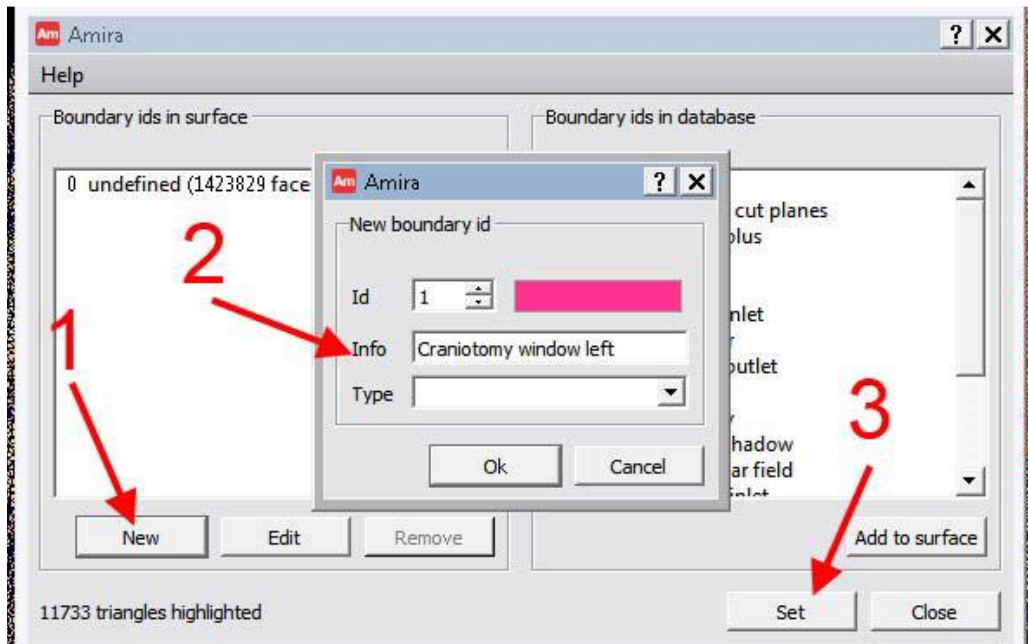


Figure 162: Amira boundary id settings

- 10.14. Save the surface under “petname_CT_skull_craniotomy_approach.surf”
- 10.15. Measure the surface area by right clicking the surface → Measure and Analyze
→ Surface Area Volume

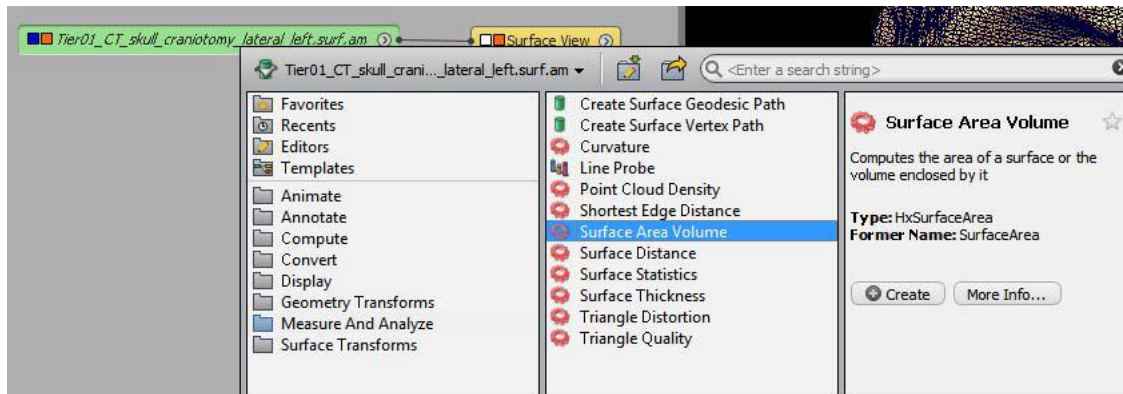


Figure 163: Amira surface area volume

10.16. Properties → Patches → Apply → Show



Figure 164: Amira patches apply

10.17. In the Surface View, change the “colours” to “boundary ids”

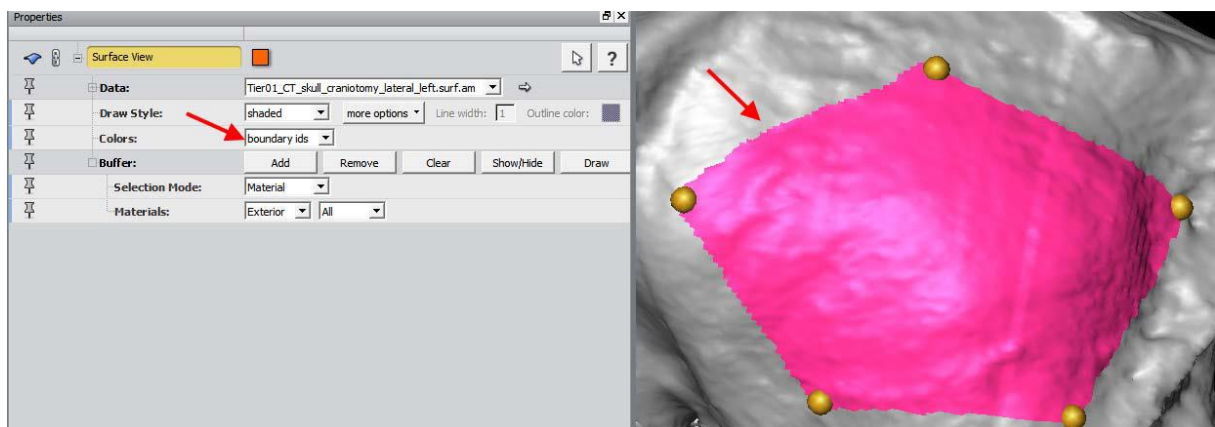


Figure 165: Amira colours bondary id

11 Simulating the Craniotomy

- 11.1. Load the surface “petname_CT_skull.surf” and the landmark file “petname_CT_drillholes_approach.landmark.Ascii” and set the landmark size to 0.5

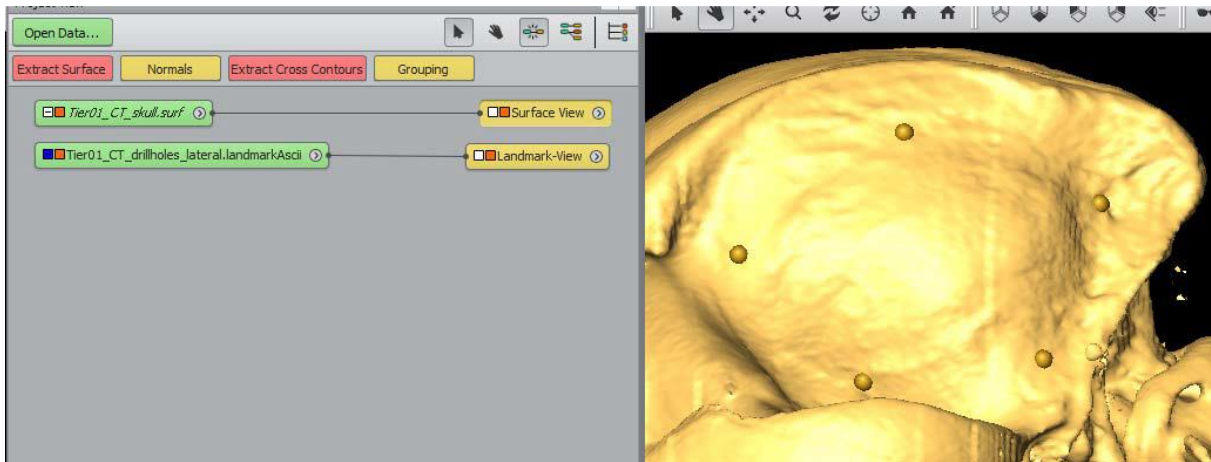


Figure 166: Amira simulate craniotomy

- 11.2. Open the Surface Editor and disable “visible triangles only”

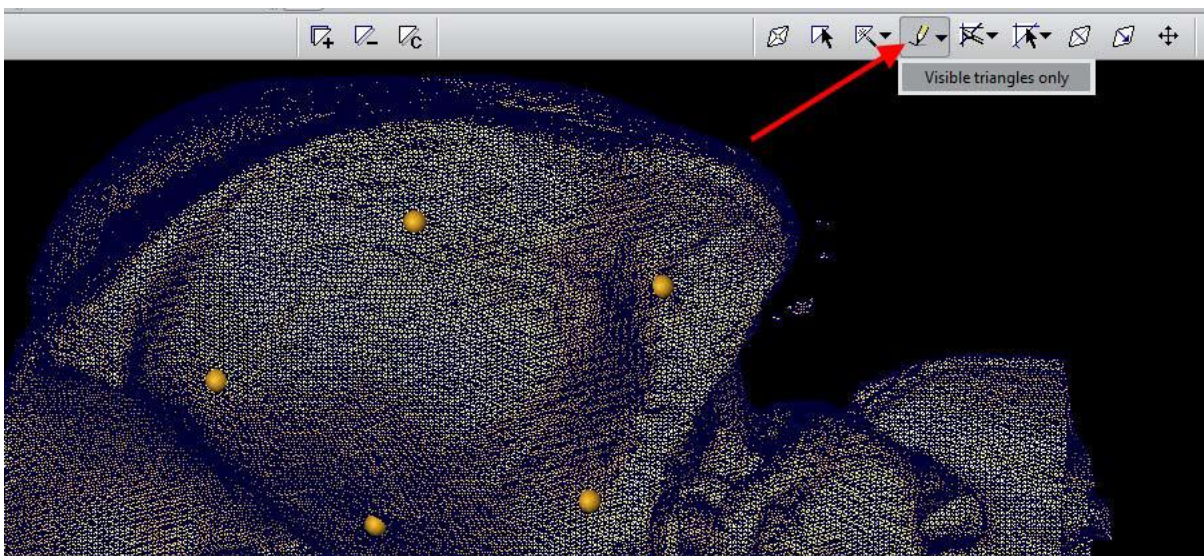


Figure 167: Amira visible triangles

11.3. Draw a contour around the landmarks

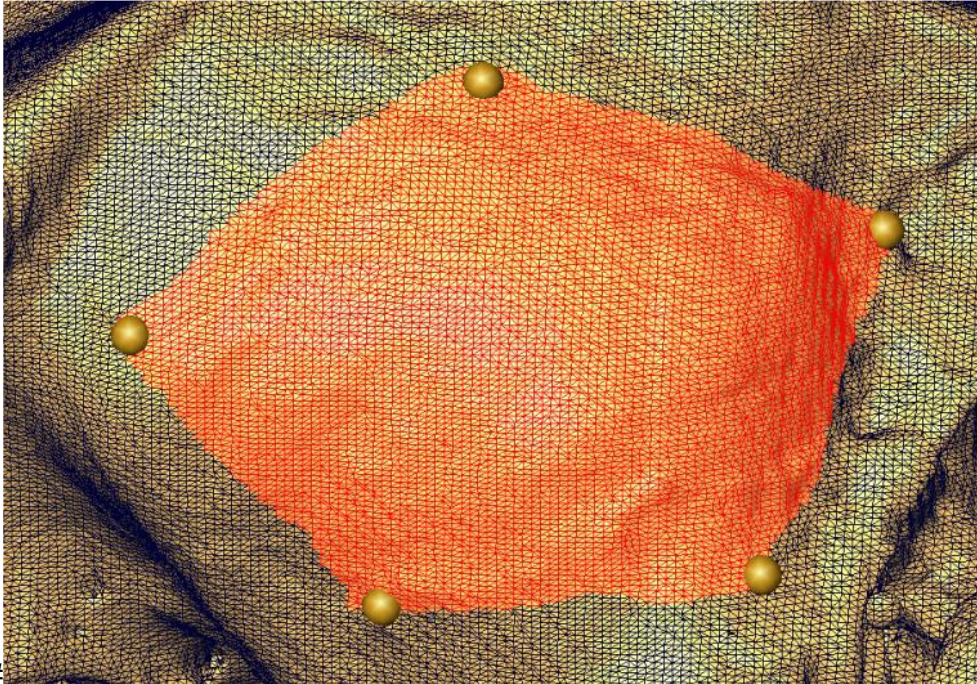


Figure 168: Amira draw contour

- 11.4. Because the “visible triangles only” was disabled, underlying material and the opposite side are selected as well. Make sure to delete (ctrl + left mouse button) the unwanted triangles.

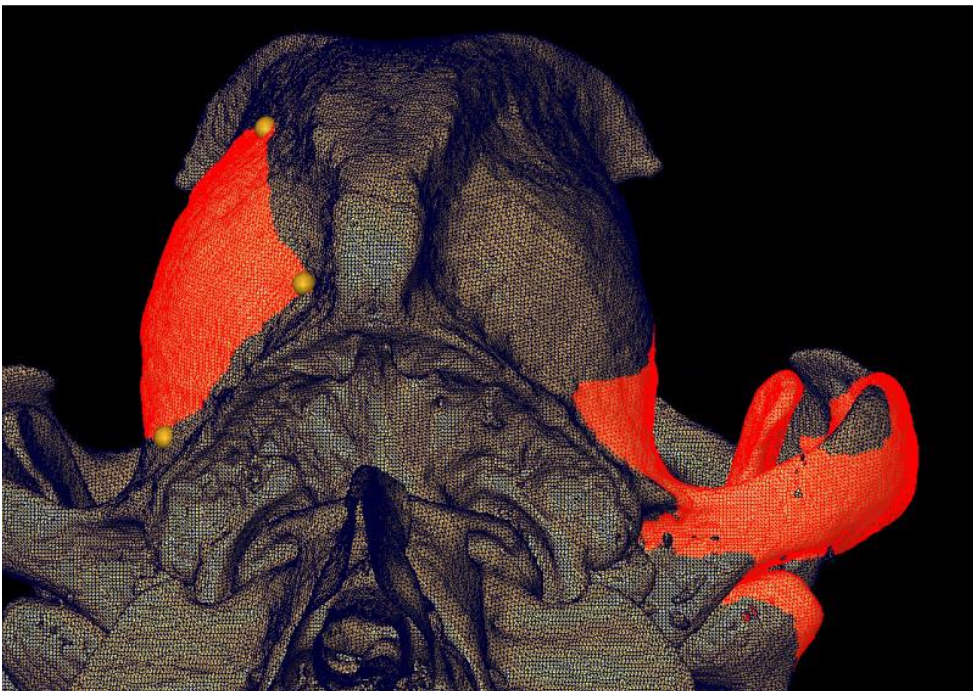


Figure 169: Amira draw error



Figure 170: Amira correct drawing

- 11.5. When the selection is complete, go to “Surface” → Edit → “Delete highlighted faces”

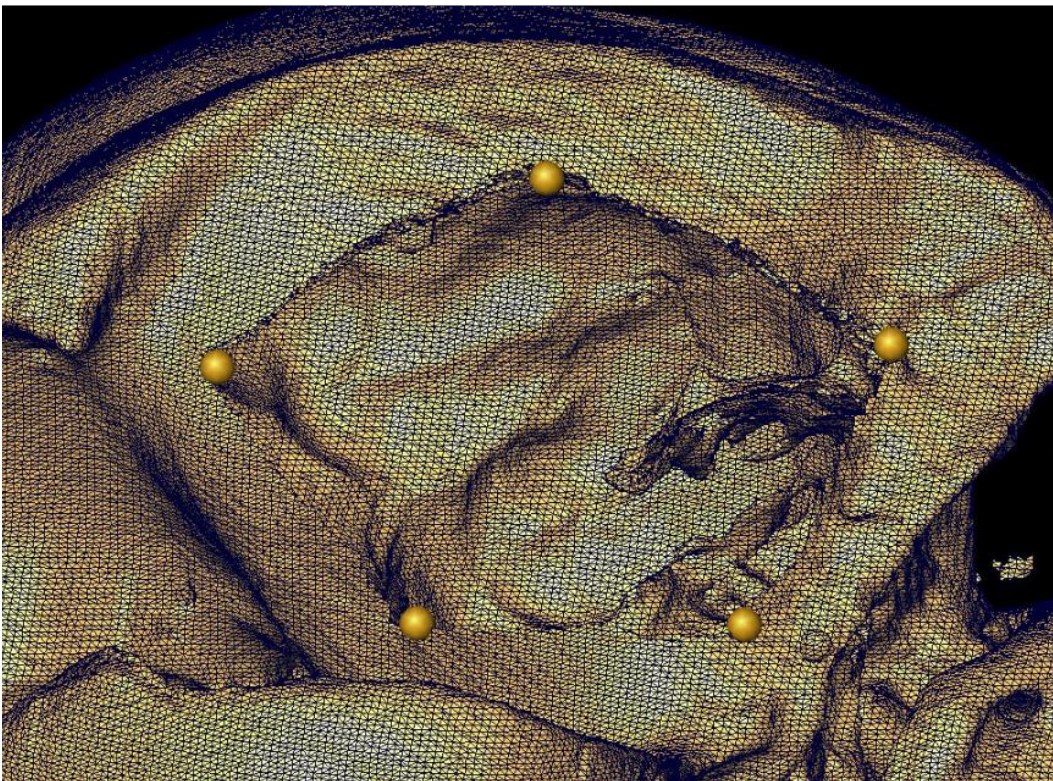


Figure 171: Amira delete faces

- 11.6. Save the surface as
"petname_CT_skull_craniotomy_window_approach_left.surf"
- 11.7. Repeat steps 11 to 11.5 for the right side if necessary
- 11.8. When a MR file is loaded, it should look like follows

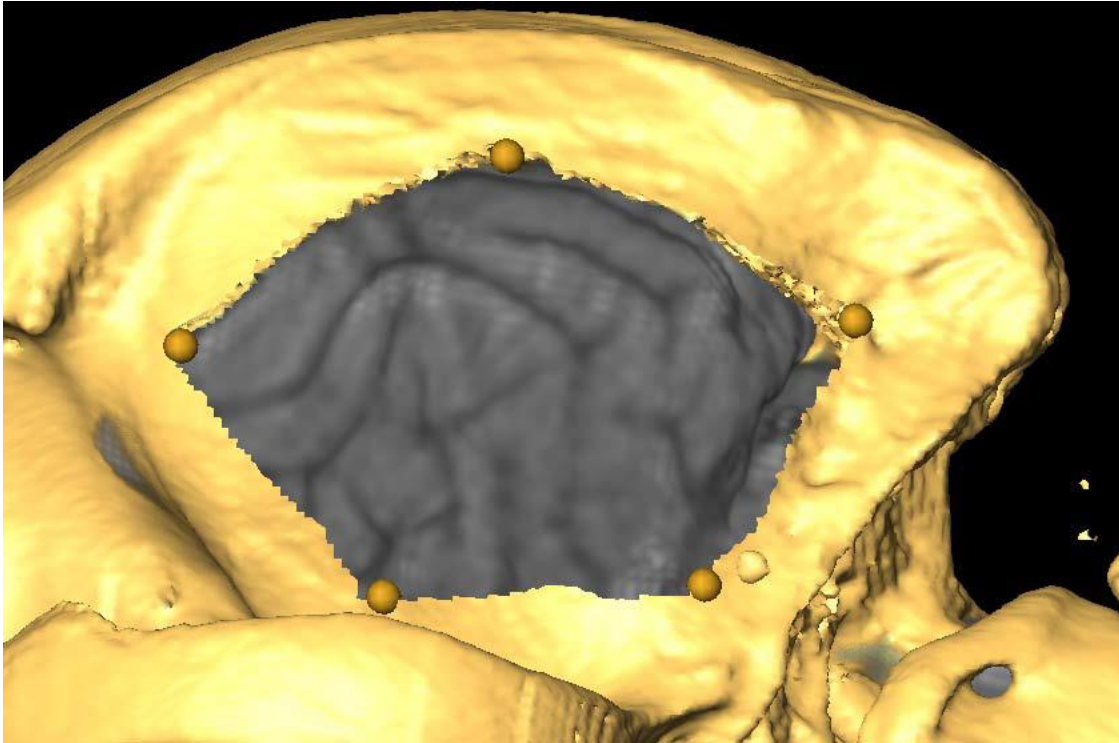


Figure 172: Amira craniotomy completed

12 Measuring the Gyri area

- 12.1. Load the “petname_CT_skull_craniotomy_window_approach_left.surf” and “petname_brain_left_gyri.surf”
- 12.2. Set the Surface View of the brain/gyri to “boundary ids” which should then look like follows (example, anatomy not correct)

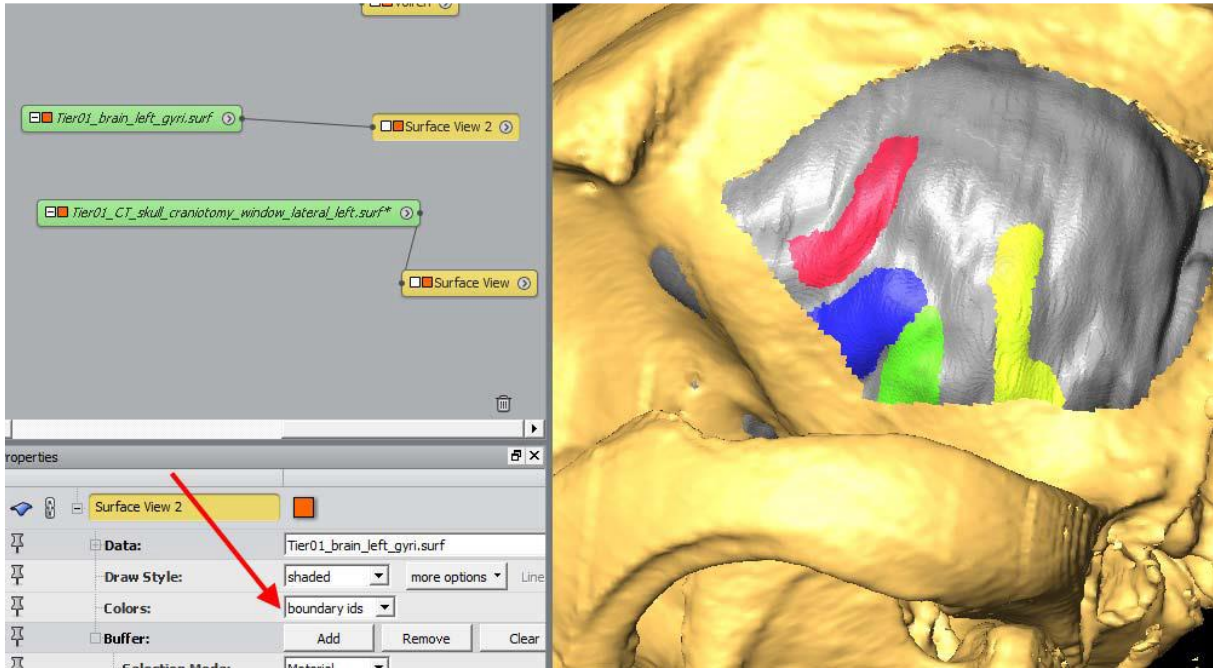


Figure 173: Amira craniotomy with brain

- 12.3. Open the Surface Editor for “petname_brain_left_gyri.surf” and choose the “Draw contour to highlight faces” tool with enabled “visible triangles only” to then draw the accessible brain are through the craniotomy window.

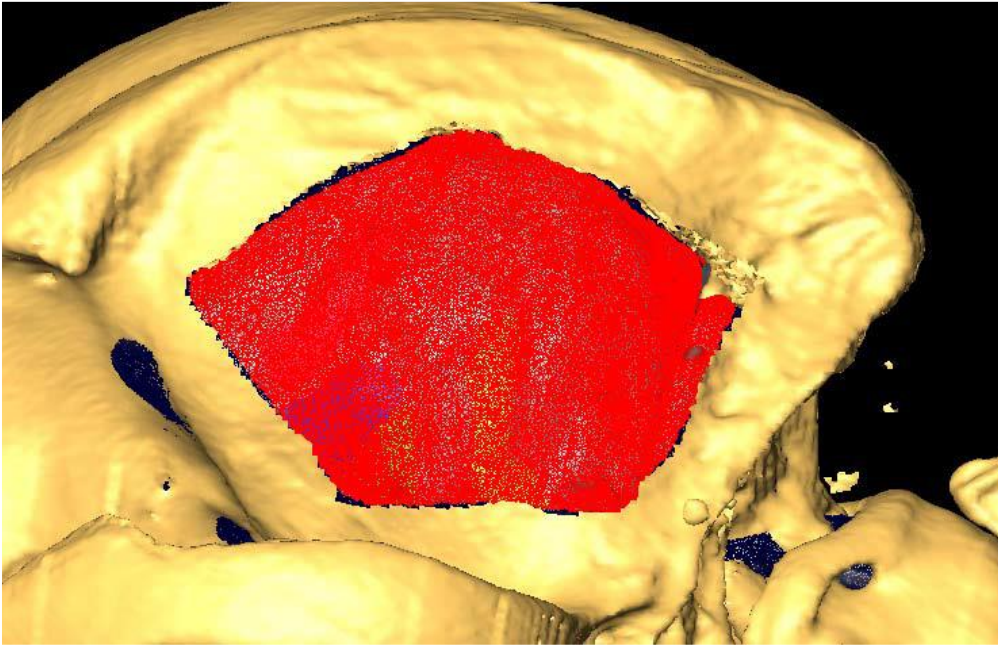


Figure 174: Amira draw craniotomy window

- 12.4. Disable the Surface view of the “petname_CT_skull_craniotomy_window_approach_left.surf” to check the selection (rotating the whole brain)

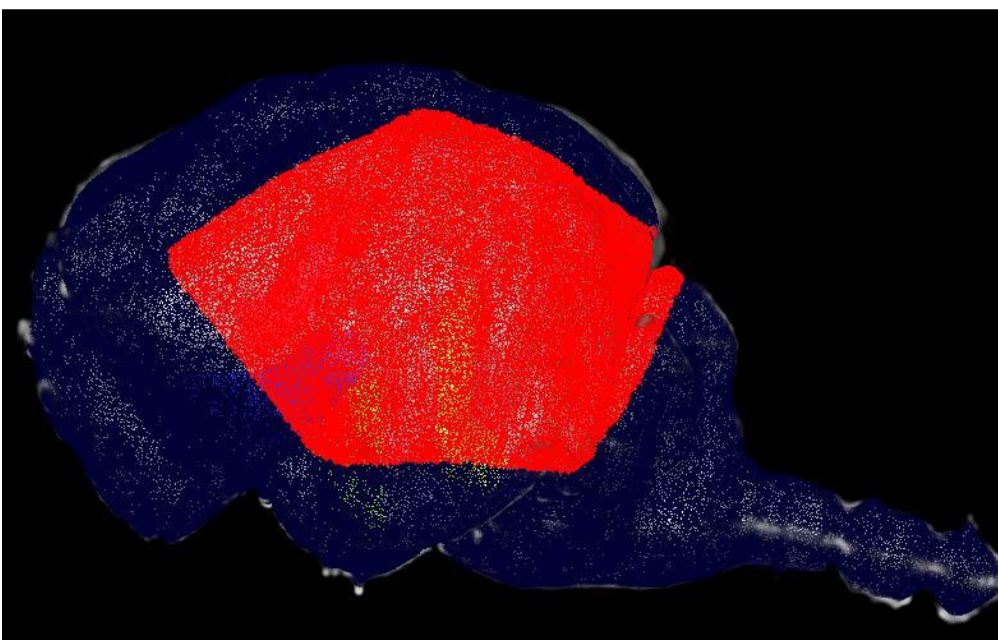


Figure 175: Amira craniotomy window on brain

12.5. Set a new boundary id for the selection

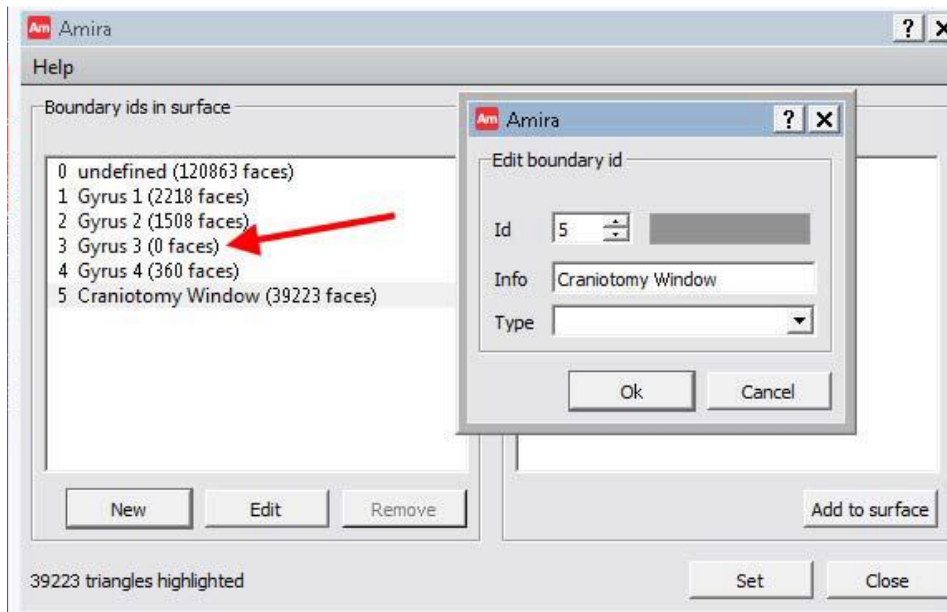


Figure 176: Amira boundary id

- 12.6. Save the file as "petname_brain_left_gyri_window.surf"
- 12.7. Measure the areas by right clicking the surface file → Measure and Analyze → Surface Area Volume. Set the properties to "patches" → Apply
- 12.8. Save the file under the suggested name and then click "show"
- 12.9. The newly generated table (unit=mm) displays the area for each patch (Patch number in the table = Patch number in the Viewer +1)

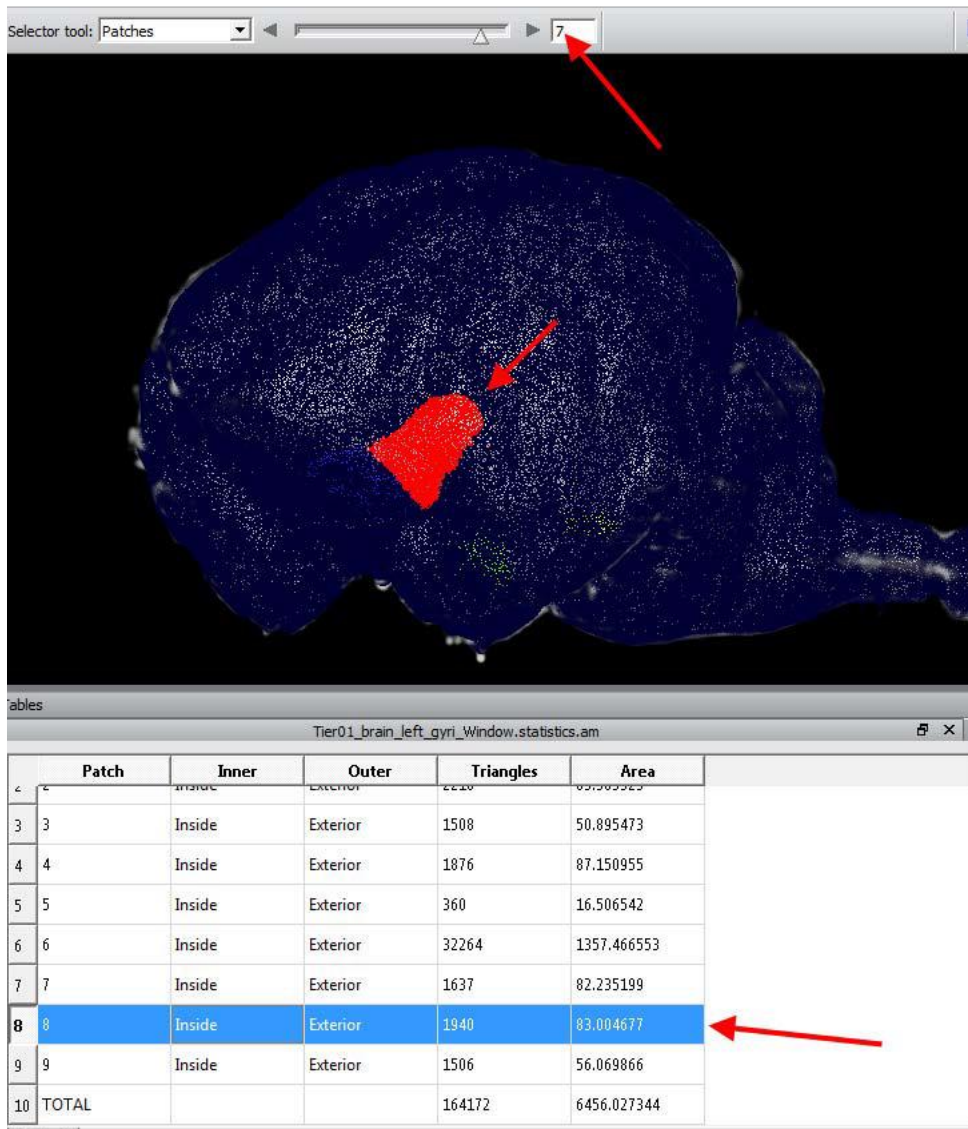


Figure 177: Amira Gyrus area

- 12.10. Write down the "Area" (right most row in the table) into a Microsoft Excel file (or similar programs)
- 12.11. Use these values for further calculations

13 Sinus frontalis

- 13.1. Load the “petname_CT_skull_craniotomy_window_approach_left.surf” and the already aligned CT stack.
- 13.2. Load an Ortho Slice tool on the CT stack, choose the right plane so the Ortho Slice is a transverse slice and navigate it one slice rostrally to the craniotomy.

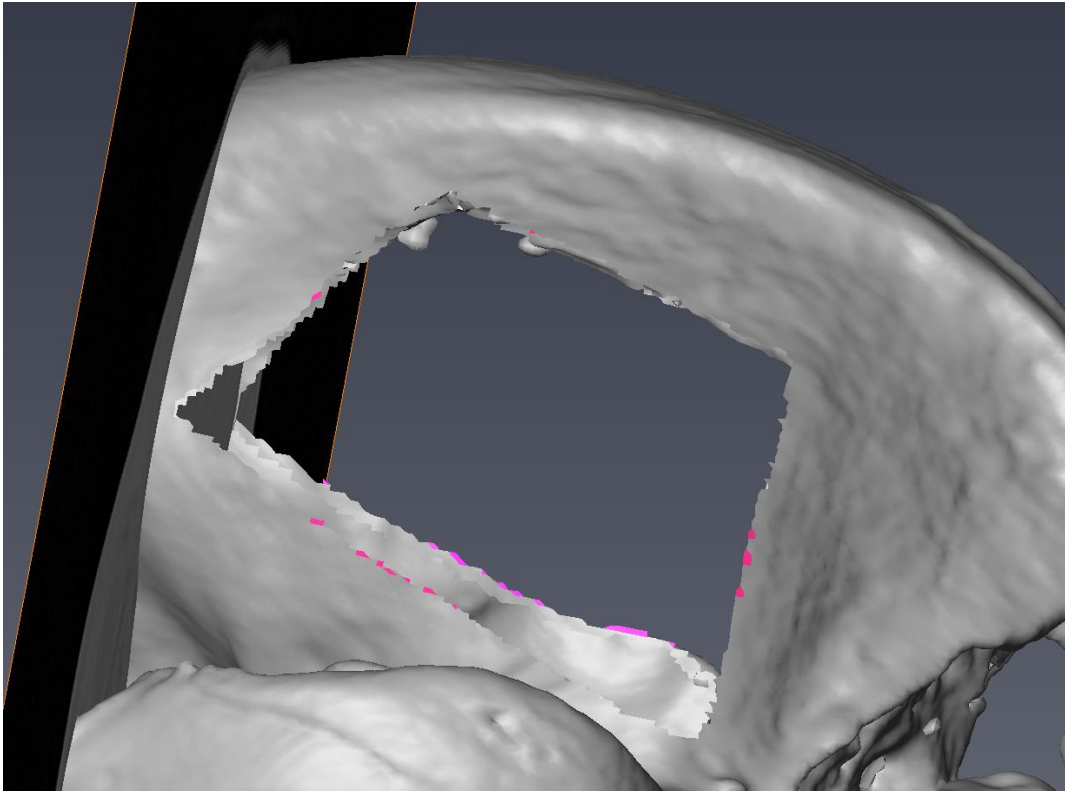
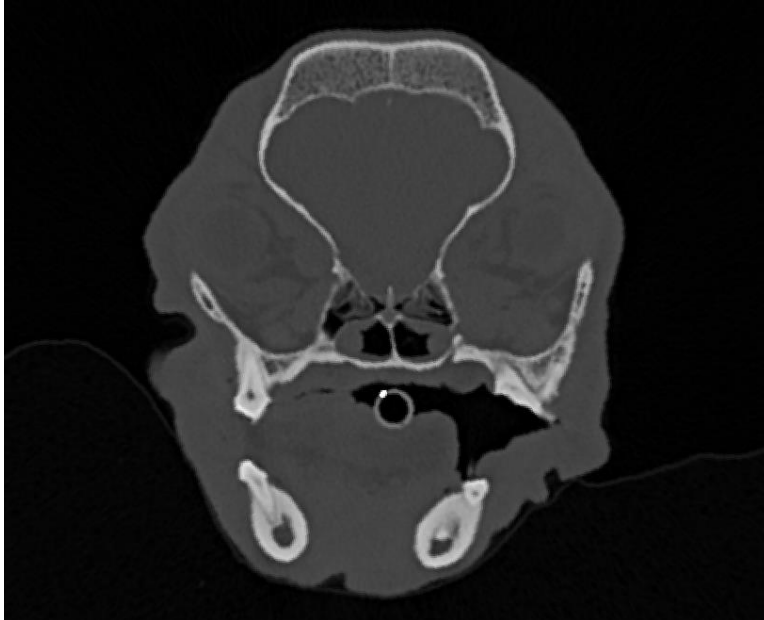


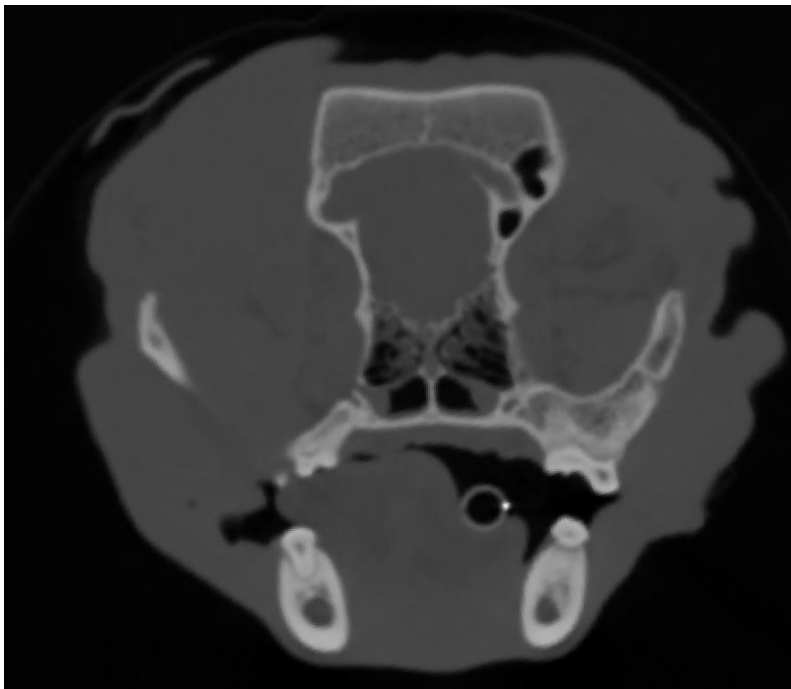
Figure 178: Amira craniotomy both sides

- 13.3. Now look at the CT scan from the front to see if a Sinus frontalis is visible or not. It cannot be opened if there is no Sinus frontalis visible. Check for any interference of craniotomy and the Sinus frontales if it is visible.



13.4.

Figure 179: Amira Sinus frontalis not opened



13.5.

Figure 180: Amira check for interference

- 13.6. Write down the gathered information

7.5 List of Figures

Figure 1: Bones of the skull, lateral aspect. (Hermanson et al. 2020)	3
Figure 2: Bones of the skull, medial aspect of sagittal section. (Hermanson et al. 2020)	3
Figure 3: Paranasal sinuses in three types of skulls (Hermanson et al. 2020)	4
Figure 4: Skull, lateral view showing craniometric points. (Hermanson et al. 2020)	6
Figure 5: Skull, dorsal view showing	6
Figure 6: Skull, ventral view showing craniometric points (Hermanson et al. 2020)	6
Figure 7: Differences between skull types (modified from Schoenebeck and Ostrander (2013))	8
Figure 8: Compared portrayal of the brain location in a German Shepherd (dolichocephalic breed) and a French Bulldog (brachycephalic breed). (Nickel et al. 2004)	9
Figure 9: Nomenclature of the gyri and sulci (lateral view) (Breit Sabine)	10
Figure 10: Nomenclature of the gyri and sulci (dorsal view) (Breit Sabine)	10
Figure 11: Cerebral lobes (Copyright 2010 by Saunders, an imprint of Elsevier Inc.) https://slideplayer.com/slide/8421143/ (accessed May 18, 2020)	12
Figure 12: Sinus durae matris, simplified, medial aspect (Salomon et al. 2020).....	14
Figure 13: Cranial venous sinuses, dorsal aspect (calvaria removed.) (Reinhard et al. 1962)	15
Figure 14: Measurements of the cranium (dorsal view) (Onar 1999)	18
Figure 15: Modified measurements of the cranium (lateral view) (Onar 1999)	19
Figure 16: Brain with all Gyri drawn in	20
Figure 17: „Approach Brachycephalic“ on a brachycephalic dog – Drill holes 1 to 5	22
Figure 18: „Approach Brachycephalic“ on a brachycephalic dog – Drill holes 1 to 5 with guiding lines in mm	22
Figure 19: Comparison „Approach Mesaticephalic“ and “Approach Brachycephalic” on a mesaticephalic dog.....	23
Figure 20: Measuring the distance of the craniotomy area to the crista sagittalis externa (in mm).....	23

Figure 21: Ortho Slice tool set one slice rostrally to the craniotomy	24
Figure 22: CT scan one slice rostral of the simulated craniotomy – the Sinus frontalis in this dog is cranial to the craniotomy and therefore unopened.	24
Figure 23: Location of the first hole (Steyrer 2018)	25
Figure 24: Location of the second hole (Steyrer 2018)	25
Figure 25: Location of the third hole (Steyrer 2018).....	26
Figure 26: Location of the fourth hole (Steyrer 2018).....	26
Figure 27: Location of the fifth hole (Steyrer 2018)	27
Figure 28: Cephalic index for each dog and median.....	29
Figure 29: Craniotomy areas of „Approach Brachycephalic“	30
Figure 30: Craniotomy areas of „Approach Mesaticephalic“	30
Figure 31: Comparison of craniotomy areas for brachycephalic dogs.....	31
Figure 32: Comparison of craniotomy areas for mesaticephalic dogs	31
Figure 33: "Approach Mesaticephalic" in Dog 3 (mesaticephalic dog)	32
Figure 34: "Approach Brachycephalic" in Dog 3 (mesaticephalic dog).....	32
Figure 35: "Approach Brachycephalic" in Dog 7 (brachycephalic dog).....	32
Figure 36: "Approach Mesaticephalic" in Dog 7 (brachycephalic dog)	32
Figure 37: „Approach Brachycephalic“ on a brachycephalic skull (Dog 5).....	35
Figure 38: „Approach Mesaticephalic“ on a brachycephalic dog (Dog 5)	35
Figure 39: Mean gyri area and their accessibility in brachycephalic dogs	39
Figure 40: Mean Gyri Area and their accessibility in mesaticephalic dogs	40
Figure 41: Craniotomy area compared to the accessible brain area in the „Approach Brachycephalic“.....	41
Figure 42: Craniotomy area compared to accessible brain area in the „Approach Mesaticephalic“	41
Figure 43: Craniotomy Area compared to the accessible brain area in the „Approach Brachycephalic“ in mesaticephalic dogs	42

Figure 44: Craniotomy Area compared to the accessible brain area in the „Approach Mesaticephalic“ in mesaticephalic dogs.....	42
Figure 45: Craniotomy area compared to the accessible brain area in the „Approach Brachycephalic“ on brachycephalic dogs.....	43
Figure 46: Craniotomy area compared to the accessible brain area in the „Approach Mesaticephalic“ on brachycephalic dogs	43
Figure 47: Approach Mesaticephalic" in Dog 1	47
Figure 48: "Approach Brachycephalic" in Dog 1	47
Figure 49: Amira home	85
Figure 50: Amira import	85
Figure 51: Amira Volren.....	86
Figure 52: Amira Volren2.....	86
Figure 53: Amira saving.....	87
Figure 54: Amira view Figure 55: Amira axes	87
Figure 56: Amira tools	88
Figure 57: Amira Isosurface.....	88
Figure 58: Amira transform.....	89
Figure 59: landmarks (Hermanson et al. 2020).....	89
Figure 60: Amira aligning.....	90
Figure 61: Amira aligning 2.....	90
Figure 62: Amira scalebars.....	91
Figure 63: Amira scalebars settings.....	91
Figure 64: Amira transform editor settings	92
Figure 65: Amira landmarks.....	92
Figure 66: Amira landmark editor	93
Figure 67: Amira Interact	93
Figure 68: Amira set landmarks.....	95

Figure 69: Amira cranial index	96
Figure 70: Amira Arcus width.....	97
Figure 71: Amira units	97
Figure 72: Amira Volren colour	98
Figure 73: Amira Volren colour green	98
Figure 74: Amira scan alignment	99
Figure 75: Amira scans aligned	100
Figure 76: Amira register images.....	100
Figure 77: Amira references link.....	101
Figure 78: Amira references linked	101
Figure 79: Amira colour wash	102
Figure 80: Amira colour wash check.....	102
Figure 81: Amira new label field	103
Figure 82: Amira segmentation.....	103
Figure 83: Amira inside material	104
Figure 84: Amira material threshold.....	104
Figure 85: Amira masked voxels	105
Figure 86: Amira threshold background.....	105
Figure 87: Amira grow selection	106
Figure 88: Amira shrink selection	106
Figure 89: Amira remove selected	107
Figure 90: Amira segmentation pick	107
Figure 91: Amira clear selection	108
Figure 92: Amira selection brush	108
Figure 93: Amira "bridges"	108

Figure 94: Amira correct selection	109
Figure 95: Amira Invert selection	109
Figure 96: Amira inverted selection	110
Figure 97: Amira selection border	110
Figure 98: Amira grow and shrink	111
Figure 99: Amira fill holes	111
Figure 100: Amira grow selection	112
Figure 101: Amira arithmetic.....	112
Figure 102: Amira arithmetic input.....	113
Figure 103: Amira arithmetic expression.....	114
Figure 104: Amira result	114
Figure 105: Amira crop editor	115
Figure 106: Amira brain crop	115
Figure 107: Amira resample	115
Figure 108: Amira resample settings	116
Figure 109: Amira low brain threshold	117
Figure 110: Amira add masked voxels.....	117
Figure 111: Amira fill holes	118
Figure 112: Amira smooth labels	118
Figure 113: Amira generate surface	119
Figure 114: Amira simplification editor.....	119
Figure 115: Amira surface view	120
Figure 116: Amira binary	120
Figure 117: Amira surface editor	120
Figure 118: Amira visible triangles.....	121

Figure 119: Amira draw style	121
Figure 120: Amira interact tool.....	121
Figure 121: Amira paramedian brain	122
Figure 122: Amira delete highlighted faces.....	122
Figure 123: Amira brain half	122
Figure 124: Amira surface editor	123
Figure 125: Amira visible triangles.....	123
Figure 126: Amira boundary ids.....	124
Figure 127: Amira boundary id settings	124
Figure 128: Amira clear buffer	125
Figure 129: Amira draw style boundary	125
Figure 130: Amira boundary id 2	125
Figure 131: Amira surface area volume.....	126
Figure 132: Amira patches	126
Figure 133: Amira show surface area	127
Figure 134: Amira resampled Volren	127
Figure 135: Amira back faces.....	128
Figure 136: Amira visible triangles.....	128
Figure 137: Amira draw Gyrus.....	129
Figure 138: Amira both faces.....	129
Figure 139: Amira set boundary id.....	130
Figure 140: Amira boundary id settings	130
Figure 141: Amira clear highlights	130
Figure 142: Amira surface view colour.....	131
Figure 143: Amira coloured Gyrus.....	131

Figure 144: Amira Gyri overlap.....	132
Figure 145: Amira Gyri drawn.....	132
Figure 146: Amira selector tool.....	133
Figure 147: Amira patch selector.....	134
Figure 148: Amira surface area volume.....	134
Figure 149: Amira patches apply.....	134
Figure 150: Amira show surface area.....	135
Figure 151: Amira patch selector.....	136
Figure 152: Amira create surface.....	137
Figure 153: Amira direct normals.....	137
Figure 154: Amira landmarks.....	138
Figure 155: Amira measure tool.....	138
Figure 156: Amira landmark size.....	139
Figure 157: Amira surface editor.....	139
Figure 158: Amira draw contour.....	140
Figure 159: Amira visible triangles.....	140
Figure 160: Amira draw craniotomy.....	141
Figure 161: Amira set boundary ids.....	141
Figure 162: Amira boundary id settings.....	142
Figure 163: Amira surface area volume.....	142
Figure 164: Amira patches apply.....	143
Figure 165: Amira colours bondary id.....	143
Figure 166: Amira simulate craniotomy.....	144
Figure 167: Amira visible triangles.....	144
Figure 168: Amira draw contour.....	145

Figure 169: Amira draw error.....	145
Figure 170: Amira correct drawing.....	146
Figure 171: Amira delete faces.....	146
Figure 172: Amira craniotomy completed	147
Figure 173: Amira craniotomy with brain.....	148
Figure 174: Amira draw craniotomy window	149
Figure 175: Amira craniotomy window on brain	149
Figure 176: Amira boundary id	150
Figure 177: Amira Gyrus area	151
Figure 178: Amira craniotomy both sides.....	152
Figure 179: Amira Sinus frontalis not opened	153
Figure 180: Amira check for interference.....	153

7.6 List of Tables

Table 1: Average measurements of three skull types. (Hermanson et al. 2020)	7
Table 2: Gyri with different naming	11
Table 3: List of Gyri and Sulci.....	11
Table 4: Information about the dogs	16
Table 5: Landmarks used to align the skulls	17
Table 6: Measurements for the cranial index.....	18
Table 7: Gyri used in this study	20
Table 8: Measurements of the skull in mm	29
Table 9: Measurements from the craniotomy to the crista sagittalis externa	33
Table 10: Access to gyri in brachycephalic dogs	33
Table 11: Access to gyri in mesaticephalic dogs.....	34
Table 12: Mean accessible gyri area in brachycephalic dogs in sqmm and %	37
Table 13: Mean accessible gyri area in mesaticephalic dogs in sqmm and %	38
Table 14: Comparison of the mean access to the area of each individual gyrus in %	50
Table 15: Vergleich der durchschnittlich zugänglichen Fläche der einzelnen Gyri in %	52
Table 16: Morphometric measurements in mm.....	57
Table 17: Craniotomy area Approach Schlager in mm.....	57
Table 18: Craniotomy area Approach Steyrer in mm	57
Table 19: Gyri area in mm Dog 1.....	58
Table 20: Gyri area in mm Dog 2.....	58
Table 21: Gyri area in mm Dog 3.....	59
Table 22: Gyri area in mm Dog 4.....	59
Table 23: Gyri area in mm Dog 5.....	60

Table 24: Gyri area in mm Dog 6.....	60
Table 25: Gyri area in mm Dog 7.....	61
Table 26: Gyri area in mm Dog 8.....	61
Table 27: Sinus frontalis.....	62
Table 28: Statistics Gyrus sylvius rostralis.....	63
Table 29: Statistics Gyrus sylvius caudalis.....	64
Table 30: Statistics Gyrus ectosylvius rostralis.....	65
Table 31: Statistics Gyrus ectosylvius medius.....	66
Table 32: Statistics Gyrus ectosylvius caudalis.....	67
Table 33: Statistics Gyrus suprasylvius rostralis.....	68
Table 34: Statistics Gyrus suprasylvius medius.....	69
Table 35: Statistics Gyrus ectomarginalis.....	70
Table 36: Statistics Gyrus suprasylvius caudalis.....	71
Table 37: Statistics Gyrus occipitalis.....	72
Table 38: Fisher test Gyrus occipitalis.....	73
Table 39: Statistics Gyrus marginalis.....	73
Table 40: Statistic tests Gyrus marginalis.....	74
Table 41: Statistics Gyrus endomarginalis.....	75
Table 42: chi-square test Gyrus endomarginalis.....	76
Table 43: Statistics Gyrus postcruciatu.....	77
Table 44: Fisher test Gyrus postcruciatu.....	78
Table 45: Statistics Gyrus praecruciatu.....	78
Table 46: Statistic tests Gyrus praecruciatu.....	79
Table 47: Statistics Gyrus proreus.....	80
Table 48: Fisher test Gyrus proreus.....	81

Table 49: Statistics craniotomy and gyri area	81
Table 50: Statistics craniotomy sides compared	82
Table 51: Statistics approaches compared	83
Table 52: Statistics morphometric analysis	84
Table 53: Amira landmarks	93
Table 54: Amira measurements	98

7.7 References

References

Bagley RS, Harrington ML, Pluhar GE, Gavin PR, Moore MP. 1997. Acute, unilateral transverse sinus occlusion during craniectomy in seven dogs with space-occupying intracranial disease. *Veterinary surgery : VS*, 26 (3): 195–201. DOI 10.1111/j.1532-950x.1997.tb01484.x.

Bilderback AL, Faissler D. 2009. Surgical management of a canine intracranial abscess due to a bite wound. *Journal of veterinary emergency and critical care (San Antonio, Tex. : 2001)*, 19 (5): 507–512. DOI 10.1111/j.1476-4431.2009.00467.x.

Boston SE. 2010. Craniectomy and orbitectomy in dogs and cats. *The Canadian Veterinary Journal*, 51 (5): 537–540.

Braun RK, Gideon LA, Riebold TW, Peters RR. 1977. Surgical approach for pinealectomy in the calf. *American journal of veterinary research*, 38 (12): 1973–1976.

Breit Sabine VU. *Nomenclature Brain*.

Cavanaugh RP, Aiken SW, Schatzberg SJ. 2008. Intraventricular tension pneumocephalus and cervical subarachnoid pneumorrhachis in a bull mastiff dog after craniotomy. *Journal of Small Animal Practice*, 49 (5): 244–248. DOI 10.1111/j.1748-5827.2007.00467.x.

Copyright 2010 by Saunders, an imprint of Elsevier Inc. Cerebral lobes. <https://slideplayer.com/slide/8421143/>.

Dewey CW, Krotscheck U, Bailey KS, Marino DJ. 2007. Craniotomy with cystoperitoneal shunting for treatment of intracranial arachnoid cysts in dogs. *Veterinary surgery : VS*, 36 (5): 416–422. DOI 10.1111/j.1532-950X.2007.00287.x.

Dickinson PJ. 2014. Advances in Diagnostic and Treatment Modalities for Intracranial Tumors. *Journal of veterinary internal medicine*, 28 (4): 1165–1185. DOI 10.1111/jvim.12370.

Evans HE, Miller ME, Hrsg. 1979. *Miller's anatomy of the dog*. Second. ed. Philadelphia: W.B. Saunders, 1181.

Goulle F, Meige F, Durieux F, Malet C, Toulza O, Isard P-F, Peiffer RL, Dulaurent T. 2011. Intracranial meningioma causing partial amaurosis in a cat. *Veterinary ophthalmology*, 14 Suppl 1: 93–98. DOI 10.1111/j.1463-5224.2011.00904.x.

Hermanson JW, DeLahunta A, Evans HE. 2020. *Miller and Evans' anatomy of the dog*. Fifth edition, 981eiten.

Janicek JC, Kramer J, Coates JR, Lattimer JC, Lacarrubba AM, Messer NT. 2006. Intracranial abscess caused by *Rhodococcus equi* infection in a foal. *Journal of the American Veterinary Medical Association*, 228 (2): 251–253. DOI 10.2460/javma.228.2.251.

Kramer J, Coates JR, Hoffman AG, Frappier BL. 2007. Preliminary anatomic investigation of three approaches to the equine cranium and brain for limited craniectomy procedures. *Veterinary surgery : VS*, 36 (5): 500–508. DOI 10.1111/j.1532-950X.2007.00297.x.

Lüps P. 1973. Biometrische Untersuchungen an der Schädelbasis des Haushundes. S.l.: s.n., 103.

M Das J, Bajaj J. 2020. StatPearls. Pneumocephalus. Treasure Island (FL).

Marquez-Grados F, Vettorato E, Corletto F. 2020. Sevoflurane with opioid or dexmedetomidine infusions in dogs undergoing intracranial surgery: a retrospective observational study. *Journal of veterinary science*, 21 (1): e8. DOI 10.4142/jvs.2020.21.e8.

Marras LC, Kalaparambath TP, Black SE, Rowed DW. 1998. Severe tension pneumocephalus complicating frontal sinus osteoma. *The Canadian journal of neurological sciences. Le journal canadien des sciences neurologiques*, 25 (1): 79–81. DOI 10.1017/s0317167100033540.

Oliver JE, Hoerlein BF, Mayhew IG, Pedersen D, Hrsg. 1987. *Veterinary neurology*. Philadelphia u.a.: Saunders, 554.: Ill., graph. Darst.

Oliver JE Jr. 1966. Principles of canine brain surgery. *Journal of the American Animal Hospital Association*, (2): 73–88.

Oliver JE Jr. 1968. Surgical approaches to the canine brain. *American journal of veterinary research*, (29): 353–378.

Onar V. 1999. A morphometric study on the skull of the German shepherd dog (Alsatian). *Anatomia, histologia, embryologia*, 28 (4): 253–256. DOI 10.1046/j.1439-0264.1999.00202.x.

Park S-H, Won J, Kim S-I, Lee Y, Park C-K, Kim S-K, Choi S-H. 2017. Molecular Testing of Brain Tumor. *Journal of pathology and translational medicine*, 51 (3): 205–223. DOI 10.4132/jptm.2017.03.08.

Pluhar GE, Bagley RS, Keegan RD, Baszler TV, Moore MP. 1996. The effect of acute, unilateral transverse venous sinus occlusion on intracranial pressure in normal dogs. *Veterinary surgery : VS*, 25 (6): 480–486. DOI 10.1111/j.1532-950x.1996.tb01447.x.

Reinhard KR, Miller ME, Evans HE. 1962. The craniovertebral veins and sinuses of the dog. *The American journal of anatomy*, 111: 67–87. DOI 10.1002/aja.1001110106.

Roberts T, McGreevy P, Valenzuela M. 2010. Human induced rotation and reorganization of the brain of domestic dogs. *PloS one*, 5 (7): e11946. DOI 10.1371/journal.pone.0011946.

Salomon F-V, Geyer H, Gille U. 2020. *Anatomie für die Tiermedizin*. Fourth., aktualisierte Auflage, 887eiten.

Schmidt MJ, Amort KH, Failing K, Klingler M, Kramer M, Ondreka N. 2014. Comparison of the endocranial- and brain volumes in brachycephalic dogs, mesaticephalic dogs and Cavalier King Charles spaniels in relation to their body weight. *Acta veterinaria Scandinavica*, 56: 30. DOI 10.1186/1751-0147-56-30.

Schmidt MJ, Biel M, Klumpp S, Schneider M, Kramer M. 2009. Evaluation of the volumes of cranial cavities in Cavalier King Charles Spaniels with Chiari-like malformation and other brachycephalic dogs as measured via computed tomography. *American journal of veterinary research*, 70 (4): 508–512. DOI 10.2460/ajvr.70.4.508.

Schoenebeck JJ, Ostrander EA. 2013. The genetics of canine skull shape variation. *Genetics*, 193 (2): 317–325. DOI 10.1534/genetics.112.145284.

Seki S, Teshima K, Ito D, Kitagawa M, Yamaya Y. 2019. Impact of intracranial hypertension on the short-term prognosis in dogs undergoing brain tumor surgery. *The Journal of veterinary medical science*, 81 (8): 1205–1210. DOI 10.1292/jvms.18-0475.

Sharkey LC, McDonnell JJ, Alroy J. 2004. Cytology of a mass on the meningeal surface of the left brain in a dog. *Veterinary clinical pathology*, 33 (2): 111–114. DOI 10.1111/j.1939-165x.2004.tb00358.x.

Song RB, Vite CH, Bradley CW, Cross JR. 2013. Postmortem evaluation of 435 cases of intracranial neoplasia in dogs and relationship of neoplasm with breed, age, and body weight. *Journal of veterinary internal medicine*, 27 (5): 1143–1152. DOI 10.1111/jvim.12136.

Steyrer. 2018. Evaluation of a newly described rostral tentorial craniotomy approach in mesaticephalic dogs, regarding its safety and constancy of accessible brain regions.

Stockard CR, Anderson OD, James WT. 1941. The genetic and endocrinic Basis for differences in form and behavior as elucidated by studies of contrasted pure-line dog breeds and their hybrids. By Charles R(upert) Stockard and collaborators. With special contributions on behavior by O. D. Anderson and W. T. James. Philadelphia: The Wistar Institute of Anatomy and Biology, 775.

Suñol A, Mascort J, Font C, Bastante AR, Pumarola M, Feliu-Pascual AL. 2017. Long-term follow-up of surgical resection alone for primary intracranial rostral tentorial tumors in dogs: 29 cases (2002-2013). *Open veterinary journal*, 7 (4): 375–383. DOI 10.4314/ovj.v7i4.14.

Toga AW, Thompson PM. 2003. Mapping brain asymmetry. *Nature reviews. Neuroscience*, 4 (1): 37–48. DOI 10.1038/nrn1009.

Uemura EE. 2015. *Fundamentals of Canine Neuroanatomy and Neurophysiology*. First. Aufl. s.l.: Wiley-Blackwell, 432.

Wayne RK. 1986. CRANIAL MORPHOLOGY OF DOMESTIC AND WILD CANIDS: THE INFLUENCE OF DEVELOPMENT ON MORPHOLOGICAL CHANGE. *Evolution; international journal of organic evolution*, 40 (2): 243–261. DOI 10.1111/j.1558-5646.1986.tb00467.x.

Wohlgemuth MV. 1985. Tension pneumocephalus. *Journal of neurosurgical nursing*, 17 (3): 146–154. DOI 10.1097/01376517-198506000-00002.

Wouters EGH, Beukers M, Theyse LFH. 2011. Surgical treatment of a cerebral brain abscess in a cat. *Veterinary and comparative orthopaedics and traumatology : V.C.O.T.*, 24 (1): 72–75. DOI 10.3415/VCOT-10-02-0018.